Reeling of Tight Fit Pipe

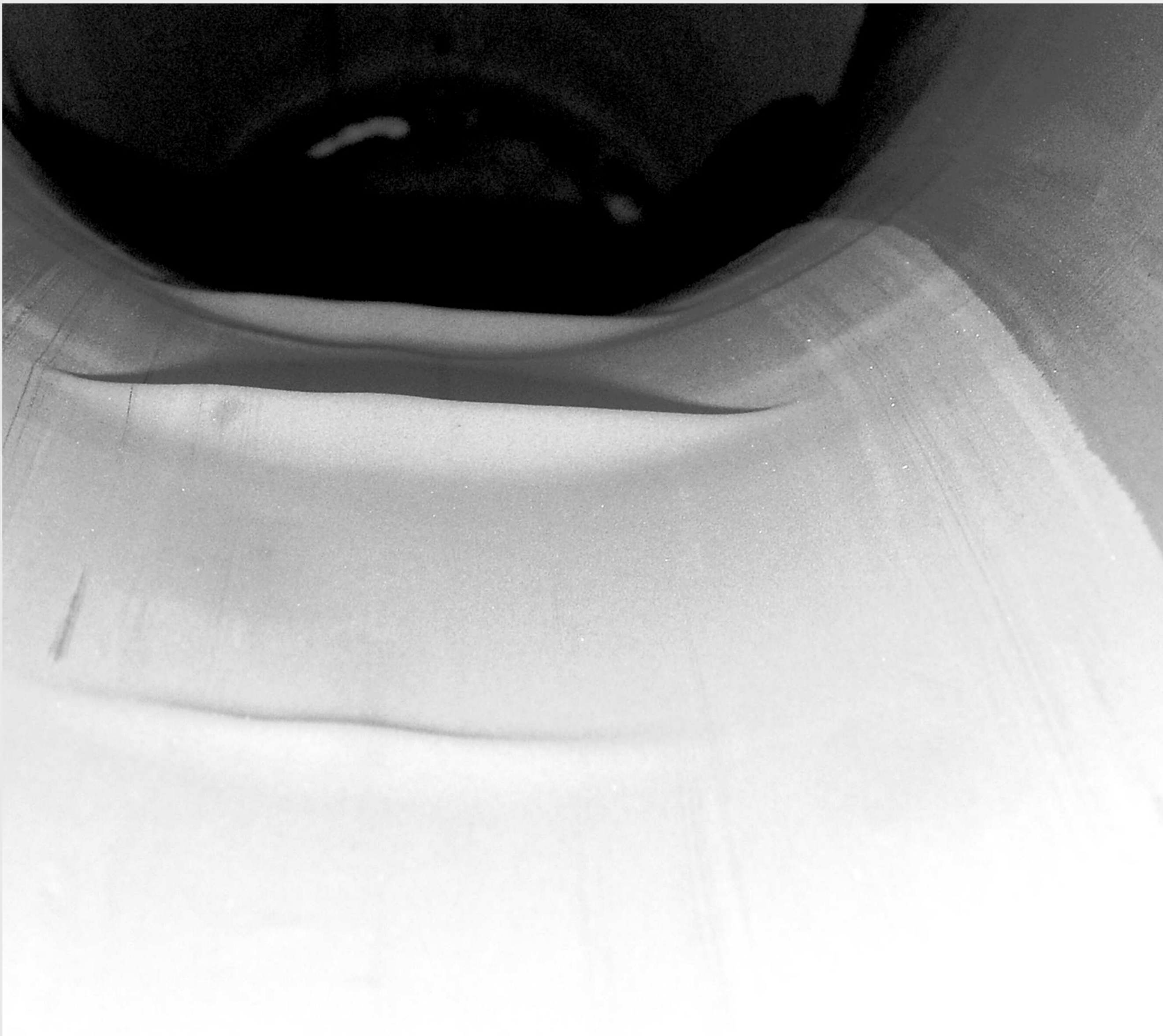

Eelke S. Focke

Reeling
of
Tight Fit Pipe

Proefschrift

ter verkrijging van de graad van doctor
aan de Technische Universiteit Delft,
op gezag van de Rector Magnificus prof. dr. ir. J.T. Fokkema,
voorzitter van het College voor Promoties,
in het openbaar te verdedigen op dinsdag 5 juni 2007 om 15:00 uur
door

Eelke Shireen FOCKE

civiel ingenieur
geboren te Willemstad, Curaçao

Dit proefschrift is goedgekeurd door de promotoren:
Prof. ir. J. Meek
Prof. ir. F.S.K. Bijlaard

Samenstelling promotiecommissie:

Rector Magnificus	voorzitter
Prof. ir. J. Meek	Technische Universiteit Delft, promotor
Prof. ir. F.S.K. Bijlaard	Technische Universiteit Delft, promotor
Ir. A.M. Gresnigt	Technische Universiteit Delft
Prof. dr. ir. J. Wardenier	Technische Universiteit Delft
Prof. ir. H.H. Snijder	Technische Universiteit Eindhoven
D. Haldane	Heriot-Watt University Edinburgh
Prof. dr. M. Rotter	University of Edinburgh

ISBN 978-90-9021849-6
Offshore Engineering, report 2007.OE.010

Published and distributed by the author in cooperation with:

Offshore Engineering
Stevinweg 1
2628 CN Delft
+31 15 278 4758
www.offshore.tudelft.nl

Cover design: Courtesy of Annemarit van Broekhoven
Printing: Gildeprint Drukkerijen

Acknowledgements

Many people and institutions have contributed directly and indirectly to this thesis. First of all I would like to thank Jan Meek for his help with finding a PhD subject and creating a PhD position combining an academic environment with industry. The confidence in me and the personal coaching have contributed to the motivation and the enjoyment of conducting this PhD project. I would like to acknowledge Frans Bijlaard for his assistance and personal support throughout the PhD trajectory. I would also like to express my sincere gratitude to Nol Gresnigt for the inspiring discussions on flanged connections, horizontally positioned test equipment and other steel and pipeline related subjects. These discussions will always be remembered heartily. Jan van der Graaf I would like to thank for his continuous support at Heerema Marine Contractors and making it practically possible for me to execute this project within the Heerema Company. I am very grateful for that. Anton de Koning I would like to recognise for his participation in this project. Furthermore, I would like to thank Dr. Nakasugi and Mr. Fujita from Kuroki T&P for their help, support and the warm welcome I always felt when visiting Japan.

I would like to acknowledge Alex Wesdorp, Martin Kik and all the welders at the Heerema Welding Centre in Vlissingen for their contribution. Visiting the Welding Centre and witnessing the welding activities was a great experience and always a fun trip to look forward to. Furthermore, I would like to recognise Albert Bosman, Edwin Scharp, Cees van Beek, Liesbeth Eekhout and all the other people in the STEVIN laboratory in Delft for their assistance to the experimental part of the project. The creative solutions to the experimental challenges concerning the full scale bending rig and the related measuring equipment impressed me immensely. I would also like to express my appreciation to Dakang Liu for his support with the simulation of the manufacturing process of Tight Fit Pipe in MARC. Moreover, I would like to thank Martijn Slaats and Annemiek Hilberink for their help and critical input to papers, presentations and to this PhD thesis. Erwan Karjadi I would like to thank for simulating the experimental work in ABAQUS. I very much enjoyed our cooperation when correlating the experimental data to the finite element results. I would also like to acknowledge all the MSc. and BSc. students working on their theses within my PhD project.

Finally, I would like to thank my friends, my family and my colleagues at Heerema Marine Contractors and the Delft University of Technology for their support throughout the PhD research. I would also like to express my gratitude to Noortje Jansen and Marlies Goorden for being my ushers at the PhD defence and to Annemarit van Broekhoven for the cover design.

This research was supported by SenterNovem, Delft University of Technology, Heerema Marine Contractors, Dosto Engineering and Kuroki T&P.

Summary

If it would be possible to install Tight Fit Pipe by means of reeling, it would be an attractive new option for the exploitation of offshore oil and gas fields containing corrosive hydrocarbons. Tight Fit Pipe is a mechanically bonded double walled pipe where a corrosion resistant alloy liner pipe is mechanically fitted inside a carbon steel outer pipe through a thermo-hydraulic manufacturing process. Reeling is a fast method of offshore pipeline installation where a pipe is spooled on a reel, which is positioned on a vessel. The vessel subsequently sails to the offshore location where the pipe is unwound, straightened and deployed to the seabed. However, reeling of Tight Fit Pipe is not yet proven technology. The reeling process imposes high plastic strains (due to bending) in the pipe, which may cause unacceptable liner pipe wrinkling and Tight Fit Pipe ovalisation. This PhD project aimed to make a contribution to the possible development of the installation of Tight Fit Pipe by means of the reeling method. The focus of this research was on the initiation and the degree of liner pipe wrinkling as well as the degree of ovalisation occurring during the spooling-on phase of the reeling process, both theoretically and experimentally; the latter by performing full scale bending tests on 12.75 inch outer diameter Tight Fit Pipe. These bending tests focussed on the spooling-on phase, because initiation of liner pipe wrinkling is expected to occur during this phase of the reeling process: the highest bending of the pipe occurs in this phase.

Axial compression tests on 10.75 and 12.75 inch outer diameter Tight Fit Pipe and small scale reeling tests on 22 mm outer diameter single walled pipe were executed prior to building the full scale bending rig. Results of these tests aided in the design of the bending rig and its measuring equipment. In order to verify the fitness for purpose of the full scale bending rig, a full scale bending test was executed on a 12.75 inch outer diameter single walled pipe in preparation of the bending tests of the 12.75 inch Tight Fit Pipes. Seven 12.75 inch Tight Fit Pipes were subsequently bent stepwise to smaller bending radii. Reel radii used for testing were 9 m, 8 m, 7.5 m, 7 m, 6.5 m, 6 m, 5.5 m and 5 m. One of the objectives of the testing was to determine the initiation of liner pipe wrinkling of which there is currently no general agreement on its definition. In this study the initiation of liner pipe wrinkling has been defined as crossing a certain threshold of the liner pipe wrinkle height, which could be based on its influence on fatigue life reduction or the size of a pig and its ability to pass wrinkles of a certain height. Further research into this subject has to be performed.

Results of the full scale bending tests of 12.75 inch Tight Fit Pipe indicated that:

1. the developed theoretical model describing the forces on the 12.75 inch Tight Fit Pipe by the full scale bending rig matched the test results well.
2. the DNV OS F101 prediction for ovalisation, assuming the liner pipe and the outer pipe wall thicknesses “added”, representing one single wall thickness in this

prediction, resulted in an underestimate of the measured ovalisation. This underestimate is attributed to the fact that this prediction is intended for bending only, while in the tests also a reaction force of the reel on the Tight Fit Pipe enhanced ovalisation.

3. the extent of the liner pipe wrinkling decreased if Tight Fit Pipe with a high mechanical bonding strength between the liner pipe and the outer pipe in the Tight Fit Pipe was used. This can be explained by the fact that the higher radial contact stress between the liner pipe and the outer pipe results in a higher axial friction between the liner pipe and the outer pipe. This higher axial friction avoids liner pipe material “feeding in” to the liner pipe wrinkle.
4. the presence of a circumferential weld in the Tight Fit Pipes with a high mechanical bonding strength caused higher liner pipe wrinkles at the lower curvatures tested. This may be the consequence of the weld resulting in a less even distribution of the contact stress between the reel and the Tight Fit Pipe during bending. Locally higher contact forces resulted in small indentations in the pipe wall that triggered the initiation of the liner pipe wrinkles.
5. the electric resistance welded longitudinal outer pipe weld did not cause higher liner pipe wrinkles at the curvatures tested. This may be explained by the fact that this weld is continuous along the length of the Tight Fit Pipe and did not function as a local imperfection.

Liner pipe wrinkling decreases with an increase of the reel diameter, a decrease of the diameter to thickness ratio of the liner pipe and an increase of the mechanical bonding strength. A sensitivity analysis of the manufacturing process of Tight Fit Pipe showed that the most efficient way to increase the mechanical bonding strength is to increase the liner pipe material strength and to minimise the contact time between the liner pipe and the outer pipe during the manufacturing process. Liner pipe wrinkling also decreases when the diameter to thickness ratio of the outer pipe is decreased because this influences ovalisation of the Tight Fit Pipe and thereby has a beneficial effect on liner pipe wrinkling. The future task is to combine the reel diameter, the diameter to thickness ratios of the liner pipe and the outer pipe and the mechanical bonding strength with the material and the geometrical properties of a Tight Fit Pipe in such a way that the requirements for e.g. the liner pipe wrinkle height are adhered to. Equations were developed that can be used to predict the liner pipe wrinkle height when bending the 12.75 inch Tight Fit Pipe used in this research on reels with radii varying between 5.5 m and 9 m, while the mechanical bonding strength is between 53 MPa and 189 MPa.

API residual compressive stress tests showed that the initial mechanical bonding strength in the 12.75 inch Tight Fit Pipe bend tested in this research was significantly reduced, irrespective of whether a high or a low initial mechanical bonding strength had been used prior to spooling-on. This decrease of the mechanical bonding strength can be explained with the normality principle used in plastic theory. These findings justify further research into this phenomenon as the eventual mechanical bonding strength after reeling installation may be vital for its anticipated application during operation.

Table of Contents

List of Symbols

a	liner pipe wrinkle height	[mm]
A_1; A_2; A_3	constants used in the prediction of the critical buckling strain by Lee [30]	[-]
$A_{L;o;TFP}$	outside surface of the liner pipe while confined in the outer pipe	[mm^2]
B	constant used in the prediction of the critical buckling strain by Lee [30]	[-]
C_{11}; C_{12}; C_{21}; C_{22}; C_3	constants used in the prediction of the critical buckling strain by Lee [30]	[-]
$d_{L;a;n}$	average diameter of the liner pipe in step n during the manufacturing process of Tight Fit Pipe	[mm]
$d_{L;a;TFP}$	average diameter of the liner pipe when it is part of the Tight Fit Pipe	[mm]
$d_{L;i;n}$	inner diameter of the liner pipe in step n during the manufacturing process of Tight Fit Pipe	[mm]
$d_{L;o}$	outer diameter of the liner pipe when it is not part of the Tight Fit Pipe	[mm]
$d_{L;o;n}$	outer diameter of the liner pipe in step n during the manufacturing process of Tight Fit Pipe	[mm]
$d_{L;o;TFP}$	outer diameter of the liner pipe when it is part of the Tight Fit Pipe	[mm]
d_n	equilibrium diameter in step n during the manufacturing process of Tight Fit Pipe	[mm]
d_o	outer diameter of the single walled pipe	[mm]
$d_{o;max}$	maximum outer diameter of the single walled pipe	[mm]
$d_{o;min}$	minimum outer diameter of the single walled pipe	[mm]
$d_{O;a;n}$	average diameter of the outer pipe in step n during the manufacturing process of Tight Fit Pipe	[mm]
$d_{O;i;n}$	inner diameter of the outer pipe in step n during the manufacturing process of Tight Fit Pipe	[mm]
$d_{O;o}$	outer diameter of the outer pipe when it is not part of the Tight Fit Pipe	[mm]
$d_{O;o;n}$	outer diameter of the outer pipe in step n during the manufacturing process of Tight Fit Pipe	[mm]
$d_{O;o;TFP}$	outer diameter of the outer pipe when it is part of the Tight Fit Pipe	[mm]
D_{reel}	reel diameter	[mm]
dM/dx	change in the bending moment M over the length dx	[N]
dr/dx	change in the orientation of the liner pipe	[-]
dx	small distance	[mm]

E_a	Young's modulus of the single walled pipe in the axial direction	[MPa]
E_L	liner pipe Young's modulus assumed identical in the hoop and axial directions	[MPa]
$E_{L;a}$	liner pipe Young's modulus in the axial direction	[MPa]
$E_{L;S}$	liner pipe secant modulus	[MPa]
$E_{L;T}$	liner pipe tangent modulus	[MPa]
$E_{L;T;n}$	liner pipe tangent modulus in situation n (1, 2, or 3)	[MPa]
E_O	outer pipe Young's modulus assumed identical in the hoop and axial directions	[MPa]
$E_{O;a}$	outer pipe Young's modulus in the axial direction	[MPa]
f	ovalisation of a pipeline	[%]
f_0	initial ovalisation of the single walled pipe	[%]
f_{AB}	ovalisation of the single walled pipe after unloading	[%]
f_e	elastic ovality (recovered during the pipe unloading)	[%]
$f_{H;average}$	average ovalisation measured by hand	[%]
f_{Hn}	ovalisation measured by hand at location n	[%]
f_{MBS}	ovalisation of the single walled pipe at maximum bending	[%]
$f_{OM;average;AB}$	average ovalisation determined by the ovalisation meters after bending (after unloading)	[%]
$f_{OM;average;MBS}$	average ovalisation determined by the ovalisation meters at maximum bending	[%]
$f_{OMn;AB}$	ovalisation determined by the ovalisation meter n after bending (after unloading)	[%]
$f_{OMn;MBS}$	ovalisation determined by the ovalisation meter n at maximum bending	[%]
$F_{FP;A}$	axial fixation point force	[N]
$F_{FP;A;max}$	axial fixation point force at $F_{HC;max}$	[N]
$F_{FP;P}$	lateral fixation point force	[N]
$F_{FP;P;max}$	lateral fixation point force at $F_{HC;max}$	[N]
F_{HC}	hydraulic cylinder force	[N]
$F_{HC;A}$	axial component of the hydraulic cylinder force	[N]
$F_{HC;max}$	maximum hydraulic cylinder force	[N]
$F_{HC;P}$	lateral component of the hydraulic cylinder force	[N]
$F_{HC;x}$	x-component of the hydraulic cylinder force	[N]
$F_{HC;x;max}$	maximum x-component of the hydraulic cylinder force	[N]
$F_{HC;y}$	y-component of the hydraulic cylinder force	[N]
$F_{HC;y;max}$	maximum y-component of the hydraulic cylinder force	[N]
$F_{L;cr}$	critical liner pipe buckling force in the axial compression tests	[N]
F_{LF}	lift force	[N]
$F_{LF;max}$	lift force at $F_{HC;max}$	[N]

$F_{L;push}$	force required to push the liner pipe out of the Tight Fit Pipe	[N]
$F_{O;cr}$	critical outer pipe buckling force in the axial compression tests	[N]
F_{reel}	reaction force of the reel on the pipe	[N]
$F_{reel;FP}$	reaction force of the reel on the pipe at the fixation point side of the reel	[N]
$F_{reel;HC;P}$	reaction force of the reel lateral on the pipe at the hydraulic cylinder side of the reel	[N]
$F_{reel;HC;y}$	reaction force of reel in y-direction on the pipe at the hydraulic cylinder side of the reel	[N]
$F_{reel;T;P}$	reaction force of the reel on the pipe during reeling in reality	[N]
$F_{T;A}$	axial force in the tensioners during reeling in reality	[N]
$F_{T;P}$	perpendicular force in the tensioners during reeling in reality	[N]
g	initial gap between the liner pipe and the outer pipe	[mm]
j	number of strain gauges used in the residual compressive stress test	[-]
k_L	liner pipe thermal conductivity	[W/mK]
k_O	outer pipe thermal conductivity	[W/mK]
k_R; k_δ	factors in the equation determining ovalisation of the single walled pipe under bending and a lateral force	[-]
l_i	influence length	[mm]
L	length of the pipe	[mm]
L_1	distance along the Tight Fit Pipe between the prebottom and the top of the liner pipe wrinkle	[mm]
L_2	distance along the Tight Fit Pipe between the top and the postbottom of the liner pipe wrinkle	[mm]
L_{axial}	distance along the Tight Fit Pipe between the start of the laser and a certain location	[mm]
$L_{axial;end;dr/dx}$	distance along the Tight Fit Pipe between the start of the laser and the end of the liner pipe wrinkle (length based on the *dr*/*dx* threshold)	[mm]
$L_{axial;post}$	distance along the Tight Fit Pipe between the start of the laser and the postbottom of the liner pipe wrinkle	[mm]
$L_{axial;pre}$	distance along the Tight Fit Pipe between the start of the laser and the prebottom of the liner pipe wrinkle	[mm]
$L_{axial;start;dr/dx}$	distance along the Tight Fit Pipe between the start of the laser and the start of the liner pipe wrinkle (length based on the *dr*/*dx* threshold)	[mm]
$L_{axial;top}$	distance along the Tight Fit Pipe between the start of the laser and the top of the liner pipe wrinkle	[mm]
$L_{contact}$	pipe length in contact with the reel	[mm]

L_{CM}	length of the curvature meter	[mm]
$L_{DM\text{-}axial}$	length between the pipe end and the displacement meter measuring the axial displacement of the pipe	[mm]
L_{EP}	length of the (single walled) elongation pipe in the Tight Fit Pipe test piece	[mm]
$L_{flange\text{-}ICP}$	distance between the flange of the test piece and the initial contact point	[mm]
$L_{flanges}$	thickness of the flanges of the test piece and the re-usable pipe together	[mm]
L_{FP}; $L_{FP;1}$; $L_{FP;2}$	distances in the bending rig	[mm]
$L_{HC\text{-}Hn}$	distance between the hydraulic cylinder connection to the re-usable pipe and the ovalisation hand measurement *n*	[mm]
$L_{HC\text{-}Km;legn}$	distance between the hydraulic cylinder connection to the re-usable pipe and the leg *n* (1, 2 or 3) of the curvature meter *m* (1 or 2)	[mm]
$L_{HC\text{-}OMn}$	distance between the hydraulic cylinder connection to the re-usable pipe and the ovalisation meter *n*	[mm]
$L_{HC\text{-}PMn}$	distance between the hydraulic cylinder connection to the re-usable pipe and the position meter *n*	[mm]
$L_{HC\text{-}SGn;m}$	distance between the hydraulic cylinder connection to the re-usable pipe and the cross-section of strain gauges *n* and *m*	[mm]
$L_{HC;x}$; $L_{HC;y}$	distances in the bending rig	[mm]
$L_{HC;y;1}$; $L_{HC;y;2}$	distances in the bending rig	[mm]
$L_{laser\ hole\text{-}ETR}$	distance between the start of the laser and the end of the test region in the Tight Fit Pipe	[mm]
$L_{laser\ hole\text{-}STR}$	distance between the start of the laser and the beginning of the test region in the Tight Fit Pipe	[mm]
$L_{laser\ hole\text{-}weld}$	distance between the start of the laser and the weld connecting the Tight Fit Pipe to the elongation pipe	[mm]
$L_{LFP\text{-}end}$	distance between the sheet of the lateral fixation point and the end of the test piece	[mm]
$L_{re\text{-}usable\ pipe}$	length of the pipe connecting the test piece to the hydraulic cylinder	[mm]
L_{sheet}	width of the sheet holding the pipe in the lateral fixation point	[mm]
L_{TFP}	length of the Tight Fit Pipe	[mm]
$L_{weld\ TFP}$	width of the weld connecting the Tight Fit Pipe to the Tight Fit Pipe in the test piece	[mm]
$L_{weld\ TFP\text{-}EP}$	width of the weld connecting the Tight Fit Pipe to the elongation pipe in the test piece	[mm]
L/m	half wave length of a local buckle in the single walled pipe	[mm]

L_L/m	half wave length of a local buckle in the liner pipe	[mm]
$L_L/m_{dr/dx}$	liner pipe wrinkle half wave length (*dr/dx* threshold)	[mm]
$L_L/m_{pre\text{-}post}$	distance between the prebottom and the postbottom surrounding the liner wrinkle top in the liner pipe	[mm]
L_O/m	half wave length of a local buckle in the outer pipe	[mm]
m	variable used in numbering (e.g. number of curvature meters etc.)	[-]
M	bending moment	[Nmm]
M_E	elastic bending moment capacity of the single walled pipe	[Nmm]
M_P	plastic bending moment capacity of the single walled pipe	[Nmm]
$M_{P;TEST\text{-}1}$	plastic bending moment capacity of the single walled pipe TEST-1	[Nmm]
$M_{P;TEST\text{-}2}$	plastic bending moment capacity of the single walled pipe TEST-2	[Nmm]
n	variable used in numbering (e.g. number of legs of a curvature meter etc.)	[-]
p	number of circumferential waves	[-]
$P_{i;max}$	maximum internal pressure during the manufacturing process of Tight Fit Pipe	[MPa]
$P_{i;n}$	internal pressure during the manufacturing process of Tight Fit Pipe in step *n*	[MPa]
q_{reel}	distributed load of the reel on the pipe	[N/m]
Q	heat flow through the liner pipe and the outer pipe	[W]
r_a	average radius of the single walled pipe	[mm]
$r_{L;a}$	average radius of the liner pipe when it is not part of the Tight Fit Pipe	[mm]
$r_{L;a;n}$	average radius of the liner pipe in step *n* during the manufacturing process of Tight Fit Pipe	[mm]
$r_{L;i;n}$	inner radius of the liner pipe in step *n* during the manufacturing process of Tight Fit Pipe	[mm]
$r_{L;i;TFP}$	inner radius of the liner pipe when it is part of the Tight Fit Pipe	[mm]
$r_{L;o;n}$	outer radius of the liner pipe in step *n* during the manufacturing process of Tight Fit Pipe	[mm]
$r_{L;o;TFP}$	outer radius of the liner pipe when it is part of the Tight Fit Pipe	[mm]
r_o	outer radius of the single walled pipe	[mm]
$r_{O;a;n}$	average radius of the outer pipe in step *n* during the manufacturing process of Tight Fit Pipe	[mm]
$r_{O;i;n}$	inner radius of the outer pipe in step *n* during the manufacturing process of Tight Fit Pipe	[mm]

$r_{O;i;TFP}$	inner radius of the outer pipe when it is part of the Tight Fit Pipe	[mm]
$r_{O;o;n}$	outer radius of the outer pipe in step *n* during the manufacturing process of Tight Fit Pipe	[mm]
$r_{O;o;TFP}$	outer radius of the outer pipe when it is part of the Tight Fit Pipe	[mm]
R	reaction (lateral) force on the pipe	[N]
R_{TFP}	bending radius of the Tight Fit Pipe	[mm]
$R_{TFP;Km}$	bending radius of the Tight Fit Pipe measured in the curvature meter *m* (1 or 2)	[mm]
R_y	plastic reaction capacity	[N]
t	wall thickness of the single walled pipe	[mm]
t_L	liner pipe wall thickness	[mm]
t_O	outer pipe wall thickness	[mm]
T_{CW}	temperature of the cooling water	[K]
T_{end}	temperature of the liner pipe and the outer pipe when removing the cooling water during the manufacturing process of Tight Fit Pipe	[K]
$T_{environment}$	environmental temperature	[K]
$T_{L;a;(PH/CH)}$	average temperature of the liner pipe while in contact with the outer pipe during the manufacturing process of Tight Fit Pipe (partial or complete liner pipe heating)	[K]
$T_{L;n}$	temperature of the liner pipe in step *n*	[K]
T_{L-O}	temperature at the liner pipe - outer pipe boundary	[K]
$T_{O;max}$	outer pipe maximum temperature	[K]
$T_{O;n}$	temperature of the outer pipe in step *n*	[K]
UA	thermal resistance of the combined liner pipe and outer pipe	[W/K]
V	shear force in the pipe	[N]
α	factor used in the equation determining ovalisation due to bending	[-]
α_{gw}	girth weld factor	[-]
α_h	maximum allowable yield to tensile strength ratio	[-]
α_L	liner pipe thermal expansion coefficient	[1/K]
α_O	outer pipe thermal expansion coefficient	[1/K]
β	angle between the pipe and the x-axis	[rad]
β_{max}	angle between the pipe and the x-axis at maximum bending	[rad]
γ	angle between the pipe and the hydraulic cylinder	[rad]
$\delta_{El;R}$	factor used in the equation determining ovalisation of a pipe under bending and a lateral force	[mm]

$\delta_{L;cr}$	critical buckling displacement of the liner pipe	[mm]
Δ	difference	[%]
$\Delta d_{L;a;n\text{-}m}$	change in the average liner pipe diameter from step *n* to *m* during the manufacturing process of Tight Fit Pipe	[mm]
$\Delta d_{L;o;n\text{-}m}$	change in the outer liner pipe diameter from step *n* to *m* during the manufacturing process of Tight Fit Pipe	[mm]
$\Delta d_{O;i;n\text{-}m}$	change in the inner outer pipe diameter from step *n* to *m* during the manufacturing process of Tight Fit Pipe	[mm]
$\Delta d_{O;o;TFP}$	change of the outer diameter of the outer pipe when the outer pipe is part of the Tight Fit Pipe	[mm]
$\Delta d_{O;o;TFP;hor}$	change of the outer pipe outer diameter in the horizontal plane when outer pipe is part of the Tight Fit Pipe	[mm]
$\Delta d_{O;o;TFP;ver}$	change of the outer pipe outer diameter in the vertical plane when outer pipe is part of the Tight Fit Pipe	[mm]
ΔL	measured displacement in the middle of the curvature meter relative to its ends	[mm]
$\Delta P_{i;n\text{-}m}$	change in the internal pressure from step *n* to *m* during the manufacturing process of Tight Fit Pipe	[MPa]
$\Delta r_{L;a;n\text{-}m}$	change in the average liner pipe radius from step *n* to *m* during the manufacturing process of Tight Fit Pipe	[mm]
$\Delta r_{L;i,TFP}$	change of the inner liner pipe radius when the liner pipe is part of the Tight Fit Pipe	[mm]
$\Delta r_{L;i,TFP;bottom}$	change of the inner liner pipe radius at the defined bottom of the liner pipe wrinkle when the liner pipe is part of the Tight Fit Pipe	[mm]
$\Delta r_{L;i,TFP;post}$	change of the inner liner pipe radius at the liner pipe wrinkle postbottom when liner pipe is part of the Tight Fit Pipe	[mm]
$\Delta r_{L;i,TFP;pre}$	change of the inner liner pipe radius at the liner pipe wrinkle prebottom when the liner pipe is part of the Tight Fit Pipe	[mm]
$\Delta r_{L;i,TFP;top}$	change of the inner liner pipe radius at the liner pipe wrinkle top when the liner pipe is part of the Tight Fit Pipe	[mm]
$\Delta r_{O;a;n\text{-}m}$	change in the average outer pipe radius from step *n* to *m* during the manufacturing process of Tight Fit Pipe	[mm]
Δs_{HC}	change in the hydraulic cylinder stroke	[mm]
$\Delta T_{L;a}$	change in the liner pipe temperature	[%]

$\Delta T_{L;n\text{-}m}$	change in the temperature of the liner pipe from step *n* to *m* during the manufacturing process of Tight Fit Pipe	[K]
$\Delta T_{O;n\text{-}m}$	change in the temperature of the outer pipe from step *n* to *m* during the manufacturing process of Tight Fit Pipe	[K]
Δx	displacement in x-direction of the hydraulic cylinder connection to the re-usable pipe	[mm]
Δx_{HC}	displacement of the hydraulic cylinder in x-direction	[mm]
Δx_{max}	maximum displacement in x-direction of the hydraulic cylinder connection to the re-usable pipe	[mm]
Δx_{res}	residual displacement in x-direction of the hydraulic cylinder connection to the re-usable pipe	[mm]
Δy	displacement in y-direction of the hydraulic cylinder connection to the re-usable pipe	[mm]
Δy_{max}	maximum displacement in y-direction of the hydraulic cylinder connection to the re-usable pipe	[mm]
Δy_{res}	residual displacement in y-direction of the hydraulic cylinder connection to the re-usable pipe	[mm]
$\Delta \varepsilon_{L;h;n\text{-}m}$	change in the liner pipe hoop strain from step *n* to *m* during the manufacturing process of Tight Fit Pipe	[-]
$\Delta \varepsilon_{O;h;n\text{-}m}$	change in the outer pipe hoop strain from step *n* to *m* during the manufacturing process of Tight Fit Pipe	[-]
$\Delta \sigma_{C;n\text{-}m}$	change in the radial contact stress between the liner pipe and the outer pipe from step *n* to *m* during the manufacturing process of Tight Fit Pipe	[MPa]
$\Delta \sigma_{L;h;n\text{-}m}$	change in the liner pipe hoop stress from step *n* to *m* during the manufacturing process of Tight Fit Pipe	[MPa]
$\Delta \sigma_{O;h;n\text{-}m}$	change in the outer pipe hoop stress from step *n* to *m* during the manufacturing process of Tight Fit Pipe	[MPa]
$\Delta \sigma_{res}$	change in the residual liner pipe hoop stress	[MPa]
ε_b	bending strain	[-]
$\varepsilon_{b;Km}$	bending strain determined by curvature meter *m* (1 or 2)	[-]
$\varepsilon_{b;SG;average}$	average bending strain measured by the strain gauges	[-]
$\varepsilon_{b;SGn}$	bending strain measured in the strain gauge *n*	[-]
ε_{cr}	critical buckling strain of the single walled pipe	[-]
$\varepsilon_{L;a}$	axial strain in the liner pipe	[-]
$\varepsilon_{L;cr}$	critical buckling strain of the liner pipe	[-]
$\varepsilon_{L;h}$	hoop strain in the liner pipe	[-]
$\varepsilon_{O;cr}$	critical buckling strain of outer pipe	[-]
$\varepsilon_{TFP;cr}$	critical buckling strain of integral Tight Fit Pipe	[-]

ζ	angle between the hydraulic cylinder and the y-axis	[rad]
ζ_{max}	angle between the hydraulic cylinder and the y-axis at maximum bending	[rad]
κ	curvature	[1/m]
λ	ratio of E_L to $E_{L;T}$	[-]
μ	friction coefficient between the liner pipe and the outer pipe in the Tight Fit Pipe	[-]
ν; ν_L; ν_O	Poisson ratio of the single walled pipe, of the liner pipe and of the outer pipe	[-]
ρ	factor used in the equation determining ovalisation due to bending	[-]
σ_C	radial contact stress between the liner pipe and the outer pipe in the Tight Fit Pipe	[MPa]
$\sigma_{L;a}$	axial stress in the liner pipe	[MPa]
$\sigma_{L;cr}$	critical buckling stress of the liner pipe	[MPa]
$\sigma_{L;h}$	hoop stress in the liner pipe	[MPa]
$\sigma_{L;h;n}$	hoop stress in the liner pipe in step *n*	[MPa]
$\sigma_{L;t;a}$	liner pipe axial maximum stress (in tension)	[MPa]
$\sigma_{L;t;h}$	liner pipe hoop maximum stress (in tension)	[MPa]
$\sigma_{L;y}$	liner pipe yield stress assumed identical in hoop and axial direction	[MPa]
$\sigma_{L;y;a}$	liner pipe axial yield stress (in tension)	[MPa]
$\sigma_{L;y;h}$	liner pipe hoop yield stress (in tension)	[MPa]
$\sigma_{O;h;n}$	hoop stress in the outer pipe in step *n*	[MPa]
$\sigma_{O;t;a}$	outer pipe axial maximum stress (in tension)	[MPa]
$\sigma_{O;t;h}$	outer pipe hoop maximum stress (in tension)	[MPa]
$\sigma_{O;y}$	outer pipe yield stress assumed identical in hoop and axial direction	[MPa]
$\sigma_{O;y;a}$	outer pipe axial yield stress (in tension)	[MPa]
$\sigma_{O;y;h}$	outer pipe hoop yield stress (in tension)	[MPa]
σ_{res}	residual liner pipe hoop stress	[MPa]
$\sigma_{t;a}$	single walled pipe axial maximum stress (in tension)	[MPa]
$\sigma_{t;h}$	single walled pipe hoop maximum stress (in tension)	[MPa]
σ_y	yield stress of the single walled pipe assumed identical in hoop and axial direction	[MPa]
$\sigma_{y;a}$	single walled pipe axial yield stress (in tension)	[MPa]
$\sigma_{y;h}$	single walled pipe hoop yield stress (in tension)	[MPa]
τ_C	axial friction between the liner pipe and the outer pipe in the Tight Fit Pipe	[MPa]
ψ	ratio of E_L to $E_{L;S}$	[-]
Ω_L; Ω_O	thermal resistance of the liner pipe and the outer pipe	[K/W]

1 Introduction

1.1 Summary of the Research Objective

The project as discussed in this PhD thesis concerns the installation of Tight Fit Pipe by means of the reeling installation method. The focus of the research is to investigate liner pipe wrinkling and ovalisation of Tight Fit Pipe during the spooling-on phase of the reeling process, both theoretically and experimentally; the latter by performing full scale bending tests.

1.2 Background Information

1.2.1 Market Development

The offshore oil and gas industry is increasingly being confronted with the technical challenges associated with the recovery of unprocessed fluids from deeper and more complex reservoirs in all parts of the world. This trend is expected only to increase in the future to meet the growing demand for oil and gas throughout the world. Furthermore, the solubility of corrosive gasses (CO_2 and H_2S dissolved in oil and gas) increases with pressure and the pressure increases with increasing reservoir depth. Since the oil and gas industry is already exploiting deeper reservoirs [54], particular attention is given to providing resistance to corrosion attack from the unprocessed fluids passing through the well tubing, the subsea flowlines and the processing facilities [49]. Note that in general a flowline is a pipeline that is used to transport unprocessed fluids from the subsea wells to the processing facilities whereas a pipeline is used to transport mainly processed fluids from the processing facilities to shore. Moreover, there is a trend in the offshore industry to minimise the number of processing facilities offshore in the development of subsea oil and gas fields wherever possible for the purpose of cost reduction [35].

As a consequence of these phenomena, a larger volume of untreated products, which can be corrosive because of the presence of water, CO_2 and/or H_2S, needs to be transported over longer distances from the subsea wells to the processing facilities. Material selection for these pipelines is influenced by the corrosivity of these products.

In many cases, the corrosivity is minimal in which case carbon steel can be applied, using corrosion inhibitors in the fluid. However, if the corrosive action is more severe, corrosion resistant alloys have to be selected (Appendix I). In such cases, double walled pipe combining a corrosion resistant alloy liner pipe with a carbon steel outer pipe, can be an attractive option. Recent market studies have shown that demand for these double walled pipes is growing because of today's strong focus on reducing maintenance cost and a more serious interest in life cycle approach for material selection [10].

There are various types of double walled pipe which can be divided into two main categories, namely the metallurgically bonded double walled pipes called "clad pipes" and the mechanically bonded double walled pipes called "lined pipes" (Appendix I). Lined pipe behaves differently than clad pipes under some loading conditions because the liner pipe is only mechanically bonded to the outer pipe. However, lined pipe requires no heat treatment after bonding, it is available in any desired combination of the inner and the outer pipe and lined pipe is less expensive in its purchase than clad pipe [35].

A promising type of lined pipe is the concept of Tight Fit Pipe. Tight Fit Pipe is a mechanically bonded double walled pipe where a corrosion resistant alloy liner pipe is mechanically fitted inside a carbon steel outer pipe through a thermo-hydraulic manufacturing process. This type of lined pipe is manufactured by Kuroki T&P Co., Ltd. in Japan. More information on different types of corrosion in offshore pipelines and measures that can be taken against corrosion can be found in Appendix I.

As far as pipe-laying is concerned, there is a strong focus nowadays (economical reasons) on so-called reeling as a method of pipe laying, particularly for offshore installation. Reeling is an installation method of pipelines where the pipe elements are welded together onshore and subsequently the pipeline is spooled on a reel, which is positioned on a vessel. The vessel then sails to the offshore location, where the pipeline is unwound, straightened and lowered to the seabed. Until now this method has only been applied for carbon steel pipelines [5] and clad pipe [53]. However, it is equally attractive for the installation of lined pipe.

If it would be possible to install Tight Fit Pipe by means of reeling, it would be an attractive new option for offshore fields containing corrosive oil and gas. Reeling of Tight Fit Pipe is not yet proven technology, however. The reeling process imposes high plastic strains (due to bending) on the pipe, which may cause unacceptable liner pipe wrinkling and pipe ovalisation. It is expected that the relatively high mechanical bonding strength available in the Tight Fit Pipe due to the thermo-hydraulic manufacturing process may result in a good resistance against bending during the reeling installation process. This adds to the motivation of investigating the possibility of installing Tight Fit Pipe by means of reeling.

1.2.2 Reeling

Reeling is a pipeline installation method that provides a rapid and efficient means of laying offshore pipelines, presently up to a maximum pipe diameter of 18 inch [5], [28]. The pipeline length that can be carried on a reel depends on the diameter and wall thickness of the pipe and the capacity of the reel (e.g. the capacity of one reel on the reeling vessel “Deep Blue” is 2750 tonnes [59]). For example, assuming no insulation coating and a diameter to thickness ratio of 17, the length of a single walled pipeline on one reel of the reeling vessel Deep Blue can vary between approximately 190 km for a 4 inch pipeline to 10 km for an 18 inch pipeline. The laying speed of reeling is considerably higher than of conventional pipe laying (S-lay and J-lay). The time required to return to a spool base for collecting more pipeline needs to be considered, however. A spool base is an onshore yard where the pipe elements are welded to a pipeline, which is subsequently spooled on a reel that is positioned on the vessel.

A characteristic of the reeling process is that it imposes high plastic strains (due to bending) in the pipeline. This results in residual stresses when the pipeline is straightened during installation. The initial and reverse bending will cause ovality of the pipeline. The degree of ovalisation during reeling should be limited as it affects the resistance of the pipe to both collapse and local buckling [23].

During the reeling process, the pipeline will undergo three different stages [45]. The first stage involves winding the pipeline (which is pre-manufactured onshore) on the reel, which is located on the vessel. Attaching the end of the pipeline to the spool, applying a holdback tension to the pipe and slowly rotating the drum achieves the winding. The pipeline is plastically deformed until it conforms to the curvature of the reel. Strains are such that the pipeline yields over most of its cross section.

The second stage in the reeling installation process involves the reeling-off process. In the beginning, the pipeline is pulled off the reel by tensioners so that it can be passed through a straightener. After a while the tension required for reeling-off is provided by the lay tension of the suspended pipeline due to its self weight and is being controlled by tensioners. The lay tension causes both an axial load and a moment as it pulls the pipeline towards the straightener.

When unreeling, the pipeline has a residual curvature depending on its properties and the diameter of the reel. Each layer of pipeline wound on the reel has a different curvature (the inner layers have a higher curvature than the outer layers). The function of the aligner (Figure 1.1) is to ensure the same curvature of the pipeline before it enters the straightener; it bends the pipeline coming from the reel to a fixed curvature, irrespective of the layer on the drum from which it has been reeled. As a result, the straightener can be set at one configuration during the whole installation process. Research has been performed to eliminate the aligner from the reeling process proposing a straightener which applies the appropriate, reverse curvature for each layer of pipe [14]. However, up till now the industry prefers the robust system of aligning the pipeline before straightening it.

It is the curvature applied to the pipeline in the aligner which is removed by the straightening process, the third stage of the reeling process. Straightening implies applying reverse bending, so that the pipeline leaves the vessel as a straight pipe. Figure 1.1 shows the reeling equipment.

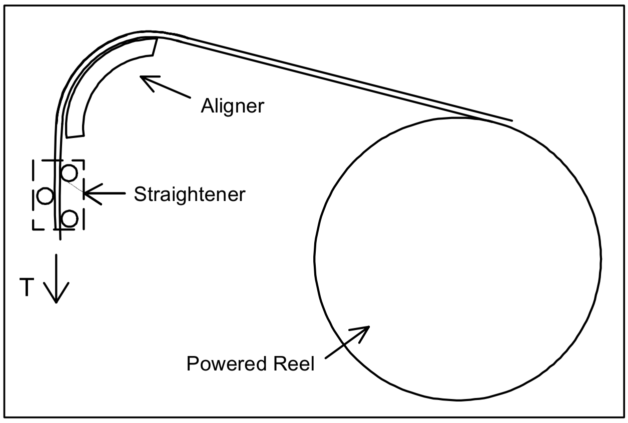

Figure 1.1 Schematic representation of the equipment used for reeling

1.2.3 Tight Fit Pipe

Tight Fit Pipe is a double walled pipe where a corrosion resistant alloy liner pipe is mechanically fitted inside a carbon steel outer pipe through a thermo-hydraulic manufacturing process (Figure 1.2). The outer pipe is heated to a certain temperature which does not deteriorate the mechanical properties of the outer pipe. Subsequently, a corrosion resistant alloy liner pipe is inserted into the heated outer pipe, while the liner pipe temperature is kept low using cooling water. Just after insertion, the water pressure in the liner pipe is increased and the liner pipe is expanded first elastically and then plastically. Further increase of the water pressure causes the outer pipe to expand elastically together with the plastically expanding liner pipe. Then, the water pressure is decreased, causing both the outer pipe and the liner pipe to shrink elastically. Subsequently the liner pipe and the outer pipe are cooled in the atmosphere. Due to the remaining deformations in the liner pipe, the outer pipe grips around the liner pipe at the end of the manufacturing process [10], [32], [33], [35], [50].

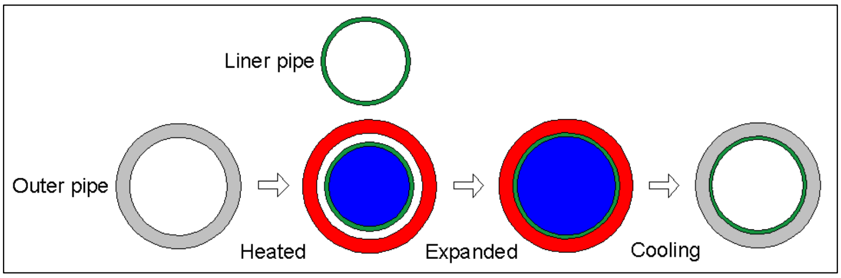

Figure 1.2 Schematic representation of the Tight Fit Pipe manufacturing process

At the end of the manufacturing process there is a residual compressive hoop stress present in the liner pipe and a residual tensile hoop stress in the outer pipe (Figure 1.3), due to the difference in temperature and the subsequent difference in shrinkage [18]. The resulting radial contact stress between the liner pipe and the outer pipe provides the mechanical bonding strength between the liner pipe and the outer pipe in the Tight Fit Pipe.

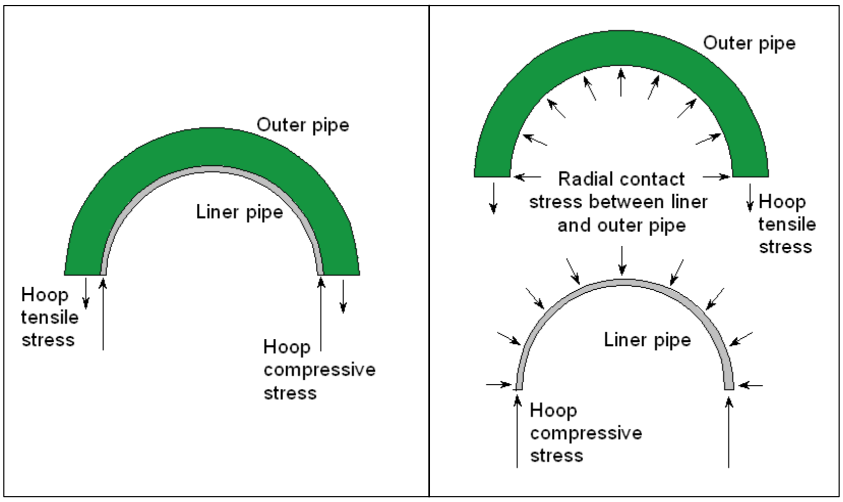

Figure 1.3 The hoop tensile stress in the outer pipe is in equilibrium with the hoop compression stress in the liner (left); the radial contact stress causes the mechanical bonding strength between the liner pipe and the outer pipe in the Tight Fit Pipe (right)

1.2.4 Tight Fit Pipe used in the Research

Several Tight Fit Pipes in two different size categories were available for tests executed in the project (Table 1.1).

The first category of Tight Fit Pipe consisted of one 12 m long (L_{TFP}) 10.75 inch outer diameter Tight Fit Pipe ($d_{O;o;TFP}$) with a 2.45 mm thick (t_L), 304L liner pipe (with a longitudinal weld) and a 9.3 mm thick (t_O), X65, seamless outer pipe. The outer diameter of this Tight Fit Pipe was 273.05 mm (10.75 inch) and the inner diameter of this Tight Fit pipe was 249.55 mm (273.05 mm – 2 · 9.3 mm – 2 · 2.45 mm = 249.55 mm). The 10.75 inch Tight Fit Pipe was provided in the beginning of the research and was used for preliminary testing in order to become acquainted with the product Tight Fit Pipe.

The second category of Tight Fit Pipe consisted of three 12 m long (L_{TFP}), 12.75 inch outer diameter Tight Fit Pipes ($d_{O;o;TFP}$), each with a 3.0 mm thick (t_L), 316L liner pipe (with a longitudinal weld) and a 14.3 mm thick (t_O), X65, electric resistance welded outer pipe [64], [65]. The outer diameters of these Tight Fit Pipes were 323.85 mm (12.75 inch) and the inner diameters of these Tight Fit Pipes were 289.25 mm (323.85 mm – 2 · 14.3 mm – 2 · 3.0 mm = 289.25 mm). Each of these three 12.75 inch Tight Fit Pipes had a different residual liner pipe hoop stress, i.e. a different mechanical bonding strength between the liner pipe and the outer pipe in the Tight Fit Pipe. These three 12.75 inch Tight Fit Pipes were used in the full scale bending testing programme.

Table 1.1 Size categories of Tight Fit Pipe used in the research

$d_{O;o;TFP}$	t_L [mm]	t_O [mm]	L_{TFP} [m]	LP Material	OP Material	OP Type
10.75	2.45	9.3	12	304L	X65	seamless
12.75	3.0	14.3	3 x 12	316L	X65	ERW

Note:
LP: Liner pipe
OP: Outer pipe
ERW: Electric resistance welded [64], [65]

1.3 Objective of the Study

The research addresses the challenges associated with the development of putting the installation of Tight Fit Pipe into practice by means of the reeling installation method. Before realisation of installing Tight Fit Pipe by means of reeling, more knowledge is required about the limit states of the Tight Fit Pipe during (1) the reeling process on board of the vessel, (2) the transfer from the reeling vessel to the seabed and (3) the operational phase.

1. During the reeling phase of the Tight Fit Pipe the most likely limit states are expected to be:
    a. liner pipe wrinkling above acceptable limits on the compression side of the bent pipe.
    b. Tight Fit Pipe ovalisation above acceptable limits hindering use or reducing external water pressure resistance.
    c. crack initiation in the Tight Fit Pipe circumferential weld due to bending.

2. During the transfer of the Tight Fit Pipe to the seabed, the most likely limit states are expected to be:
   a. collapse of the Tight Fit Pipe due to external water pressure.
   b. collapse of the Tight Fit Pipe due to external water pressure in combination with bending (e.g. in the sagbend).
   c. crack initiation in the Tight Fit Pipe circumferential weld due to bending in the sagbend and/or fatigue.

3. During the operational phase of the Tight Fit Pipe, the most likely limit states are expected to be:
   a. crack initiation in the circumferential weld of the Tight Fit Pipe due to fatigue.
   b. liner pipe wrinkling above acceptable limits due to compressive stresses (e.g. due to heating of a constrained pipe).
   c. crack initiation at the liner pipe wrinkles.

The objective of this research was to investigate the influence of reeling (i.e. bending) on liner pipe wrinkling and ovalisation of the Tight Fit Pipe (limit states 1a and 1b above). In order to investigate this, full scale bending tests on Tight Fit Pipe were performed in this research. In these tests the initiation and the degree of liner pipe wrinkling as well as the degree of ovalisation of the Tight Fit Pipe occurring during the spooling-on phase of the reeling process were determined. This phase of the reeling process is most critical with respect to liner pipe wrinkling, because during this phase the Tight Fit Pipe experiences maximum bending.

Moreover, in these tests the influence on liner pipe wrinkling during bending was determined for (1) the mechanical bonding strength between the liner pipe and the outer pipe in the Tight Fit Pipe, (2) the presence of the electric resistance welded longitudinal outer pipe weld and (3) the presence of the Tight Fit Pipe circumferential weld (connecting the Tight Fit Pipe elements).

The research question therefore is: “what is the degree of liner pipe wrinkling and ovalisation of the Tight Fit Pipe during the spooling-on phase of the reeling process, determined both theoretically and experimentally; the latter by performing full scale bending tests?”

1.4 Study Approach

This thesis study and its reporting are structured as follows: Chapter 1 comprises the introduction explaining the objective, the research question and the motivation of the research. Also definitions of reeling and Tight Fit Pipe are provided in this chapter.

In order to obtain more knowledge about the mechanical bonding strength between the liner pipe and the outer pipe in the Tight Fit Pipe at the end of the manufacturing process, a computer model of the manufacturing process of Tight Fit Pipe was developed. In this model the mechanical bonding strength can be determined as a result of input parameters such as the heat and the internal pressure applied during the manufacturing process. The mechanical bonding strength was expected to be of influence on liner pipe wrinkling (Chapter 2).

In Chapter 3 the material and the geometric properties of the single walled pipes and the Tight Fit Pipes used in this research are discussed as well as the mechanical bonding strengths of these Tight Fit Pipes. This data was needed to be able to compare experimental results with theoretical predictions for the tests as executed.

Buckling of pipelines subjected to bending (applied to the Tight Fit Pipe during reeling) correlates in a number of respects to buckling of axially compressed pipelines. Axial compression tests on short Tight Fit Pipe test pieces are relatively easy to perform compared to bending tests. Moreover, an axial compression machine was readily available while the full scale bending rig still had to be built. Therefore, in order to gain a better understanding of the local buckling behaviour of Tight Fit Pipe, several axial compression tests were performed on the available 10.75 and 12.75 inch outer diameter Tight Fit Pipes (Chapter 4).

In order to obtain a better understanding of reeling in practice and reeling simulation by bending tests, small scale bending tests were performed on 22 mm outer diameter single walled pipes (Chapter 5). Results from these tests contributed to the design and construction of a full scale bending rig for executing bending tests on Tight Fit Pipe.

One bending test was executed on a 12.75 inch outer diameter single walled test piece to verify the suitability of the full scale bending rig for the purpose of the full scale bending tests on 12.75 inch outer diameter Tight Fit Pipe (Chapter 6). The test piece consisted of two 12.75 inch single walled pipes connected by a weld.

Seven reeling simulation tests were subsequently executed on 12.75 inch Tight Fit Pipe (Chapter 7) in order to investigate the initiation and the degree of liner pipe wrinkling as well as the degree of ovalisation of the Tight Fit Pipe as a function of the reel diameter. Other objectives were to determine the influence on liner pipe wrinkling of (1) the mechanical bonding strength between the liner pipe and the outer pipe in the Tight Fit Pipe, (2) the electric resistance welded longitudinal outer pipe weld and (3) the presence of the Tight Fit Pipe circumferential weld.

2 Manufacturing Process of Tight Fit Pipe

2.1 Introduction

In this chapter the Tight Fit Pipe manufacturing process is addressed in order to obtain a better understanding of the mechanical bonding strength between the liner pipe and the outer pipe in the Tight Fit Pipe at the end of the manufacturing process. The mechanical bonding strength can be quantified by quantifying the residual liner pipe hoop stress (Figure 1.3). An increase in the mechanical bonding strength between the liner pipe and the outer pipe indicates an increase in the radial contact stress between the liner pipe and the outer pipe and an increase in the residual liner pipe hoop stress (Figure 1.3).

The mechanical bonding strength was expected to be of influence on the liner pipe wrinkling behaviour during bending. Therefore, the manufacturing process of Tight Fit Pipe was simulated in various computer models. These computer models allow for variation of parameters in such a way that theoretically an optimum mechanical bonding strength can be obtained which results in minimal liner pipe wrinkling during reeling. For example, by decreasing the amount of heating up of the liner pipe during the manufacturing process in the computer model, a higher mechanical bonding strength can be obtained, which may reduce liner pipe wrinkling during reeling.

A two dimensional analytical model and a three dimensional, one layer thick, finite element model have been developed to simulate the manufacturing process of Tight Fit Pipe. The analytical model is a simple model, easy to use and therefore very suitable for a quick assessment of the influence of a certain parameter on the mechanical bonding strength between the liner pipe and the outer pipe in the Tight Fit Pipe. The three dimensional, one layer thick, finite element model is a more advanced model in that it does not disregard the change in the liner pipe and the outer pipe wall thicknesses throughout the manufacturing process and a better representation of the material characteristics is possible. It has been used for the verification of the analytical model.

During the manufacturing process of the Tight Fit Pipe, the cooled liner pipe comes in contact with the heated outer pipe. The increased temperature of the liner pipe as a result of contact with the hot outer pipe showed to be an important parameter influencing the mechanical bonding strength at the end of the manufacturing process. Therefore, this parameter is discussed in Subsection 2.2. In Subsection 2.3, the analytical model and the finite element model are described. In Subsection 2.4, results from these models are compared with Kuroki T&P factory results. In Subsection 2.5 a sensitivity analysis is presented, in which the analytical model is used to determine which parameters are most influential on the mechanical bonding strength.

2.2 Liner Pipe Temperature during the Manufacturing Process of Tight Fit Pipe

For six Tight Fit Pipes, the mechanical bonding strength between the liner pipe and the outer pipe measured in the Kuroki T&P factory (using the residual compressive stress test described in Subsection 3.4.2) was compared to predictions made in the two dimensional analytical model and in the three dimensional, one layer thick, finite element model. Both models are described hereafter.

As pointed out, the temperature increase of the cooled liner pipe as a result of contact with the hot outer pipe during the manufacturing process of Tight Fit Pipe appeared to be an important parameter influencing the mechanical bonding strength [18]. In order to determine the influence of this liner pipe temperature increase, this increase in the liner pipe temperature needed to be determined first. For each of the six Tight Fit Pipes the average temperature of the liner pipe due to contact with the outer pipe ($T_{L;a;PH}$) was determined using equations stated in Appendix II [34]. Several assumptions were made:

1. The outer boundary temperature of the outer pipe equalled the oven temperature and the inner boundary temperature of the liner pipe equalled the cooling water temperature.
2. All heat transfer between the liner pipe and the outer pipe was assumed to be obtained by conduction; heat transfer by radiation between the liner pipe and the outer pipe was neglected. It is understood that the amount of conductivity is determined by the contact surface between the liner pipe and the outer pipe.
3. Heating of the cooling water was ignored.
4. The dimensions of the liner pipe and the outer pipe were based on dimensions at the end of the manufacturing process.
5. Although the contact time between the liner pipe and the outer pipe does influence the amount of heating of the liner pipe, this was not taken into account for reasons of simplification. A steady state model of heating the liner pipe due to contact with the hot outer pipe was developed.

The liner pipe, while in contact with the outer pipe, was assumed either to heat up to this average temperature $T_{L;a;PH}$ (partial heating) or to heat up to the same temperature as the outer pipe (complete heating; $T_{L;a;CH} = T_{O;max}$) in the two dimensional analytical model and in the three dimensional, one layer thick, finite element model (Table 2.1). By using the models with these two different liner pipe temperatures, the influence of the liner pipe temperature on the residual liner pipe hoop stress, i.e. on the mechanical bonding strength between the liner pipe and the outer pipe in the Tight Fit Pipe, was investigated. No measurements of the liner pipe temperature during the manufacturing process have been performed.

Table 2.1 Calculated average liner pipe temperatures resulting from contact with the hot outer pipe for six Tight Fit Pipe test cases

	1	2	3	4	5	6
$T_{L;a;CH} = T_{O;max}$ [K]	638	655	650	655	580	680
$T_{L;a;PH}$ [K]	352	355	375	374	366	388

2.3 Analytical and Finite Element Models of the Manufacturing Process of Tight Fit Pipe

2.3.1 Analytical Model of the Tight Fit Pipe Manufacturing Process

In this subsection the two dimensional analytical model is described that was developed to obtain a better understanding of the mechanical bonding strength between the liner pipe and the outer pipe at the end of the manufacturing process of Tight Fit Pipe. The mechanical bonding strength between the liner pipe and the outer pipe in the Tight Fit Pipe was expected to be of influence on the liner pipe wrinkling behaviour during reeling (i.e. bending). The mechanical bonding strength can be quantified by quantifying the residual liner pipe hoop stress (Figure 1.3).

In the two dimensional analytical model the manufacturing process of Tight Fit Pipe is represented by mathematical equations. The liner pipe and the outer pipe characteristics (e.g. the liner pipe and the outer pipe diameter) as well as the manufacturing process parameters (e.g. the heating temperature of the outer pipe) are used as input. The residual liner pipe hoop stress, i.e. the mechanical bonding strength between the liner pipe and the outer pipe, is the output of the analytical model. The two dimensional analytical model is easy in use and therefore suitable for a quick assessment of the influence of a certain parameter on the mechanical bonding strength between the liner pipe and the outer pipe at the end of the manufacturing process of Tight Fit Pipe. In order to keep the model simple and easy to use, the following assumptions have been made:

1. The residual liner pipe hoop stress calculated by the two dimensional, cross-sectional, analytical model was assumed to represent the residual liner pipe hoop stress in an actual Tight Fit Pipe, which is a three dimensional object. In the three dimensional Tight Fit Pipe the radial contact stress between the liner pipe and the outer pipe (Figure 1.3) indicates an axial friction between the liner pipe and the outer pipe along the Tight Fit Pipe length. If the radial contact stress increases, the axial friction increases as well: more force is needed to overcome this axial friction and push the liner pipe out of the outer pipe in the Tight Fit Pipe. In the two dimensional model there is no length available for this axial friction. When the two dimensional, cross-sectional model of Tight Fit Pipe is altered into a three dimensional model of the Tight Fit Pipe, sufficient length of Tight Fit Pipe needs to

be available in the three dimensional model for the axial friction between the liner pipe and the outer pipe to develop (Figure 2.1). The axial friction between the liner pipe and the outer pipe compresses the liner pipe in axial direction introducing an axial compressive strain. This axial compressive strain contributes to the residual liner pipe hoop stress. The residual liner pipe hoop stress calculated in the two dimensional analytical model therefore underestimates the residual liner pipe hoop stress present in an actual Tight Fit Pipe. The relation between the axial strain, the hoop strain, the axial stress and the hoop stress in the liner pipe of the Tight Fit Pipe is explained in Equations (3.1) and (3.2).

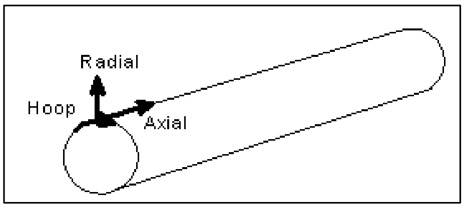

Figure 2.1 Definition of the axial, hoop and radial direction in the Tight Fit Pipe

2. During the manufacturing process it was assumed that the liner pipe was either heated to $T_{L;a;PH}$ (partial heating) or that it was heated to the same temperature of the outer pipe ($T_{L;a;CH}$ = $T_{O;max}$; complete heating).
3. The temperature of the outer pipe was assumed to be equal to the (measured) oven temperature (e.g. 673 K (400 °C)). Cooling down of the outer pipe due to contact with the cooled liner pipe was neglected. This assumption was based on the fact that the oven functions throughout the manufacturing process. The hydraulic cooling and expansion plug (Figure 2.2) inserted into the liner pipe throughout the manufacturing process, was however not designed to cool the liner pipe while expanding it. The cooling and expansion plug can either expand the liner pipe or cool it, but cannot do both at the same time.

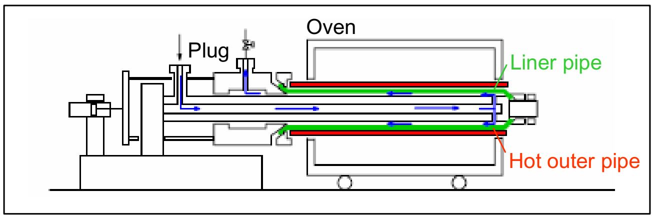

Figure 2.2 The manufacturing process of Tight Fit Pipe: the outer pipe, heated in the oven, is positioned over the liner pipe, which is cooled by water, inserted through the plug

4. The environmental temperature ($T_{environment}$) was assumed 298 K (25 °C).

5. In the last stage of the manufacturing process of Tight Fit Pipe (Figure 1.2), the Tight Fit Pipe was cooled down from the oven temperature T_{oven} (e.g. 673 K) to the environmental temperature $T_{environment}$ (298 K). T_{end}, the temperature at which active water cooling of the liner pipe (Figure 2.2) was stopped, was assumed to be 343 K (70 °C). So, the Tight Fit Pipe cooled down from T_{oven} to T_{end} by pumping water through the plug cooling the liner pipe. The Tight Fit Pipe cooled down from T_{end} to $T_{environment}$ without cooling the liner pipe.
6. The liner pipe and the outer pipe wall thicknesses were assumed not to change during the manufacturing process in order to reduce the complexity of the model.
7. Perfect elastic plastic liner pipe material behaviour was assumed in order to reduce the complexity of the model.
8. The decrease of the outer pipe yield stress and Young's modules ($\sigma_{O;y}$ and E_O) and the increase of the outer pipe thermal expansion coefficient (α_O), due to heating in the oven during the manufacturing process of Tight Fit Pipe (Figure 2.2), were not taken into account. The decrease of the liner pipe yield stress and Young's modules ($\sigma_{L;y}$ and E_L) and the increase of the liner pipe thermal expansion coefficient (α_L), due to the increase of the liner pipe temperature as a result of contact with the heated outer pipe during the manufacturing process of Tight Fit Pipe (Subsection 2.2), were also not taken into account.
9. Reduction of the liner pipe yield stress due to the Bauschinger effect (the softening which the material exhibits upon reverse loading) was neglected.

The influence of the assumptions 2, 6, 7 and 8 on the residual liner pipe hoop stress (the outcome of the analytical model) is investigated in Subsections 2.4 and 2.5. In Table 2.2 the ten steps as simulated in the analytical model can be seen.

Table 2.2 Steps in the analytical model of the manufacturing process of Tight Fit Pipe

Step	Description
1	Start of the manufacturing process
2	Cooling down of the liner pipe from $T_{environment}$ to T_{CW}
3	Heating up of the outer pipe from $T_{environment}$ to $T_{O;max}$
4	Elastic expansion of the liner pipe to the yield stress
5	Elastic plastic expansion of the liner pipe until it touches the outer pipe
6	Increase of the internal pressure to maximum ($P_{i;max}$)
7a, 7b	Partial ($T_{L;a;PH}$) or complete ($T_{L;a;CH}$) heating of the liner pipe due to contact with the hot outer pipe
8a, 8b, 8c	Reduction of the internal pressure from $P_{i;max}$ to atmospheric level
9a, 9b	Cooling down of the liner pipe and the outer pipe to T_{end} while actively cooling the liner pipe using the plug (Figure 2.2)
10a, 10b	Cooling down of the liner pipe and the outer pipe without cooling of the liner pipe from T_{end} to $T_{environment}$

The ten steps as simulated in the analytical model are described below. The analytical model and the related equations can be found in Appendix II [15], [18].

In step 1 the dimensions of the liner pipe and the outer pipe are stated. The hoop stress in the liner pipe and the outer pipe in step 1 are zero. In step 2 the liner pipe is cooled down by the hydraulic cooling and expansion plug (Figure 2.2) from the environmental temperature ($T_{environment}$) to the temperature of the cooling water (T_{CW}). In step 3 the outer pipe is heated from the environmental temperature ($T_{environment}$) to the oven temperature ($T_{O;max}$).

In step 4 the internal pressure causes the liner pipe to reach the yield stress. In step 5 the liner pipe is expanded by the internal pressure until it touches the outer pipe. An increase in the diameter, caused by the internal pressure combined with a constant yield stress (perfect elastic plastic material behaviour) actually reduces the internal pressure. This phenomenon is simplified by assuming that no increase in the internal pressure is needed to increase the size of the liner pipe after the yield stress has been reached. The influence of this simplification is small and can be neglected, however. At the end of step 6 the maximum internal pressure ($P_{i;max}$) is present in the hydraulic cooling and expansion machine. This results in a tensile hoop stress in the liner pipe and in the outer pipe at the end of step 6.

In step 7 the liner pipe is heated due to contact with the hot outer pipe. It is assumed that the liner pipe is either heated to $T_{L;a;PH}$ (partial heating) or that it is heated to the same temperature of the outer pipe ($T_{L;a;CH} = T_{O;max}$; complete heating). No measurements of the liner pipe temperature during the manufacturing process have been performed.

Firstly in step 7a, the expansion of the liner pipe due to heating as a result of contact with the hot outer pipe is calculated, while the expansion of the liner pipe is not restricted by the outer pipe. Secondly, in step 7b, the unrestrictedly expanded, heated liner pipe is fitted “back” in the outer pipe. An equilibrium diameter establishes itself in between the inner diameter of the outer pipe in step 7a and the outer diameter of the unrestrictedly expanded, heated up, liner pipe in step 7a.

As mentioned, at the end of step 6, a tensile hoop stress is present in both the liner pipe and the outer pipe. As a result of heating of the liner pipe while restricted in expansion by the outer pipe in step 7, the hoop stress in the liner pipe reduces and can even become a compressive hoop stress. The outer pipe experiences an increase of the tensile hoop stress. This change in the tensile hoop stress in the outer pipe from step 6 to 7 needs to be added to the tensile hoop stress in the outer pipe in step 6. The change in hoop stress in the liner pipe from tensile in step 6 (positive value) to compression in step 7 (negative value) needs to be accounted for. It is possible that the liner pipe heats up so much in step 7 that the hoop stress in the liner pipe changes from tensile yield to compressive yield.

In step 8, the internal pressure is reduced to atmospheric level while the liner pipe is still heated due to contact with the outer pipe. In order to calculate the dimensions and the hoop stresses of the liner pipe and the outer pipe at the end of step 8, firstly in step 8a, dimensions and stresses of the liner pipe and the outer pipe are calculated for the situation where the internal pressure is assumed to be reduced to atmospheric level and the liner pipe is assumed not to be heated due to contact with the outer pipe. Secondly in step 8b, the expansion of the liner pipe as a result of contact with the hot outer pipe is calculated, assuming the expansion of the liner pipe is not restricted by the outer pipe (the internal pressure is at atmospheric level which does not cause the liner to expand further). Thirdly in step 8c, the unrestrictedly expanded, heated liner pipe is fitted "back" in the outer pipe while the internal pressure is still at atmospheric level. Calculations in step 8b and 8c are identical to the calculations in step 7a and step 7b.

In step 9 the outer pipe is cooled down to temperature T_{end} (343 K (70 °C)), the temperature at which active cooling of the liner pipe by the plug (Figure 2.2) is stopped. Because active cooling of the liner pipe is stopped at temperature T_{end}, the liner pipe then obtains the same temperature T_{end} as the outer pipe. It is therefore assumed that the liner pipe and the outer pipe both cool down in step 9 to T_{end}. In order to calculate the dimensions and hoop stresses of the liner pipe and the outer pipe at the end of step 9, step 9 comprises two steps. Firstly in step 9a, the liner pipe and the outer pipe are assumed to cool down independently from each other and due to their difference in temperature and material characteristics, they decrease to different dimensions. Secondly in step 9b, the liner pipe is fitted "back" in the outer pipe, thereby calculating an equilibrium diameter and the related stresses as has been described in step 7.

If the liner pipe heats up significantly during the manufacturing process, the decrease in diameter of the liner pipe during the cooling down phase may be more than the decrease in diameter of the outer pipe from step 8 to 9. The fact that the thermal expansion coefficient of the liner pipe is larger than the thermal expansion coefficient of the outer pipe for the test cases considered in this research (the test cases are explained in Subsection 2.4.2), attributes to this phenomenon. The liner pipe is then assumed to expand into the outer pipe resulting in a decrease in the compressive liner pipe hoop stress from step 8 to 9. If the liner pipe heats up only a small amount during the manufacturing process, the liner pipe may decrease less in diameter than the outer pipe from step 8 to 9, depending on the temperature difference and the thermal expansion coefficient difference between the liner pipe and the outer pipe. The liner pipe is then compressed into the outer pipe resulting in an increase in the compressive liner pipe hoop stress from step 8 to 9. However, if the liner pipe yields in compression during step 8, it cannot absorb an increase in the compressive hoop stress and the liner pipe continues to yield in compression during step 9.

In step 10 the liner pipe and the outer pipe cool down from T_{end} to the environmental temperature ($T_{environment}$). Firstly in step 10a the liner pipe and the outer pipe are assumed to cool down to the environmental temperature independently from each other.

Secondly in step 10b, the liner pipe is assumed to be fitted “back” in the outer pipe. Calculations are identical to the calculations in step 7a and step 7b. It is checked at every step whether the hoop stress in the outer pipe does not exceed the outer pipe yield stress in order to verify the outer pipe elastic behaviour.

2.3.2 Finite Element Model of the Tight Fit Pipe Manufacturing Process

The manufacturing process of Tight Fit Pipe was simulated in a three dimensional, one layer thick, finite element model: a thermal mechanical three dimensional solid element (class hex20) was used based on the requirement of accuracy in combination with contact of both pipes during the manufacturing process [31].

Due to the axi-symmetric properties of the pipe, only a small part of the circumference of the pipe needed to be simulated in the finite element model. Arbitrarily, 1/72 of the circumference of the liner pipe and the outer pipe was modelled in the three dimensional, one layer thick, finite element model (Figure 2.3).

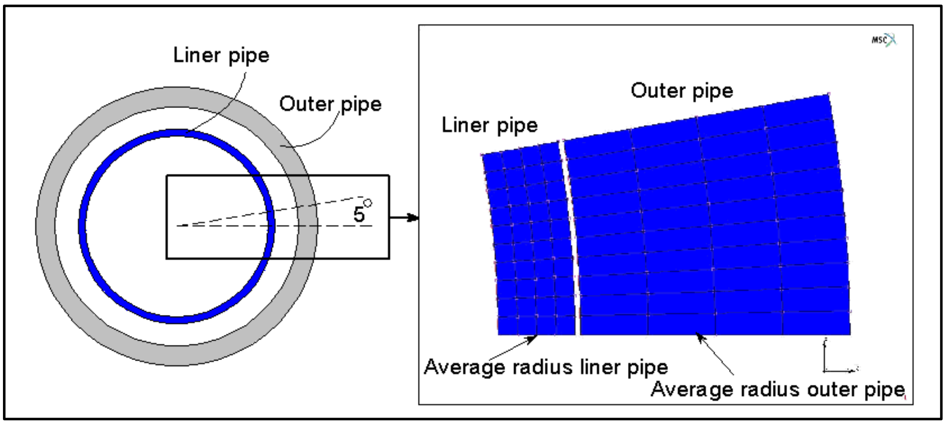

Figure 2.3 Three dimensional, one layer thick, finite element model of the manufacturing process of Tight Fit Pipe

The liner pipe and the outer pipe characteristics as well as the manufacturing process parameters were used as input in the finite element model. The residual liner pipe hoop stress was the output of the finite element model. Load on the separate liner pipe and the outer pipe in order to “obtain” a Tight Fit Pipe at the end of the manufacturing process were applied in the finite element model in seven subsequent steps (Table 2.3).

Table 2.3 Steps in the three dimensional, one layer thick, finite element model simulating the manufacturing process of Tight Fit Pipe

Step	Description
1	Cooling down of the liner pipe from $T_{environment}$ to T_{CW}
2	Heating up of the outer pipe from $T_{environment}$ to $T_{O;max}$
3	Increase of the internal pressure to $P_{i;max}$ while the outer pipe temperature is kept constant at $T_{O;max}$ and the liner pipe temperature is kept constant at T_{CW}
4	Partial ($T_{L;a;PH}$) or complete ($T_{L;a;CH}$) heating of the liner pipe, while the internal pressure is constant and maximal at $P_{i;max}$ and the outer pipe is continuously heated at $T_{O;max}$
5	Decrease of the internal pressure from $P_{i;max}$ to atmospheric level, while the liner pipe and the outer pipe are continuously heated
6	Decrease of the temperature to T_{end} of both the liner pipe and the outer pipe
7	Liner pipe and outer pipe cool down from T_{end} to $T_{environment}$

Assumptions 1, 2, 3, 4, 5, 8 and 9, applicable to the two dimensional analytical model (Subsection 2.3.1) were also valid for the three dimensional, one layer thick, finite element model. The influence of the assumptions 2 and 8 on the residual liner pipe hoop stress (the outcome of the finite element model) is investigated in Subsections 2.4 and 2.5.

2.3.3 Comparison between Analytical and Finite Element Model

There are a few differences between the analytical model and the finite element model:

1. The analytical model is less advanced than the finite element model in that the wall thickness is kept constant throughout the manufacturing process and perfect elastic plastic material representation is used.
2. The analytical model is less complicated in use than the finite element model and it takes less time to run (five minutes compared to one hour).
3. The analytical model enables a quick understanding of the influence of the various parameters, which is important for the choice of the process variables in the manufacturing process.
4. The finite element model is a three dimensional, one layer thick model, while the analytical model only comprises the cross-section of the Tight Fit Pipe. The liner pipe yield stress is used in the analytical model as the yield criterion for the liner pipe. In the finite element model the von Mises stress is used as the yield criterion which is set equal to the liner pipe yield stress.

The finite element model was developed to verify the analytical model. Both models are compared to factory data hereafter in Subsection 2.4.

2.4 Comparing the Analytical and the Finite Element Models with Practice

2.4.1 Overview of Analytical and Finite Element Models

The analytical model and the finite element model were compared to measured data from the Kuroki T&P factory. Two considerations were made:

1. Liner pipe temperature

No measurements of the liner pipe temperature during the manufacturing process have been performed. Therefore, the analytical model and the finite element model have been developed assuming the liner pipe to heat to $T_{L;a;PH}$ (partial heating) or to $T_{L;a;CH}$ (complete heating).

2. Material representation

The finite element model was developed to verify the analytical model. Because the analytical model uses perfect elastic plastic liner pipe material representation, this model was compared to a finite element model assuming perfect elastic plastic liner pipe material representation as well. The finite element model using perfect elastic plastic liner pipe material representation was also compared to a finite element model assuming strain hardening for the liner pipe. In this finite element model, the true stress strain curve for the liner pipe material, calculated from the measured liner pipe engineering stress strain curve (Appendix II), was used. By comparing these finite element models with measured data from Kuroki T&P, it was determined how the liner pipe material representation influenced the comparison with practice.

Keeping the two considerations mentioned above in mind, two different situations were considered in the analytical model and four situations were considered in the finite element model. These situations were compared to factory data.

Two different situations were considered in the analytical model:

1. AM-1: partial heating of the liner pipe was assumed and liner pipe perfect elastic plastic material behaviour (no strain hardening).
2. AM-2: complete heating of the liner pipe was assumed and liner pipe perfect elastic plastic material behaviour (no strain hardening).

Four different situations were considered in the finite element model:

1. FEA-1: partial heating of the liner pipe was assumed and liner pipe perfect elastic plastic material behaviour (no strain hardening).
2. FEA-2: partial heating of the liner pipe was assumed and liner pipe strain hardening material behaviour.

3. FEA-3: complete heating of the liner pipe was assumed and liner pipe perfect elastic plastic material behaviour (no strain hardening).
4. FEA-4: complete heating of the liner pipe was assumed and liner pipe strain hardening material behaviour.

It will be shown later in this thesis that for some test cases (the test cases are explained in Subsection 2.4.2) the residual liner pipe hoop stresses, predicted by the analytical and the finite element models, compare well with the measurements from the Kuroki T&P factory, while for other test cases no correlation was found at all (Subsection 2.4.3). This may be the result of unknown phenomena in the manufacturing process of Tight Fit Pipe which were not taken into account in the models. Because of this and due to the current absence of measurements of the liner pipe temperature during the manufacturing process, an accurate comparison of the predicted and the measured residual liner pipe hoop stresses could not be carried out.

A sensitivity analysis was performed using the models (Subsections 2.5 and 2.6) to provide more insight into the various parameters of the manufacturing process of Tight Fit Pipe and to provide an indication of which parameters should be modified to improve the residual liner pipe hoop stress. In the recommendations of this thesis it is advised to verify the findings of the sensitivity analysis by testing in the factory. It is also advised to measure the temperature of the liner pipe during the manufacturing process.

2.4.2 Input Data for Analytical and Finite Element Models

The residual liner pipe hoop stresses determined in the models were compared to the residual liner pipe hoop stresses measured for six different Tight Fit Pipes manufactured in the Kuroki T&P factory. As experimenting with Tight Fit Pipe manufacturing in the Kuroki T&P factory is not part of the research, measured data (i.e. measured residual liner pipe hoop stress) was used from six different Tight Fit Pipes which have been manufactured in the factory over the last few years. The fact that these Tight Fit Pipes differ from each other in many different respects (Table 2.4) makes verification of the analytical and the finite element model less straightforward.

Input data for the six test cases (E_L, α_L, etc.) can be found in Table 2.4. For both the analytical model and the finite element model, the outer pipe Young's modulus (E_O) was 200000 MPa, identical in axial and hoop direction. An outer pipe thermal expansion coefficient (α_O) of 0.000013 was used. For all liner pipes a Poisson ratio (ν_L) of 0.27 was applied. For the analytical model and the finite element model, the liner pipe Young's modulus (E_L) and yield stress ($\sigma_{L;y}$) were assumed identical in axial and hoop direction. These data and the data in Table 2.4 were received from Kuroki T&P. Liner pipe material characteristics can be found in Appendix II.

Table 2.4 Input data used in the analytical model and in the finite element model for six test cases

	1	2	3	4	5	6
Material OP[1)]	C95	C95	C95	C95	X65	X65
Material LP	SUS 304[2)]	UNS N08825[3)]	SUS 304[2)]	UNS N08031[3)]	SUS 304[2)]	SUS 304[2)]
$d_{O;o}$ [mm]	114.3	114.3	193.7	193.7	273.1	273.1
t_O [mm]	11.5	11.5	8.9	8.9	9.3	9.3
$d_{L;o}$ [mm]	88.9	88.9	169.0	170.5	250.0	250.0
t_L [mm]	2.0	1.6	2.0	2.0	2.5	2.5
g [mm]	2.4	2.4	6.84	5.34	4.6	4.6
$\sigma_{L;y}$ [MPa]	294	353	316	435	308	308
E_L [MPa]	193190	192210	193190	198100	193190	193190
α_L [1/K]	1.6E-05	1.4E-05	1.6E-05	1.4E-05	1.4E-05	1.4E-05
$P_{i;max}$ [MPa]	116	102	57	58	34	32
$T_{O;max}$ [K]	638	655	650	655	580	680
T_{CW} [K]	283	293	298	293	300	298
$T_{L;a;PH}$ [K]	352	355	375	374	366	388
$T_{L;a;CH}$ [K]	638	655	650	655	580	680

Note:
OP: Outer pipe
LP: Liner pipe
1) API 5L code [3]
2) JIS standard (stainless steel products) corresponding to ASTM standard 304 [62]
3) ASTM standard [63]

2.4.3 Comparison of the Output of the Analytical and the Finite Element Models with Measured Data

For each of the six test cases a comparison was made between the residual liner pipe hoop stress measured in the Kuroki T&P factory and the values resulting from the analytical model and the finite element model.

In Table 2.5 the residual liner pipe hoop stress measured in the Kuroki T&P factory is compared with the residual liner pipe hoop stress resulting from the finite element model, assuming perfect elastic plastic liner pipe material behaviour. In the model the liner pipe was assumed to heat up either partially (FEA-1) or completely (FEA-3) during the manufacturing process. It can be seen in Table 2.5 that a 37 % to 46 % lower assumed liner pipe temperature (the difference between partial and complete liner pipe heating) during the manufacturing process can result in an increase in the residual liner pipe hoop stress ranging from 11 % (test case 4) to 171 % (test case 3).

Table 2.5 Comparison of the residual liner pipe hoop stress from FEA-1 and FEA-3 with measured factory data

Test Case	σ_{res} factory [MPa]	σ_{res} FEA-1 [MPa]	σ_{res} FEA-3 [MPa]	$\Delta\sigma_{res}$ FEA-1 - FEA-3 [%]	$\Delta T_{L;a}$ [%]
1	-195	-273	-123	121	-45
2	-156	-350	-298	17	-46
3	-194	-296	-109	171	-42
4	-119	-404	-365	11	-43
5	-138	-304	-240	26	-37
6	-187	-288	-254	13	-43

Note:

σ_{res} FEA-1: σ_{res} in the finite element model assuming partial heating of the liner pipe and perfect elastic plastic liner pipe material behaviour

σ_{res} FEA-3: σ_{res} in the finite element model assuming complete heating of the liner pipe and perfect elastic plastic liner pipe material behaviour

$\Delta\sigma_{res}$ FEA-1 - FEA-3: σ_{res} in FEA-1 minus σ_{res} in FEA-3 divided by σ_{res} in FEA-3

$\Delta T_{L;a}$: $T_{L;a;PH}$ minus $T_{L;a;CH}$ divided by $T_{L;a;CH}$

In Table 2.6 the residual liner pipe hoop stress measured in the Kuroki T&P factory is compared with the residual liner pipe hoop stress resulting from the finite element model, assuming strain hardening liner pipe material behaviour. In the model the liner pipe was assumed to heat up either partially (FEA-2) or completely (FEA-4) during the manufacturing process. A 37 % to 46 % lower assumed liner pipe temperature (the difference between partial and complete liner pipe heating) can result in an increase in the residual liner pipe hoop stress ranging from 0 % (test case 4) to 63 % (test case 1).

Table 2.6 Comparison of the residual liner pipe hoop stress from FEA-2 and FEA-4 with measured factory data

Test Case	σ_{res} factory [MPa]	σ_{res} FEA-2 [MPa]	σ_{res} FEA-4 [MPa]	$\Delta\sigma_{res}$ FEA-2 - FEA-4 [%]	$\Delta T_{L;a}$ [%]
1	-195	-377	-231	63	-45
2	-156	-463	-412	12	-46
3	-194	-399	-261	53	-42
4	-119	-477	-477	0	-43
5	-138	-382	-346	11	-37
6	-187	-386	-335	15	-43

Note:

σ_{res} FEA-2: σ_{res} in the finite element model assuming partial heating of the liner pipe and strain hardening liner pipe material behaviour

σ_{res} FEA-4: σ_{res} in the finite element model assuming complete heating of the liner pipe and strain hardening liner pipe material behaviour

$\Delta\sigma_{res}$ FEA-2 - FEA-4: σ_{res} in FEA-2 minus σ_{res} in FEA-4 divided by σ_{res} in FEA-4

$\Delta T_{L;a}$: $T_{L;a;PH}$ minus $T_{L;a;CH}$ divided by $T_{L;a;CH}$

The residual liner pipe hoop stress thus seems to be sensitive to the (assumed) temperature of the liner pipe.

In Table 2.7 the measured residual liner pipe hoop stress is compared with the residual liner pipe hoop stress resulting from the finite element model, assuming partial liner pipe heating. In the model either perfect elastic plastic liner pipe material behaviour (FEA-1) or strain hardening liner pipe material behaviour (FEA-2) was assumed. It can be seen in Table 2.7 that strain hardening has much influence on the residual liner pipe hoop stress. E.g. for test case 2, the difference in results between the models FEA-1 and FEA-2 is 72 %: 197 % (the difference between the factory data and FEA-2) minus 125 % (the difference between the factory data and FEA-1).

Table 2.7 Comparison of the residual liner pipe hoop stress from FEA-1 and FEA-2 with measured factory data

Test Case	σ_{res} factory [MPa]	σ_{res} FEA-1 [MPa]	σ_{res} FEA-2 [MPa]	$\Delta\sigma_{res}$ FEA-1 - factory [%]	$\Delta\sigma_{res}$ FEA-2 - factory [%]
1	-195	-273	-377	40	93
2	-156	-350	-463	125	197
3	-194	-296	-399	53	106
4	-119	-404	-477	240	301
5	-138	-304	-382	120	177
6	-187	-288	-386	54	107

Note:

σ_{res} FEA-1: σ_{res} in the finite element model assuming partial heating of the liner pipe and perfect elastic plastic liner pipe material behaviour

σ_{res} FEA-2: σ_{res} in the finite element model assuming partial heating of the liner pipe and strain hardening liner pipe material behaviour

$\Delta\sigma_{res}$ FEA-1 - factory: σ_{res} in FEA-1 minus σ_{res} from the factory divided by σ_{res} from the factory

$\Delta\sigma_{res}$ FEA-2 - factory: σ_{res} in FEA-2 minus σ_{res} from the factory divided by σ_{res} from the factory

In Table 2.8 the measured residual liner pipe hoop stress is compared with the residual liner pipe hoop stress resulting from the finite element model, assuming complete liner pipe heating. In the model either perfect elastic plastic liner pipe material behaviour (FEA-3) or strain hardening liner pipe material (FEA-4) was assumed. It can be seen in Table 2.8 (just as in Table 2.7) that the liner pipe strain hardening has much influence on the residual liner pipe hoop stress.

Table 2.8 Comparison of the residual liner pipe hoop stress from FEA-3 and FEA-4 with measured factory data

Test Case	σ_{res} factory [MPa]	σ_{res} FEA-3 [MPa]	σ_{res} FEA-4 [MPa]	$\Delta\sigma_{res}$ FEA-3 - factory [%]	$\Delta\sigma_{res}$ FEA-4 - factory [%]
1	-195	-123	-231	-37	19
2	-156	-298	-412	91	164
3	-194	-109	-261	-44	35
4	-119	-365	-477	207	301
5	-138	-240	-346	74	151
6	-187	-254	-335	36	79

Note:

σ_{res} FEA-3: σ_{res} in the finite element model assuming complete heating of the liner pipe and perfect elastic plastic liner pipe material behaviour

σ_{res} FEA-4: σ_{res} in the finite element model assuming complete heating of the liner pipe and strain hardening liner pipe material behaviour

$\Delta\sigma_{res}$ FEA-3 - factory: σ_{res} in FEA-3 minus σ_{res} from the factory divided by σ_{res} from the factory

$\Delta\sigma_{res}$ FEA-4 - factory: σ_{res} in FEA-4 minus σ_{res} from the factory divided by σ_{res} from the factory

It can be seen in Table 2.7 and Table 2.8 that there is a significant variation in the differences between the factory data and the finite element model results among the six test cases. The same can be seen among the six test cases in Table 2.9 for the differences between the factory data and the results from the analytical model.

Table 2.9 Comparison of the residual liner pipe hoop stress from AM-1 and AM-2 with measured factory data

Test Case	σ_{res} factory [MPa]	σ_{res} AM-1 [MPa]	σ_{res} AM-2 [MPa]	$\Delta\sigma_{res}$ AM-1 - factory [%]	$\Delta\sigma_{res}$ AM-2 - factory [%]
1	-195	-286	-236	47	21
2	-156	-353	-353	126	126
3	-194	-300	-194	55	0
4	-119	-434	-425	265	257
5	-138	-305	-291	121	111
6	-187	-305	-285	63	52

Note:

σ_{res} AM-1: σ_{res} in the analytical model assuming partial heating of the liner pipe and perfect elastic plastic liner pipe material behaviour

σ_{res} AM-2: σ_{res} in the analytical model assuming complete heating of the liner pipe and perfect elastic plastic liner pipe material behaviour

$\Delta\sigma_{res}$ AM-1 - factory: σ_{res} in AM-1 minus σ_{res} from the factory divided by σ_{res} from the factory

$\Delta\sigma_{res}$ AM-2 - factory: σ_{res} in AM-2 minus σ_{res} from the factory divided by σ_{res} from the factory

The degree of correlation between the results from the models and the measured data from the factory can differ significantly per test case. For example, the result from finite element model FEA-4 for test case 1 in Table 2.8 matches factory data relatively well: there is a 19 % difference. The result from the identical finite element model FEA-4 for test case 4 in Table 2.8 does not match the factory data at all: there is a 301 % difference. These results suggest that unknown parameters of the manufacturing process influence the residual liner pipe hoop stress. This makes it currently not possible for the models to accurately predict the residual liner pipe hoop stress at the end of the manufacturing process.

In Table 2.10 results from the analytical model are compared with results from the finite element model assuming partial and complete heating for the six test cases.

Table 2.10 Comparison of the residual liner pipe hoop stress from the analytical model with the residual liner pipe hoop stress from the finite element model

Test Case	σ_{res} FEA-1 [MPa]	σ_{res} FEA-3 [MPa]	σ_{res} AM-1 [MPa]	σ_{res} AM-2 [MPa]	$\Delta\sigma_{res}$ AM-1 - FEA-1 [%]	$\Delta\sigma_{res}$ AM-2 - FEA-3 [%]
1	-273	-123	-286	-236	5	91
2	-350	-298	-353	-353	1	18
3	-296	-109	-300	-194	1	77
4	-404	-365	-434	-425	7	16
5	-304	-240	-305	-291	0	21
6	-288	-254	-305	-285	6	12

Note:

σ_{res} AM-1:	σ_{res} in the analytical model assuming partial heating of the liner pipe and perfect elastic plastic liner pipe material behaviour
σ_{res} AM-2:	σ_{res} in the analytical model assuming complete heating of the liner pipe and perfect elastic plastic liner pipe material behaviour
σ_{res} FEA-1:	σ_{res} in the finite element model assuming partial heating of the liner pipe and perfect elastic plastic liner pipe material behaviour
σ_{res} FEA-3:	σ_{res} in the finite element model assuming complete heating of the liner pipe and perfect elastic plastic liner pipe material behaviour
$\Delta\sigma_{res}$ AM-1 - FEA-1:	σ_{res} in AM-1 minus σ_{res} in FEA-1 divided by σ_{res} in FEA-1
$\Delta\sigma_{res}$ AM-2 - FEA-3:	σ_{res} in AM-2 minus σ_{res} in FEA-3 divided by σ_{res} in FEA-3

Differences between the finite element model and the analytical model (Table 2.10) can be the result of the phenomenon that the finite element model is a three dimensional, one layer thick, finite element model, while the analytical model only comprises the cross-section of the Tight Fit Pipe (identified as **phenomenon 1**). The liner pipe yield stress is used in the analytical model as the yield criterion for the liner pipe. In the finite element model the von Mises stress is used as the yield criterion which is set equal to the liner pipe yield stress. This can result in differences in the liner pipe hoop stress and the liner pipe radius in the different steps of the manufacturing process when comparing the analytical model with the finite element model. The different steps of the manufacturing process have been explained in Subsection 2.3.1. For example for test case 1, from step 5 to step 6 (Figure 2.4), when the liner pipe and the outer pipe together are expanded by the internal pressure, the hoop and the radial stress play a role in the determination of the yield criterion in the finite element model. The pipe is free to move in the axial direction and the axial stress is thus zero. In the analytical model only the hoop stress defines yielding from step 5 to step 6. This explains the difference in the liner pipe behaviour between both models from step 5 to step 6 (Figure 2.4).

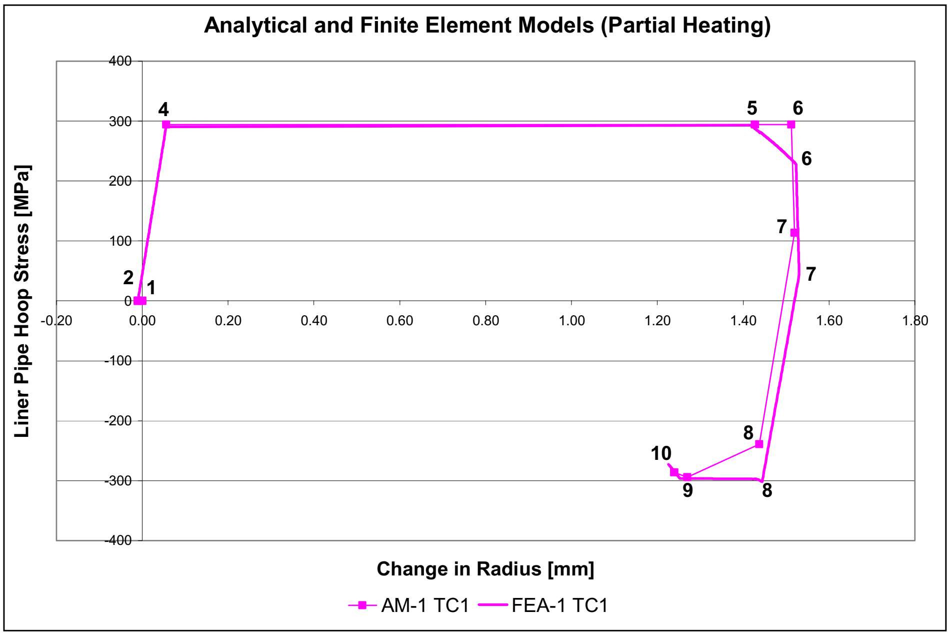

Figure 2.4 Comparison between the analytical and the finite element model (test case 1)

In Table 2.10 it can also be seen that the results from the analytical model correlate well with results from the finite element model assuming partial heating of the liner pipe. Results from the analytical model correlate less to results from the finite element model when complete heating of the liner pipe is assumed. This may be the result of the phenomenon that in the analytical model the changes of the liner pipe and outer pipe wall thicknesses are not taken into account while in the finite element model these changes are taken into account (identified as **phenomenon 2**). A higher liner pipe temperature (complete heating) influences the change in wall thickness more and thus the outcome of the finite element model. In test cases 1 and 3 the liner pipe thermal expansion coefficient is relatively high compared to the other test cases (Table 2.4) influencing the change in wall thickness due to heat more and thus the outcome of the finite element model more. This may explain the 92 % and 78 % difference in Table 2.10 between the analytical model AM-2 and the finite element model FEA-3 for test cases 1 and 3 while the differences for the other test cases are smaller. For test case 3, assuming complete liner pipe heating, the liner pipe radius becomes 0.07 mm smaller than the outer pipe radius from step 8 to step 10 (cooling down of the liner pipe and the outer pipe to $T_{environment}$), causing a reduction of the residual liner pipe hoop stress of 122 MPa. Assuming complete liner pipe heating, the neglected changes of the liner pipe and the outer pipe wall thicknesses due to heat comprise 0.01 mm and 0.04 mm from step 8 to step 10, respectively. The difference between the liner pipe radius and the outer pipe radius (0.07 mm) is thus in the same order of magnitude as the neglected changes in their wall thicknesses due to heat (0.01 mm and 0.04 mm, respectively).

For example for test case 1, from step 8 to step 9, when the internal pressure is reduced to atmospheric level, phenomenon 2 also explains the difference in the liner pipe behaviour between the analytical and the finite element model, assuming partial liner pipe heating (Figure 2.4). In the finite element model yielding in compression is reached in step 8 while the yield stress in compression is not yet reached in step 8 in the analytical model. From step 8 to step 9, the liner pipe and the outer pipe cool down from $T_{L;a;PH}$ and $T_{O;max}$, respectively, to the temperature T_{end}. From step 8 to step 9 in the analytical model the liner pipe hoop stress reaches the yield stress in compression. From step 8 to step 9 in the finite element model the liner pipe hoop stress wants to become more compressive, but is unable to, because the yield stress in compression already has been reached. So, in step 9, the hoop stresses in the liner pipe in both the finite element model and in the analytical model have reached the yield stress in compression.

Taking Table 2.5 to Table 2.10 and Figure 2.4 into account, it can be concluded that a correct assumption of the temperature of the cooled liner pipe as a result of contact with the heated outer pipe during the manufacturing process and correctly modelling of the liner pipe material (yield stress and amount of strain hardening) are important. These parameters influence the predicted residual liner pipe hoop stress at the end of the manufacturing process in the analytical model and in the finite element model quite severely. If these two parameters are not correctly assumed in the models, it can result in incorrect predictions for the residual liner pipe hoop stress at the end of the manufacturing process. It also seems that incorrectly calculated values for the residual liner pipe hoop stress may be the consequence of unknown phenomena, other than the unknown liner pipe temperature, during the manufacturing process of Tight Fit Pipe which are not taken into account in the models: predicted results correlate relatively well with the measured data of some test cases while for other test cases no correlation is found at all.

2.5 Sensitivity Analysis

2.5.1 Objective of the Sensitivity Analysis

The analytical model and the finite element model were developed to investigate the Tight Fit Pipe manufacturing process in order to obtain a better understanding of the magnitude of the residual liner pipe hoop stress, i.e. the mechanical bonding strength, at the end of the manufacturing process. This is important as the mechanical bonding strength is expected to be of influence on liner pipe wrinkling during reeling.

The analytical model and the finite element model allow for variation in the parameters in such a way that theoretically an optimum residual liner pipe hoop stress can be obtained which is expected to result in minimal liner pipe wrinkling during reeling. When changing the parameters, in order to achieve this optimum, it is necessary to understand which parameters have the most influence on the residual liner pipe hoop stress. A sensitivity analysis was therefore carried out. In this sensitivity analysis, input parameters were changed to investigate their influence on the residual liner pipe hoop stress. The sensitivity of the residual liner pipe hoop stress to the following parameters was investigated:

1. Temperature dependent material characteristics of the liner and the outer pipe:
    a. Liner pipe and the outer pipe yield stresses ($\sigma_{L;y}$ and $\sigma_{O;y}$)
    b. Liner pipe and the outer pipe thermal expansion coefficients (α_L and α_O)
    c. Liner pipe and the outer pipe Young's moduli (E_L and E_O)
2. Geometric characteristics of the liner pipe and the outer pipe:
    a. Liner pipe and the outer pipe wall thicknesses (t_L and t_O)
    b. Initial gap between the liner pipe and the outer pipe (g)
3. Characteristics of the manufacturing process:
    a. Oven temperature ($T_{O;max}$)
    b. Internal pressure ($P_{i;max}$)

An additional objective of the first part of the sensitivity analysis (1a, 1b and 1c above: the sensitivity of the residual liner pipe hoop stress to the temperature dependent material characteristics (Subsection 2.5.2)) was to provide information on the effect of assuming the values constant (not influenced by the heat) in the models. The variation of these parameters in the sensitivity analysis was based on the change of the value of these parameters due to heating during the manufacturing process. In the second (2a and 2b above) and third part (3a and 3b above) of the sensitivity analysis (Subsection 2.5.3 and 2.5.4) a variation in a parameter of 30 % was based on the need to take a variation that is of the same order of magnitude as the maximum variation used in the first part of the sensitivity analysis. The different sensitivity analyses can then be best compared. At the same time the 30 % variation also caused a noticeable variation in the residual liner pipe hoop stress.

The sensitivity analysis was executed using the analytical model assuming both partial and complete heating. Partial heating of the liner pipe is identified as the liner pipe heating up to 373 K (100 °C; the approximate average for the six test cases in Table 2.4). Complete heating of the liner pipe is identified as heating the liner pipe up to 673 K (400 °C; the approximate average for the six test cases Table 2.4).

2.5.2 Temperature Dependent Material Characteristics of the Liner Pipe and the Outer Pipe

Temperature dependent material characteristics of the liner pipe and the outer pipe are material characteristics which values depend on the temperature of the material:

1. Liner pipe 0.2 % yield stress ($\sigma_{L;y}$)
2. Outer pipe yield stress ($\sigma_{O;y}$)
3. Liner pipe thermal expansion coefficient (α_L)
4. Outer pipe thermal expansion coefficient (α_O)
5. Young's modulus of the liner pipe (E_L)
6. Young's modulus of the outer pipe (E_O)

The thermal expansion coefficient increases in value with increasing temperature. The yield stress and the Young's modulus decrease in value with increasing temperature.

The values of the parameters mentioned above were assumed not to change due to variation in temperature throughout the manufacturing process of Tight Fit Pipe in the analytical model and in the finite element model. This has been mentioned in the assumptions in Subsections 2.3.1 (analytical model) and 2.3.2 (finite element model). It is however required to be aware of the influence of these assumptions on the output of the models, i.e. on the residual liner pipe hoop stress. Therefore, the investigation into the sensitivity of the residual liner pipe hoop stress due to variation of these parameters was at the same time also an investigation into the influence of the assumption keeping these parameters constant in value throughout the manufacturing process.

1. Liner pipe 0.2 % yield stress

The yield stress at 0.2 % strain of stainless steel at 100 °C is 18 % lower than the value at 20 °C, while at 400 °C it has decreased with 40 % [61]. Therefore, an 18 % reduction in the yield stress was implemented in the analytical model AM-1 while a 40 % reduction of the yield stress was implemented in the analytical model AM-2.

In Table 2.11 it can be seen that an 18 % reduction in the liner pipe yield stress at 100 °C results in approximately an 18 % reduction in the residual liner pipe hoop stress in the analytical model AM-1A. The 40 % reduction in the liner pipe yield stress at 400 °C results in a 40 % reduction in the residual liner pipe hoop stress in the analytical model AM-2A. The input parameters for each of the six test cases in Table 2.11 can be found in Table 2.4.

Table 2.11 Influence of the reduction of the liner pipe yield stress on the residual liner pipe hoop stress

Test Case	σ_{res} AM-1 [MPa]	σ_{res} AM-2 [MPa]	σ_{res} AM-1A [MPa]	σ_{res} AM-2A [MPa]	$\Delta\sigma_{res}$ AM-1 - AM-1A [%]	$\Delta\sigma_{res}$ AM-2 - AM-2A [%]
1	-286	-236	-233	-118	-18	-50
2	-353	-353	-289	-212	-18	-40
3	-300	-194	-244	-68	-19	-65
4	-434	-425	-356	-250	-18	-41
5	-305	-291	-250	-168	-18	-42
6	-305	-285	-250	-162	-18	-43

Note:

σ_{res} AM-1:	σ_{res} in the analytical model assuming partial heating of the liner pipe and perfect elastic plastic liner pipe material behaviour (Table 2.9)
σ_{res} AM-2:	σ_{res} in the analytical model assuming complete heating of the liner pipe and perfect elastic plastic liner pipe material behaviour (Table 2.9)
σ_{res} AM-1A:	σ_{res} in the analytical model assuming partial heating of the liner pipe, perfect elastic plastic liner pipe material behaviour and a reduced liner pipe yield stress
σ_{res} AM-2A:	σ_{res} in the analytical model assuming complete heating of the liner pipe, perfect elastic plastic liner pipe material behaviour and a reduced liner pipe yield stress
$\Delta\sigma_{res}$ AM-1 - AM-1A:	σ_{res} in AM-1A minus σ_{res} in AM-1 divided by σ_{res} in AM-1
$\Delta\sigma_{res}$ AM-2 - AM-2A:	σ_{res} in AM-2A minus σ_{res} in AM-2 divided by σ_{res} in AM-2

2. Outer pipe yield stress

The outer pipe yield stress reduces by 20 % when heated to 400 °C (compared to the value at 20 °C) [61]. The finite element model was used to study the sensitivity of the residual liner pipe hoop stress to the outer pipe yield stress because this was not possible in the analytical model. The outer pipe yield stress was decreased by 20 % in the finite element models FEA-2 and FEA-4.

It can be seen in Table 2.12 that a 20 % decrease in the outer pipe yield stress has no effect when the liner pipe is only partially heated up, because the outer pipe yield stress was not reached (FEA-2A). However, when the liner pipe was heated up completely (FEA-4A), a 20 % decrease in the outer pipe yield stress either resulted in a significant or in no decrease in the residual liner pipe hoop stress at the end of the manufacturing process. This depended on whether the reduced outer pipe yield stress was reached (test case 3, 5 and 6) or was not reached (test case 1, 2 and 4) during the manufacturing process. The input parameters for each of the six test cases in Table 2.12 can be found in Table 2.4.

Table 2.12 Influence of the outer pipe yield stress reduction on the residual liner pipe hoop stress

Test Case	σ_{res} FEA-2 [MPa]	σ_{res} FEA-4 [MPa]	σ_{res} FEA-2A [MPa]	σ_{res} FEA-4A [MPa]	$\Delta\sigma_{res}$ FEA-2 - FEA-2A [%]	$\Delta\sigma_{res}$ FEA-4 - FEA-4A [%]
1	-377	-231	-377	-231	0	0
2	-463	-412	-463	-412	0	0
3	-399	-261	-399	-259	0	-1
4	-477	-477	-477	-475	0	0
5	-382	-346	-382	-124	0	-64
6	-386	-335	-386	-206	0	-39

Note:

σ_{res} FEA-2: σ_{res} in the finite element model assuming partial heating of the liner pipe and strain hardening liner pipe material behaviour (Table 2.6)

σ_{res} FEA-4: σ_{res} in the finite element model assuming complete heating of the liner pipe and strain hardening liner pipe material behaviour (Table 2.6)

σ_{res} FEA-2A: σ_{res} in the finite element model assuming partial heating of the liner pipe, strain hardening liner pipe material behaviour and a reduced outer pipe yield stress

σ_{res} FEA-4A: σ_{res} in the finite element model assuming complete heating of the liner pipe, strain hardening liner pipe material behaviour and a reduced outer pipe yield stress

$\Delta\sigma_{res}$ FEA-2 - FEA-2A: σ_{res} in FEA-2A minus σ_{res} in FEA-2 divided by σ_{res} in FEA-2

$\Delta\sigma_{res}$ FEA-4 - FEA-4A: σ_{res} in FEA-4A minus σ_{res} in FEA-4 divided by σ_{res} in FEA-4

3. Liner pipe thermal expansion coefficient

The thermal expansion coefficient of the liner pipe (stainless steel) at 100 °C is 3 % higher than the value at 20 °C, while at 400 °C it has increased with 9 % [60]. An increase of 3 % of the thermal expansion coefficient of the liner pipe was implemented in the analytical model AM-1 and an increase of 9 % was implemented in the analytical model AM-2.

Table 2.13 shows that an increase in the thermal expansion coefficient of the liner pipe decreases the residual liner pipe hoop stress at the end of the manufacturing process and that the effect becomes more significant when the liner heats up more (AM-1B and AM-2B). The input parameters for each of the six test cases in Table 2.13 can be found in Table 2.4.

Table 2.13 Influence of the liner pipe thermal expansion coefficient increase on the residual liner pipe hoop stress

Test Case	σ_{res} AM-1 [MPa]	σ_{res} AM-2 [MPa]	σ_{res} AM-1B [MPa]	σ_{res} AM-2B [MPa]	$\Delta\sigma_{res}$ AM-1 - AM-1B [%]	$\Delta\sigma_{res}$ AM-2 - AM-2B [%]
1	-286	-236	-283	-156	-1	-34
2	-353	-353	-353	-330	0	-6
3	-300	-194	-297	-114	-1	-41
4	-434	-425	-431	-352	-1	-17
5	-305	-291	-302	-237	-1	-19
6	-305	-285	-302	-211	-1	-26

Note:

σ_{res} AM-1: σ_{res} in the analytical model assuming partial heating of the liner pipe and perfect elastic plastic liner pipe material behaviour (Table 2.9)

σ_{res} AM-2: σ_{res} in the analytical model assuming complete heating of the liner pipe and perfect elastic plastic liner pipe material behaviour (Table 2.9)

σ_{res} AM-1B: σ_{res} in the analytical model assuming partial heating of the liner pipe, perfect elastic plastic liner pipe material behaviour and an increased liner pipe thermal expansion coefficient

σ_{res} AM-2B: σ_{res} in the analytical model assuming complete heating of the liner pipe, perfect elastic plastic liner pipe material behaviour and an increased liner pipe thermal expansion coefficient

$\Delta\sigma_{res}$ AM-1 - AM-1B: σ_{res} in AM-1B minus σ_{res} in AM-1 divided by σ_{res} in AM-1

$\Delta\sigma_{res}$ AM-2 - AM-2B: σ_{res} in AM-2B minus σ_{res} in AM-2 divided by σ_{res} in AM-2

4. Outer pipe thermal expansion coefficient

The outer pipe thermal expansion coefficient increases by 12 % when heated to 400 °C (compared to the value at 20 °C) [60]. The thermal expansion coefficient of the outer pipe was increased by 12 % in the analytical models AM-1 and AM-2.

It can be seen in Table 2.14 that an increase of the outer pipe thermal expansion coefficient of 12 % can either result in an increase in the residual liner pipe hoop stress (e.g. test case 3) or it can have no influence at all (e.g. test case 2) (AM-1C and AM-2C).

An increase in the value of the outer pipe thermal expansion coefficient can result in an increase of residual liner pipe hoop stress because the outer pipe can shrink more tightly around the liner pipe during the cooling down process (e.g. test case 3). The increase of the outer pipe thermal expansion coefficient had no effect in test case 2, because the residual liner pipe hoop stress already equalled the yield stress at the end of the manufacturing process when the outer pipe thermal expansion coefficient at 20 °C was used.

Table 2.14 Influence of the outer pipe thermal expansion coefficient increase on the residual liner pipe hoop stress

Test Case	σ_{res} AM-1 [MPa]	σ_{res} AM-2 [MPa]	σ_{res} AM-1C [MPa]	σ_{res} AM-2C [MPa]	$\Delta\sigma_{res}$ AM-1 - AM-1C [%]	$\Delta\sigma_{res}$ AM-2 - AM-2C [%]
1	-286	-236	-294	-294	3	25
2	-353	-353	-353	-353	0	0
3	-300	-194	-312	-286	4	48
4	-434	-425	-435	-435	0	3
5	-305	-291	-308	-308	1	6
6	-305	-285	-308	-308	1	8

Note:

σ_{res} AM-1: σ_{res} in the analytical model assuming partial heating of the liner pipe and perfect elastic plastic liner pipe material behaviour (Table 2.9)

σ_{res} AM-2: σ_{res} in the analytical model assuming complete heating of the liner pipe and perfect elastic plastic liner pipe material behaviour (Table 2.9)

σ_{res} AM-1C: σ_{res} in the analytical model assuming partial heating of the liner pipe, perfect elastic plastic liner pipe material behaviour and an increased outer pipe thermal expansion coefficient

σ_{res} AM-2C: σ_{res} in the analytical model assuming complete heating of the liner pipe, perfect elastic plastic liner pipe material behaviour and an increased outer pipe thermal expansion coefficient

$\Delta\sigma_{res}$ AM-1 - AM-1C: σ_{res} in AM-1C minus σ_{res} in AM-1 divided by σ_{res} in AM-1

$\Delta\sigma_{res}$ AM-2 - AM-2C: σ_{res} in AM-2C minus σ_{res} in AM-2 divided by σ_{res} in AM-2

5. Young's modulus of the liner pipe

At 100 °C, the liner pipe Young's modulus decreases by 4 %, while it decreases by 16 % at 400 °C (compared to the value at 20 °C) [61]. Calculations indicate that the influence of this reduction of the liner pipe Young's modulus due to heating on the residual liner pipe hoop stress can be neglected.

6. Young's modulus of the outer pipe

The outer pipe Young's modulus decreases by 30 % at 400 °C (compared to the value at 20 °C) [61]. The 30 % reduction in the outer pipe Young's modulus results in a negligible influence on the residual liner pipe hoop stress.

2.5.3 Geometric Characteristics of the Liner and Outer Pipe

Geometric characteristics of the liner pipe and the outer pipe are characteristics which can vary due to an allowable tolerance in this parameter. The sensitivity of the residual liner pipe hoop stress to the following geometric characteristics has been investigated:

1. Liner wall thickness (t_L)
2. Outer pipe wall thickness (t_O)
3. Initial gap between the liner and the outer pipe (g)

1. Liner wall thickness

Calculations indicate that the influence of a 30 % variation in the liner pipe wall thickness on the residual liner pipe hoop stress is minimal compared to the influence the liner pipe yield stress has on the residual liner pipe hoop stress.

Figure 2.5 shows the influence of a more extreme variation in the liner pipe wall thickness ($t_L/3$ and $t_L{\cdot}3$) for test case 1, assuming complete liner pipe heating. For test case 1, the outer pipe wall thickness (t_O) is 11.50 mm, while the liner pipe wall thickness is 2.00 mm (t_L), 0.67 mm ($t_L/3$) or 6.00 mm ($t_L{\cdot}3$). Also the influence of more extreme variation in the liner pipe wall thickness ($t_L/3$ and $t_L{\cdot}3$) for test case 3 can be seen in Figure 2.5, assuming partial liner pipe heating. For test case 3, the outer pipe wall thickness (t_O) is 8.92 mm, while the liner pipe wall thickness is 2.00 mm (t_L), 0.67 mm ($t_L/3$) or 6.00 mm ($t_L{\cdot}3$).

The liner pipe wall thickness has less influence on the residual liner pipe hoop stress (identical to the liner hoop stress in step 10) than the level of the liner pipe yield stress in compression (Figure 2.5). Assuming partial liner pipe heating, the liner pipe always yields in compression in step 9 (cooling down of the liner pipe and the outer pipe to T_{end}). Assuming complete liner pipe heating, the liner pipe always yields in compression in step 8 (reduction of the internal pressure to atmospheric level). The influence of the liner pipe wall thickness on the residual liner pipe hoop stress becomes more significant as the temperature of the liner pipe increases during the manufacturing process.

The codes [3] indicate only an allowable tolerance of the liner pipe wall thickness of -12.5 % and + 15 %, however.

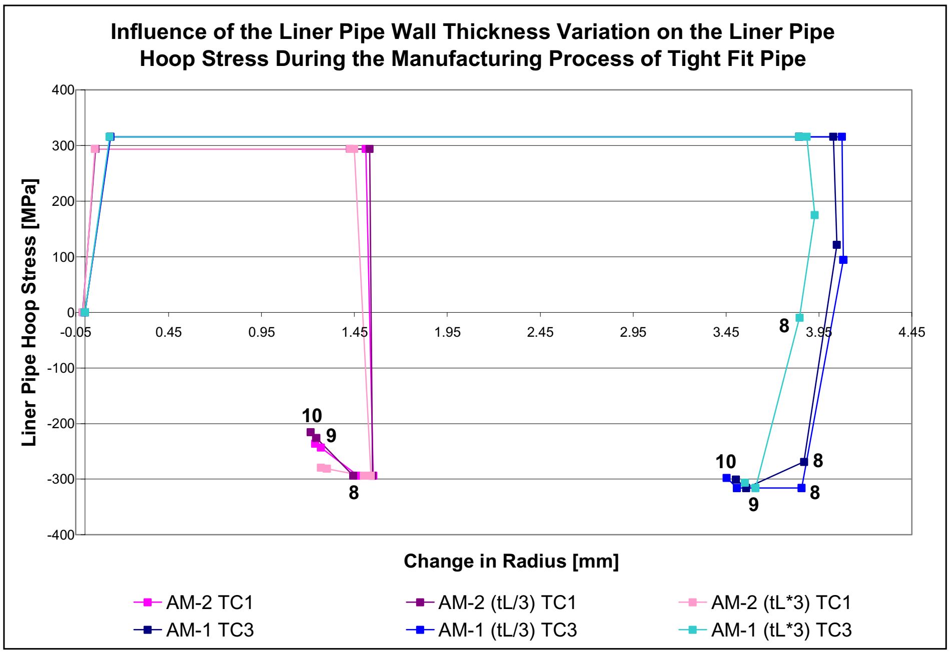

Figure 2.5 Sensitivity of the manufacturing process of Tight Fit Pipe (step 8, 9 and 10 are indicated) to variation in the liner pipe wall thickness

2. Outer pipe wall thickness

Calculations indicate that the influence of a 30 % variation in the outer pipe wall thickness on the residual liner pipe hoop stress is small compared to the influence the liner pipe yield stress has on the residual liner pipe hoop stress. Moreover, codes [3] indicate an allowable tolerance of the outer pipe wall thickness of - 12.5 % and + 15 %.

3. Initial gap between the liner and outer pipe

Calculations indicate that the influence of a 30 % variation in the initial gap on the residual liner pipe hoop stress is minimal. The gap depends on the liner pipe and the outer pipe wall thicknesses, which have a tolerance of - 12.5 % and + 15 % and on the liner pipe and the outer pipe outer diameters, which have a tolerance of ± 0.75 % [3].

2.5.4 Characteristics of the Manufacturing Process

Parameters of the manufacturing process comprise the following:

1. Maximum outer pipe temperature ($T_{O;max}$)
2. Internal pressure ($P_{i;max}$)

1. Maximum outer pipe temperature

The residual liner pipe hoop stress can be sensitive to a 30 % decrease in the maximum outer pipe temperature, depending on the parameters of the test case.

2. Internal Pressure

A 30 % decrease in the internal pressure has minimum influence on the residual liner pipe hoop stress (partial or complete liner heating) compared to the influence the liner pipe yield stress has on the residual liner pipe hoop stress.

2.6 Overview of the Sensitivity Analysis

For partial and complete heating, an overview of the sensitivity of the residual liner pipe hoop stress to the parameters above can be found in Table 2.15 and Figure 2.6. The influence of a parameter shown in Figure 2.6 is calculated by dividing the variation in percentages of the input by the variation in percentages of the output.

Table 2.15 Sensitivity analysis of the manufacturing process of Tight Fit Pipe

	PARTIAL LINER PIPE HEATING		COMPLETE LINER PIPE HEATING	
	Δ *parameter* [%]	$\Delta\sigma_{res}$ average [%]	Δ *parameter* [%]	$\Delta\sigma_{res}$ average [%]
Liner pipe yield stress ($\sigma_{L;y}$)	-18	-18	-40	-47
Outer pipe yield stress ($\sigma_{O;y}$)	-20	0	-20	-17
Liner pipe Young's Modulus (E_L)	-4	0	-16	+2
Outer pipe Young's Modulus (E_O)	-30	0	-30	+1
Liner pipe thermal expansion coefficient (α_L)	+3	-1	+9	-24
Outer pipe thermal expansion coefficient (α_O)	+12	+1	+12	+15
Liner pipe wall thickness (t_L)	-30	0	-30	-2
Outer pipe wall thickness (t_O)	-30	0	-30	-3
Initial gap (g)	-30	0	-30	0
Outer pipe heat ($T_{O;max}$)	-30	-10	-30	0
Internal pressure ($P_{i;max}$)	-30	0	-30	0

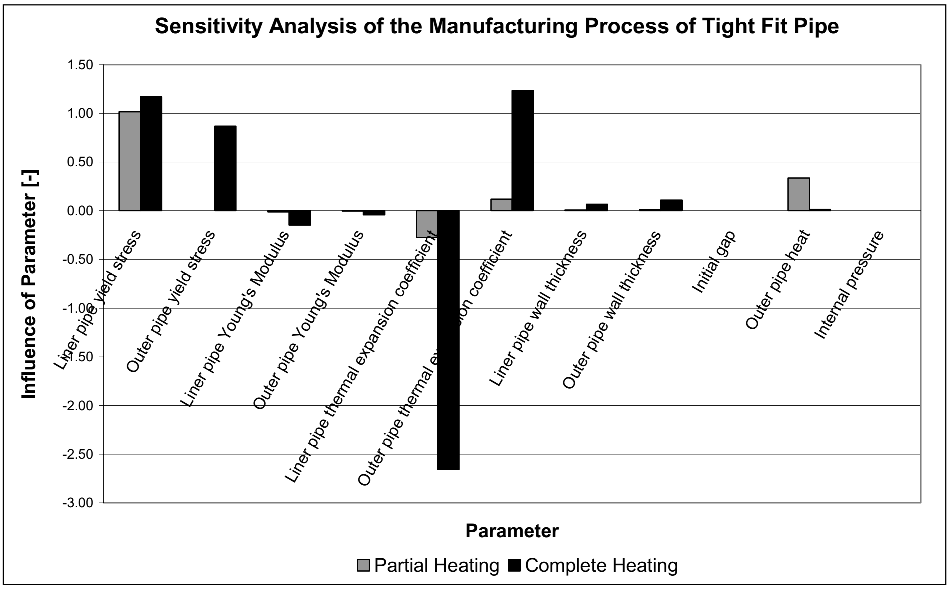

Figure 2.6 Sensitivity analysis of the manufacturing process of Tight Fit Pipe

It can be seen that the residual liner pipe hoop stress is most sensitive to the liner pipe material strength (yield stress) and the liner pipe thermal expansion coefficient (Table 2.15 and Figure 2.6). The influence of these liner pipe characteristics increases as the assumed temperature of the liner pipe during the manufacturing process increases (compare partial heating with complete heating in Table 2.15 and Figure 2.6). Thus, the amount of heating of the liner pipe as a result of contact with the hot outer pipe is also of importance.

It has been stated earlier that the computer models allow for variation of the parameters in such a way that theoretically an optimum mechanical bonding strength between the liner pipe and the outer pipe in the Tight Fit Pipe can be obtained. This optimum mechanical bonding strength is expected to minimise liner pipe wrinkling during reeling. Assuming that a high mechanical bonding strength between the liner pipe and the outer pipe, i.e. a high residual liner pipe hoop stress, results in minimal liner pipe wrinkling (this statement will be proven in Chapter 7), a high mechanical bonding strength needs to be achieved at the end of the manufacturing process of Tight Fit Pipe in order to minimise liner pipe wrinkling during reeling.

It can be concluded that the most efficient way to increase the mechanical bond and thereby expect to minimise the risk of liner pipe wrinkling, is to:

1. increase the liner pipe material strength.
2. minimise the contact time between the liner pipe and the outer pipe during the manufacturing process; the liner pipe then heats up only moderately.
3. decrease the thermal expansion coefficient of the liner; however, this influence will only be minimal when the liner pipe only heats up slightly.

As mentioned in the assumptions of the analytical model and the finite element model, the change in the value of the temperature dependent variables as a consequence of heating was neglected. As a result of this assumption, the residual liner pipe hoop stress in the models is:

1. underestimated by a maximum of 15 % (complete heating of the liner pipe (Table 2.15)), as a result of the fact that the increase of the outer pipe thermal expansion coefficient due to heating is neglected.
2. is overestimated by 24 % (complete heating of the liner pipe (Table 2.15)), as a result of the fact that the increase of the liner pipe thermal expansion coefficient due to heating is neglected.
3. is overestimated by 47 % (complete heating of the liner pipe (Table 2.15)) as a result of the fact that the decrease of the liner pipe yield stress due to heating is neglected.

It should be realised that the liner pipe temperature during the manufacturing process is currently an assumed value.

2.7 Conclusions

In order to obtain a better understanding of the mechanical bonding strength in the Tight Fit Pipe, i.e. the residual liner pipe hoop stress, at the end of the manufacturing process, computer models have been developed to simulate the manufacturing process of Tight Fit Pipe.

Comparison of the residual liner pipe hoop stress with the measured factory data shows that the models cannot yet predict the residual liner pipe hoop stress accurately. Therefore, a sensitivity analysis was carried out to improve the understanding of the influence of the various parameters on the residual liner pipe hoop stress. This sensitivity analysis shows that the temperature of the cooled liner pipe, while in contact with the heated outer pipe, proves to be an important parameter. The current absence of measurements of the liner pipe temperature during the manufacturing process contributes to the inability to predict the residual liner pipe hoop stress more accurately with the present models. The sensitivity analysis also shows that the residual liner pipe hoop stress is very sensitive to the liner pipe yield stress and strain hardening and the liner pipe thermal expansion coefficient.

The computer models enable variation of the input parameters in such a way that theoretically an optimum residual liner pipe hoop stress, i.e. an optimum mechanical bonding strength at the end of the manufacturing process of Tight Fit Pipe can be obtained. Assuming that a high mechanical bonding strength minimises the risk of liner pipe wrinkling during reeling (this statement will be proven in Chapter 7), a high mechanical bonding strength needs to be pursued in the manufacturing process of Tight Fit Pipe.

The sensitivity analysis shows that the most efficient way to increase the mechanical bonding strength, i.e. the residual liner pipe hoop stress is to increase the liner pipe material strength and to minimise the contact time between the liner and the outer pipe during the manufacturing process. If more efficient cooling of the liner pipe were possible, this would also help to increase the residual liner pipe hoop stress. The risk of liner pipe wrinkling is then expected to be minimised, making the Tight Fit Pipe most probably better suitable for installation by reeling.

3 Properties of the Available Pipes

3.1 Introduction

One of the objectives of the full scale bending tests on Tight Fit Pipe was to determine the influence of the mechanical bonding strength between the liner pipe and the outer pipe in the Tight Fit Pipe on liner pipe wrinkling during reeling. In order to study this influence, three 12.75 inch outer diameter Tight Fit Pipes with different mechanical bonding strengths (high and low) were bent in a full scale bending rig. The mechanical bonding strength was determined for each of these three Tight Fit Pipes prior to bend testing them in the full scale bending rig. The mechanical bonding strength was also determined for a 10.75 inch outer diameter Tight Fit Pipe as preparation for determining this property for the 12.75 inch Tight Fit Pipe. The material and the geometrical properties were also determined for these Tight Fit Pipes as well as for the other pipes used in this research.

An overview of the different tests performed in the research and of the pipes needed for these tests can be found in Subsection 3.2. The material properties as well as the geometric properties of the pipes are provided in Subsection 3.3, while in Subsection 3.4 the mechanical bonding strengths of the Tight Fit Pipes are determined.

3.2 Overview of the Tests and the Test Specimens

Table 3.1 provides an overview of the tests performed and the pipes used in these tests.

Table 3.1 Overview of the tests performed and of the pipes needed for these tests

Test	Description	Pipes
Saw cutting tests	Subsection 3.4.1	10.75 inch TFP
Residual compressive stress tests	Subsection 3.4.2	10.75 and 12.75 inch TFP
Liner pipe push out tests	Subsection 3.4.3	10.75 inch TFP
Axial compression tests	Chapter 4	10.75 and 12.75 inch TFP
Small scale bending tests	Chapter 5	22 mm single walled pipes with wall thicknesses varying from 1.3 to 4.3 mm
Full scale bending tests	Chapter 6	12.75 inch single walled pipe with 21.77 mm and 18.65 mm wall thickness
Full scale bending tests	Chapter 7	12.75 inch TFP

Note:
TFP: Tight Fit Pipe

The 10.75 inch outer diameter Tight Fit Pipe consisted of a 9.3 mm thick, X65, seamless outer pipe and a 2.45 mm thick, 304L liner pipe (with a longitudinal weld). The 12.75 inch outer diameter Tight Fit Pipe consisted of a 14.3 mm thick, X65, electric resistance welded outer pipe and a 3.0 mm thick, 316L liner pipe (with a longitudinal weld).

To determine experimentally the strength of the mechanical bond of a Tight Fit Pipe section, a ring, cut from this Tight Fit Pipe section, was used. It was investigated experimentally on a 10.75 inch Tight Fit Pipe how cutting off this Tight Fit Pipe ring from a Tight Fit Pipe section influenced the mechanical bonding strength between the liner pipe and the outer pipe in the Tight Fit Pipe ring. This so called “saw cutting test” (Subsection 3.4.1) was performed using a 10.75 inch Tight Fit Pipe, because of the limited availability of the 12.75 inch Tight Fit Pipe.

Prior to bending the 12.75 inch Tight Fit Pipes in the full scale bending rig, the high or low mechanical bonding strengths of each of these Tight Fit Pipes were determined. This was either done by the residual compressive stress test (Subsection 3.4.2) or by the liner pipe push out test (Subsection 3.4.3). In order to become familiar with experimental determination of the mechanical bonding strength, these tests were performed first on the 10.75 inch Tight Fit Pipe, before testing the 12.75 inch Tight Fit Pipe.

Prior to bend testing the 12.75 inch Tight Fit Pipes in the full scale bending rig, the bending rig first needed to be designed and constructed. Test results from axial compression tests on the 10.75 and 12.75 inch Tight Fit Pipes (Chapter 4) and test results from small scale bending tests on 22 mm outer diameter single walled pipes with wall thicknesses varying from 1.3 to 4.3 mm (Chapter 5) provided valuable information for the design of the full scale bending rig and its measuring equipment. The full scale bending rig was tested for its fitness for purpose by bending a 12.75 inch single walled test piece (Chapter 6). The test piece consisted of a 12.75 inch single walled pipe with a wall thickness of 21.77 mm (TEST-1) connected by a weld to another 12.75 inch single walled pipe with a wall thickness of 18.65 mm (TEST-2).

The three 12.75 inch Tight Fit Pipes available for the testing in the full scale bending rig were all given a different colour code in order to distinguish between the different Tight Fit Pipes and thus between the different mechanical bonding strengths. Tight Fit Pipes coded ORANGE and GREEN were Tight Fit Pipes with a high mechanical bonding strength while the Tight Fit Pipe coded WHITE was a Tight Fit Pipe with a low mechanical bonding strength. Bend testing Tight Fit Pipes with different mechanical bonding strengths (high and low) and measuring liner pipe wrinkling during these tests provided information on the influence of the mechanical bonding strength on liner pipe wrinkling during bending.

3.3 Material and Geometric Properties of the Pipes

3.3.1 Test Set-up

The material characteristics of the pipes were determined by performing tensile tests (at a speed of 1 mm/min). Tensile testing was performed on the three 12.75 inch Tight Fit Pipes (WHITE, ORANGE and GREEN) and on the two single walled 12.75 inch pipes (TEST-1 and TEST-2). It should be noted that the outer pipe wall thickness of the 12.75 inch Tight Fit Pipe and the wall thicknesses of the two available single walled 12.75 inch pipes (TEST-1 and TEST-2) were thick enough to manufacture a coupon in the hoop direction (Figure 3.1). However, the liner pipe of the 12.75 inch Tight Fit Pipe was too thin for this type of coupon in the hoop direction. Therefore, the curved liner pipe coupon in the hoop direction (Figure 3.1) was flattened so that it fitted the grips of the test machine.

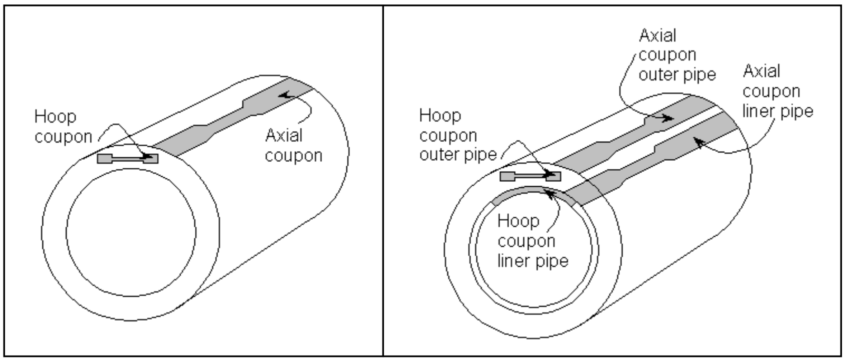

Figure 3.1 Coupons for the tensile testing in the axial and hoop directions taken from the single walled pipe (left) and from the liner pipe and the outer pipe of a Tight Fit Pipe (right)

3.3.2 Test Results

The stress strain diagram between 0 % and 5 % strain of the ORANGE Tight Fit Pipe can be seen in Figure 3.2. This stress strain diagram is taken as an example; the stress strain diagrams of the other 12.75 inch Tight Fit Pipes and the stress strain diagrams of the 12.75 inch single walled pipes can be found in Appendix III. Tensile testing was not performed on the 10.75 inch Tight Fit Pipe, but the material characteristics of this Tight Fit Pipe have been received from Kuroki T&P.

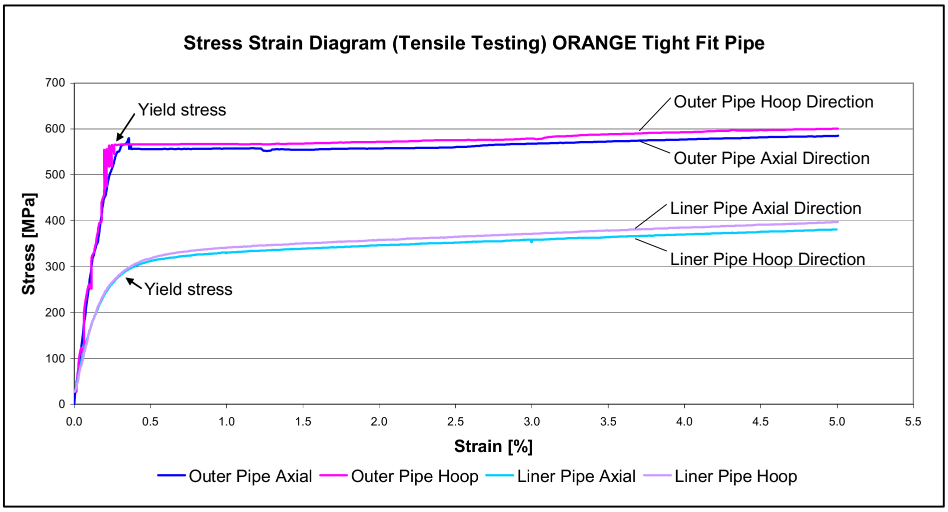

Figure 3.2 Stress strain diagram of the ORANGE Tight Fit Pipe between 0 % and 5 % strain determined in the tensile testing

Figure 3.2 indicates that the material first experiences elastic deformation after which it reaches the yield stress. Subsequently the material experiences plastic deformation while strain hardening occurs as well. The stress strain diagrams of the liner pipe and the outer pipe were determined in the axial and hoop directions. The tested specimens of the 12.75 inch Tight Fit Pipe's liner pipe and outer pipe, as well as those of the two single walled 12.75 inch pipes, taken from the pipes in the axial and hoop directions, can be seen in Figure 3.3.

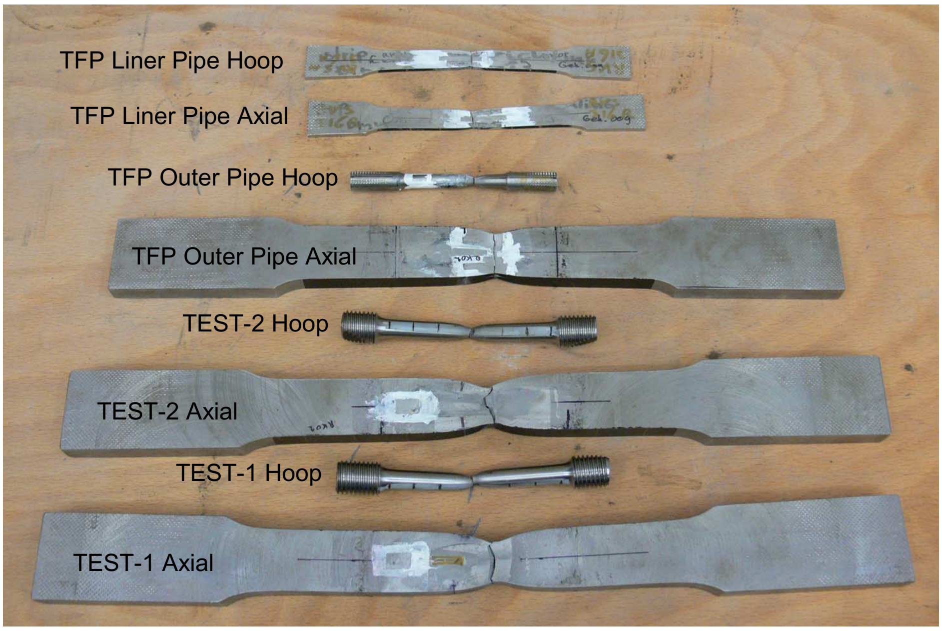

Figure 3.3 Coupons in the axial and hoop directions, after performance of the tensile testing

Characteristics of the 10.75 inch Tight Fit Pipe, the three 12.75 inch Tight Fit Pipes and the two single walled pipes (TEST-1 and TEST-2) can be found in Table 3.2. For each of the pipes, material characteristics are provided such as the Young's modulus ($E_{L;a}$, $E_{O;a}$ and E_O), the yield strengths in the axial direction ($\sigma_{L;y;a}$, $\sigma_{O;y;a}$, $\sigma_{y;a}$), the yield strengths in the hoop direction ($\sigma_{L;y;h}$, $\sigma_{O;y;h}$, $\sigma_{y;h}$), the tensile strengths in the axial direction ($\sigma_{L;t;a}$, $\sigma_{O;t;a}$, $\sigma_{t;a}$) and the tensile strengths in the hoop direction ($\sigma_{L;t;h}$, $\sigma_{O;t;h}$, $\sigma_{t;h}$). The yield strengths of the materials in the axial and hoop directions were derived from the stress strain diagrams which can be found in Appendix III. The yield stress is defined as the stress needed to cause 0.2 % permanent elongation in the material after unloading. The Poisson ratios of the pipes (ν, ν_L and ν_O) are assumed 0.3. In Table 3.2 also the geometric properties such as the outer diameter and the wall thicknesses of the 10.75 and 12.75 inch Tight Fit Pipes ($d_{O;o;TFP}$, t_L, t_O) are presented as well as the outer diameter and the wall thicknesses of the 12.75 inch single walled pipes (d_o and t). Geometric properties of the pipes were measured using a sliding calliper or measuring tape. The residual liner pipe hoop stresses of the Tight Fit Pipes (σ_{res}) are also stated in Table 3.2. Determination of the residual liner pipe hoop stresses of these Tight Fit Pipes is described in Subsection 3.4.2.

Table 3.2 Material and geometric characteristics of pipes used in this research

		WHITE	ORANGE	GREEN	TEST-1	TEST-2
σ_{res} [MPa]	-187	-53	-178	-199	-	-
		low	high	high		
OP Material	X65	X65	X65	X65	X52	X52
LP Material	304L	316L	316L	316L	-	-
OP Type	seam-less	ERW	ERW	ERW	seam-less	seam-less
d_o or $d_{O;o;TFP}$ [inch]	10.75	12.75	12.75	12.75	12.75	12.75
$d_{O;o;TFP}$ [mm]	273.10	324.55	324.70	324.85	322.93	323.72
t or t_O [mm]	9.30	14.35	14.48	14.53	21.77	18.65
$d_{L;o;TFP}$ [mm]	249.6	295.85	295.74	295.79	-	-
t_L [mm]	2.45	3.00	2.93	2.95	-	-
$\sigma_{L;y;a}$ [MPa]	308	308	298	295	-	-
$\sigma_{L;t;a}$ [MPa]	-	-	548	552	-	-
$\sigma_{L;y;h}$ [MPa]	-	-	305	286	-	-
$\sigma_{L;t;h}$ [MPa]	-	-	572	570	-	-
$\sigma_{y;a}$ or $\sigma_{O;y;a}$ [MPa]	-	538	556	563	361	354
$\sigma_{t;a}$ or $\sigma_{O;t;a}$ [MPa]	-	-	595	596	500	503
$\sigma_{y;h}$ or $\sigma_{O;y;h}$ [MPa]	-	-	566	588	366	361
$\sigma_{t;h}$ or $\sigma_{O;t;h}$ [MPa]	-	-	609	624	519	521
$E_{L;a}$ [MPa]	193190	193000	193000	193000	-	-
E_a or $E_{O;a}$ [MPa]	200000	200000	200000	200000	200000	200000

Note:
OP: Outer pipe
LP: Liner pipe
ERW: Electric resistance welded
The Young's modulus of the liner pipe ($E_{L;a}$) of the 10.75 inch Tight Fit Pipe was received from Kuroki T&P measurements while the Young's modulus of the liner pipe of the 12.75 inch Tight Fit Pipe was obtained from Reference [67]. The Young's moduli of the outer pipes of the 10.75 and 12.75 inch Tight Fit Pipes were obtained from Reference [68].

3.4 Tight Fit Pipe Mechanical Bonding Strength

3.4.1 Saw Cutting Tests

3.4.1.1 Test Set-up

Two saw cutting tests were performed on the 10.75 inch Tight Fit Pipe to investigate how the magnitude of the mechanical bonding strength in a Tight Fit Pipe ring is influenced by cutting this Tight Fit Pipe ring from a longer Tight Fit Pipe section [16]. While cutting two rings of Tight Fit Pipe from the 10.75 inch Tight Fit Pipe section, the change in the axial strain in the liner pipe was measured using several uni-axial strain gauges at the inside of the Tight Fit Pipe along the longitudinal axis (Figure 3.4). Moreover, in the first saw cutting test, three bi-axial strain gauges were attached to the liner pipe, in the middle of the 200 mm long Tight Fit Pipe ring to be cut off (so 100 mm from the edge). In the second test, also 100 mm from the edge of the Tight Fit Pipe ring, three bi-axial strain gauges were attached to the inside of the liner pipe and to the outside of the outer pipe. The bi-axial strain gauges provided information on the changes in the residual axial and hoop strains in the Tight Fit Pipe ring cut from the longer Tight Fit Pipe section. From these strain changes measured in the Tight Fit Pipe ring, the change in the residual liner pipe hoop stress, i.e. the change in the mechanical bonding strength in the Tight Fit Pipe ring, was determined.

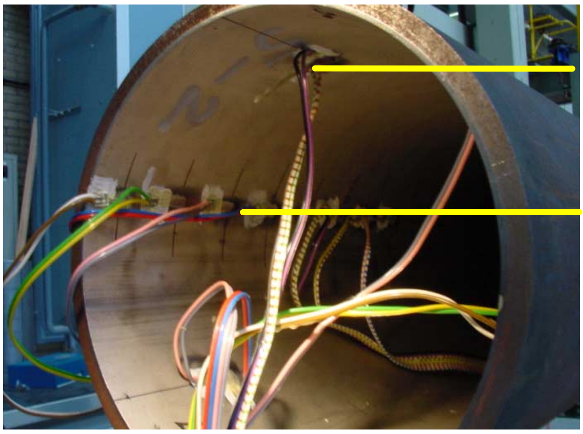

Figure 3.4 Uni-axial strain gauges positioned along the longitudinal axis and bi-axial strain gauges positioned in the middle of the test specimen cut in the saw cutting test

3.4.1.2 Test Results

The changes in the axial and hoop strains measured by the bi-axial strain gauges (Figure 3.4) in the two Tight Fit Pipe rings while cutting them from a longer Tight Fit Pipe section can be found in Table 3.3 to Table 3.5. The changes in the axial and hoop stresses in the two Tight Fit Pipe rings due to cutting them from a longer Tight Fit Pipe section were calculated using Equations (3.1) and (3.2) together with these measured axial and hoop strains [1]. These results are also presented in Table 3.3 and Table 3.5. The material characteristics used in Equations (3.1) and (3.2) can be found in Table 3.2. In Table 3.3 to Table 3.5 a minus indicates a compression stress or strain while a positive sign refers to a tensile stress or strain.

$$\sigma_{L;h} = \frac{E_L}{\left(1-(\nu_L)^2\right)} \cdot \left(\frac{\Sigma \varepsilon_{L;h}}{j} + \nu_L \cdot \frac{\Sigma \varepsilon_{L;a}}{j} \right) \tag{3.1}$$

$$\sigma_{L;a} = \frac{E_L}{\left(1-(\nu_L)^2\right)} \cdot \left(\frac{\Sigma \varepsilon_{L;a}}{j} + \nu_L \cdot \frac{\Sigma \varepsilon_{L;h}}{j} \right) \tag{3.2}$$

Table 3.3 Changes in the strains and stresses in the liner pipe, 100 mm from the edge, for the first 200 mm Tight Fit Pipe ring, cut from the Tight Fit Pipe section

	Strain [μ]	Stress [MPa]
Average change in the axial strain and stress in the middle of the Tight Fit Pipe which is cut off	21	3
Average change in the hoop strain and stress in the middle of the Tight Fit Pipe which is cut off	-23	-4

Table 3.4 Changes in the strains and stresses in the liner pipe, 100 mm from the edge, for the second 200 mm Tight Fit Pipe ring, cut from the Tight Fit Pipe section

	Strain [μ]	Stress [MPa]
Average change in the axial strain and stress in the middle of the Tight Fit Pipe which is cut off	49	9
Average change in the hoop strain and stress in the middle of the Tight Fit Pipe which is cut off	-30	-3

Table 3.5 Changes in the strains and stresses in the outer pipe, 100 mm from the edge, for the second 200 mm Tight Fit Pipe ring, cut from the Tight Fit Pipe section

	Strain [μ]	Stress [MPa]
Average change in the axial strain and stress in the middle of the Tight Fit Pipe which is cut off	-6	-3
Average change in the hoop strain and stress in the middle of the Tight Fit Pipe which is cut off	-26	-6

Table 3.3 and Table 3.4 indicate that the liner pipe of the Tight Fit Pipe ring became longer due to cutting this ring from the longer Tight Fit Pipe section. This can be explained by the fact that saw cutting caused a change in the axial friction between the liner pipe and the outer pipe at the cutting location. This caused a decrease in the

compressive axial stress in the liner pipe present after manufacturing the Tight Fit Pipe. At the same time the change in the axial friction between the liner pipe and the outer pipe resulted in a decrease in the tensile axial stress in the outer pipe, present after manufacturing the Tight Fit Pipe, thereby causing the outer pipe of the Tight Fit Pipe ring to become shorter (Figure 3.5). In Table 3.4 and Table 3.5 it can be seen that in the Tight Fit Pipe ring both the liner pipe and the outer pipe became smaller in diameter and no gap occurred between the outer pipe and the liner pipe. It should be taken into consideration that the measured values of the axial and hoop strains are relatively small.

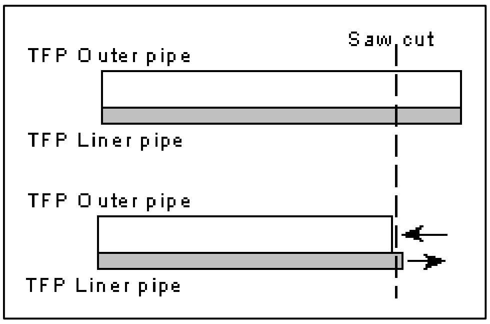

Figure 3.5 Saw cutting a Tight Fit Pipe and the influence this has on the behaviour of the liner pipe and the outer pipe

Table 3.3 and Table 3.4 show that the influence on the mechanical bonding strength in a Tight Fit Pipe ring, when cutting this ring from a longer Tight Fit Pipe section is marginal; the residual liner pipe hoop stress of this 10.75 inch outer diameter Tight Fit Pipe ring was 187 MPa (Subsection 3.4.2).

The influence of cutting a Tight Fit Pipe ring from a longer Tight Fit Pipe section extends approximately 250 mm (one diameter) into the longer Tight Fit Pipe section for this 10.75 inch Tight Fit Pipe (Figure 3.6).

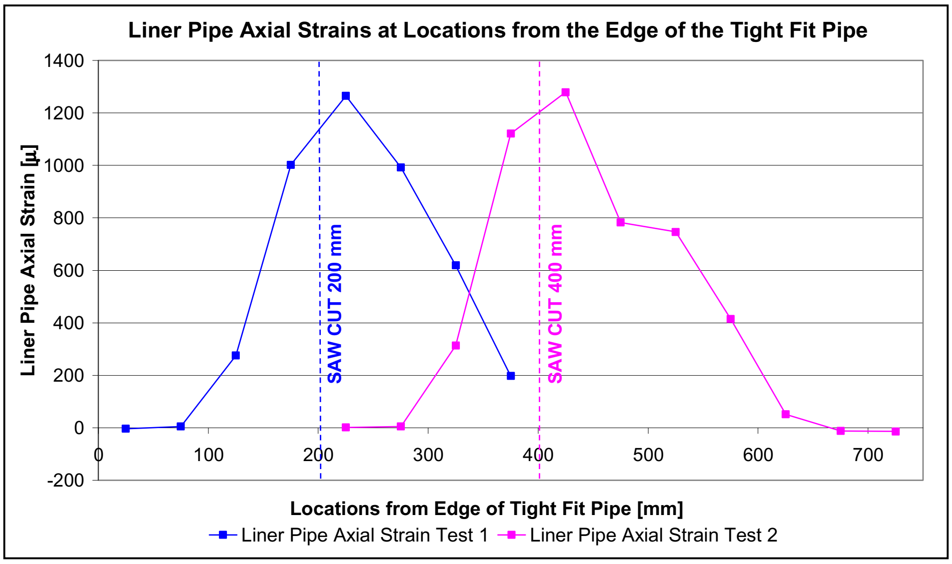

Figure 3.6 Change in the axial liner pipe strain due to saw cutting a Tight Fit Pipe ring from a Tight Fit Pipe section (test results from the uni-axial strain gauges (Figure 3.4))

3.4.2 Residual Compressive Stress Test

3.4.2.1 Test Set-up

In the residual compressive stress test, the corrosion resistant alloy liner pipe is taken out of the outer pipe restriction by saw cutting the outer pipe over the length of a Tight Fit Pipe ring (Figure 3.7) [1]. Three bi-axial strain gauges were placed on the inside surface of the corrosion resistant alloy liner pipe of this Tight Fit Pipe ring. The changes in the hoop and the axial strains were measured in the tests and the residual hoop and axial stresses were calculated using Equations (3.1) and (3.2) [1] as well as the material characteristics from Table 3.2.

The mechanical bonding strengths of each of the 12.75 inch Tight Fit Pipes, used in full scale bending tests, were determined using the residual compressive stress test. This was done prior to bend testing these Tight Fit Pipes in the full scale bending rig. Due to restrictions in the availability of the 12.75 inch Tight Fit Pipe and also because the exact length of Tight Fit Pipe ring to be used in this test is not specified in the applicable codes [1], 100 mm long Tight Fit Pipe rings were used.

In order to become familiar with the experimental determination of the bonding strength of a Tight Fit Pipe and due to the limitation of the available 12.75 inch Tight Fit Pipe, the residual compressive stress tests were performed first on the 10.75 inch Tight Fit Pipe [16], before these tests were executed on the 12.75 inch Tight Fit Pipes. Seven 10.75 inch Tight Fit Pipe rings with different lengths were used in these tests to investigate whether the length of the ring influenced the measured changes in the axial and hoop strains.

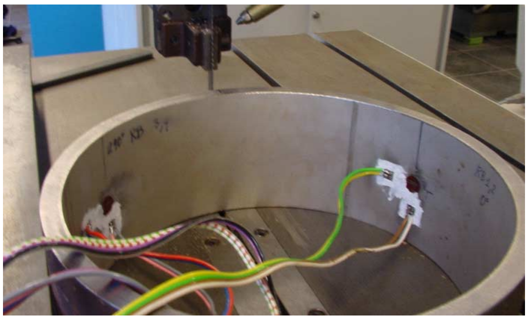

Figure 3.7 Taking the corrosion resistant alloy liner pipe out of the 10.75 inch Tight Fit Pipe outer pipe in the residual compressive stress test

3.4.2.2 Test Results

Table 3.6 indicates that the length of the Tight Fit Pipe ring (L_{TFP}) has negligible influence on the hoop strain ($\varepsilon_{L;h}$) measured. The length of the specimen does influence the axial strain ($\varepsilon_{L;a}$) measured, however. For the 50 and 100 mm Tight Fit Pipe specimens, the liner pipe became shorter after the residual compressive stress test, while for the 200 mm Tight Fit Pipe specimens, the liner pipe became longer after cutting away the outer pipe. Using the measured hoop and axial strains, the residual liner pipe hoop stress ($\sigma_{L;h}$) and the residual liner pipe axial stress ($\sigma_{L;a}$) can be determined using Equations (3.1) and (3.2). In Table 3.6 a minus indicates a compression stress or strain while a positive sign refers to a tensile stress or strain.

Table 3.6 Residual compressive liner pipe hoop and axial strains and stresses measured in the 10.75 inch Tight Fit Pipe

Test	1	2	3	4	5	6	7
L_{TFP} [mm]	50	50	100	100	200	200	200
$\varepsilon_{L;h}$ [μ]	895	786	941	823	800	874	837
$\varepsilon_{L;a}$ [μ]	-224	-239	-145	-98	196	251	67
$\sigma_{L;h} = \sigma_{res}$ [MPa]	-176	-152	-190	-169	-182	-201	-182
$\sigma_{L;a}$ [MPa]	-9	1	-29	-32	-93	-109	-68

It was expected in the residual compressive stress test that the liner pipe became larger in diameter and longer in length. This expectation resulted from the fact that when the outer pipe shrinks around the liner pipe during the manufacturing process of Tight Fit Pipe, a compressive hoop strain and a compressive axial strain are being generated in the liner pipe. This results in a smaller diameter and shorter length of the liner pipe. In the residual compressive stress test, the phenomenon that the removal of the outer pipe causes the liner pipe to expand in length (axial direction) and in diameter (radial direction) is for the moment identified as **phenomenon I** (Figure 3.8). Phenomenon I is the opposite of the axial and radial shrinkage of the liner pipe during manufacturing.

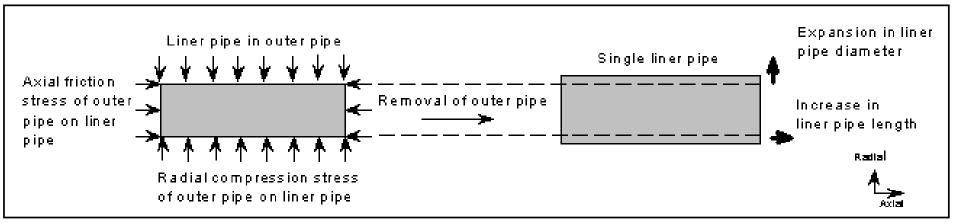

Figure 3.8 Phenomenon I, an increase of the diameter and the length of the liner pipe due to the outer pipe removal

For a short piece of Tight Fit Pipe, the axial friction between the liner pipe and the outer pipe is relatively more distorted by saw cutting than in case of a longer piece of Tight Fit Pipe. The axial friction between the liner pipe and the outer pipe compresses the liner pipe in the axial direction. When relatively more axial friction between the liner pipe and the outer pipe is disrupted, the liner pipe is less compressed axially. When the outer pipe is then subsequently cut from the inner pipe during the residual compressive stress test, the radial strain change is positive and is related to a negative axial strain change. The material needed for the increase in diameter needs to be obtained from a decrease in axial direction through the Poisson ratio. For the moment this phenomenon is identified as **phenomenon II** (Figure 3.9).

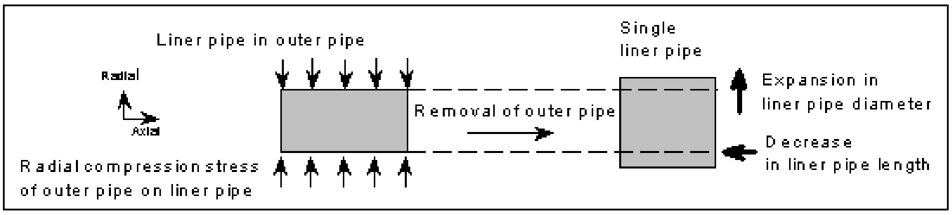

Figure 3.9 Phenomenon II, an increase of the liner pipe diameter and a decrease of the liner pipe length, due to the outer pipe removal

In the residual compressive stress tests, phenomenon II, indicating a positive radial strain change related to a negative axial strain change, dominated for the 50 mm and 100 mm Tight Fit Pipe specimens. Phenomenon I, indicating a positive radial strain change related to a positive axial strain change, dominated for the 200 mm test pieces. With an increase in the Tight Fit Pipe specimen length in the residual compressive stress test, phenomenon I (an increase in the liner pipe diameter and length at the outer pipe removal) becomes increasingly dominant.

So, in a 100 mm long Tight Fit Pipe specimen less axial friction is present between the liner pipe and the outer pipe to compress the liner pipe axially than in a 200 mm specimen [43] or in an even longer Tight Fit Pipe section. The liner pipe in the 100 mm long Tight Fit Pipe is therefore less axially compressed than the liner pipe in the 200 mm Tight Fit Pipe specimen or the liner pipe in an even longer Tight Fit Pipe section. When the outer pipe is removed from the liner pipe in the residual compressive stress test, less positive axial strain is therefore measured in the 100 mm long Tight Fit Pipe than is measured in a 200 mm piece of Tight Fit Pipe. In a 100 mm long Tight Fit Pipe, less axial strain contributes to the compressive residual liner pipe hoop stress than in a 200 mm Tight Fit Pipe or in an even longer Tight Fit Pipe section (Equations (3.1) and (3.2) and Table 3.2). It should therefore be taken into account that the residual compressive stress test on a short piece of Tight Fit Pipe provides an underestimation of the residual liner pipe hoop stress in a longer Tight Fit Pipe section (Table 3.6). Table 3.6 also indicates that with an increase in the Tight Fit Pipe length from 50 mm to 100 mm to 200 mm, the residual liner pipe axial stress becomes more compressive.

Results for the measured hoop and axial strains in the 100 mm long (L_{TFP}) 12.75 inch Tight Fit Pipe rings can be found in Table 3.7. The residual liner pipe hoop stress ($\sigma_{L;h}$) and the residual liner pipe axial stress ($\sigma_{L;a}$) are determined from the measured hoop and axial strains ($\varepsilon_{L;h}$ and $\varepsilon_{L;a}$) using Equations (3.1) and (3.2) and the material characteristics of the 12.75 inch Tight Fit Pipes as stated in Table 3.2.

Table 3.7 Residual compressive liner pipe hoop and axial strains and stresses measured in the 12.75 inch Tight Fit Pipes

	WHITE		ORANGE		GREEN	
	1	2	3	4	5	6
L_{TFP} [mm]	100	100	100	100	100	100
$\varepsilon_{L;h}$ [μ]	296	309	1049	907	1074	1086
$\varepsilon_{L;a}$ [μ]	-157	-182	-426	-484	-481	-475
$\sigma_{L;h} = \sigma_{res}$ [MPa]	-53	-54	-195	-162	-197	-200
$\sigma_{L;a}$ [MPa]	15	19	24	45	34	32
Average $\sigma_{L;h}$ [MPa]	-53		-178		-199	

Table 3.7 shows that for the different 12.75 inch Tight Fit Pipes an increase in the positive hoop strain correlates to an increase in negative axial strain. An increase in positive hoop strain means that the liner pipe became larger in diameter in the residual compressive stress test. An increase in negative axial strain indicates that the liner pipe became shorter in length in the residual compressive stress test. The material needed for the increase in diameter was provided for by the decrease in material in length

through the Poisson ratio. So, for the 100 mm long 12.75 inch Tight Fit Pipe ring, Phenomenon II, described above, dominates over phenomenon I (Figure 3.9).

As mentioned before, the residual compressive stress test on a 100 mm long 12.75 inch Tight Fit Pipe cannot provide an indication of the residual axial stress present in the liner pipe in a longer Tight Fit Pipe section. It can be seen in Table 3.7 that the residual axial stress (determined from 100 mm long 12.75 inch Tight Fit Pipe specimens) is a tension stress, while according to theory the residual axial stress in the liner pipe in a longer Tight Fit Pipe section has to be compressive. If the residual compressive stress tests would be performed on 200 mm long 12.75 inch Tight Fit Pipe specimens, the residual axial liner pipe stress is expected to be more compressive due to the increase in the axial friction present between the liner pipe and the outer pipe.

In order to provide an indication of the variation in the residual liner pipe hoop stress within one Tight Fit Pipe, fabricated in a 12 m length, several residual compressive stress test results are compared to each other in Table 3.8.

Table 3.8 Variation in the residual liner pipe hoop stresses in the Tight Fit Pipes

	$\sigma_{L;h}$ = σ_{res} [MPa]	Δ [%]
10.75 inch Tight Fit Pipe - 50 mm	-176	16
10.75 inch Tight Fit Pipe - 50 mm	-152	
10.75 inch Tight Fit Pipe - 100 mm	-190	13
10.75 inch Tight Fit Pipe - 100 mm	-169	
10.75 inch Tight Fit Pipe - 200 mm	-182	11
10.75 inch Tight Fit Pipe - 200 mm	-201	
10.75 inch Tight Fit Pipe - 200 mm	-182	
12.75 inch Tight Fit Pipe - 100 mm WHITE	-53	2
12.75 inch Tight Fit Pipe - 100 mm WHITE	-54	
12.75 inch Tight Fit Pipe - 100 mm ORANGE	-195	20
12.75 inch Tight Fit Pipe - 100 mm ORANGE	-162	
12.75 inch Tight Fit Pipe - 100 mm GREEN	-197	2
12.75 inch Tight Fit Pipe - 100 mm GREEN	-200	

Note:

Δ [%] The most negative value minus the least negative value divided by the least negative value; e.g. ((-176 MPa + 152 MPa)/ 152 MPa) = 16 %)

Table 3.8 shows that there are differences in the residual liner pipe hoop stress ($\sigma_{L;h}$ = σ_{res}) along the Tight Fit Pipe, varying between 2 % and 20 % for the 10.75 and 12.75 inch Tight Fit Pipes. The 12.75 inch WHITE, ORANGE and GREEN Tight Fit Pipe rings used in the residual compressive stress tests were taken out of the longer Tight Fit Pipe sections next to each other. The 10.75 inch Tight Fit Pipe specimens were taken out of the Tight Fit Pipe at random locations.

3.4.3 Liner Pipe Push Out Test

3.4.3.1 Test Set-up

The principle of the liner pipe push out test is that the liner pipe is being pushed out of the outer pipe and the required (static) force ($F_{L;push}$) is recorded. The push out force depends on the radial contact force (σ_C) between the liner pipe and the outer pipe and the coefficient of friction μ [13]. The coefficient of friction depends on the roughness of the liner pipe, the roughness of the outer pipe and dirt, oil, oxides, etc. present in between the liner pipe and the outer pipe. The push out force is a measure for the axial load transfer between the liner pipe and the outer pipe (the axial friction (τ_C)) and thus for the mechanical bonding strength in a Tight Fit Pipe indicated by the residual liner pipe hoop stress ($\sigma_{L;h}$) (Equations (3.3) to (3.6)).

$$F_{L;push} = \tau_C \cdot A_{L;o;TFP} \tag{3.3}$$

$$\tau_C = \sigma_C \cdot \mu \tag{3.4}$$

$$A_{L;o;TFP} = \pi \cdot 2 \cdot r_{L;o;TFP} \cdot L_{TFP} \tag{3.5}$$

$$\sigma_C = \frac{t_L \cdot \sigma_{L;h}}{r_{L;o;TFP}} \tag{3.6}$$

For three different lengths of 10.75 inch Tight Fit Pipe (50 mm, 100 mm and 200 mm) the liner pipe was pushed out of the outer pipe (Figure 3.10). Three uni-axial strain gauges were attached on the inside of the liner pipe at respectively 60° (SG1), 180° (SG2) and 300° (SG3) of the circumference. These were located at the same positions as the displacement measuring devices on the outside (HP1, HP2 and HP3).

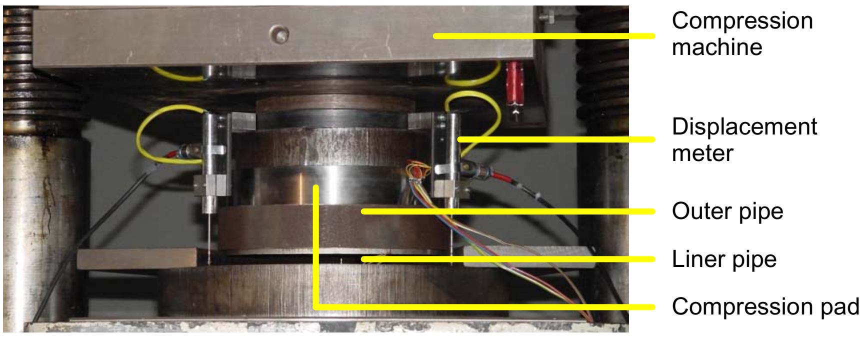

Figure 3.10 Liner pipe push out test: pushing the liner pipe out of the outer pipe

3.4.3.2 Test Results

Table 3.9 indicates that the (static) push out force ($F_{L;push}$) increases with an increase in the Tight Fit Pipe length. In Figure 3.11 it can be seen that the relation between the length of the Tight Fit Pipe specimen (L_{TFP}) and the required push out force ($F_{L;push}$) is polynomial. This is the result of geometrical stiffening occurring as a result of the relatively higher push out force together with the Poisson ratio for longer Tight Fit Pipe specimen in the liner pipe push out tests. For longer lengths of Tight Fit Pipe specimen, the liner pipe is pushed harder against the outer pipe, which results in a higher radial contact stress, a higher axial friction between the liner pipe and the outer pipe and thus in turn, in a high push out force.

Table 3.9 Test data from the liner pipe push out tests on 10.75 inch Tight Fit Pipe

Test	1	2	3	4	5	6
L_{TFP} [mm]	50	50	100	100	200	200
$F_{L;push}$ [KN]	-41	-63	-122	-135	-374	-316
$\sigma_{L;h}$ [MPa]	-164	-164	-180	-180	-188	-188
μ [-]	0.32	0.51	0.44	0.49	0.63	0.54
$\varepsilon_{L;a}$ [μ]	-	-186	144	125	734	547

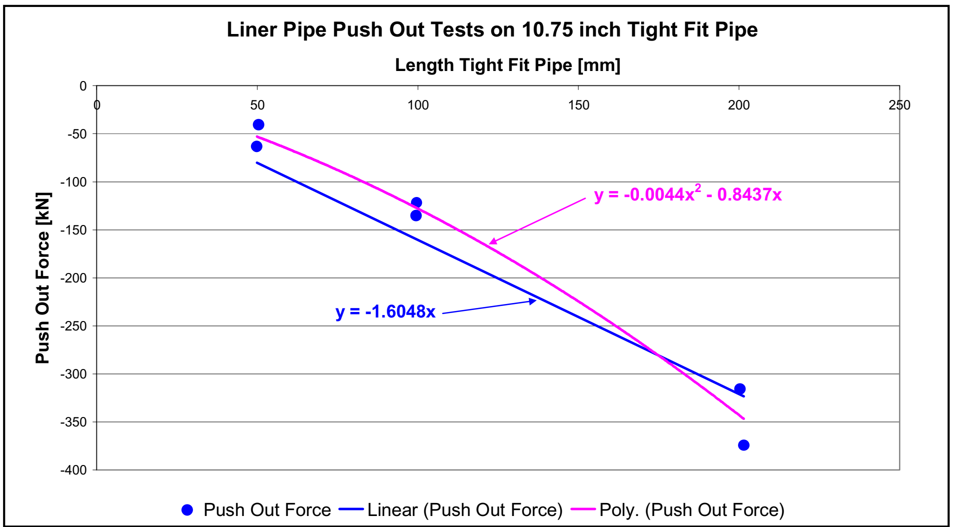

Figure 3.11 Relations between the liner pipe push out force and the length of the Tight Fit Pipe specimens

In order to predict the residual liner pipe hoop stress from the push out force, the friction coefficient between the liner pipe and the outer pipe needs to be known. The friction coefficient of the 10.75 inch Tight Fit Pipe is not known. This friction coefficient can be determined using Table 3.2 and Equations (3.3) to (3.6), however. Due to the polynomial increase of the liner pipe push out force with increasing Tight Fit Pipe length, the derived friction coefficient (using Equations (3.6) to (3.3)) also seems to have a polynomial increase with an increase in the Tight Fit Pipe length (Table 3.9). This is of course not correct, since the friction coefficient is a constant value not dependent on the Tight Fit Pipe length. If a friction coefficient of e.g. 0.32 is taken from the measurements (the lowest friction coefficient determined in the liner pipe push out tests on different lengths of 10.75 inch Tight Fit Pipe) and if the compressive residual liner pipe hoop stress is calculated from the liner pipe push out force for e.g. the 200 mm long Tight Fit Pipe specimen, a very high and unrealistic value for the residual liner pipe hoop stress is obtained. This is the result of the geometrical stiffening as a consequence of the relatively high push out force together with the Poisson ratio for long Tight Fit Pipe test lengths in the liner pipe push out tests.

It can therefore be concluded that if the liner pipe push out test is used to determine the strength of the mechanical bond between the liner pipe and the outer pipe, it is advised to use a short Tight Fit Pipe specimen (e.g. 50 mm). The mechanical bonding strength between the liner pipe and the outer pipe in the Tight Fit Pipe is then minimally influenced by the test method.

The liner pipe push out tests indicate, in agreement with the residual compressive stress tests, that the liner pipe of the 50 mm long Tight Fit Pipe specimens become shorter (a negative axial strain ($\varepsilon_{L;a}$) in Table 3.9) after the liner pipe was pushed out of the outer pipe while the liner pipes from the 100 mm and 200 mm long Tight Fit Pipe specimens became longer in length (a positive axial strain ($\varepsilon_{L;a}$) in Table 3.9). So, for the 50 mm Tight Fit Pipe rings, Phenomenon II (Figure 3.9) was dominant, while for the 100 mm and 200 mm specimens, Phenomenon I (Figure 3.8) was more pronounced.

3.4.4 Comparison of the Residual Compressive Stress Test with the Liner Pipe Push Out Test

As mentioned earlier, two different test methods can be used to quantify the mechanical bonding strength between the liner pipe and the outer pipe in the Tight Fit Pipe. The residual compressive stress test quantifies the residual liner pipe hoop stress while the liner pipe push out test results in a (static) push out force. Both parameters are a measure for the mechanical bonding strength between the liner pipe and the outer pipe in the Tight Fit Pipe.

When comparing the residual compressive stress test with the liner pipe push out test, a preference tends to go to the residual compressive stress test. The main reason for this is that the outcome of the liner pipe push out test, the liner pipe push out force, depends on the length of the Tight Fit Pipe test specimen. In the residual compressive stress test, the outcome, namely the residual liner pipe hoop stress, depends to a much lesser extent on the length of the Tight Fit Pipe test specimen. This makes the residual compressive stress test a more robust test to identify the mechanical bonding strength between the liner pipe and the outer pipe in a Tight Fit Pipe.

3.5 Conclusions

The mechanical bonding strength between the liner pipe and the outer pipe in a Tight Fit Pipe section can be determined experimentally on a ring of Tight Fit Pipe, which is cut from this section. Two different test methods were executed to quantify the mechanical bonding strength of the Tight Fit Pipes used in this research. The residual compressive stress test quantifies the residual liner pipe hoop stress as an indication of the mechanical bonding strength. The liner pipe push out test results in a liner pipe push out force as an indication of the mechanical bonding strength. When comparing both tests, preference tends to go to the residual compressive stress test. The outcome of this test, namely the residual liner pipe hoop stress, depends to a lesser extent on the length of the Tight Fit Pipe test specimen than in case of the liner pipe push out force. This makes the residual compressive stress test a more robust test to determine the mechanical bonding strength of a Tight Fit Pipe section.

It can also be concluded that cutting a ring of Tight Fit Pipe from a longer Tight Fit Pipe section did not significantly influence the mechanical bonding strength in this ring.

Determining the mechanical bonding strength of a Tight Fit Pipe is of importance because part of the overall research aim is to experimentally determine the influence of the mechanical bonding strength on liner pipe wrinkling during reeling.

4 Behaviour of Tight Fit Pipe under Axial Compression

4.1 Introduction

Buckling of pipes due to bending correlates in a number of respects to buckling of axially compressed pipes: the buckling mode shapes are similar, snap buckling may occur and the buckling stress is sensitive to initial imperfections [44]. Moreover, an axial compression machine was readily available in the laboratory, while the full scale bending rig still had to be built. Therefore, prior to carrying out bending tests on Tight Fit Pipe, axial compression tests on Tight Fit Pipe were performed in order to gain a better understanding of the behaviour of Tight Fit Pipe under compression.

In Subsection 4.2 an overview of the three types of axial compression tests on Tight Fit Pipe as executed in this research is presented. The three types of axial compression tests are subsequently described in Subsections 4.3, 4.4 and 4.5.

4.2 Overview of the Axial Compression Tests

The axial compression tests were performed on two Tight Fit Pipe configurations:

1. A 10.75 inch outer diameter Tight Fit Pipe with a 2.45 mm thick, 304L liner pipe (with a longitudinal weld) and a 9.3 mm thick, X65, seamless outer pipe.
2. A 12.75 inch outer diameter Tight Fit Pipe with a 3.0 mm thick, 316L liner pipe (with a longitudinal weld) and a 14.3 mm thick, X65, electric resistance welded outer pipe.

The material and geometric properties of these two Tight Fit Pipes as well as their mechanical bonding strengths can be found in Table 3.2. In this chapter, three types of axial compression tests performed on the 10.75 and 12.75 inch Tight Fit Pipe are described:

1. Buckling of the single liner pipe
2. Buckling of the liner pipe confined and pre-stressed in the outer pipe
3. Buckling of the integral Tight Fit Pipe

1. Buckling of the single liner pipe

The liner pipes were removed from the Tight Fit Pipe configuration in the residual compressive stress tests (Subsection 3.4.2) and in the liner pipe push out tests

(Subsection 3.4.3) and subsequently loaded and buckled under axial compression. These tests were performed on liner pipes from the 10.75 and 12.75 inch Tight Fit Pipe.

2. Buckling of the liner pipe confined and pre-stressed in the outer pipe

In the Tight Fit Pipe configuration, only the liner pipe was loaded and buckled due to axial compression while positioned and pre-stressed inside the outer pipe. For the 10.75 inch test specimens, one value of liner pipe pre-stress (i.e. one value of the residual liner pipe hoop stress) was used, whilst for the 12.75 inch test specimens, two different values of pre-stress were employed.

3. Buckling of the integral Tight Fit Pipe

The combined liner pipe and outer pipe (the composite Tight Fit Pipe) were loaded and buckled under axial compression. A 10.75 inch test specimen with one value for the liner pipe pre-stress, i.e. with one value for the residual liner pipe hoop stress, was used.

The three types of tests were performed to establish the difference in buckling strength and deformation capacity between the single liner pipe (axial compression test 1) and the liner pipe while confined and pre-stressed in the outer pipe (axial compression tests 2 and 3).

Due to the very gradual occurrence of local buckles and the fact that the first signs of a local buckle (which can occur before the maximum axial force) is rather uncertain [25], the buckling force in the axial compression tests is identified as the maximum axial force that can be applied on the test specimen (Figure 4.1). The buckling strain is defined as the strain occurring when the buckling force is reached at the peak of the curve.

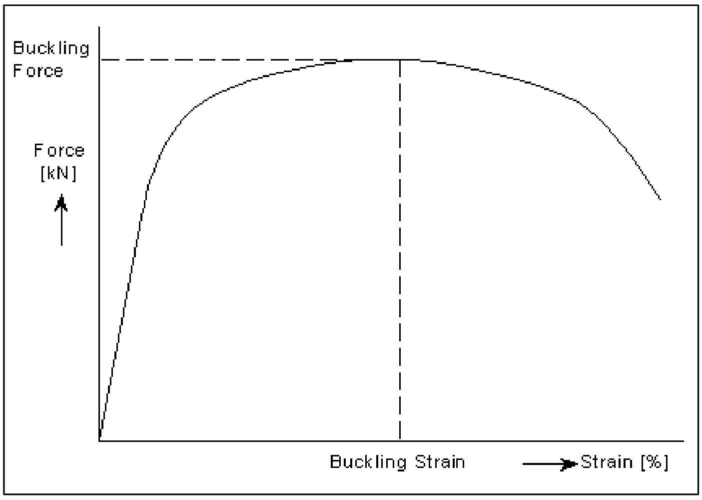

Figure 4.1 Definition of the buckling force and the buckling strain (figure not to scale)

4.3 Buckling of the Single Liner Pipe (Test Type 1)

4.3.1 Objective of the Tests

The objective of the buckling tests on liner pipes from the 10.75 and 12.75 inch outer diameter Tight Fit Pipe was to establish the buckling behaviour of the single liner pipe. A second objective of the buckling tests on the liner pipe, obtained from the 12.75 inch Tight Fit Pipe, was to determine whether the residual liner pipe hoop stress (Figure 1.3), which was present in the liner pipe as a result of the Tight Fit Pipe manufacturing process, influenced the axial buckling capacity of the liner pipe alone. The residual liner pipe hoop stress was removed by cutting the outer pipe from the liner pipe in the residual compressive stress tests described in Subsection 3.4.2.

4.3.2 Test Set-up for Buckling of the Liner Pipe Isolated from the 10.75 Inch Tight Fit Pipe

The test set-up of the buckling tests on the liner pipe from the 10.75 inch Tight Fit Pipe can be seen in Figure 4.2. An extra hinge with low friction was positioned on top of a compression pad (Figure 4.3) between the liner pipe and the compression machine to ensure that the compression machine did not bend the pipe. In the single liner pipe buckling tests, as described in this subsection, the compression pad functioned as a support for the extra hinge. However, the compression pad was designed to be utilized in the liner pipe buckling tests when the liner pipe was confined and pre-stressed inside the outer pipe (axial compression test type 2). The compression pad exactly fitted the liner pipe and did not touch the outer pipe. Therefore it compressed the liner pipe only.

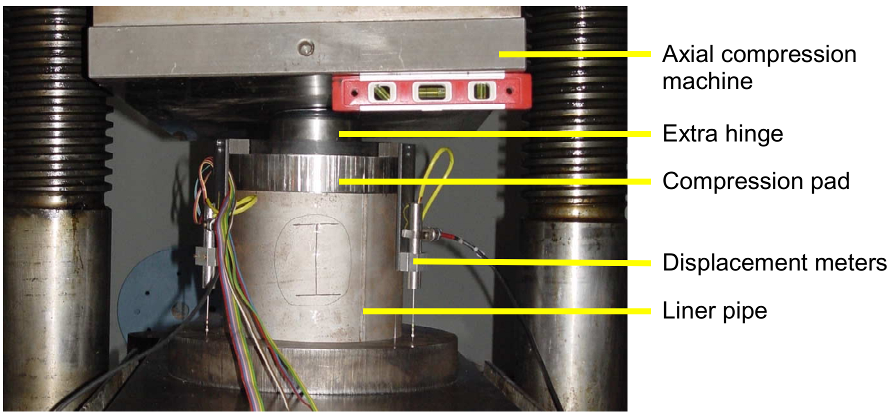

Figure 4.2 Test set-up for the liner pipe from the 10.75 inch Tight Fit Pipe

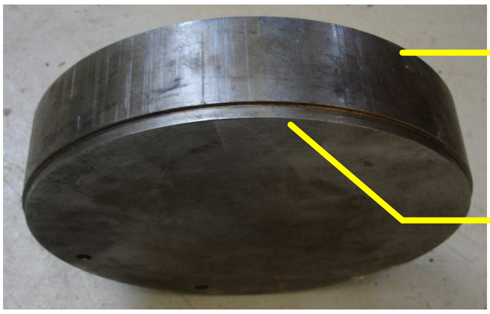

Figure 4.3 Compression pad

Some of the test pieces were equipped with three strain gauges at 60°, 180° and 300° of the circumference on the inside of the liner pipe at mid level of the height of the liner pipe. Three displacement meters were positioned at the same locations on the outside. The other test pieces were equipped with 12 strain gauges divided equally over the height of the test specimen, at 0°, 90°, 180° and at 270° of the circumference on the inside. No displacement meters were used for these test pieces. When no displacement meters were used, the number of strain gauges was increased from 3 to 12, because the strain gauges measure locally while the displacement meters measure globally.

Five 100 mm long and four 200 mm long liner pipes were made available for axial compression tests. All were obtained from a 10.75 inch Tight Fit Pipe with an initial residual liner pipe hoop stress of 187 MPa (Figure 1.3).

4.3.3 Test Set-up for Buckling of the Liner Pipe Isolated from the 12.75 Inch Tight Fit Pipe

The test set-up of the buckling tests on liner pipes obtained from the 12.75 inch Tight Fit Pipe can be seen in Figure 4.4. This test set-up differed from the buckling tests on the liner pipes from the 10.75 inch Tight Fit Pipe: a plate was used instead of an axial compression pad to support the extra hinge between the liner pipe and the compression machine. The compression pad could not be used in this test series because it did not completely cover the wall thickness of the single liner pipe, causing bending moments in the liner pipe wall. This phenomenon was noticeable due to high values of strain measurements when the stresses in the liner pipe were lower than the yield stress (the stiffness should obey the Young's modulus). When the plate, that transferred the axial force to the single liner pipe over the full top area, was used, the measured liner pipe stiffness was in good agreement with the Young's modulus. On the outside of the liner pipe, the test pieces were equipped with nine strain gauges, equally spaced over the height, at 0°, 120° and 240° of the circumference.

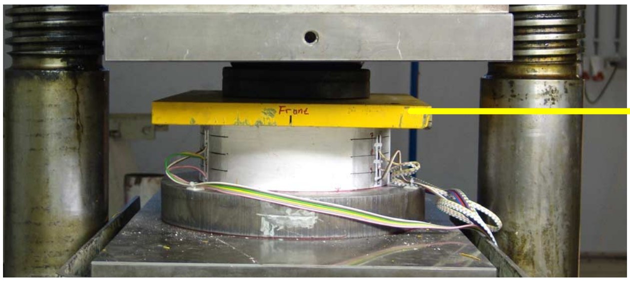

Compression plate

Figure 4.4 Test set-up for the liner pipe from the 12.75 inch Tight Fit Pipe

Three 100 mm long liner pipes were obtained from the 12.75 inch Tight Fit Pipe with different residual liner pipe hoop stresses (Table 4.1) and used for compression testing. Single liner pipe buckling tests were only executed on 100 mm long liner pipes from the 12.75 inch outer diameter Tight Fit Pipe because these were the remains of the residual compressive stress tests executed on the 12.75 inch Tight Fit Pipes (Subsection 3.4.2). Due to limited availability of this 12.75 inch Tight Fit Pipe no other lengths of liner pipes from this Tight Fit Pipe were tested in axial compression.

4.3.4 Tests Results

The buckling strain of the liner pipe ($\varepsilon_{L;cr}$) and the liner pipe buckling force ($F_{L;cr}$) as well as the half wave length of the liner pipe (L_L/m) are independent of the length of the liner pipe specimen, as long as the liner pipe specimen is equal to or longer than the half wave length [4]. Therefore, in the evaluation of the results of the buckling tests on liner pipes from 10.75 inch Tight Fit Pipe, the results of the 100 mm and 200 mm long liner pipe buckling tests can be considered as one test series. Results of the individual 100 mm and 200 mm buckling tests on liner pipes from the 10.75 inch Tight Fit Pipe, as well as the average results of these tests can be found in Table 4.1.

Results of the buckling tests on the 100 mm long liner pipes from the 12.75 inch Tight Fit Pipe can be found in Table 4.2. Table 4.2 indicates that the size of the residual liner pipe hoop stress (σ_{res}), which was present in the liner pipe when it was still part of the 12.75 inch Tight Fit Pipe, appears not to influence the buckling capacity of the single liner pipe.

Table 4.1 Buckling results for the 100 mm and 200 mm long liner pipes from the 10.75 inch Tight Fit Pipe

Test (100 mm)	$F_{L;cr}$ [kN]	$\varepsilon_{L;cr}$ SG [%]	$\varepsilon_{L;cr}$ DM [%]	L_L/m [mm]
1	-591	-0.27	-0.34	32
2	-546	-0.20	-0.37	36
3	-469	-0.16	-0.20	33
4	-568	-0.15	-0.31	32
5	-586	-0.30	-	36
Test (200 mm)	$F_{L;cr}$ [kN]	$\varepsilon_{L;cr}$ SG [%]	$\varepsilon_{L;cr}$ DM [%]	L_L/m [mm]
6	-573	-0.26	-0.33	32
7	-582	-0.30	-0.26	34
8	-582	-0.40	-0.27	38
9	-593	-0.30	-	36
Average	-565	-0.26	-0.30	34

Note:
SG: Strain gauge
DM: Displacement meter

Table 4.2 Buckling results for the 100 mm long liner pipes from the 12.75 inch Tight Fit Pipe

Test	σ_{res} [MPa]	Tight Fit Pipe	$F_{L;cr}$ [kN]	$\varepsilon_{L;cr}$ SG [%]	L_L/m [mm]
1	178	ORANGE	-812	-0.38	42
3	53	WHITE	-768	-0.46	47
4	53	WHITE	-770	-0.47	45
Average	-	-	-783	-0.44	45

Note:
SG: Strain gauge

Two to three axi-symmetric buckles were present in the 100 mm long liner pipes of the 10.75 and 12.75 inch Tight Fit Pipes and six to seven axi-symmetric buckles were present in the 200 mm long liner pipes from the 10.75 inch Tight Fit Pipe. In all the single liner pipe buckling tests, one of the buckles in the buckled liner pipes was more noticeable than the others. The results of the axial compression tests on liner pipes from the 10.75 and 12.75 inch Tight Fit Pipes were compared to the results calculated with several buckling formulae. Equations (4.1), (4.2), (4.3) and (4.4) were used to predict the buckling strain of single wall pipes due to axial compression.

Batterman [4]:

$$\varepsilon_{L;cr} = \frac{2 \cdot E_L \cdot t_L}{E_{L;S} \cdot r_{L;a}} \cdot \frac{1}{\left\{3 \cdot \left[(3 \cdot \psi + 2 - 4 \cdot \nu_L) \cdot \lambda - (1 - 2 \cdot \nu_L)^2\right]\right\}^{0.5}} \qquad (4.1)$$

Gresnigt [23]:

$$\varepsilon_{L;cr} = 0.25 \cdot \left(\frac{t_L}{r_{L;a}} \right) - 0.0025 \tag{4.2}$$

Gerard [21]:

$$\varepsilon_{L;cr} = \frac{\sqrt{\frac{E_{L;T}}{E_{L;S}}} \cdot \frac{t_L}{r_{L;a}}}{\sqrt{3 \cdot \left(1 - (\nu_L)^2 \right)}} \tag{4.3}$$

Lee [30]:

$$\varepsilon_{L;cr} = \frac{\sigma_{L;cr}}{E_{L;S}} = \frac{1}{E_{L;S}} \cdot \left[\sqrt{\frac{\left(2 \cdot A_3 \cdot \left(2 \cdot \sqrt{A_1} + B\right)\right)}{\left(2 \cdot \sqrt{A_1} + A_2\right)}} \cdot \left(\frac{1}{C_{11}} \right) \cdot \left(\frac{t_L}{r_{L;a}} \right) \right] \tag{4.4}$$

$$A_1 = \frac{C_{22}}{C_{11}} \; ; \; A_2 = \frac{(C_3 - 2 \cdot C_{12})}{C_{11}} \; ; \; A_3 = \frac{1}{\left\{ 6 \cdot \left[(C_{22}/C_{11}) - \left(C_{12} \cdot C_{21}/(C_{11})^2 \right) \right] \right\}} \tag{4.5}$$

$$B = 2 \cdot (C_{12}/C_{11}) + \left\{ \left[4 \cdot (C_{11} \cdot C_{22} - C_{12} \cdot C_{21}) \right] / C_{11} \cdot C_3 \right\} \tag{4.6}$$

$$C_{11} = \frac{1}{E_{L;T}} \; ; \; C_{12} = C_{21} = \frac{\nu_L}{E_L} + \frac{1}{2} \cdot \left(\frac{1}{E_{L;T}} - \frac{1}{E_L} \right) ; \; C_{22} = \frac{1}{4} \cdot \left(\frac{1}{E_{L;T}} + \frac{3}{E_{L;S}} \right) ;$$
$$C_3 = \frac{3}{E_{L;S}} - \left(\frac{[1 - 2 \cdot \nu_L]}{E_L} \right) \tag{4.7}$$

Equations (4.8), (4.9) and (4.10) were used to predict the half wave length of the buckle.

Batterman [4]:

$$\frac{L_L}{m} = \frac{1}{2} \cdot \frac{\pi \cdot \left[t_L \cdot r_{L;a} \cdot (\lambda + 3 \cdot \psi) \right]^{0.5}}{\left\{ 3 \cdot \left[(3 \cdot \psi + 2 - 4 \cdot \nu_L) \cdot \lambda - (1 - 2 \cdot \nu_L)^2 \right] \right\}^{0.25}} \tag{4.8}$$

Gerard [21]:

$$\frac{L_L}{m} = \pi \cdot \sqrt{\left(\frac{1}{4} + \frac{3}{4} \cdot \frac{E_{L;T}}{E_{L;S}} \right)} \cdot \sqrt{\frac{r_{L;a} \cdot t_L}{3}} \cdot \left[\frac{E_{L;S}}{E_{L;T}} \right]^{0.25} \tag{4.9}$$

Lee [30]:

$$\frac{L_L}{m}=\frac{\pi \cdot r_{L;a}}{p}\cdot\left(\frac{1}{A_1}\right)^{-0.25} \tag{4.10}$$

$$p=\sqrt{\frac{r_{L;a}}{t_L}\cdot\sqrt{2/A_3\cdot\left(2\cdot\sqrt{A_1}+B\right)\cdot\left(2\cdot\sqrt{A_1}+A_2\right)}} \tag{4.11}$$

The Young's moduli of the 304L liner pipe of the 10.75 inch Tight Fit Pipe and the 316L liner pipe of the 12.75 inch Tight Fit Pipe (E_L) were 193193 MPa and 193000 MPa, respectively (Table 3.2). The secant moduli of the liner pipes of the 10.75 and 12.75 inch Tight Fit Pipe ($E_{L;S}$) were determined from the buckling tests by dividing the average buckling stress by the average buckling strain in the axial compression tests type 1. The secant moduli of the 304L and 316L liner pipes were 99340 MPa and 69598 MPa, respectively, while the tangent moduli of the 304L and 316L liner pipes ($E_{L;T}$) were both 10000 MPa.

Comparison between the test results and the theoretical predictions for the liner pipe critical buckling strain ($\varepsilon_{L;cr}$) and the liner pipe half wave length (L_L/m) can be found in Table 4.3 for the liner pipes from the 10.75 inch Tight Fit Pipe and in Table 4.4 for the liner pipes from the 12.75 inch Tight Fit Pipe.

Table 4.3 Comparison of the average experimental buckling results with buckling formulae, for a liner pipe from a 10.75 inch Tight Fit Pipe

	Tests[1)]	Equation (4.1)	Equation (4.2)	Equation (4.3)	Equation (4.4)
$\varepsilon_{L;cr}$ SG [%]	-0.26	-0.42	-0.25	-0.42	-1.12
$\varepsilon_{L;cr}$ DM [%]	-0.30				
L_L/m [mm]	34	33	-	33	47

Note:
SG: Strain gauge
DM: Displacement meter
1) Average taken from Table 4.1.

Table 4.4 Comparison of the average experimental buckling results with buckling formulae, for a liner pipe from a 12.75 inch Tight Fit Pipe

	Tests[1)]	Equation (4.1)	Equation (4.2)	Equation (4.3)	Equation (4.4)
$\varepsilon_{L;cr}$ SG [%]	-0.44	-0.52	-0.26	-0.52	-1.17
L_L/m [mm]	45	37	-	37	57

Note:
SG: Strain gauge
1) Average taken from Table 4.2.

Table 4.3 and Table 4.4 show that the theoretical prediction for the critical buckling strain by Gresnigt (Equation (4.2)) underestimates the experimental value for the buckling strain. This can be expected since this equation is a design formula and should be considered as conservative. The theoretical predictions for the critical buckling strain by Batterman and Gerard (Equations (4.1) and (4.3)) overestimate the experimental value for the buckling strain. This can be explained by the fact that these equations are based on elastic plastic analysis of buckling of cylindrical shells and do not take imperfections into account. That the prediction by Lee (Equation (4.4)) overestimates the predictions by Batterman and Gerard can be explained by the fact that Lee considers the circumferential wave formation while Batterman and Gerard assume axi-symmetrical buckling. In inelastic buckling this circumferential mode can lead to a relatively higher buckling load [30].

It should also be noted that the predictions of the critical buckling strain by Batterman, Gerard and Lee are sensitive to the value assumed for the tangent modulus. If the tangent modulus of the 316L liner pipe from the 12.75 inch Tight Fit Pipe is varied from 10000 MPa ($E_{L;T1}$) to 4500 MPa ($E_{L;T2}$) or 20000 MPa ($E_{L;T3}$) (Figure 4.5), the estimation for the critical buckling strain varies between 0.52 %, 0.35 % and 0.73 %, respectively. A minor variation in the assumed tangent modulus results in a different prediction for the critical buckling strain.

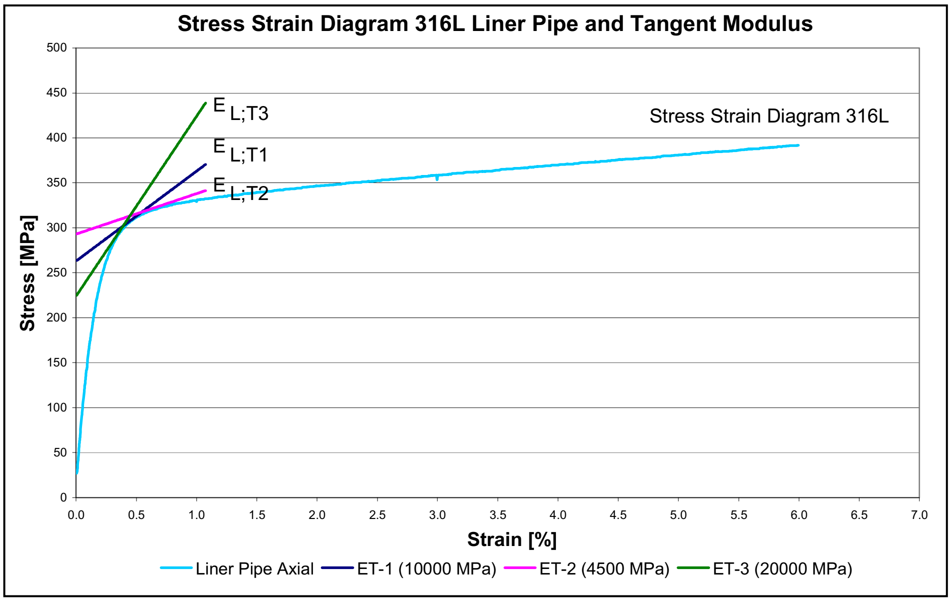

Figure 4.5 Stress strain diagram of the 316L liner pipe from the 12.75 inch Tight Fit Pipe

Figure 4.6 shows that the most significant buckle occurred in the middle of the liner pipe from the 12.75 inch Tight Fit Pipe, while for the liner pipe from the 10.75 inch Tight Fit Pipe the most significant buckle occurred mostly at the bottom or the top of the specimen. This can be explained by the fact that the plate transferred the axial force better into the liner pipe from the 12.75 inch Tight Fit Pipe than the compression pad did into the liner pipe from the 10.75 inch Tight Fit Pipe.

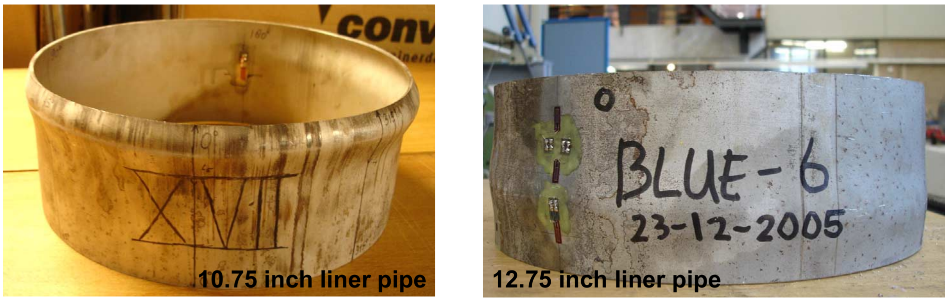

Figure 4.6 Axi-symmetric buckle in the liner pipe, obtained from 10.75 and 12.75 inch Tight Fit Pipe

4.4 Buckling of the Liner Pipe Pre-stressed in the Outer Pipe (Test Type 2)

4.4.1 Objective of the Tests

The first objective of the buckling tests of the liner pipes pre-stressed in the outer pipes was to investigate how much the buckling strength (buckling strain and force) increased by positioning and pre-stressing the liner pipe inside the outer pipe. A second objective of the 12.75 inch Tight Fit Pipe tests was to determine whether the mechanical bonding strength of the Tight Fit Pipe influenced the buckling strength and the buckling strain of the liner pipe while confined inside the outer pipe. A second objective of the 10.75 inch Tight Fit Pipe tests was to determine whether the length of the specimen influenced the buckling strength of the liner (whilst confined and pre-stressed inside the outer pipe). Axial compression tests on 10.75 inch Tight Fit Pipe with a low and high residual liner pipe hoop stress were not performed, because these pipes were not available; only 10.75 inch Tight Fit Pipe with a high residual liner pipe hoop stress (187 MPa) was available to be used in the axial compression testing.

4.4.2 Test Set-up

In these buckling tests the liner pipe was axially compressed until buckling while confined and pre-stressed inside the outer pipe. Only the liner pipe was axially compressed by a compression pad (Figure 4.3) that exactly fitted the liner pipe but did not touch the outer pipe (Figure 4.7). The test set-up was identical for both Tight Fit Pipe sizes (10.75 and 12.75 inch Tight Fit Pipe). Strain gauge wires passed through the compression pad to the inside of the Tight Fit Pipe (the strain gauges were attached to the inside of the liner pipe). The compression pad was lifted several times during the tests to investigate whether liner pipe buckling had occurred.

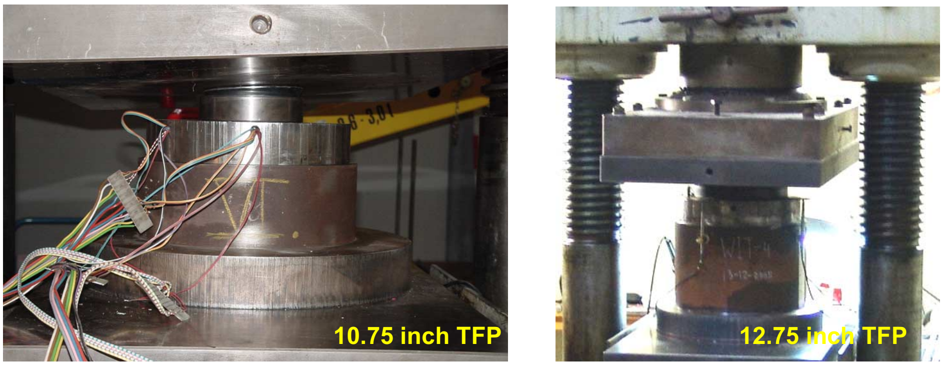

Figure 4.7 Test set-up for liner pipe buckling tests, while confined and pre-stresses inside the outer pipe (10.75 and 12.75 inch Tight Fit Pipe (TFP))

The liner pipes from the 10.75 inch Tight Fit Pipe in this test series were identically provided with measuring equipment as the single liner pipes from the 10.75 inch Tight Fit Pipe when they were loaded under axial compression (Subsection 4.3). Some specimens were equipped with a combination of three strain gauges and three displacement meters, others with twelve strain gauges only. Four of these tests in total were conducted on 10.75 inch Tight Fit Pipe.

All 12.75 inch Tight Fit Pipe test pieces were equipped with four strain gauges at 0°, 90°, 180° and 270° of the circumference, on the inside of the Tight Fit Pipe at midlevel of the height of the specimen and with four displacement meters at the same locations on the outside. Four of these buckling tests in total were conducted. Two of these tests were conducted on liner pipes with a residual liner pipe hoop stress of 53 MPa while the two others were executed on liner pipes which were more tightly confined inside the outer pipe, having a residual liner pipe hoop stress of 199 MPa.

4.4.3 Test Results

The results of the buckling tests on the 100 mm and 200 mm long liner pipes confined and pre-stressed in the outer pipe can be found in Table 4.5 and Figure 4.8 for the 10.75 inch Tight Fit Pipe and in Table 4.6 and Figure 4.9 for the 12.75 inch Tight Fit Pipe. Figure 4.8 shows that for the liner pipe from the 10.75 inch Tight Fit Pipe the axial force was first increased to approximately 300 kN. The liner pipe was then unloaded and the compression pad (Figure 4.3) was lifted to be able to inspect the liner pipe for buckling. No liner pipe buckling was found. Next, the force was increased to approximately 700 kN. The liner pipe was subsequently unloaded and inspected for buckling after the compression pad had been lifted. Still no liner pipe buckling was found. Liner pipe buckling occurred after the axial load had been increased to 800 kN. The axial force was subsequently increased until the critical buckling force ($F_{L;cr}$) and strain ($\varepsilon_{L;cr}$) had been reached. The same procedure was used for the 12.75 inch Tight Fit Pipe in Figure 4.9.

Table 4.5 Buckling results for the liner pipe pre-stressed in the outer pipe, for the 100 mm and 200 mm long 10.75 inch Tight Fit Pipe

Test (100 mm)	$F_{L;cr}$ [kN]	Liner Pipe Buckling [kN]	$\varepsilon_{L;cr}$ SG [%]	$\varepsilon_{L;cr}$ DM [%]	L_l/m [mm]
1	-983	-901 to -983[1)]	-1.88	-	28
2	-962	-803 to -962	-1.87	-	32
Test (200 mm)	$F_{L;cr}$ [kN]	Liner Pipe Buckling [kN]	$\varepsilon_{L;cr}$ SG [%]	$\varepsilon_{L;cr}$ DM [%]	L_l/m [mm]
3	-979	-904 to -979	-	-1.89	25
4	-974	-838 to -974[2)]	-1.76	-2.75	28
5	-910	-800 to -910[3)]	-0.92	-	24
Average	-961		-1.61	-2.32	27

Note:

SG: Strain gauge

DM: Displacement meter

1) At 901 kN a small buckle was felt (not seen) at 180°-235° and around 0°

2) At 838 kN a small buckle was felt (not seen) at 180°

3) At 800 kN a small buckle was felt (not seen) between 180° and 300° in middle of Tight Fit Pipe

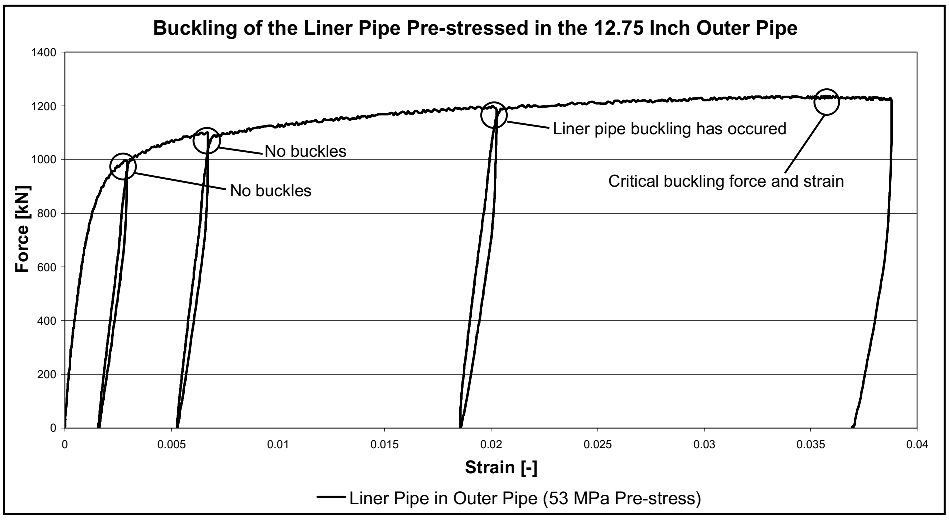

Figure 4.8 Liner pipe buckling (10.75 inch Tight Fit Pipe; test 5 as defined in Table 4.5)

Table 4.6 Buckling results for the liner pipe pre-stressed in the outer pipe, for the 12.75 inch Tight Fit Pipe

Test	L_{TFP} [mm]	σ_{res} [MPa]	Liner Pipe Buckling [kN]	$F_{L;cr}$ [kN]	$\varepsilon_{L;cr}$ SG [%]	$\delta_{L;cr}$ DM [mm]	L_L/m [mm]
1	208	-199	-300 to -1499	-1700	-3.33	11.45	44
2	135	-199	-1135 to -1302	-1971	-7.09 1)	11.43	36
Average		-199		-1835	-5.21	11.44	40
3	205	-53	-300 to -1199	-1211	-2.62	6.08	38
4	210	-53	-1101 to -1200	-1237	-3.58	9.17	32
Average		-53		-1224	-3.10	7.63	35

Note:
SG: Strain gauge
DM: Displacement meter
1) This buckling strain is an estimation based on the correctly measured maximum buckling force in relation to the last correctly measured strain of -5.91 % at -1802 kN.

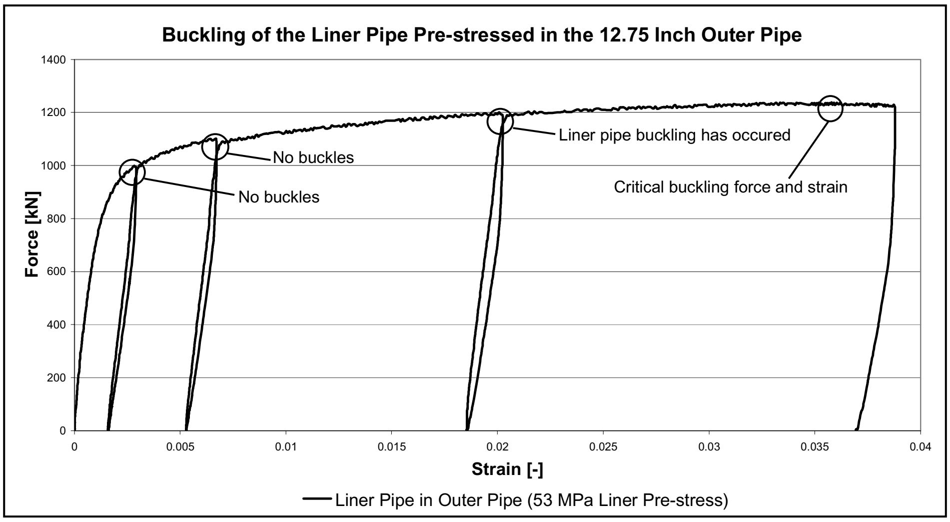

Figure 4.9 Liner pipe buckling (12.75 inch Tight Fit Pipe; test 4 as defined in Table 4.6)

When comparing the buckling behaviour of the liner pipe confined and pre-stressed in the outer pipe, with the buckling behaviour of the single liner pipe (Table 4.2 and Table 4.1), it can be seen that the buckling force and the buckling strain of the liner pipe are significantly higher when the liner pipe is confined and pre-stressed inside the outer pipe (Table 4.5 and Table 4.6). The increase in the liner pipe buckling force can be explained by the fact that part of the axial compression force was transferred to the outer pipe by the axial friction between the liner pipe and the outer pipe together with the fact that the liner pipe could only buckle inwards due to the presence of the outer pipe. The fact that the axial friction avoids the liner pipe material “feeding in” to the liner pipe wrinkle, together with the fact that the liner pipe could only buckle inwards due to the presence of the outer pipe, increases the liner pipe buckling strain.

When comparing Table 4.2 with Table 4.1 and Table 4.5 with Table 4.6 respectively, it is clear that the increase of the liner pipe buckling strength from test series 1 to 2 is different for both Tight Fit Pipe sizes. For the 10.75 inch Tight Fit Pipe, the liner pipe buckling force increased from 565 kN for the single liner pipe (test type 1) to 961 kN for the liner pipe confined in the outer pipe with a residual liner pipe hoop stress of 187 MPa (test type 2). The ratio of increase was 1.70. For the 12.75 inch Tight Fit Pipe, the liner pipe buckling force increased from 783 kN for the single liner pipe to 1835 kN for the liner pipe confined in the outer pipe with a residual liner pipe hoop stress of 199 MPa and to 1224 MPa for the liner pipe confined in the outer pipe with a residual liner pipe hoop stress of 53 MPa. The ratios of increase were 2.34 and 1.56, respectively.

Furthermore, it appeared that the critical liner pipe buckling strain for the 10.75 inch Tight Fit Pipe increased from 0.26 % for the single liner pipe (test type 1) to 1.61 % for the liner pipe confined in the outer pipe with a residual liner pipe hoop stress of 187 MPa (test type 2). The ratio of increase was 6.19. For the 12.75 inch Tight Fit Pipe, the critical liner pipe buckling strain increased from 0.44 % for the single liner pipe to 5.21 % for the liner pipe confined in the outer pipe with a residual liner pipe hoop stress of 199 MPa and to 3.10 % for the liner pipe confined in the outer pipe with a residual liner pipe hoop stress of 53 MPa. The ratios of increase were 11.84 and 7.05, respectively.

A satisfactory explanation for this difference has not been found yet, since only a small number of tests were performed and also because the 10.75 and 12.75 inch Tight Fit Pipe differed from each other in many respects (Table 4.7). As has been pointed out (Table 4.7), the outer pipe in the 10.75 inch Tight Fit Pipe was seamless while the outer pipe of the 12.75 inch Tight Fit Pipe was an electric resistance welded pipe. The electric resistance welded, 12.75 inch outer pipe had a longitudinal weld but the 10.75 inch outer pipe had not. Liner pipe buckling prior to failure in the 12.75 inch Tight Fit Pipe always appeared first at the location of the outer pipe longitudinal weld (Figure 4.10), while liner pipe buckling prior to failure in the 10.75 inch Tight Fit Pipe occurred at various locations, probably depending on the distribution of imperfections.

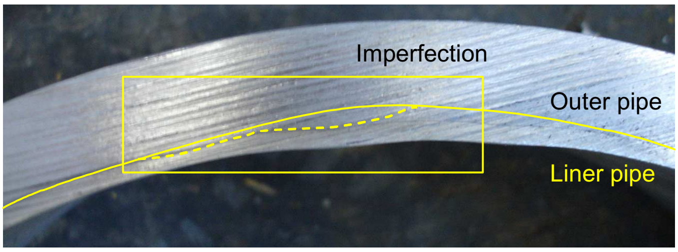

Figure 4.10 Wave like imperfection in the liner pipe due to the electric resistance welded longitudinal outer pipe weld

The 12.75 inch electric resistance welded outer pipe also differed from the seamless 10.75 inch outer pipe in that it had lower surface roughness and thus a lower friction coefficient μ. This influenced the relationship between the radial contact stress and the axial friction between the liner pipe and the outer pipe in the Tight Fit Pipe (Equation (3.4)). The relationship between the radial contact stress and the axial friction was thus different for the 10.75 inch Tight Fit Pipe and the 12.75 inch Tight Fit Pipe. It should also be taken into account that, through the Poisson ratio, the applied axial loading (which is different for both pipe sizes) influenced the radial contact stress, and thus the axial friction, between the liner pipe and the outer pipe, as explained earlier.

Table 4.7 Buckling results for the 10.75 and 12.75 inch Tight Fit Pipe test samples

10.75 inch Tight Fit Pipe	$F_{L;cr}$ [kN]	$\varepsilon_{L;cr}$ [%]	σ_{res} [MPa]	$d_{L;o}/t_L$ [-]	Outer Pipe Material	Liner Pipe Material
Liner Pipe	-565	-0.26	-	103	-	304L ($\sigma_{L;y}$ = 308 MPa)
Liner in Outer Pipe	-961	-1.61	-187	104	X65, seamless	
Liner and Outer Pipe	-5007	-1.03	-187	104		
12.75 inch Tight Fit Pipe						
Liner Pipe	-783	-0.44	-	97	-	316L ($\sigma_{L;y}$ = 300 MPa)
Liner in Outer Pipe	-1835	-5.21	-199	98	X65, ERW	
Liner in Outer Pipe	-1224	-3.10	-53	98		

Note:
ERW: Electric resistance welded

The strain gauge results of the 100 mm and 200 mm long 10.75 inch Tight Fit Pipe specimens (Table 4.5) indicate that the buckling strain ($\varepsilon_{L;cr}$) measured by the strain gauges was independent of the length of the specimens. This can also be seen for the 135 mm and the 200 mm long 12.75 inch Tight Fit Pipe specimens (Table 4.6). However, care should be taken when converting the displacement at buckling (measured by displacement meters) into the buckling strain. Due to the fact that the buckles were local, the displacement at buckling ($\delta_{L;cr}$) was approximately the same for a long and a shorter Tight Fit Pipe. If this same displacement at buckling were to be divided by a longer length for a longer Tight Fit Pipe, this would result in a smaller buckling strain. For this reason, displacement at buckling measured by the displacement meters in the 12.75 inch Tight Fit Pipe test series is expressed in Table 4.6 for the 135 mm and 200 mm long specimens, rather than the buckling strain. In the 10.75 inch test series, displacement from displacement measurements cannot be compared for the 100 and 200 mm long specimens, since displacement meters were only used when buckling the 200 mm specimens. Due to difficulties in operating the displacement meters for the 100 mm long 10.75 inch Tight Fit Pipe, they were replaced by an increase in the number of strain gauges for the 100 mm long Tight Fit Pipe specimens.

In Table 4.6 (12.75 inch Tight Fit Pipe) it can be seen that the buckling strength of the liner pipe increased significantly when the pre-stress in the liner pipe, i.e. the residual liner pipe hoop stress, increased. An increase in the residual liner pipe hoop stress means an increase in the radial contact stress and the axial friction between the liner pipe and the outer pipe. An increase in the axial friction between the liner pipe and the outer pipe increases the obstruction for the occurrence of local buckles: it becomes more difficult for the liner pipe material to “feed in” to the buckle when the axial friction between the liner pipe and the outer pipe increases.

4.5 Buckling of the Integral Tight Fit Pipe (Test Type 3)

4.5.1 Objective of the Test

The objective of this test was to determine the buckling strength of the 10.75 inch Tight Fit Pipe under compression.

4.5.2 Test Set-up

In this test the Tight Fit Pipe test specimen consisting of the combined liner pipe and outer pipe was loaded to buckling. The special extra hinge was removed from the test set-up (Figure 4.11). The axial forces in test types 1 and 2 were too low for the standard hinge of the axial compression machine to work adequately and therefore the extra special hinge had been added in these tests.

The steel plate on top of the Tight Fit Pipe allowed for passage of the strain gauge wires from the inside of the Tight Fit Pipe to the outside (Figure 4.11). The plate was lifted several times during the test to investigate whether liner buckling had occurred. The buckling strength of the 12.75 inch Tight Fit Pipe exceeded the capacity of the testing machine (5000 kN) so no axial compression tests on the 12.75 inch Tight Fit Pipe could be performed. The buckling load of the 10.75 inch Tight Fit Pipe was 5007 kN, resulting in one 10.75 inch Tight Fit Pipe buckling test to be successfully executed.

The 200 mm long 10.75 inch Tight Fit Pipe test specimen was equipped with 24 strain gauges. 12 strain gauges were positioned at 0°, 90°, 180° and 270° of the circumference on the inside surface of the liner pipe equally divided over the height of the specimen. 12 strain gauges were positioned at the same locations on the outside surface of the outer pipe also equally divided over the height of the specimen. Furthermore, 4 displacement meters were located on the outside of the Tight Fit Pipe, also at 0°, 90°, 180° and 270° of the circumference (Figure 4.11).

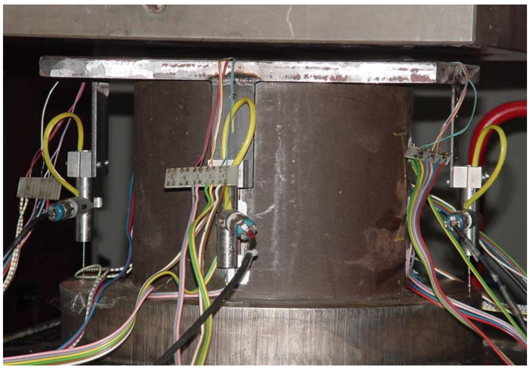

Figure 4.11 Test set-up of the axial compression test of the 10.75 inch Tight Fit Pipe

4.5.3 Test Results

In Table 4.8 the test results can be found: the critical buckling force, the critical buckling strain and the half wave length of the liner pipe ($F_{L;cr}$, $\varepsilon_{L;cr}$ and L_L/m, respectively) and of the outer pipe ($F_{O;cr}$, $\varepsilon_{O;cr}$ and L_O/m, respectively). The critical buckling strain of the liner pipe is higher when the liner pipe and the outer pipe are loaded in conjunction (Table 4.8) than when testing the liner pipe only (Table 4.1). The explanation for this increase is identical to the case where the liner pipe was confined in the outer pipe (Table 4.5).

Table 4.8 Buckling 10.75 inch Tight Fit Pipe; liner and outer pipe results

	$F_{L;cr}$ & $F_{O;cr}$ [kN]	$\varepsilon_{L;cr}$ & $\varepsilon_{O;cr}$ SG [%]	$\varepsilon_{L;cr}$ & $\varepsilon_{O;cr}$ DM [%]	L_L/m & L_O/m [mm]
Liner Pipe	-4783 to -5007	-1.03	-	28
Outer Pipe	-5007	-1.33	-1.77	60

Note:
SG: Strain gauge
DM: Displacement meter

The increase in the buckling force was the result of the fact that the buckling capacity of the liner pipe was determined by the buckling capacity of the outer pipe. The yield stress, the Young's modulus and the wall thickness of the 304L liner pipe were 308 MPa, 193190 MPa and 2.45 mm (Table 3.2), respectively. The yield stress of the X65 outer pipe was estimated at 552 MPa, based on the average of the yield stress measurements from the X65 outer pipe of the 12.75 inch Tight Fit Pipes (Table 3.2). The Young's modulus and the wall thickness of the X65 outer pipe were 200000 MPa and 9.3 mm, respectively (Table 3.2). Inspection of the liner pipe during the test indicated that no buckles were present at a compression force of -4783 kN. Hence it can be concluded that buckles only occurred in the liner pipe shortly prior to, or at, failure of the outer pipe.

When buckling the integral Tight Fit Pipe (test type 3), buckling strains of the liner pipe and the outer pipe ($\varepsilon_{L;cr}$ and $\varepsilon_{O;cr}$) were measured during the test. The buckling strain of the liner pipe in test type 3 was slightly lower than the buckling strain of the liner pipe in test type 2. This can be explained by the fact that in test type 3 the liner pipe and the outer pipe were both compressed and buckled while in test type 2 only the liner pipe was compressed. Buckling of the outer pipe in test type 3 adds to the distortion of the radial contact stress and thus the axial friction between the liner pipe and the outer pipe. The axial friction increases the buckling capacity of the liner pipe. The buckled Tight Fit Pipe can be seen in Figure 4.12.

Figure 4.12 10.75 inch liner pipe and outer pipe (inside and outside) after testing the integral Tight Fit Pipe in compression

4.6 Conclusions

The conclusions are based on experiments with specimens from the 10.75 and 12.75 inch outer diameter Tight Fit Pipe (Table 4.9).

Test type 1: buckling of the single liner pipe (10.75 and 12.75 inch Tight Fit Pipe)
The equation by Gresnigt [23] underestimated the experimentally determined liner pipe buckling strain. Predictions based on elastic plastic analysis of cylindrical shell buckling not taking imperfections into account (Batterman [4], Gerard [21] and Lee [30]) resulted in an overestimation of the experimental values.

Test type 2: buckling of the liner pipe, pre-stressed in the outer pipe (10.75 and 12.75 inch Tight Fit Pipe)

1. Compared to single liner pipe buckling, the buckling force and the buckling strain of the liner pipe increase when confined and pre-stressed in an outer pipe (Table 4.9). The increase in the liner pipe buckling force can be explained by the fact that part of the axial compression force was transferred to the outer pipe by the axial friction between the liner pipe and the outer pipe together with the fact that

the liner pipe could only buckle inwards due to the presence of the outer pipe. The fact that the axial friction avoids the liner pipe material “feeding in” to the liner pipe wrinkle, together with the fact that the liner pipe could only buckle inwards due to the presence of the outer pipe, increases the liner pipe buckling strain.

2. The buckling force of the liner pipe increases when the mechanical bonding strength between the liner pipe and the outer pipe in the Tight Fit Pipe, i.e. the residual liner pipe hoop stress, increases (Table 4.9).
3. Liner buckling prior to failure in the 12.75 inch Tight Fit Pipe always occurred at the location of the outer pipe electric resistance welded longitudinal outer pipe weld, while liner buckling prior to failure in the 10.75 inch Tight Fit Pipe occurred at various locations, probably depending on the distribution of the imperfections.

Test type 3: buckling of the integral Tight Fit Pipe (10.75 inch Tight Fit Pipe)

1. Compared to single liner buckling, the buckling force of the liner pipe ($F_{L;cr}$) in the integral Tight Fit Pipe was higher (Table 4.9). This is the result of the buckling force of the liner pipe being determined by the buckling force of the integral Tight Fit Pipe.
2. The buckling strain of the liner pipe ($\varepsilon_{L;cr}$) when buckling the integral Tight Fit Pipe in axial compression test type 3 was slightly lower than the buckling strain of the liner pipe when buckled while confined and pre-stressed in the outer pipe (axial compression test type 2). This is due to the fact that the outer pipe buckled as well in the test distorting the radial contact stress between the liner pipe and the outer pipe.
3. Buckles in the liner occurred shortly prior to, or at failure of the outer pipe.

Table 4.9 Overview of axial compression tests on 10.75 and 12.75 inch Tight Fit Pipe

Tight Fit Pipe [inch]	Test	$F_{L;cr}$ [kN]	$\varepsilon_{L;cr}$ SG [%]	$\varepsilon_{L;cr}$ DM [%]	L_l/m [mm]
10.75	Liner Pipe	-565	-0.26	-0.30	34
10.75	Liner <u>in</u> Outer Pipe	-961	-1.61	-2.32	27
10.75	Liner <u>and</u> Outer Pipe	-5007	-1.03	-1.77	28
12.75	Liner Pipe	-783	-0.44	-	45
12.75	Liner <u>in</u> Outer Pipe (σ_{res} = -199 MPa)	-1835	-5.21	11.44	40
12.75	Liner <u>in</u> Outer Pipe (σ_{res} = -53 MPa)	-1224	-3.10	7.63	35

Note:
SG: Strain gauges
DM: Displacement meters

It can be concluded that the axial compression tests contributed to the understanding of the buckling behaviour of the Tight Fit Pipe.

5 Small Scale Reeling Simulation of Single Walled Pipe

5.1 Introduction

Small scale bending tests were conducted on eleven 22 mm outer diameter single walled pipes with wall thicknesses varying between 1.3 mm and 4.3 mm in preparation of the full scale bending tests on Tight Fit Pipe. In the small scale bending tests observations and experiences with the forces applied by the small scale bending rig on the pipe were used in the design of the full scale bending rig. Small scale bending tests were also executed to become familiar with performing bending tests [19].

This chapter starts by explaining how in reality the spooling-on phase during the actual reeling installation process is executed (Subsection 5.2). Next, the reeling simulation tests in the small scale bending rig are described (Subsection 5.3). The test set-up of the small scale bending rig is shown in Subsection 5.3.1 and the test results are compared to theoretical predictions in Subsection 5.3.2. In Subsection 5.4 it is discussed how the bending tests (both in the full scale bending rig and in the small scale bending rig) resemble the spooling-on phase of the actual reeling process in reality.

5.2 Spooling-on during Actual Reeling

When spooling a pipeline on a reel in reality (Figure 5.1), the beginning of the pipeline is attached and fixed to the reel. The pipeline is then bent on the reel by paying out pipeline through the tensioners which jointly with the driving moment of the reel keep the pipeline under tension. The pipeline is positioned on the drum in several layers.

Figure 5.1 Spooling pipeline on the reeling vessel “Deep Blue”

The bending moment in the pipeline increases from the tensioners to the reel (Figure 5.2). On the reel the bending moment changes only when the radius changes, e.g. when the pipeline is reeled as a next layer on the drum. No change in bending moment within one layer of pipeline means that the shear force is zero ($\frac{dM}{dx} = V = 0$) within this layer. The first layer of pipeline is the most critical, because in this layer the pipeline experiences the largest curvature.

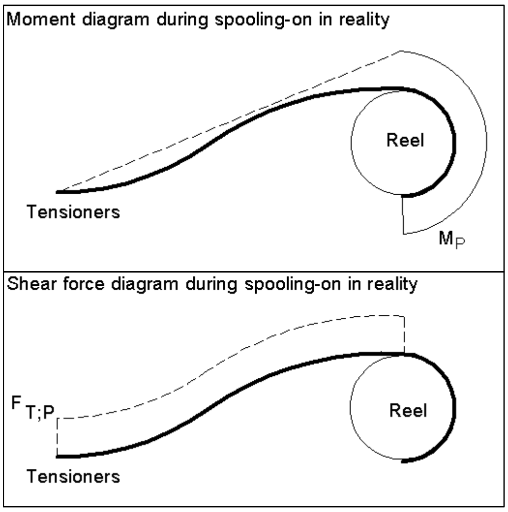

Figure 5.2 Moment and shear force diagram of the pipeline during spooling-on in the actual reeling process (excluding the weight of the pipe)

Because there is no shear force in the pipe that is in contact with the reel, the perpendicular force in the tensioners, $F_{T;P}$ in Figure 5.3, needs to be in equilibrium with the reaction force of the reel on the pipe, $F_{reel;T;P}$ in Figure 5.3. Figure 5.3 is valid for a horizontal reel (i.e. Global Industries "Chicasaw" [7]). When the reel is positioned vertically (i.e. Technip "Deep Blue" [5], [28], [59]), the perpendicular force in the tensioners ($F_{T;P}$) plus the weight of the pipeline, are in equilibrium with the reaction force of the reel on the pipeline ($F_{reel;T;P}$). The full scale bending rig in the laboratory and thus the small scale bending rig in the laboratory as preparation, both bent pipes in the horizontal plane. Therefore, Figure 5.2 and Figure 5.3 are applicable to these bending rigs. In the horizontal spooling-on process onboard of the reeling vessel the pipeline is supported between the reel and the tensioners. In the full scale bending rig the pipe was supported by rollers. In Figure 5.3 the equilibrium of the forces on the pipeline comprises two parts. In the first part the perpendicular force in the tensioners ($F_{T;P}$) is in equilibrium with the reaction force of the reel laterally to the pipeline ($F_{reel;T;P}$). In the second part the tension force ($F_{T;A}$) is in equilibrium with the distributed load of the reel on the pipe (q_{reel}). It should be noted that the reaction force of the reel on the pipeline ($F_{reel;T;P}$) is in fact a distributed load. However, for reasons of simplicity, this distributed load is treated as a concentrated load. In Figure 5.3 the axial friction between the reel and the pipeline is not taken into account for reasons of simplicity as well, because the stresses due to the axial load on the pipeline are negligible compared to the bending moment and the shear force applied on the pipeline.

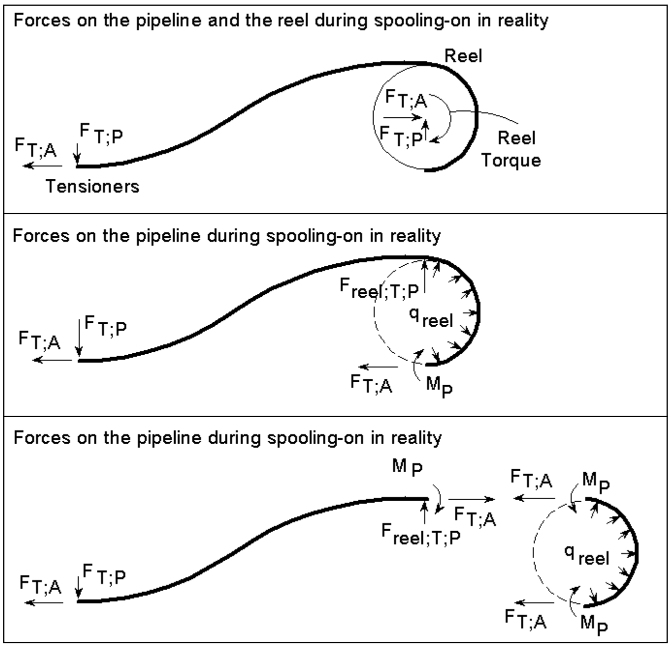

Figure 5.3 Forces on the pipeline during spooling-on in the actual reeling process

During spooling-on of the pipeline, the distance between the tensioners and the reel can vary for different reeling vessels but remains constant during the spooling-on process. The tension force is normally kept constant during the reeling process. However, it is possible to increase the tension force during the reeling process, which may be required in order to prevent local buckling [11], [6].

5.3 Reeling with the Small Scale Bending Rig

5.3.1 Test set-up

Bending tests on eleven 22 mm outer diameter single walled pipes (PIPE1 to PIPE11; Table 5.1) were performed in four different geometrical sets, each having a different wall thickness (t). Material testing of the pipes was performed indirectly: the yield stress of a pipe (σ_y) was calculated from the bending moment in the pipe (M) when positioned on the reel. The bending moment in the pipe was calculated by multiplying the measured force in the hydraulic cylinder (F_{HC}) with the arm between the hydraulic cylinder and the reel ($L_{HC;x}$ in Figure 5.4). The bending moment could also be calculated by multiplying the lateral fixation point force ($F_{FP;P}$) with the arm between the fixation point and the reel (L_{FP} in Figure 5.4). The bending moment determined by the hydraulic cylinder force should theoretically be equal to the bending moment determined by the lateral fixation point force. When the pipe was positioned on the reel, the plastic bending moment capacity of the pipe (M_P) was almost reached. It was thus assumed that the average of the bending moments (determined by the hydraulic cylinder force and the lateral fixation point force) in the pipe bent on the reel equalled the plastic bending capacity. This bending moment was used to determine the yield stress of the pipe (Table 5.1).

Certain testing parameters (the diameter of the reel (D_{reel}), the distances in the bending rig (L_{FP}, $L_{FP;1}$ and $L_{LF;2}$), the type of the fixation point and applying a lift force (F_{LF}) or not) were changed in order to investigate the influence of these parameters on the behaviour of the pipe during bending (Table 5.1). For all tests (Table 5.1), the distance between the initial contact point of the pipe with the reel and the hydraulic cylinder ($L_{HC;x}$) was 515 mm.

Table 5.1 Characteristics of the test pipes and the bending tests

PIPE	t [mm]	σ_y [MPa]	D_{reel} [mm]	L_{FP}		Fixation Point	F_{LF} [N]
				$L_{FP;1}$	$L_{FP;1}$		
				[mm]			
1	2.6	214	545	480		roll	0
2	4.3	360	545	480		hinge	0
3	4.3	367	545	300		hinge	0
5	1.3	302	545	300		hinge	0
7	1.3	300	350	375		hinge	0
4	2.2	253	545	300		hinge	0
6	2.2	275	545	480		hinge	0
8	2.2	261	350	480		hinge	0
9	2.2	250	350	480		fixed	0
10	2.2	289	350	182	298	fixed	398
11	2.2	266	350	182	193	fixed	398

Note:
The yield stress of the pipe (σ_y) was calculated from the bending moment in the pipe (M).

A schematic representation of the small scale bending rig and a picture of the small scale bending rig in the laboratory can be seen in Figure 5.4. The pipe was connected to the fixation point on one side whilst the pipe was pulled against the reel by a hydraulic cylinder on the other side (Figure 5.5).

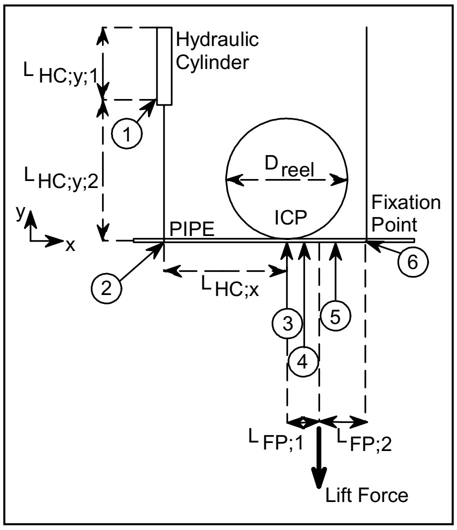

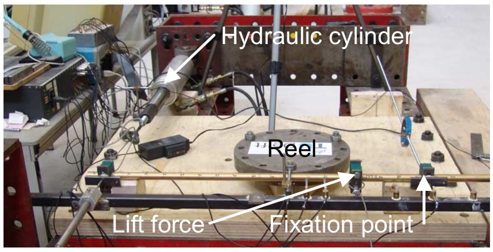

Figure 5.4 Test set-up for an un-bent pipe; left a schematic overview, right a picture of the test set-up in the laboratory (ICP = initial contact point of the pipe with the reel)

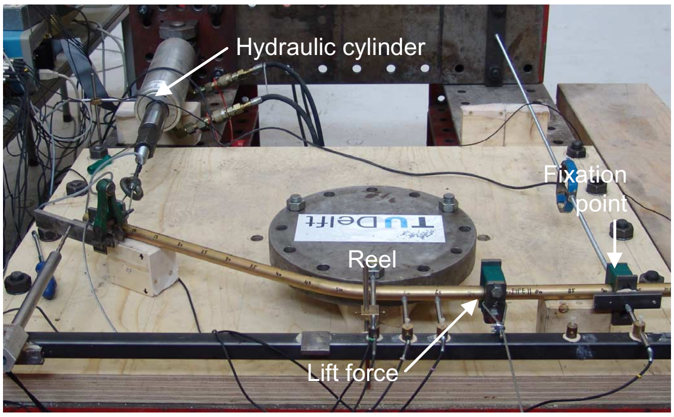

Figure 5.5 A bent pipe in the small scale bending rig

The hydraulic cylinder force was measured by the hydraulic cylinder itself while the lateral fixation point force was measured by a load cell at the fixation point. The movement of the hydraulic cylinder in x-direction was measured at location 1 (Figure 5.4) by a displacement meter. Displacement meters were also used at locations 2, 3, 4, 5 and 6 (Figure 5.4) to measure the displacement of the pipe in y-direction. At location 6 (Figure 5.4), the displacement of the pipe in x-direction was measured. A displacement meter was used at location 3 (Figure 5.4) to measure the displacement of the reel in y-direction.

In the bending tests PIPE10 and PIPE11 (Table 5.1) a “lift” force (F_{LF}) was used. The “lift” force lifted the pipe slightly from the reel, reducing the initial reaction force of the reel on the pipe in the beginning of the test (F_{reel}). Unintended buckling and undesired ovality was thereby avoided. In Figure 5.6 it is shown how the lift force, applied to the pipe by weights (maximally 398 N) pulling laterally on the pipe (Figure 5.4) reduced F_{reel}. F_{reel}, acting as a lateral force on the pipe, enhanced ovalisation [38] and could cause unintended buckling in the beginning of the test.

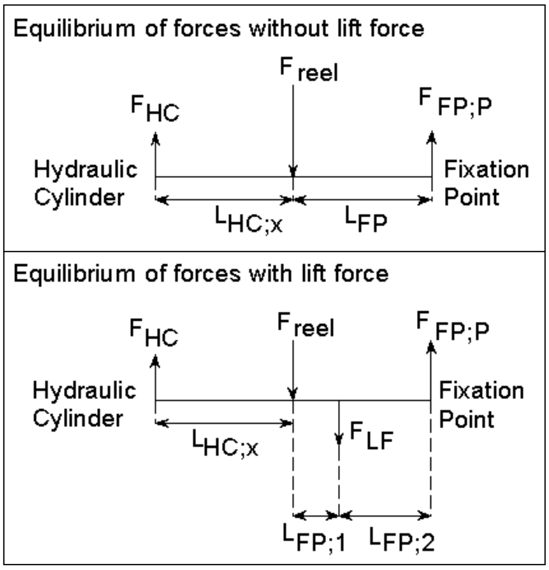

Figure 5.6 Reduction of the reaction force of the reel on the pipe due to the lift force

5.3.2 Comparison of the Experimental Data with the Theoretical Predictions

5.3.2.1 Forces in the Bending Rig

Observations and experiences with the forces applied by the small scale bending rig on the pipe were used in the design of the full scale bending rig. In the reeling simulation tests two phases were identified (Figure 5.7):

I: The pipe contacts the reel only at the initial contact point
II: The pipe contacts the reel over an increasing length $L_{contact}$

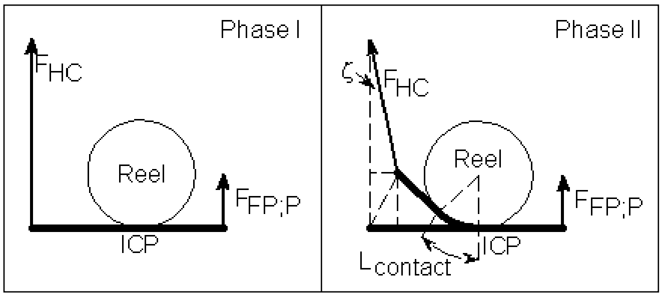

Figure 5.7 Reeling simulation test: start and after plastic deformation at the initial contact point (ICP)

In Phase I the hydraulic cylinder force (F_{HC}) and thus the lateral fixation point force ($F_{FP;P}$) increased until the plastic bending moment (related to the reel radius) was reached at the initial contact point. When the plastic bending moment had been reached at the initial contact point (i.e. the end of Phase I and the start of Phase II) the pipe started curving against the reel. In Phase II the increase in the hydraulic cylinder force (F_{HC}) caused an increasing pipe length ($L_{contact}$) to come into contact with the reel (Figure 5.7). In the bending tests the hydraulic cylinder changed its orientation (angle ζ in Figure 5.7 and Figure 5.8). This resulted in the x- and y-components of the hydraulic cylinder force ($F_{HC;x}$ and $F_{HC;y}$) to change in magnitude during the test and hence the axial and perpendicular components of the hydraulic force ($F_{HC;A}$ and $F_{HC;P}$). During Phase I (the initial contact point alone touched the reel) the orientation of the hydraulic cylinder (angle ζ) changed slightly due to bending of the pipe. This initial change was neglected and for reasons of simplicity all change in the hydraulic cylinder orientation was assumed to occur in Phase II.

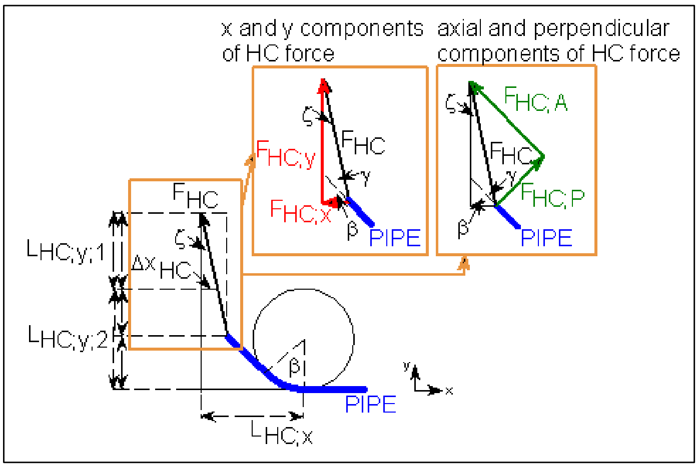

Figure 5.8 Components of the hydraulic cylinder force (HC force) for PIPE1 to PIPE11

During the reeling simulation tests, Δx_{HC} and F_{HC} were measured. These results were used to calculate the x- and y-components of the hydraulic cylinder force using Equations (5.1) to (5.3).

$$\zeta = a\tan\left(\frac{\Delta x_{HC}}{L_{HC;y;1}}\right) \tag{5.1}$$

$$F_{HC;x} = F_{HC} \cdot \sin(\zeta) \tag{5.2}$$

$$F_{HC;y} = F_{HC} \cdot \cos(\zeta) \tag{5.3}$$

In order to determine the axial and perpendicular components of the hydraulic cylinder force during testing (Equations (5.4) to (5.7)), it was necessary to measure the changing angles β and γ (Figure 5.8). Since the importance of these angles was only realised after testing, they could only be estimated at the end of the bending test when the maximum pipe length was in contact with the reel ($L_{contact}$). In the full scale bending rig it was possible to measure angle β during the bending test.

$$\beta = \left(\frac{L_{contact}}{(D_{reel}/2)}\right) \tag{5.4}$$

$$\gamma = \frac{\pi}{2} - \zeta - \beta \tag{5.5}$$

$$F_{HC;A} = F_{HC} \cdot \cos(\zeta) \tag{5.6}$$

$$F_{HC;P} = F_{HC} \cdot \sin(\zeta) \tag{5.7}$$

At the end of Phase I (Figure 5.9), when the plastic bending moment was reached at the initial contact point, the reaction force of the reel on the pipe (F_{reel}) still equalled the hydraulic cylinder force (F_{HC}) plus the lateral fixation point force ($F_{FP;P}$). In Phase II (Figure 5.9) the reaction force from the reel on the pipe (F_{reel}) was divided in two components: one ($F_{reel;FP}$) was in equilibrium with the lateral fixation point force ($F_{FP;P}$) and the other ($F_{reel;HC;y}$) was in equilibrium with the y-component of the hydraulic cylinder force ($F_{HC;y}$). For the pipe section in contact with the reel, there was no change in bending moment as the curvature was determined by reel size. Because there was no change in bending moment, there was also no shear force. Therefore the y-component of the hydraulic cylinder and the fixation point force needed to be in equilibrium with the reaction forces $F_{reel;HC;y}$ and $F_{reel;FP}$, respectively. This equilibrium was also met during actual reeling.

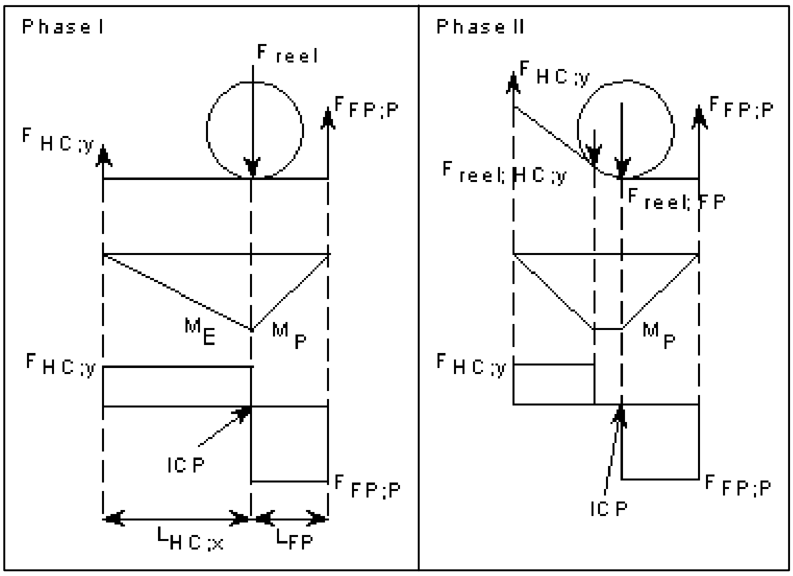

Figure 5.9 Phases I and II in the reeling simulation tests: (ICP = initial contact point)

In Phase II of the reeling simulation test the equilibrium of the forces on the pipe comprised two parts (Figure 5.10). In the first part, the perpendicular component of the hydraulic cylinder force ($F_{HC;P}$) was in equilibrium with the reaction force of the reel acting laterally on the pipe ($F_{reel;HC;P}$). The lateral fixation point force ($F_{FP;P}$) was in equilibrium with the reaction force of the reel on the pipe at the fixation force side of the reel ($F_{reel;FP}$). In the second part, the axial component of the hydraulic cylinder force ($F_{HC;A}$) was in equilibrium with the distributed load of the reel on the pipe (q_{reel}) and the axial force at the fixation point ($F_{FP;A}$). The axial friction between the pipe and the reel was disregarded for reasons of simplicity.

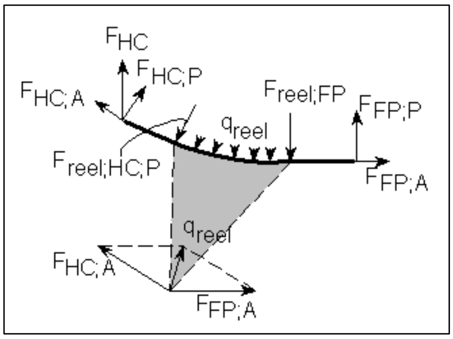

Figure 5.10 Equilibrium of the forces in Phase II of the reeling simulation test

In Phase I both the hydraulic cylinder force (F_{HC}) and the fixation point force ($F_{FP;P}$) increased (and thus the reaction force of the reel on the pipe (F_{reel})). In Phase II only the hydraulic cylinder force (F_{HC}) increased (and thus $F_{reel;HC;P}$). The axial component of the hydraulic cylinder force ($F_{HC;A}$) increased during the bending test (and thus also q_{reel} and $F_{FP;A}$) due to the increased hydraulic cylinder force (F_{HC}) and the changing angle ζ (Figure 5.8). Because the distance between the fixation point and the initial contact point (L_{FP}) and the distance between the lift force point and the initial contact point ($L_{FP;1}$) remained constant throughout the test and the bending moment reached its maximum (approximately the plastic bending moment capacity) at the end of Phase I, the lateral fixation point force ($F_{FP;P}$) and thus the reaction force of the reel on the pipe $F_{reel;FP}$ did not increase anymore after the plastic bending moment capacity had been reached at the end of Phase I.

The plastic bending moment capacity for the pipes (PIPE1 to PIPE11) was calculated using Equation (5.8) [11].

$$M_P = (d_o - t)^2 \cdot t \cdot \sigma_y \tag{5.8}$$

The force in the hydraulic cylinder at the end of Phase I (Figure 5.9) was predicted using Equation (5.9). The lateral fixation point force was determined using Equation (5.10).

$$F_{HC} = \frac{M_P}{L_{HC;x}} \tag{5.9}$$

$$F_{FP;P} = \frac{M_P}{L_{FP}} \tag{5.10}$$

When testing PIPE10 and PIPE11 a lift force (F_{LF}) was added with the objective of reducing the initial reaction force of the reel on the pipe (F_{reel} in Figure 5.6). The influence of the lift force (F_{LF}) on the hydraulic cylinder force (F_{HC}) and the lateral fixation point force ($F_{FP;P}$) at the end of Phase I was determined using Equations (5.11) and (5.12). The initial reaction force of the reel on the pipe (F_{reel}) can be determined using Equation (5.13).

$$F_{HC} = \frac{M_P}{L_{HC;x}} \tag{5.11}$$

$$F_{FP;P} = \frac{M_P + F_{LF} \cdot L_{FP;1}}{L_{FP}} \tag{5.12}$$

$$F_{reel} = F_{HC} + F_{FP;P} - F_{LF} \tag{5.13}$$

The predicted and the measured perpendicular and axial components of the hydraulic cylinder force ($F_{HC;P}$ and $F_{HC;A}$) at the end of the bending test when the maximum pipe length was in contact with the reel ($L_{contact}$), are compared to the test results in Table 5.2. In bending test PIPE 11 angle ζ became distorted because the measuring equipment accidentally broke down during the test. For this reason the axial and perpendicular components of the hydraulic cylinder force could not be calculated for this test.

Table 5.2 Comparison of the predicted and the measured components of the hydraulic cylinder force at the end of Phase II

PIPE	$L_{contact}$ [mm]	$F_{HC;P}$ test [N]	$F_{HC;P}$ theory [N]	$F_{HC;A}$ test [N]	$F_{HC;A}$ theory [N]
1	43	516	443	85	73
2	90	1271	1070	486	390
3	108	1261	1135	575	513
5	50	468	362	103	69
7	25	364	341	60	50
4	108	561	529	260	239
6	100	648	567	279	234
8	50	503	482	158	150
9	40	545	453	146	110
10	40	547	524	138	127

The predictions correlate acceptably to the test results (Table 5.2). Differences between the experimental and the theoretical results can be explained by the fact that the average yield stresses of the pipes have been used in the predictions, which were calculated from the average bending moments resulting from the hydraulic cylinder force and the lateral fixation point force. If only the bending moments as a result of the hydraulic cylinder would be used to determine the yield stresses of the pipes and these yield stresses would be used in the predictions of the hydraulic cylinder components, correlation would be better. Moreover, there is a difference between the theoretically and the experimentally determined angle ζ due to the fact that in the theoretical predictions, the bending of the pipe itself is not taken into account, thereby underestimating angle ζ. Angle ζ is used in determination of the axial and lateral components of the hydraulic cylinder force. Furthermore, measurement inaccuracies in for example the contact length of the pipe with the reel ($L_{contact}$) can cause discrepancies between theory and practice.

The reaction force of the reel on the pipe (F_{reel}) at the end of Phase I was calculated from the measured hydraulic cylinder force (F_{HC}) and the measured lateral fixation point force ($F_{FP;P}$) for PIPE9 (no lift force) and for PIPE10 (lift force (F_{LF})) in Table 5.3. By adding a lift force of 398 N (the maximum weights available in the laboratory) in test PIPE10, the reaction force of the reel on the pipe was reduced by 113 N compared to PIPE9, at the onset of the pipe curving to the reel (the end of Phase I). The fact that the lift force does not reduce the reaction force of the reel with the same value as the lift force itself is the result of the lift force increasing the lateral fixation point force, which in turn increases the reaction force of the reel on the pipe. A sensitivity analysis shows that the reaction force of the reel on the pipe decreases with 20 % when the lift force increases with 50 % for the small scale reeling bending rig configuration of PIPE10.

Table 5.3 F_{reel} in test PIPE9 (no lift force) and PIPE10 (lift force) at the end of Phase I

PIPE	F_{HC} test [N]	$F_{FP;P}$ test [N]	F_{LF} [N]	F_{reel} [N]
9	420	449	-	868
10	498	655	398	755

The relation between the hydraulic cylinder force and the lateral fixation point force during testing of PIPE 9 (no lift force) and PIPE 10 (lift force) can be seen in Figure 5.11. Both forces increased until the end of Phase I was reached. In Phase II the hydraulic cylinder force still increased due to the decrease in the distance between the reel and the hydraulic cylinder. The lateral fixation point force remained constant, because the distance between the fixation point and the reel and the distance between the lift force and the reel remained constant.

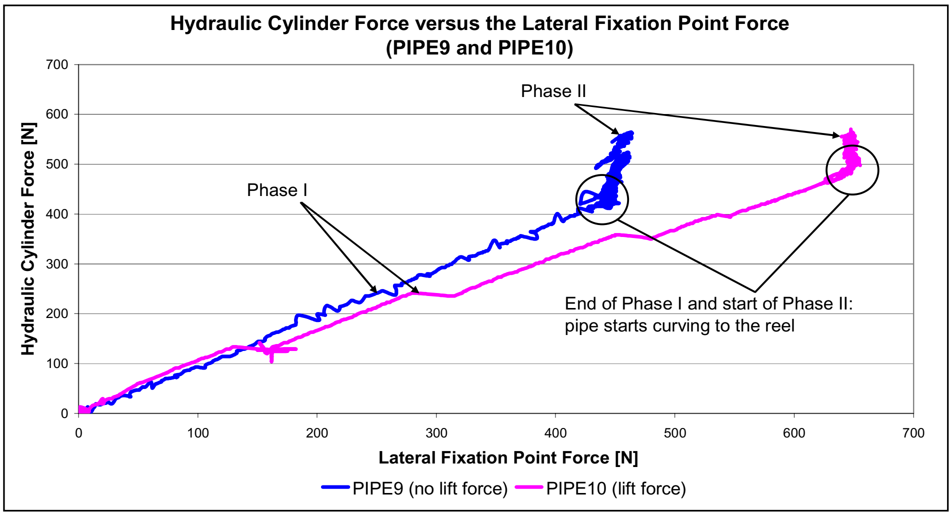

Figure 5.11 Hydraulic cylinder force versus the lateral fixation point force (PIPE9 and PIPE10)

5.3.2.2 Ovalisation of the Pipe

Ovalisation of the pipe (f) affects the resistance of the pipe to collapse due to external water pressure and local buckling [23]. Although the main objective of the small scale bending rig was to prepare for the full scale bending rig, ovalisation was investigated because of its importance during reeling. According to the DNV OS F101 standard [11], the amount of ovalisation due to bending, together with the out of roundness tolerances from the fabrication process of the pipe (Figure 5.12 and Equation (5.14)), should not exceed 3 %.

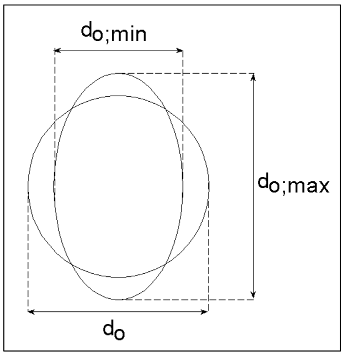

Figure 5.12 Ovalisation

$$f = \left(d_{O;\max} - d_{O;\min}\right) / d_O \tag{5.14}$$

Ovality measurements of the pipe taken after the bending tests (Table 5.4) using a sliding calliper, were taken sufficiently far from the initial contact point, because ovalisation was distorted there: the initial contact point moved a few millimetres towards the hydraulic cylinder at the start of the bending test (Figure 5.13). Ovality measurements of the pipe taken after the bending tests (Table 5.4) represented the maximum ovality measured in the curved pipe. It should be realised that the degree of ovalisation of the 22 mm outer diameter pipes was small and difficult to measure.

Figure 5.13 Movement of the initial contact point towards the hydraulic cylinder

In Table 5.4 ovalisation of the pipe measured after the reeling simulation tests (f_{AB}) is compared with ovalisation of the pipe, predicted using the DNV Offshore Standard OS-F101 [11] design formula (Equation (5.15)). This design formula for ovalisation is valid at maximum bending strain for the pure bending case (f_{MBS}).

$$f_{MBS} = f_0 + \left(0.030 \cdot \left(1 + \frac{d_o}{120 \cdot t} \right) \cdot \left(2 \cdot \varepsilon_b \cdot \frac{t}{d_o} \right)^2 \right) \tag{5.15}$$

Table 5.4 Comparison of the measured and the predicted ovalisation

PIPE	f_{AB} test [%] (measured after unloading)	f_{MBS} DNV [%] (maximum bending strain)
1	1.8	1.4
2	-	-
3	-	-
5	6.4	5.9
7	-	-
4	3.6	2.0
6	3.2	2.0
8	3.6	4.5
9	3.2	4.5
10	2.5	4.5
11	4.5	4.5

Table 5.4 shows that for some bending tests the measured values for the ovalisation after unloading (f_{AB}) were lower than the values according to the DNV Offshore Standard OS-F101 [11] formula at maximum bending (f_{MBS}). Part of these differences were the result of Equation (5.15) being a design formula predicting a “safe” value for ovalisation. Moreover, Equation (5.15) predicts ovalisation at maximum bending strain while measurements were performed after the bending test. During unloading of the pipe, a reduction of the ovalisation occurred [29]. Ovalisation at maximum bending strain in the small scale reeling tests was not measured. Ovalisation meters measuring ovality during the test were used in the full scale testing, however.

For some bending tests, the measured ovalisation of the pipe, unloaded after the test, was larger than the Offshore Standard OS-F101 [11] prediction for ovalisation at maximum bending strain. This may be due to the DNV Offshore Standard OS-F101 (2000) being valid for pure bending while ovalisation during reeling is the result of bending, a reaction force of the reel on the pipe and axial tension (Figure 5.3 and Figure 5.10). The reaction force of the reel on the pipe in combination with the tension force increase ovalisation during bending [38]. It should be realised that ovalisation of the 22 mm outer diameter pipes was minimal and difficult to measure.

5.3.2.3 Local Buckling of the Pipe

In order for the pipe to have enough resistance against collapse once it has been installed on the seabed, local buckling of the pipe has to be avoided. Excessive local buckling also obstructs a pig from passing through the pipe. More information why local buckling should be avoided can be found in Subsection 7.3.4. Although the main objective of the small scale bending rig was to prepare for the full scale bending rig, local buckling was investigated because of its importance during reeling.

Local buckling is assumed to be avoided if the maximum bending strain in the pipe remains below the predicted critical buckling strain. In the tests, local buckling was visually verified. It should be realised that the detection of the local buckle in the test depended on the eyesight of the person evaluating the local buckle. Whether local buckling occurred was therefore a subjective phenomenon. Since the main objective of the small scale reeling tests was to prepare for the full scale reeling tests of Tight Fit Pipe, a more accurate device to measure local buckling was not developed. A more accurate device to measure local buckling of the liner pipe was made for the bending tests of Tight Fit Pipe, however. It should also be noted that there is currently no agreement on the definition of a local buckle. In the full scale bending tests of Tight Fit Pipe, a definition of local buckling of the liner pipe was developed (Subsection 7.3.4).

In the small scale bending tests, one pipe was bent on a large reel with a reel diameter of 545 mm (PIPE5) while another pipe, with the same dimensions, was bent on a smaller reel with a reel diameter of 350 mm (PIPE7). Curvature and strain measurements were not performed. The maximum bending strains occurring in the pipes PIPE5 and PIPE7 during the small scale reeling tests were therefore calculated using Equations (5.16) and (5.17).

$$\kappa = \frac{1}{(D_{reel}/2) + r_o} \qquad (5.16)$$

$$\varepsilon_b = \kappa \cdot r_o \qquad (5.17)$$

Murphy and Langner [36] developed an empirical equation (Equation (5.18)) to predict the critical buckling strain of a pipe in bending. This equation can also be found in API RP1111 [2].

$$\varepsilon_{cr} = 0.5 \cdot \frac{t}{d_o} \qquad (5.18)$$

On the basis of available experimental results, Gresnigt [23] developed Equation (5.19) to predict the critical buckling strain (assuming no initial ovalisation) of a pipe.

$$\varepsilon_{cr} = 0.25 \cdot \frac{t}{r_a} - 0.0025 \tag{5.19}$$

The DNV Offshore Standard OS-F101 [11] uses Equation (5.20) to predict the critical buckling strain of pipe.

$$\varepsilon_{cr} = 0.78 \cdot \left(\frac{t}{d_o} - 0.01 \right) \cdot \alpha_h^{-1.5} \cdot \alpha_{gw} \tag{5.20}$$

The predictions for the critical buckling strain (ε_{cr}) by Murphy and Langner [36], Gresnigt [23] and the DNV Offshore Standard OS-F101 [11] are compared with the maximum bending strain (ε_b) in PIPE5 and PIPE7 in Table 5.5. Visual inspection of the pipe indicated that local buckling occurred between 1.98 % bending strain and 3.05 % bending strain.

Table 5.5 Comparison of the predicted critical buckling strain with the strain measurements in PIPE5 and PIPE7

	Test	Theoretical predictions		
PIPE	ε_b [%]	ε_{cr} Equation (5.18) [%]	ε_{cr} Equation (5.19) [%]	ε_{cr} Equation (5.20) [%]
5	-1.98	-2.95	-2.89	-4.01
7	-3.05			

When comparing the buckling equations by Murphy and Langner [36], Gresnigt [23] and the DNV Offshore Standard OS-F101 [11] with the measured data, it should be taken into account that these equations are based on experimental data from pure bending tests, not taking the reaction force of the reel on the pipe into account. The reaction force of the reel on the pipe enhances local buckling of the pipe. This may be one of the reasons why the DNV Offshore Standard OS-F101 equation overestimates the critical buckling strain measured in the small scale reeling tests. Moreover, it should be taken into account that the guidance note in this standard states that for diameter to thickness ratios smaller than 20 this equation may only be utilised provided that full scale testing, observation or former experience indicates a sufficient safety margin. The diameter to thickness ratio of PIPE5 and PIPE7 is 17.

The predictions for the critical buckling strain by Gresnigt [23] and Murphy and Langner [36] compared well with the measured strains during the bending tests. To this, two remarks must be made:

1. When comparing the local buckling predictions by Gresnigt [23] and Murphy and Langner [36] to (general) four point bending test results, these equations predict a (safe) underestimation of the critical buckling strain in the lower diameter to

thickness ratio region of below 40. This is the consequence of the fact that these equations were initially not developed for pipelines with these diameter to thickness ratios (less than 40). Because of the low diameter to thickness ratio of PIPE5 and PIPE7 (17), these equations would **underestimate** the experimentally determined critical buckling strains of PIPE5 and PIPE7.

2. The predictions by Gresnigt [23] and Murphy and Langner [36] are based on four point bending test results (pure bending), which do not take a reaction force of the reel onto the pipe into account. Comparing these predictions with the buckling test results from reeling (bending and a reaction force of the reel onto the pipe), will thus result in an **overestimation** of the test results, because the reaction force of the reel onto the pipe enhances local buckling.

Both phenomena compensate each other resulting in the predictions for the critical buckling strain by Gresnigt [23] and Murphy and Langner [36] to compare well with the strains in the bending tests.

5.4 Differences between Actual Reeling and Simulated Reeling in a Bending Rig

The spooling-on phase of the reeling process was simulated by small scale bending testing to prepare for the full scale bending testing. It was necessary to be aware of how the bending tests (small scale and full scale) resembled the spooling-on phase and how the bending tests differed from the actual spooling-on process. It needed to be determined whether these differences could be neglected or how they could be accounted for. When comparing actual reeling with simulation of reeling in a bending rig (small scale and full scale), several differences were identified:

1. During actual reeling the reaction force of the reel on the pipeline ($F_{reel;T;P}$) is in equilibrium with the perpendicular force in the tensioner ($F_{T;P}$ in Figure 5.3) and the reaction force of the reel on the pipeline is small due to a large distance between the reel and the tensioner. In the bending rig the reaction force of the reel on the pipe ($F_{reel;HC;P}$) was in equilibrium with the perpendicular component of the hydraulic cylinder force ($F_{HC;P}$ in Figure 5.8) and the reaction force of the reel on the pipe was relatively large due to the relatively small distance between the reel and the hydraulic cylinder.
2. During actual reeling the reaction force of the reel on the pipeline ($F_{reel;T;P}$) is constant because of the fixed distance between the tensioners and reel on board of the reeling vessel. In the bending rig the reaction force of the reel on the pipe ($F_{reel;HC;P}$) was not constant in value. This reaction force of the reel on the pipe increased as more pipe became in contact with the reel and the distance between the reel and the hydraulic cylinder decreased.
3. During actual reeling, the tension force in the pipeline delivered by the tensioners ($F_{T;A}$ in Figure 5.3) is constant. In the bending rig the tension force in the pipe caused by the axial component of the hydraulic cylinder ($F_{HC;A}$) was increasing in

value throughout the test due to the increasing hydraulic cylinder force and the changing orientation of the hydraulic cylinder (Figure 5.8).

4. During actual reeling a pipeline with welds is being reeled while in the small scale reeling test only pipes without a weld were reeled. However, in the full scale bending rig pipes with a weld were reeled (Chapter 6 and 7).

The main difference between actual reeling and reeling in the bending rig is the difference in the reaction force of the reel on the pipe. This force may be small and constant during actual reeling and relatively large and varying in the bending rig. Furthermore, during actual reeling the tension force is usually constant whilst in the bending rig the value was continuously changing.

As the reaction force of the reel on the pipe may be larger in the bending test than in reality and as this enhances ovality and local buckling, ovalisation of the pipe in the bending rig could be larger than in reality. Also the start of local buckling was influenced by a larger reaction force of the reel on the pipe in the test than in reality. However, since the reaction force of the reel on the pipe will be known throughout the full scale bending tests to be performed (by measuring the hydraulic cylinder force and the angles ζ and β), the influence of this force on ovality and local buckling can be accounted for. Moreover, due to the fact that ovality of the pipe measured in the bending test could exceed ovality measured during actual reeling, the bending test provided a conservative, and therefore safe, approach to ovalisation. The phenomenon of local buckling was also approached conservatively in the bending tests compared to actual reeling. It should also be taken into account that the distance between the reel and the tensioners during actual reeling varies per vessel resulting in a different reaction force of the reel on the pipe.

The influence of the tension force on the ovality of the pipe is much less than the influences of the bending moment or the perpendicular reaction force [23]. Therefore, the fact that the axial tension force is constant during actual reeling whereas it changed in the bending rig was expected to have minimal influence on ovalisation and local buckling.

From the above it can be concluded that the bending tests in the bending rig (either full scale or small scale) were able to provide reliable information on the ovalisation and the local buckling behaviour of a pipe during actual reeling. The most important parameters influencing ovalisation and local buckling being the size of the reel and the related curvature and bending strain applied on the pipe, were identical to actual reeling in the reeling simulation tests. Although there were differences between actual reeling and the reeling simulation, these differences could be neglected or they could be accounted for.

5.5 Conclusions

In preparation of the design of a full scale bending rig for reeling simulation of 12.75 inch outer diameter Tight Fit Pipe, small scale bending tests were executed on eleven 22 mm outer diameter single walled pipes. The developed theoretical model describing the forces on the pipe by the small scale bending rig proved to be acceptable and could be used in the design of the full scale bending rig. The eventual full scale bending rig had the same test set-up as the small scale bending rig at the end of the small scale reeling simulation testing: the pipe was axially and laterally fixed on one side while a hydraulic cylinder pulled the pipe against different reel sizes in order to study the initiation and the degree of local buckling as well as the degree of ovalisation of the pipe with increasing curvature. Also a lift force was present in the eventual full scale bending rig. The small scale bending test experience was useful in the preparation and the execution of the full scale bending tests.

Although the main objective of the small scale bending rig was to prepare for the full scale bending rig, ovalisation and local buckling were investigated because of their importance during reeling. Although ovalisation was difficult to measure due to the small size of the pipe, the ovality of the pipes measured after the bending tests approached the DNV Offshore Standard OS-F101 prediction for ovalisation at maximum bending strain.

The predictions for the critical buckling strain by Gresnigt [23] and Murphy and Langner [36] compared well with the measured strains during the bending tests. To this, two remarks must be made:

1. When comparing the local buckling predictions by Gresnigt [23] and Murphy and Langner [36] to (general) four point bending test results, these equations predict a (safe) underestimation of the critical buckling strain in the lower diameter to thickness ratio region of below 40. This is the consequence of the fact that these equations were initially not developed for pipelines with these diameter to thickness ratios (less than 40). Because of the low diameter to thickness ratio of PIPE5 and PIPE7 (17), these equations would **underestimate** the experimentally determined critical buckling strains of PIPE5 and PIPE7.
2. The predictions by Gresnigt [23] and Murphy and Langner [36] are based on four point bending test results (pure bending), which do not take a reaction force of the reel onto the pipe into account. Comparing these predictions with the buckling test results from reeling (bending and a reaction force of the reel onto the pipe), will thus result in an **overestimation** of the test results, because the reaction force of the reel onto the pipe enhances local buckling.

Both phenomena compensate each other resulting in the predictions for the critical buckling strain by Gresnigt [23] and Murphy and Langner [36] to compare well with the strains in the bending tests.

6 Full Scale Reeling Simulation of Single Walled Pipe

6.1 Introduction

The objective of the full scale bending test on a 12.75 inch outer diameter single walled pipe was to prepare for the full scale bending tests on the 12.75 inch outer diameter Tight Fit Pipes. By testing this single walled pipe in the bending rig prior to testing the Tight Fit Pipes, the fitness for purpose of the full scale bending rig was verified. Another objective of the reeling simulation test on the single walled pipe was to test the influence of a different bending moment capacity of subsequent pipes in a pipeline. Although the manufacturing process aims to fabricate pipes with constant material and geometric properties there will always be some variation per pipe element [3]. Therefore, the test piece that was bent consisted of two 12.75 inch outer diameter single walled pipes with different wall thicknesses, which were connected by a weld.

The test set-up is described first (Subsection 6.2), focussing on the rig itself (Subsection 6.2.1), the measuring equipment used (Subsection 6.2.2) and the properties of the test piece (Subsection 6.2.3). Comparison of the experimental results with the theoretical predictions is subsequently reported in Subsection 6.3.

6.2 Test Set-up

6.2.1 Full Scale Bending Rig

The test pipe was bent step by step to smaller bending radii in order to investigate its local buckling behaviour. Reel radii available were 9 m, 8 m, 7.5 m, 7 m, 6.5 m, 6 m, 5.5 m and 5 m. While step by step bending the pipe on the decreasing reel sizes, the forces present in the bending rig were monitored as well as the bending strain in the pipe and the pipe’s ovalisation and local buckling.

The test set-up of the full scale bending rig (Figure 6.1 and Figure 6.2) was similar to the test set-up of the small scale bending rig (Chapter 5).

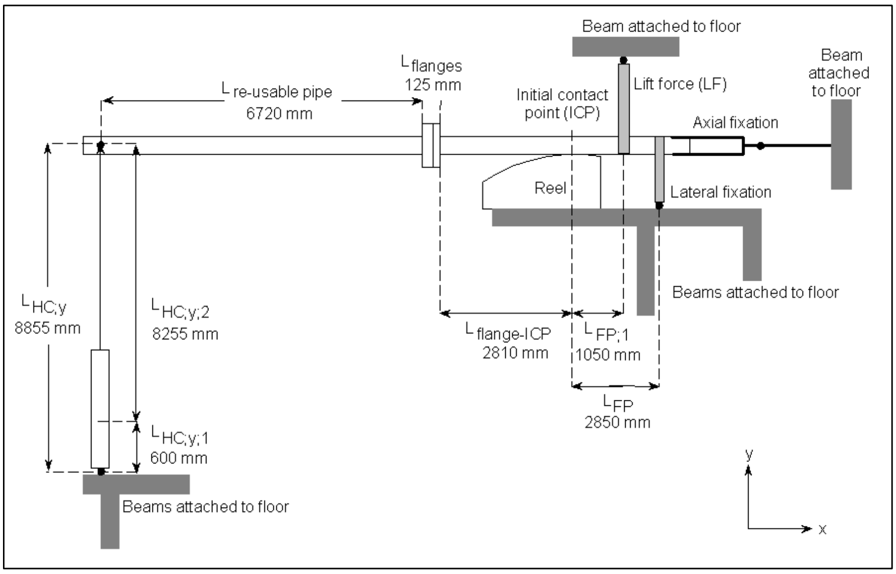

Figure 6.1 Schematic overview of the full scale bending rig (not to scale)

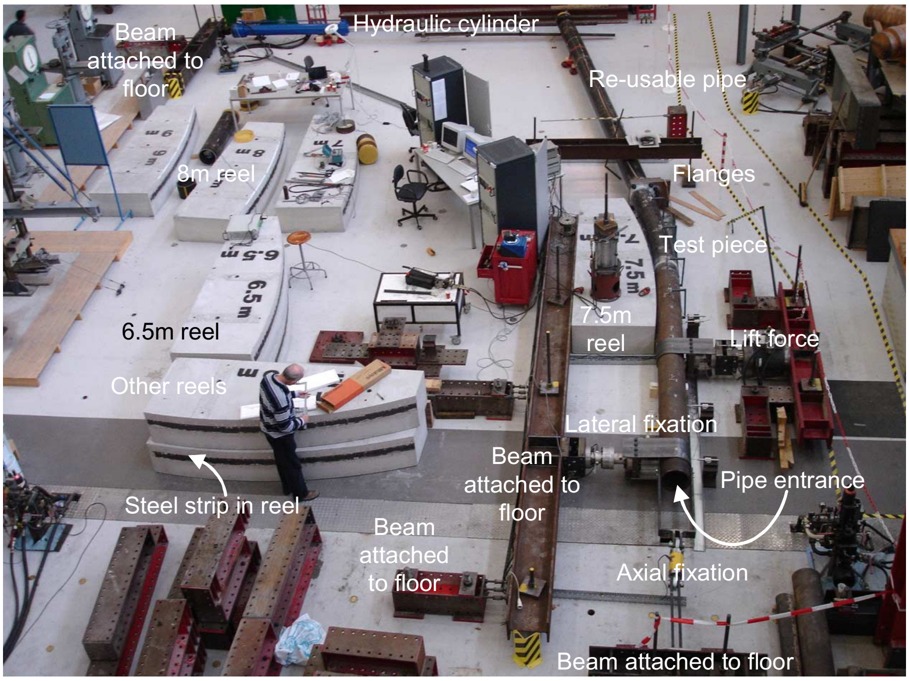

Figure 6.2 Full scale bending rig in the laboratory

The five main elements of the full scale bending rig (Figure 6.1 and Figure 6.2) are described in more detail below:

1. Test piece
2. Fixation of the pipe
3. Hydraulic cylinder
4. Reels
5. Lift force

1. Test piece

In Figure 6.1, Figure 6.2 and Figure 6.3 it can be seen that in the bending rig the test-piece was connected to the re-usable pipe by means of a flanged connection (Figure 6.3). The length between the reel and the hydraulic cylinder (in the form of the re-usable pipe) was needed in order to reduce the reaction force of the reel on the pipe during the bending test (Chapter 5). The maximum length of the re-usable pipe of 6720 mm was determined by space restrictions in the laboratory. How the difference between the length between the reel and the hydraulic cylinder in a laboratory and the length between the reel and the tensioners in reality influences the results of the bending tests (e.g. ovalisation and local buckling), has been explained in Subsection 5.4. In the beginning of the test, the reaction force of the reel on the pipe was reduced by adding a lift force (Chapter 5).

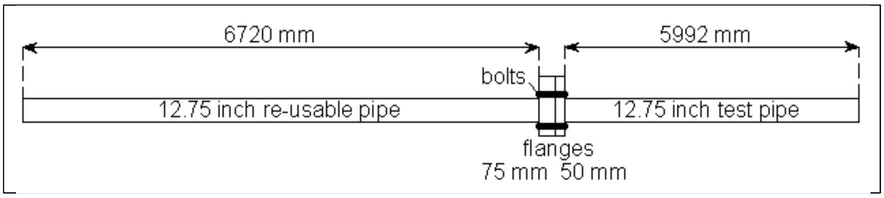

Figure 6.3 Schematic overview of the test piece connected to the re-usable pipe by means of flanges and bolts (not to scale)

The flange of the test piece was 50 mm thick and connected to a 75 mm thick flange at the end of the re-usable pipe (Figure 6.3). The flange of the re-usable pipe was thicker than the flanges of the test pieces in order to avoid plastic deformation of that flange. The 50 mm thick flanges at the end of the test pieces were only being used in one bending test, so some plastic deformation could be tolerated. The flanges were connected by means of M39, 10.9 bolts which were placed as close as possible to the pipe in order to transfer the bending moment without plastically deforming the flange itself (Figure 6.4).

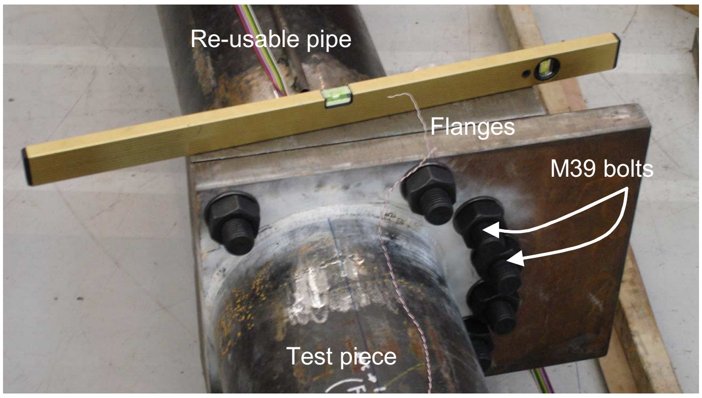

Figure 6.4 Test piece connected to the re-usable pipe by flanges and M39, 10.9 bolts

2. Fixation of the pipe

Movements of the test piece in the axial and lateral directions were restricted (Figure 6.1 and Figure 6.5). The axial fixation structure was designed such that an internal scanning device for liner pipe wrinkling (local buckling of the liner pipe) measurement used in the Tight Fit Pipe bending tests (Chapter 7) could enter the pipe from this side (Figure 6.2). The other side of the test piece was closed by the flange. A load cell in the axial fixation structure enabled measurement of the axial force. Two hinges allowed rotation in the horizontal and vertical planes.

The lateral fixation of the test piece consisted of a steel sheet around the pipe connected to a load cell. The steel sheet supported the pipe while at the same time allowing good transfer of the forces into the pipe. The load cell was connected to a hinged structure, which facilitated the pipe to move slightly in the x-direction (Figure 6.1) during the bending test. The axial and lateral fixation structures were attached to the floor by relatively large diameter, pre-stressed steel rods.

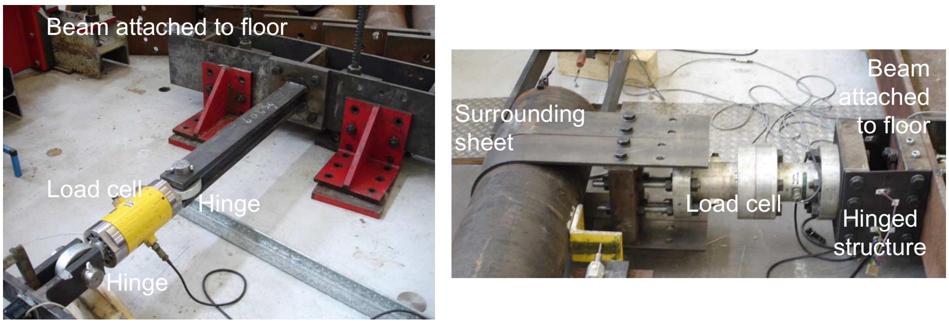

Figure 6.5 Axial fixation (left) and lateral fixation (right) of the test piece in the full scale bending rig

3. Hydraulic cylinder

A hydraulic cylinder with a stroke of 2000 mm was used. The maximum displacement when bending the pipe on the 5 m radius reel was 3728 mm. By means of a pinned connection (Figure 6.6) in the connecting rod, the length of the connecting member could be adapted (Figure 6.7). The hydraulic cylinder and the re-usable pipe were both positioned on wheels which allowed them both to easily move horizontally during the bending process (Figure 6.6 and Figure 6.7). The hydraulic cylinder was connected to a beam by a hinge which facilitated the hydraulic cylinder to rotate in the horizontal plane. This beam was connected to the floor by steel rods under pre-tension (Figure 6.6).

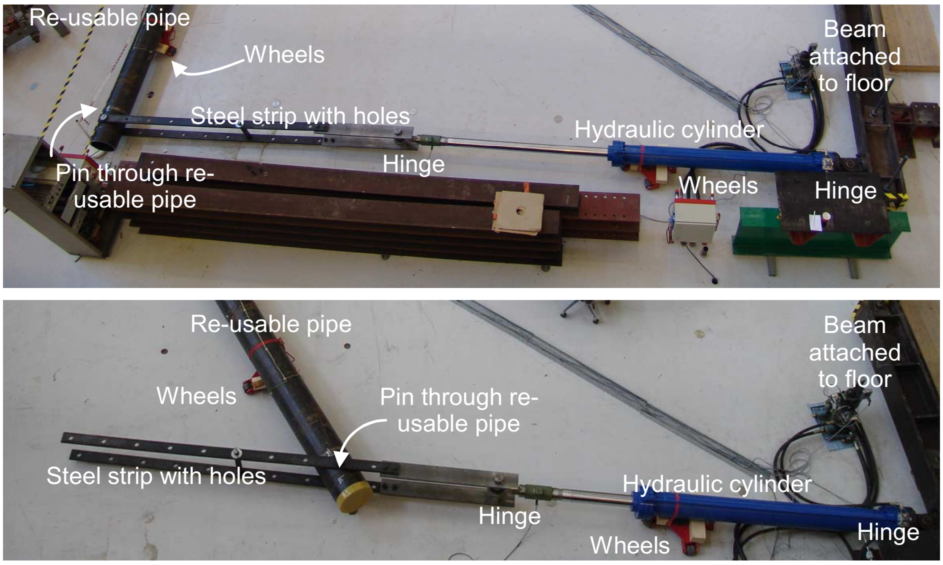

Figure 6.6 Connection of the hydraulic cylinder to the re-usable pipe in the bending rig

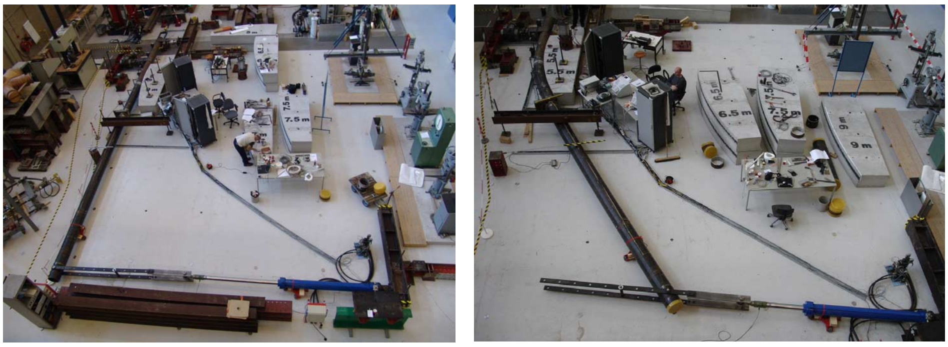

Figure 6.7 Bending the test pipe to the reels of decreasing sizes; the 9 m radius reel (left) and the 6.5 m radius reel (right)

4. Reels

Eight reels with different radii were simulated by curved, reinforced concrete formers with a steel strip in the curved side to avoid crushing of the concrete on the contact point of the pipe with the curved former, i.e. the reel (Figure 6.2). The reel was prevented from moving by attaching it to the floor by three steel rods under pre-tension (Figure 6.8). A beam, also attached to the floor by steel rods under pre-tension, located behind the reel, prevented the reel from moving as well (Figure 6.8).

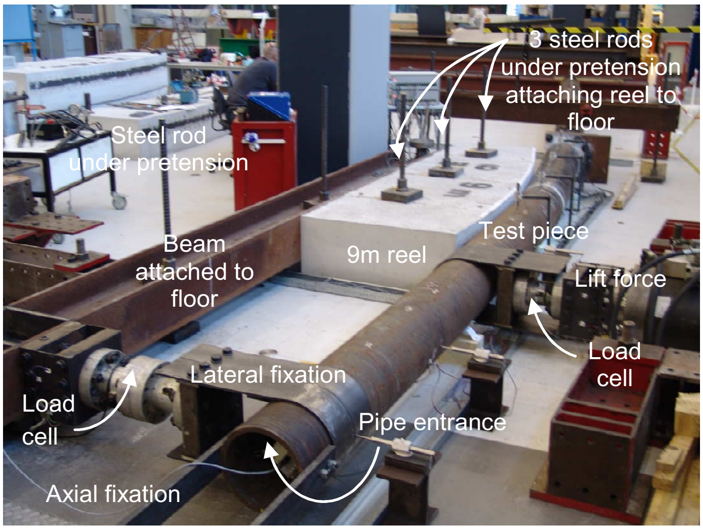

Figure 6.8 The movement of reel was restricted by attaching the reel and the beam located behind the reel to the floor by rods under pre-tension

5. Lift force

As has been explained in Chapter 5, at the end of Phase I (Figure 5.9), when the plastic bending moment was reached at the initial contact point, the reaction force of the reel on the pipe (F_{reel}) equalled the hydraulic cylinder force (F_{HC}) plus the lateral fixation point force ($F_{FP;P}$). Then, just after Phase I and throughout Phase II (Figure 5.9), the reaction force of the reel on the pipe (F_{reel}) was divided into two components: one ($F_{reel;FP}$) was in equilibrium with the lateral fixation point force ($F_{FP;P}$) and the other ($F_{reel;HC;y}$) was in equilibrium with the y-component of the hydraulic cylinder force ($F_{HC;y}$). Just after Phase I in the beginning of Phase II, neglecting the bending of the pipe itself for reasons of simplicity, $F_{HC;y} \approx F_{HC} = F_{reel;HC}$. It is thus desirable to reduce the initial reaction force of the reel (F_{reel}) to a value not exceeding the hydraulic cylinder force (F_{HC}) in the beginning of Phase II. Phase II resembled reeling in reality. In this manner unrealistic ovalisation and local buckling at the initial contact point could be avoided.

Using Equations (5.8), (5.11), (5.12) and (5.13), it was predicted that a lift force 1.6 times the magnitude of the lateral fixation point force was needed to reduce the reaction force of the reel on the pipe (F_{reel}) at the end of Phase I. This reaction force needed to be reduced to the value of the hydraulic cylinder force at the beginning of Phase II ($F_{HC} \approx F_{HC;y} = F_{reel;HC}$). The beginning of Phase II is identical to the end of Phase I. Using available equipment, only a lift force 0.8 times the magnitude of the lateral fixation point force could be applied. This resulted in a predicted reaction force of the reel on the pipe at the end of Phase I of 125 kN, while the predicted hydraulic cylinder force at the end of Phase I was 74 kN. To compensate for this boundary effect, measurements for ovalisation and local buckling were taken sufficiently far away from the initial contact point. Moreover, it should be realised that these forces were actually distributed loads but were assumed to be concentrated loads for reasons of simplicity. A distributed load is less detrimental with regard to ovalisation and local buckling. It will be seen later that in the full scale bending tests of Tight Fit Pipe the lift force will not be used anymore, because even if no lift force was applied, excessive ovalisation and local buckling at the initial contact point did not occur.

The lift force in the full scale bending test of 12.75 inch single walled pipe was applied in an identical manner as the lateral fixity of the pipe (Figure 6.8).

6.2.2 Measuring Equipment in the Full Scale Bending Rig

During the test four main areas of interest were monitored:

1. Forces in the bending rig
2. Strain and curvature of the pipe
3. Ovalisation of the pipe
4. Local buckling of the pipe

1. Forces in the bending rig

The hydraulic cylinder force was measured by a load cell. The forces restraining the axial and lateral movements of the pipe were measured by load cells positioned at the axial and lateral fixation points (Figure 6.5). The lift force was measured in the load cell located in the lift force configuration (Figure 6.8).

During testing, the displacement of the hydraulic cylinder in the x-direction (Δx_{HC} in Figure 5.8) was measured by a displacement meter located 600 mm from the hinged connection of the hydraulic cylinder with the beam (Figure 6.9). From the measured displacement in the x-direction of the hydraulic cylinder, the rotation of the hydraulic cylinder (angle ζ in Figure 5.8) was calculated. Angle ζ enabled determination of the movement of the end of the re-usable pipe in the x- and y-directions as well as the x- and y-components of the hydraulic cylinder force. These variables were required for example as input parameters for a finite element model of the full scale bending test [20], [27].

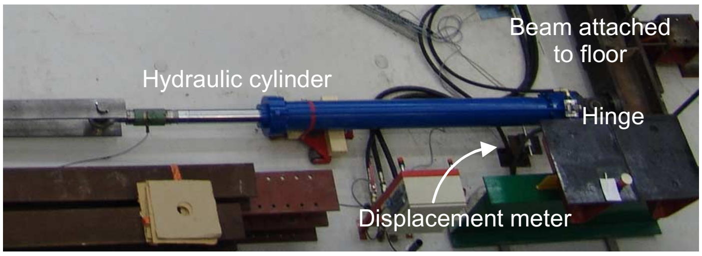

Figure 6.9 Displacement meter measuring the movement of the hydraulic cylinder

Angle β (Figure 5.8) needed to be measured throughout the test to determine the transverse and axial components of the hydraulic cylinder force at the end of the pipe ($F_{HC;A}$ and $F_{HC;P}$). These could then be used to determine the forces that influenced ovalisation and local buckling of the pipe during the bending test: the transverse reaction force of the reel on the pipe ($F_{reel;HC;P}$), the tension force in the pipe and the distributed load of the reel on the pipe (q_{reel}) [38].

1 mm thick copper strips (Figure 6.10), attached at regular intervals along the curved part of the concrete reel, were used to determine the point of contact from which angle β could be determined. As the pipe came in contact with a copper strip, the hydraulic cylinder force, needed to bring this length of pipe in contact with the reel, was recorded. The position of the copper strips along the reel (defining the different lengths of pipe being in contact with the reel), together with the measured hydraulic force, defined the transverse and axial components of the hydraulic cylinder force at the end of the pipe during the various stages in the test.

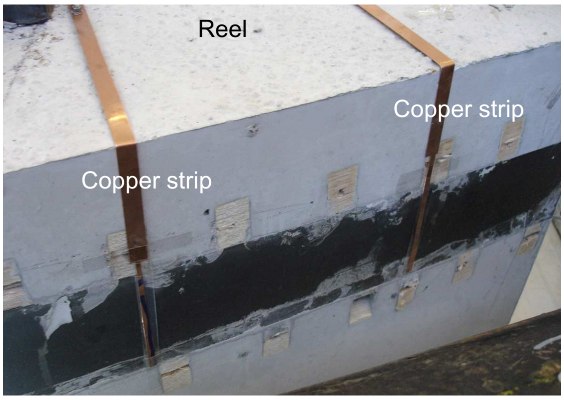

Figure 6.10 Copper strips attached at regular intervals along the curved part of the concrete reel, used to determine the point of contact of the pipe with the reel

2. Strain and curvature of the pipe

Strain was measured by uni-axial strain gauges attached to the pipe in the tension zone and in the compression zone (numbers 1 to 16 in Figure 6.11). Strain gauge 12 was not used since it would have been located at the initial contact point in the compression zone. The strain gauges in the compression zone became squeezed once the pipe was in contact with the curved former, simulating the reel.

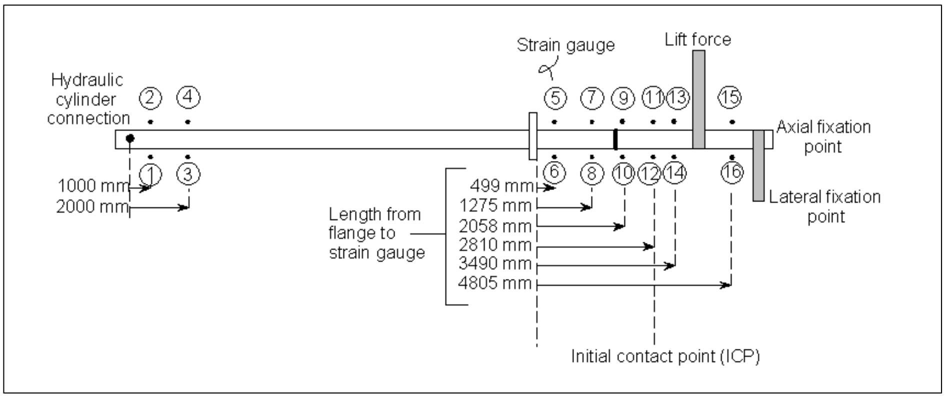

Figure 6.11 Schematic overview of the distribution of the axial strain gauges (numbers 1 to 16) over the pipe

3. Ovalisation of the pipe

Ovalisation (Figure 5.12 and Equation (5.14)) was measured at four locations along the pipe by ovalisation meters positioned at 499 mm, 1275 mm, 2058 mm and 2810 mm from the flange (Figure 6.11). The ovalisation was measured at the same locations where the strain gauges were mounted. Ovalisation was measured by hand using a sliding calliper prior to and stepwise after bending. Ovalisation meters measured ovalisation during the test. The ovalisation meter consisted of a steel U frame attached to the bottom of the pipe. A displacement meter in the top of the frame measured the vertical increase of the outer diameter of the pipe (Figure 6.12).

Only the increase in the outer diameter in the vertical plane could be measured due to the presence of the reel. During ovalisation, the decrease in the diameter in the horizontal plane is not identical to the (measured) increase in the diameter in the vertical plane. A ratio was defined between the horizontal change in the diameter and the vertical change in the diameter measured by hand after each bending stage. The horizontal change in diameter at maximum bending and after unloading was determined by multiplying the vertical change in diameter measured by the ovalisation meter at maximum bending and after unloading by this ratio. Ovalisation at maximum bending and after unloading was determined by the ovalisation meters in this manner. It was assumed that the ratio between the horizontal and vertical changes in diameter at maximum bending is the same as after bending. The value of ovalisation at maximum bending was compared to predictions for ovalisation valid when the pipe was bent on the reel.

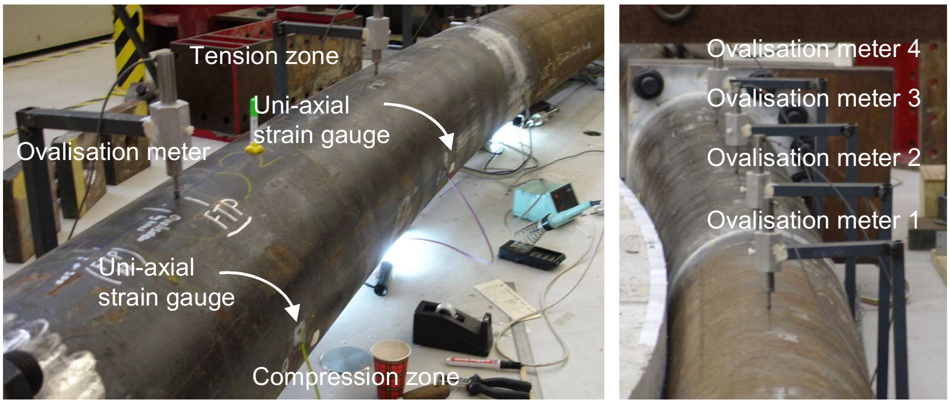

Figure 6.12 Axial strain gauges and ovalisation meters attached to the pipe

4. Local buckling of the pipe

Identification of the occurrence of local buckling of the pipe was done by visual inspection after the bending test. Temporary absence of the reel during the replacement of a reel by a smaller size, allowed for identification of a local buckle. As in the small scale reeling simulation tests (Chapter 5), it should be realised that the detection of a local buckle of the pipe in the test depended on the eyesight of the person evaluating the local buckle. Whether local buckling occurred was therefore a subjective phenomenon. Since the main objective of this test was to verify the fitness for purpose of the bending rig, a more accurate device to measure local buckling of the pipe was not developed. As mentioned earlier, a more accurate device to measure local buckling of the liner pipe was made for the bending tests of Tight Fit Pipe, however. It should also be noted that there is currently no agreement on the definition of a local buckle. In the full scale bending tests of Tight Fit Pipe, a definition of local buckling of the liner pipe has been defined.

6.2.3 Test pipe

Although the manufacturing process aims to fabricate pipes with constant material and geometric properties, there will always be some variation per pipe element [3]. This results in differences in the bending strength properties of the pipes. If by chance a pipe with a high bending moment capacity (strong pipe) is spooled on the reel prior to a pipe with less bending moment capacity (weak pipe), buckling may occur in the weaker pipe close to the weld due to strain concentration at that location (Figure 6.13).

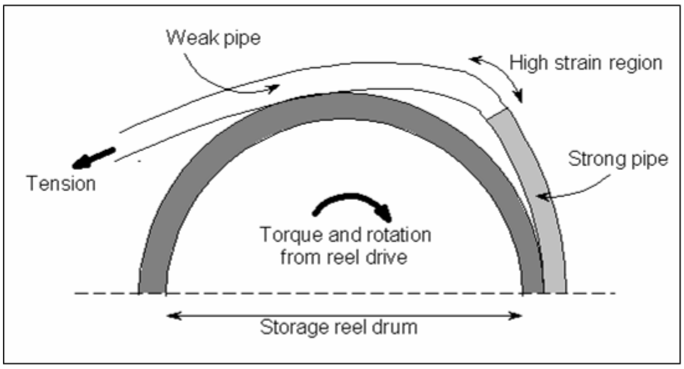

Figure 6.13 Effect of the variation in the properties of the reeled pipe

In order to simulate this situation, the test piece that was bent in the test rig consisted of a 21.77 mm thick, 12.75 inch outer diameter pipe (TEST-1) connected by a weld to an 18.65 mm thick, 12.75 inch outer diameter pipe (TEST-2). Pipes TEST-1 and TEST-2 were connected to each other in such way that TEST-1 was bent prior to TEST-2 (Figure 6.14).

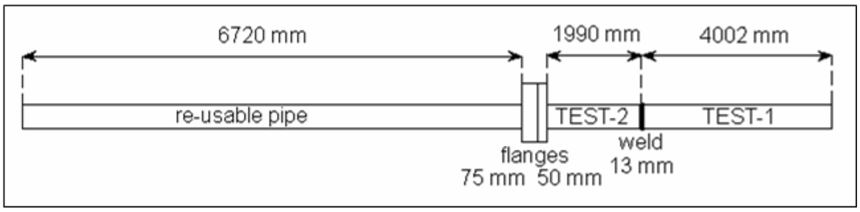

Figure 6.14 Schematic overview of the test piece to be bent in the full scale bending rig

In order to avoid large plastic deformations in the weld during reeling, the weld needs to be overmatching. The DNV OS-F101 standard [11] states that the yield strength of the welding consumable needs to be overmatching within the range of 80-200 MPa above the specified minimum yield strength of the base material. It can be seen in Table 6.1 that the weld was highly overmatching, although not within the range required by the DNV OS-F101 standard. This was due to the fact that the pipes (TEST-1 and TEST-2) were less strong than expected. Material testing defined the yield strength ($\sigma_{y;a}$) and the tensile strength ($\sigma_{t;a}$) of the pipes TEST-1 and TEST-2 (Subsection 3.3) while the yield strength and the tensile strength of the weld were determined from the welding specifications. Other properties of the pipes TEST-1 and TEST-2 that can be found in Table 6.1 are the wall thickness (t), the outer diameter (d_o), the length (L), the Young's modulus in the axial direction (E_a) and the calculated plastic bending moment capacity (M_P). The length of the weld (L) can also be found in Table 6.1.

Table 6.1 Properties of the pipes TEST-1 and TEST-2 and the connecting weld

	t [mm]	d_o [mm]	$\sigma_{y;a}$ [MPa]	$\sigma_{t;a}$ [MPa]	L [mm]	E_a [MPa]	M_P [kNm]
TEST-1	21.77	322.92	361	500	4002	200000	713
TEST-2	18.65	323.72	354	503	1990	200000	614
Weld	-	-	651	712	13	-	-

The 21.77 mm thick, 12.75 inch outer diameter pipe TEST-1 was machined next to the weld in order to reduce the risk of early buckling in the 18.65 mm thick pipe TEST-2. From the weld into the thick pipe, the pipe was first machined from 21.77 mm to a constant wall thickness of 19.49 mm over an average length of 302 mm. Then, a transition of average 16 mm in length ensured a change from 19.49 mm to 21.77 mm (Figure 6.15).

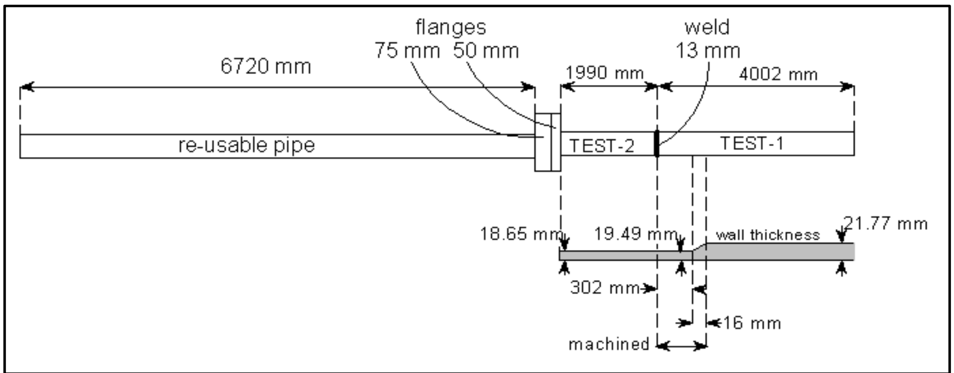

Figure 6.15 Schematic overview of the machined part of the pipe TEST-1

6.3 Comparison of the Experimental Data with the Theoretical Predictions

6.3.1 Forces in the Bending Rig

In Figure 6.16 the stepwise increase in the hydraulic cylinder force and the hydraulic cylinder rotation (angle ζ; Figure 5.8) can be seen for different reel sizes. In the bending test the pipe was bent to the 9 m radius reel by three strokes of the hydraulic cylinder because the stroke of the hydraulic cylinder was not enough to pull the pipe against this reel in one go. These three steps resulted in tests “9m-1”, “9m-2” and “9m-3” (Figure 6.16).

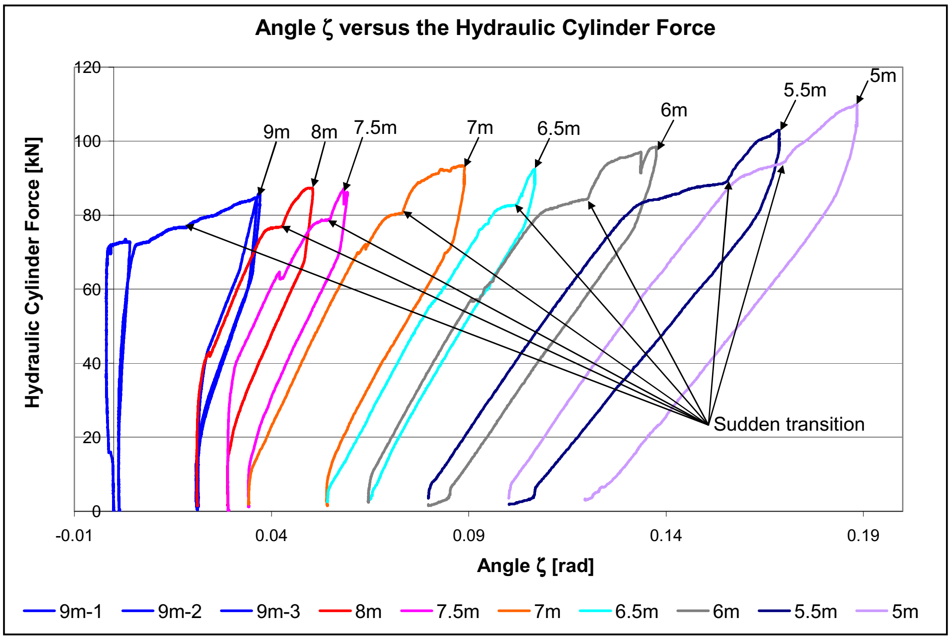

Figure 6.16 Angle ζ (defined in Figure 5.8) versus the hydraulic cylinder force

As has been described for the small scale reeling tests (Chapter 5), two phases are distinguished in a bending test. In Phase I the hydraulic cylinder force (F_{HC}) increases until the plastic bending moment has been reached in the initial contact point. In Phase II more pipe comes in contact with the reel reducing the distance between the reel and the hydraulic cylinder thereby increasing the hydraulic cylinder force. The lateral fixation point force ($F_{FP;P}$) increases in Phase I but thereafter remains constant in Phase II.

During bending, there was a sudden increase in the hydraulic cylinder force, after a short yielding plateau had been reached in the hydraulic cylinder force (Figure 6.16). This sudden increase in the hydraulic cylinder force can be explained by the fact that when the pipe was bent on the reel, the pipe was not in contact with the reel in the region surrounding the weld (Figure 6.13 and Figure 6.17). Only the pipe length next to the initial contact point and pipe length at the end of the test piece were in contact with the reel. Due to the sudden decrease in the length between the reel and the hydraulic cylinder when the end of the test piece came in contact with the reel, the hydraulic cylinder force needed to increase in order to generate the bending moment at the new contact point.

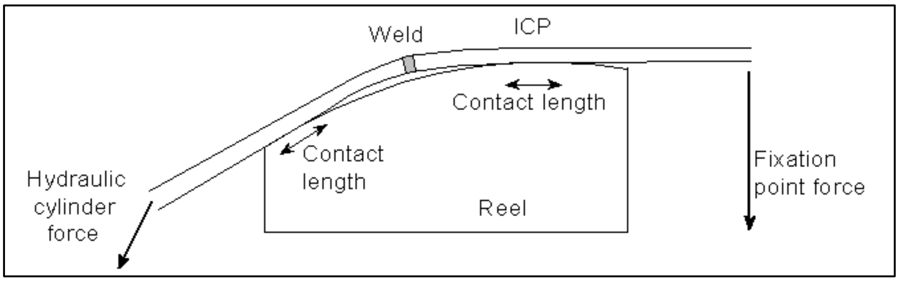

Figure 6.17 Pipe not completely in contact with the reel while bending it on the reel (ICP = initial contact point of the pipe with the reel)

The fact that the region surrounding the weld was not in contact with the reel caused the copper strip position meters (Figure 6.10) in this region not to give a signal. The copper strip near the initial contact point and the copper strip near the end of the reel did give a signal of the pipe being in contact with the reel. The pipe length in contact with the reel was recorded manually (Figure 6.17).

In Table 6.2 the measured maximum hydraulic cylinder force ($F_{HC;max}$) and its x- and y-components ($F_{HC;x;max}$ and $F_{HC;y;max}$) can be found for each reel size in the bending test. Furthermore, the maximum displacements and the residual displacements after unloading in the x- and y-directions of the connection between the hydraulic cylinder and the re-usable pipe (Δx_{max}, Δy_{max}, Δx_{res} and $\Delta y_{res;}$ Figure 6.18) can be found in Table 6.2. $F_{HC;x;max}$ and $F_{HC;y;max}$ were used as input in the finite element analysis while Δx_{max}, Δy_{max}, Δx_{res} and Δy_{res} were used in the finite element analysis for verification purposes [27].

Table 6.2 Maximum measured forces and displacements during the bending test

	$F_{HC;max}$ [kN]	$F_{HC;x;max}$ [kN]	$F_{HC;y;max}$ [kN]	Δx_{max} [mm]	Δy_{max} [mm]	Δx_{res} [mm]	Δy_{res} [mm]
9 m-1	73	0	73	22	1318	12	715
9 m-2	85	3	85	238	2222	157	1549
9 m-3	86	3	86	245	2252	154	1566
8 m	87	4	87	314	2479	204	1803
7.5 m	87	5	87	360	2688	237	1910
7 m	93	8	93	523	2904	363	2169
6.5 m	92	10	92	624	3028	424	2301
6 m	98	13	98	755	3392	500	2600
5.5 m	103	17	101	887	3638	603	2857
5 m	110	21	108	960	3819	692	3086

It should be noted in Table 6.2 that the maximum hydraulic cylinder force is relatively high when bending the pipe to the 7 m radius reel. This can be explained by the fact that in these tests the end of bending the pipe to the reel was not yet defined. This problem was solved in the Tight Fit Pipe bending tests by always terminating the bending of the pipe to the reel when the pipe came in contact with the last position meter along the curved reel (position meter PM8 in Figure 7.12).

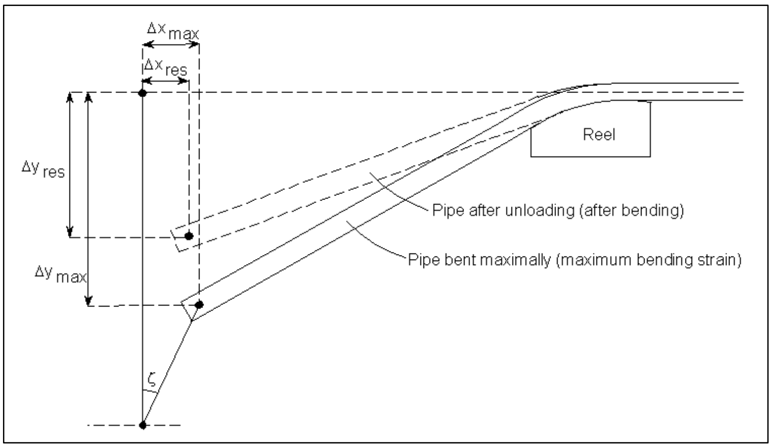

Figure 6.18 Definition of Δx_{max}, Δy_{max}, Δx_{res}, Δy_{res} in the bending test

The hydraulic cylinder force (F_{HC}), the rotation of the hydraulic cylinder (angle ζ), the change in the hydraulic cylinder stroke (Δs_{HC}) as well as the length between the hydraulic cylinder connection to the re-usable pipe and the connection of the hydraulic cylinder to the floor ($L_{HC;y}$ in Figure 6.1) were values measured in the bending test. The x- and y-components of the hydraulic cylinder force in the test ($F_{HC;x}$, $F_{HC;x;max}$, $F_{HC;y}$ and $F_{HC;y;max}$) and the maximum and the residual displacements of the connection between the hydraulic cylinder and the re-usable pipe in the x- and y-directions (Δx_{max}, Δy_{max}, Δx_{res}, Δy_{res} (Figure 6.18)) were calculated by Equations (5.1), (5.2), (5.3), (6.1) and (6.2) using these measurements.

$$\Delta x = \left(L_{HC;y} - \Delta s_{HC}\right) \cdot \sin(\varsigma) \tag{6.1}$$

$$\Delta y = L_{HC;y} - \left(L_{HC;y} - \Delta s_{HC}\right) \cdot \cos(\varsigma) \tag{6.2}$$

Table 6.3 shows the maximum hydraulic cylinder force ($F_{HC;max}$) for all reel sizes in the test. Also the lift force ($F_{LF;max}$) and the lateral and axial fixation point forces ($F_{FP;P;max}$ and $F_{FP;A;max}$) for all reel sizes in the test at the maximum hydraulic cylinder force are shown in Table 6.3.

Table 6.3 Measured forces of the bending rig on the pipe at maximum measured hydraulic cylinder force

	$F_{HC;max}$ [kN]	$F_{LF;max}$ [kN]	$F_{FP;P;max}$ [kN]	$F_{FP;A;max}$ [kN]	$F_{LF;max}$ / $F_{FP;P;max}$ [-]
9 m-1	73	265	342	3	0.78
9 m-2	85	248	295	11	0.84
9 m-3	86	252	300	6	0.84
8 m	87	266	319	3	0.84
7.5 m	87	288	345	-2	0.84
7 m	93	270	323	5	0.84
6.5 m	92	298	356	-1	0.84
6 m	98	280	334	7	0.84
5.5 m	103	295	351	8	0.84
5 m	110	287	342	10	0.84

The hydraulic cylinder force and the lateral fixation point force at the end of Phase I and at the end of Phase II can be predicted for all reel radii using Equations (5.9), (5.10) and (5.12) and Equation (6.3) to (6.7) after using Equation (5.4) to predict angle β (the angle between the pipe and the x-axis; Figure 5.8). Although it has been explained that the pipe was not in contact with the reel in the region surrounding the weld at maximum bending (Figure 6.17), the complete length of pipe was assumed to be in contact with the reel in order to determine angle β (Figure 5.8) in the bending test.

$$\Delta x = L_{HC;x} - \left(\left(D_{reel}/2\right)\cdot\sin(\beta)\right) - \left(\left(L_{HC;x} - L_{contact}\right)\cdot\cos(\beta)\right) \tag{6.3}$$

$$\Delta y = L_{HC;y} - \left(\left(D_{reel}/2\right) - \left(\left(D_{reel}/2\right)\cdot\cos(\beta)\right)\right) - \left(\left(L_{HC;x} - L_{contact}\right)\cdot\sin(\beta)\right) \tag{6.4}$$

$$F_{HC;y} = \frac{M_P}{\left(\left(L_{HC;x} - L_{contact}\right)\cdot\cos(\beta)\right)} \tag{6.5}$$

$$\varsigma = a\tan\left(\frac{\Delta x}{\Delta y}\right) \tag{6.6}$$

$$F_{HC} = \frac{F_{HC;y}}{\cos(\varsigma)} \tag{6.7}$$

In Figure 6.19 a comparison can be found between the predicted and the measured hydraulic cylinder force and the lateral fixation point force at the end of Phases I and II for the 9 m radius reel.

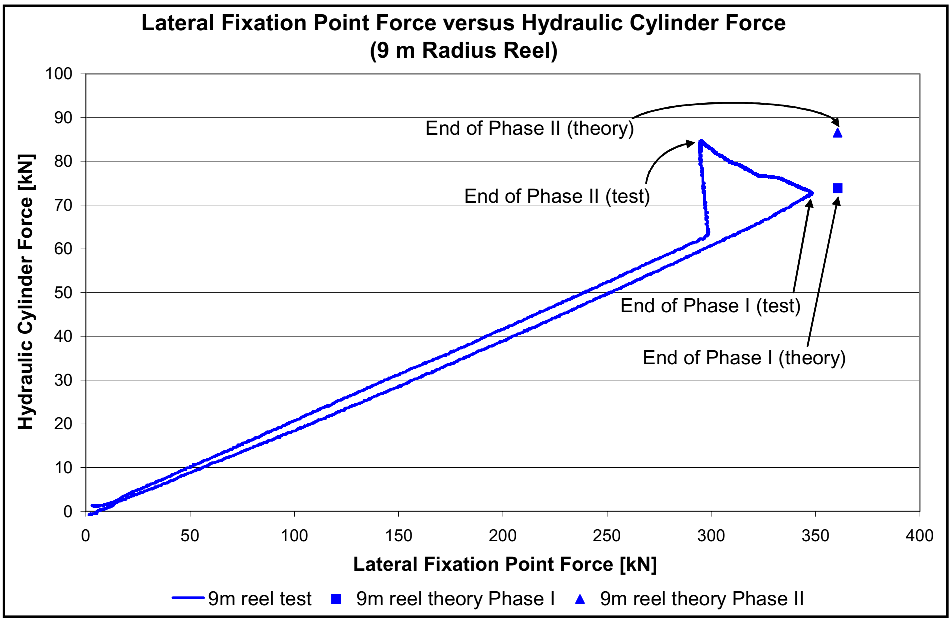

Figure 6.19 Hydraulic cylinder force versus the lateral fixation point force

The theoretical values of the hydraulic cylinder force at the end of Phases I and II as well as the theoretical value of the lateral fixation point force at the end of Phase I correlate well with the experimental values (Figure 6.19): differences are 2 %, 2 % and 4 %, respectively.

It has been theoretically predicted and experimentally proven in the small scale reeling tests (with and without a lift force) that the lateral fixation point force remains constant once the plastic bending moment has been reached at the initial contact point at the end of Phase I. However, Figure 6.19 shows that the lateral fixation point force starts decreasing at the end of Phase I, resulting in the experimental lateral fixation point force at the end of Phase II to be overestimated by 22 % by the theoretical prediction.

The decrease of the lateral fixation point force at the end of Phase I can be explained by the presence of the difference in the bending moment capacity of the pipes at both sides of the weld, $M_{P;TEST\text{-}1}$ and $M_{P;TEST\text{-}2}$. The pipe TEST-2, in contact with the reel in Phase II cannot have a bending moment larger than its plastic bending moment capacity $M_{P;TEST\text{-}2}$. The bending moment in pipe TEST-1 at the end of Phase I ($M_{P;TEST\text{-}1}$) had thus to be reduced in Phase II from $M_{P;TEST\text{-}1}$ to $M_{P;TEST\text{-}2}$ in order to accommodate $M_{P;TEST\text{-}2}$ in pipe TEST-2. The lateral fixation point force thus also reduced in value in the bending test after Phase I. If the plastic bending moment capacity of pipe TEST-2 ($M_{P;TEST\text{-}2}$) would have been used in the prediction of the lateral fixation point force at the end of Phase II, there would have been a 5 % difference between the theoretical prediction and the experimental result.

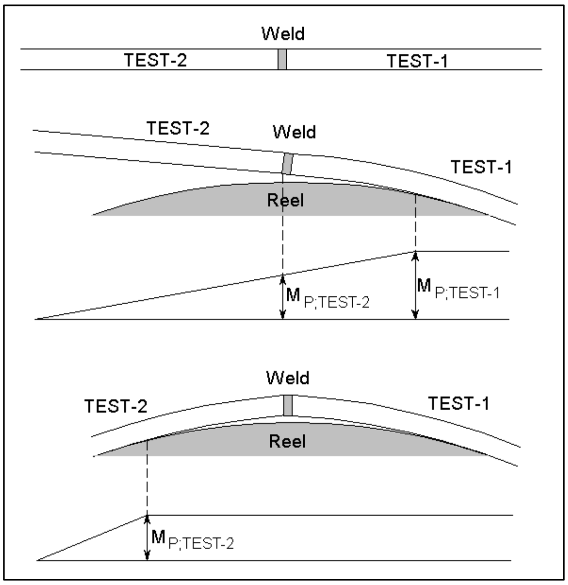

Figure 6.20 Bending the test piece, with geometric differences between the pipe sections (TEST-1 and TEST-2), on a reel

The lift force was removed from the test set-up prior to performing Tight Fit Pipe bending tests. It appeared not to be required to avoid excessive ovalisation and local buckling in the beginning of the test, while it does complicate the finite element analysis [20], [27].

6.3.2 Strain and Curvature in the Pipe

In order to measure the maximum bending strain in the pipe during testing, strain gauges were attached to the outside of the pipe in the tension and in the compression zone (Figure 6.11). The strain gauge measurements failed in this bending test and could thus not be reported. In later tests these problems were solved by using different kinds of strain gauges.

6.3.3 Ovalisation of the Pipe

The stiffening effect of the flanges reduces ovalisation in adjacent cross sections. This effect, the effect of the load introduction at the ends of the reel and the lift force had an influence on the ovalisation at locations 1 and 4 (Figure 6.12). The ovalisation at locations 2 and 3 in the central part (measuring length) were not influenced by these end effects. Ovalisation meter OM2 identified ovalisation of pipe TEST-1 when the pipe was bent on the reel while ovalisation meter OM3 stated the ovalisation of pipe TEST-2 also when the pipe was bent on the reel. It should be noted that OM2 was located in the machined region of TEST-1, providing the pipe with a wall thickness of 19.45 mm. Ovalisation values determined at maximum bending by the ovalisation meters OM2 and OM3 ($f_{OM2;MBS}$ and $f_{OM3;MBS}$) were compared in Table 6.4 to predictions for the ovalisation (f_{MBS}) stated by the DNV OS F101 code [11].

Table 6.4 Comparison of the measured and the predicted pipe ovalisation at locations 2 and 3 (TEST-1 and TEST-2, respectively), when the pipe was bent on the reel

	Test $f_{OM2;MBS}$ [%]	DNV OS F101 f_{MBS} (location 2) [%]	Test $f_{OM3;MBS}$ [%]	DNV OS F101 f_{MBS} (location 3) [%]
9m-1	0.19	1.16	0.09	1.29
9 m-2	1.57	1.16	2.50	1.29
9 m-3	1.54	1.16	2.55	1.29
8 m	1.40	1.47	3.47	1.63
7.5 m	2.04	1.67	3.83	1.85
7 m	2.39	1.91	4.64	2.11
6.5 m	2.56	2.20	4.99	2.44
6 m	2.41	2.57	5.29	2.86
5.5 m	2.91	3.05	5.71	3.38
5 m	3.41	3.67	6.72	4.07

Ovalisation of a pipe due to bending, under the influence of a reaction force on the pipe, can be predicted using equations (6.8) to (6.17) [47]. Equations (6.8) to (6.14) define ovalisation at maximum bending and Equations (6.15) to (6.17) define the residual ovalisation after unloading, where d_o is in [m]. The equations are based on the design criteria (Equation (5.15)) reported in DNV OS F101 [11] for pure bending.

$$k_R = \frac{d_o}{t} \Big/ 14 \tag{6.8}$$

$$k_\delta = 1 + \frac{(d_o - 0.6)}{2} \tag{6.9}$$

$$R = F_{HC;P} \tag{6.10}$$

$$\delta_{EI,R} = 1.203 \cdot \frac{R}{t \cdot E_a} \cdot \left(\frac{d_o}{2 \cdot t}\right)^{1.22} \tag{6.11}$$

$$\alpha = 0.03\ ,\ \rho = 120 \tag{6.12}$$

$$R_y = 3.9 \cdot \sigma_{y;a} \cdot t^2 \tag{6.13}$$

$$f_{MBS} = f_0 + \left(k_\delta \cdot \frac{2 \cdot \delta_{EI,R}}{d_o}\right) + \left(\left(\alpha \cdot \left(1 + \frac{d_o}{\rho \cdot t}\right)\right) + \left(\frac{R}{R_y \cdot k_R}\right)\right) \cdot \left(2 \cdot \varepsilon_b \cdot \frac{d_o}{t}\right)^2 \tag{6.14}$$

$$\varepsilon_{cr} = \left(0.78 \cdot \left(\frac{t}{d_o} - 0.01\right) \cdot \alpha_h^{-1.5} \cdot \alpha_{gw}\right) \cdot \left(1 - \sqrt{\frac{d_o/t}{80}} \frac{R}{R_y}\right) \tag{6.15}$$

$$f_e = \left(f_{MBS} - f_0\right) \cdot \left(1 - \frac{\varepsilon_b}{\varepsilon_{cr}}\right) \tag{6.16}$$

$$f_{AB} = f_{MBS} - f_e \tag{6.17}$$

The equations are actually meant to be used to determine ovalisation for 20 inch to 40 inch outer diameter pipelines (X60 to X80 material grade with yield to tensile strength ratio's of 0.84, 0.91 and 0.94 and a diameter to thickness ratio varying from 15 to 45) due to bending the pipeline over a stinger roller during S-lay up to a maximum bending strain of 1 %. The pipes TEST-1 and TEST-2 are of a different diameter (12.75 inch), of a different material grade (X52), with different yield to tensile strength ratio's (respectively 0.70 and 0.72), but with applicable diameter to thickness ratios (15 and 17 for TEST-1 and TEST-2, respectively), bent to a maximum bending strain of approximately 3 % (instead of 1 %). Comparison of these predictions for the ovalisation with the experimental results of the full scale bending test is still worthwhile, however. It creates an understanding of the influence of the reaction force (of the reel on the pipe) on the ovalisation of the pipe.

In Table 6.5 and Table 6.6 ovalisation at maximum bending was compared to a theoretical prediction of the ovalisation at maximum bending based on the DNV OS F101 code [11] designed for pure bending only. Ovalisation measured at maximum bending was also compared to ovalisation predictions at maximum bending based on bending and a reaction force of the reel on the pipe (reaction force *R*) occurring during reeling. The transverse component of the hydraulic cylinder force ($F_{HC;P}$) necessary to bring OM2 and OM3 in contact with the reel, was set equal to the reaction force of the reel on the pipe (e.g. *R* = 66 kN for TEST-1). This was defined by the theory as described in Chapter 5. Ovalisation at maximum bending was predicted using $F_{HC;P}$ as a reaction force *R* of the reel on the pipe TEST-1 (R / R_y = 66 kN / 535 kN = 12 %) in Equations (6.15) to (6.17).

It should be realised that Equation (6.14) predicts ovalisation at maximum bending using a reaction force (*R*) of the reel on the pipe, a point load, while in fact the reaction of the reel on the pipe was more of a distributed load [27]. Theoretically, a concentrated load contributes more to ovalisation than a distributed load. It was therefore decided that the ovalisation at maximum bending was also calculated using a reduced point load (e.g. R / R_y = 13 kN / 535 kN = 2 %) in Equations (6.8) to (6.14), possibly resembling more the distributed character of the reaction of the reel on the pipe. This value of 2 % was chosen because predictions for the ovalisation resembled experimental data better. This resulted in the predictions at maximum bending (f_{MBS}) to compare better with the experimental results ($f_{OM2;MBS}$ and $f_{OM3;MBS}$) in Table 6.5 and Table 6.6. Experimental results for the ovalisation at maximum bending were also compared to Equations (6.8) to (6.14), assuming zero reaction force R (Table 6.5 and Table 6.6). Assuming zero reaction force R of the reel on the pipe generated the same results as Equation (5.15) [47].

Table 6.5 Comparison of the measured data with various predictions for the ovalisation of the pipe at location 2 (TEST-1) when the pipe is bent on the reel

	Test	Ref [11]	Ref [47]	Ref [47]	Ref [47]
TEST-1	$f_{OM2;MBS}$ [%]	f_{MBS} Pure Bending [%]	f_{MBS} (R / R_y = 0 %) [%]	f_{MBS} (R / R_y = 2 %) [%]	f_{MBS} (R / R_y = 12 %) [%]
9 m-3	1.54	1.16	1.16	1.90	4.87
8 m	1.40	1.47	1.47	2.39	6.09
7.5 m	2.04	1.67	1.67	2.71	6.89
7 m	2.39	1.91	1.91	3.10	7.87
6.5 m	2.56	2.20	2.20	3.58	9.07
6 m	2.41	2.57	2.57	4.18	10.58
5.5 m	2.91	3.05	3.05	4.94	12.50
5 m	3.41	3.67	3.67	5.94	15.00

Table 6.6 Comparison of the measured data with various predictions for the ovalisation of the pipe at location 3 (TEST-2) when the pipe is bent on the reel

	Test	Ref [11]	Ref [47]	Ref [47]	Ref [47]
TEST-1	$f_{OM3;MBS}$ [%]	f_{MBS} Pure Bending [%]	f_{MBS} (R / R_y = 0 %) [%]	f_{MBS} (R / R_y = 3 %) [%]	f_{MBS} (R / R_y = 14 %) [%]
9 m-3	2.55	1.29	1.29	2.17	5.69
8 m	3.47	1.63	1.63	2.73	7.13
7.5 m	3.83	1.85	1.85	3.09	8.08
7 m	4.64	2.11	2.11	3.54	9.23
6.5 m	4.99	2.44	2.44	4.08	10.65
6 m	5.29	2.86	2.86	4.77	12.42
5.5 m	5.71	3.38	3.38	5.64	14.68
5 m	6.72	4.07	4.07	6.78	17.61

The ovalisation results measured by hand after unloading for TEST-1 and for TEST-2 (f_{H2} and f_{H3}) are compared, respectively in Table 6.7 and in Table 6.8, with several predictions for the ovalisation after bending (f_{AB}; Equations (6.15) to (6.17)). The same set-up as in Table 6.5 and Table 6.6 is used in Table 6.7 and in Table 6.8.

Table 6.7 Comparison of the measured data with various predictions for the residual ovalisation of the pipe at location 2 (TEST-1) after bending the pipe on the reel

	Test	Ref [47]	Ref [47]	Ref [47]
TEST-1	f_{H2} [%]	f_{AB} (R / R_y = 0 %) [%]	f_{AB} (R / R_y = 2 %) [%]	f_{AB} (R / R_y = 12 %) [%]
9 m-3	-	0.50	0.88	2.48
8 m	1.29	0.71	1.24	3.49
7.5 m	1.46	0.85	1.50	4.21
7 m	1.65	1.05	1.83	5.14
6.5 m	1.70	1.30	2.27	6.37
6 m	2.28	1.64	2.87	8.02
5.5 m	3.17	2.12	3.69	10.32
5 m	3.43	2.79	4.86	13.58

Note:
Hand measurement data for the pipe bending test on the 9 m radius reel was not available

Table 6.8 Comparison of the measured data with various predictions for the residual ovalisation of the pipe at location 3 (TEST-2) after bending the pipe on the reel

	Test	Ref [47]	Ref [47]	Ref [47]
TEST-2	f_{H3} [%]	f_{AB} (R / R_y = 0 %) [%]	f_{AB} (R / R_y = 3 %) [%]	f_{AB} (R / R_y = 14 %) [%]
9 m-3	-	0.59	1.07	3.13
8 m	2.71	0.83	1.51	4.41
7.5 m	3.24	1.00	1.82	5.32
7 m	4.05	1.23	2.23	6.50
6.5 m	4.34	1.53	2.77	8.06
6 m	4.50	1.93	3.49	10.16
5.5 m	4.64	2.49	4.50	13.08
5 m	4.84	3.28	5.93	17.22

Note:
Hand measurement data for the pipe bending test on the 9 m radius reel was not available

It can be seen in Table 6.5 to Table 6.8 that the prediction for the ovalisation by DNV OS F101 (Equation (5.15)) underestimates most values for the ovalisation measured in the bending testing. This can be explained by the fact that this prediction is based on test results from four point bending tests in which the reaction force of the reel on the pipe, enhancing ovalisation, is not taken into account [36], [47]. Table 6.5 to Table 6.8 also show that assuming R / R_y equal to 12 % (R equals approximately 66 kN) results in a severe overestimation of the ovalisation of the pipes TEST-1 and TEST-2. Furthermore, Table 6.5 to Table 6.8 indicate that the predicted ovalisation, based on Equation (6.14), is sensitive to the assumed reaction force used in the equation.

When the pipe was bent on the 9 m radius reel, the locations of the ovalisation meters OM2 and OM3 and those of the hand measurements H2 and H3 were in contact with the 9 m radius reel. The reaction force of the reel on the pipe enhanced ovalisation due to bending, measured at the locations of OM2, OM3, hand measurement 2 and hand measurement 3. It should be realised that the locations of OM2 and OM3 as well as the locations of the hand measurements 2 and 3 were not in contact with the reel during the bending tests around the smaller reel sizes (e.g. 8 m, 7.5 m etc.). These tests are thus comparable to four point bending tests, but may be influenced by nearby contact points. The fact that the ovalisation increased due to contact with the reel in the test on the 9 m radius reel, but not in all the subsequent tests on smaller radii reels, made it difficult to compare measured ovalisation data with theoretically predictions (Table 6.5 to Table 6.8). The predictions do not take prior bending history of the pipe into account, but assume the pipe to be bent directly on the specific reel size.

In the bending test it was found that the reel rotated first clockwise when the pipe was only in contact with the reel at the initial contact point (left in Figure 6.21). This rotation was mainly due to the reel rotating slightly around its rotation point towards the beam, located behind the reel in order to fill the small gap between the reel and the beam. This gap was the result of the fact that it was impossible in practice to align the reel completely with the beam located behind it. The rotation of the reel was possible due to the fact that the rods, connecting the reel to the floor under pretension, were able to move slightly within the holes, through which the rods connected the reel to the floor.

When more pipe came in contact with the reel, the reel rotated back counter clockwise to its original position (right in Figure 6.21). The fact that the beam located behind and supporting the reel (Figure 6.1) was slightly bent when maximum pipe length was in contact with the reel, caused more reel rotation counter clockwise. This rotation of the reel during the bending tests sometimes resulted in undesired sudden movements of the reel, resulting in failure of the ovalisation meters (they fell off the pipe).

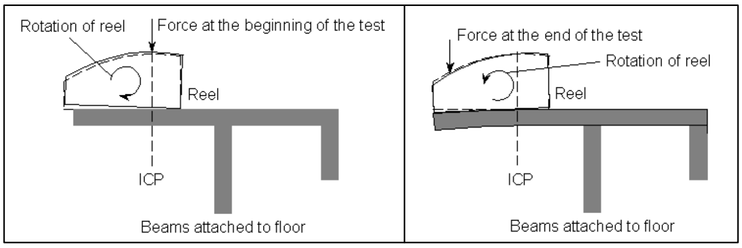

Figure 6.21 Rotation of the reel during the bending test (top view of the test set-up; ICP = initial contact point)

Finite element analysis showed that the rotation of the reel influenced which part of the pipe length was in contact with the reel and would thus be submitted to the reaction force of the reel [27]. Ovalisation in OM3 increased due to the fact that the reel rotation caused the OM3 location to come in contact in with the reel while this location would not be in contact with the reel if no reel rotation occurred.

It was therefore decided at the end of this bending test of the single walled pipe that two extra beams should be added to the bending rig behind the concrete former i.e. the reel to reduce the counter clockwise rotation of the reel as a result of bending of this beam. The clockwise and the counter clockwise rotation of the reel as a result of the fact that it was impossible to align the reel exactly with the beam and due to the fact there was always some movement of the rod in their holes, was not further restricted. This was because this rotation was minimal not causing the ovalisation meters to fall of the pipe. It was also not considered a problem in the Tight Fit Pipe bending tests because these test pieces had no variation in the geometrical and material variations. There was thus no significant part of the Tight Fit Pipe test piece not in contact with the reel, causing ovalisation variation along the length of the test piece.

6.3.4 Local Buckling of the Pipe

A local buckle was first noticed in the weaker pipe (TEST-2) after bending the pipe on the 6 m radius reel (Figure 6.22).

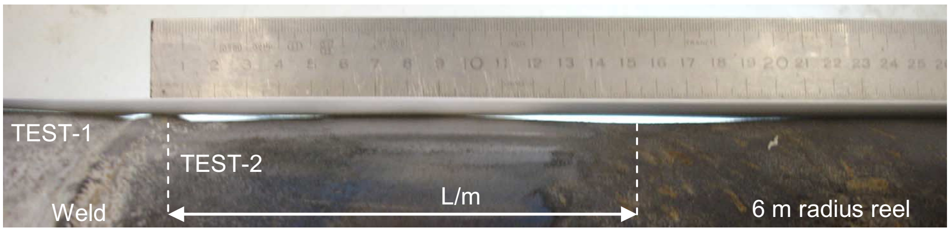

Figure 6.22 Local buckling of the pipe after bending the pipe on the 6 m radius reel

The prediction of the critical buckling strain (ε_{cr}) by Murphy and Langner (Equation (5.18)) [36], by Gresnigt (Equation (5.19)) [23] and by the DNV Offshore Standard OS-F101 (Equation (5.20)) [11] exceeded the global buckling strain (ε_b in Table 6.9) determined by Equations (5.16) and (5.17). The global bending strain at buckling was used in Table 6.9 because (local) strain measurements failed in the testing. It should be noted that in reality the local bending strain and the local curvature at buckling were larger than the global bending strain and the global curvature at buckling because of the extra bending in the weaker pipe TEST-2 (Figure 6.20). Furthermore, the depth of the local deformation was still rather small and it can be questioned whether this should be defined as local buckling (Figure 6.22). Usually, local buckling is defined as the point in the moment curvature diagram where due to the local deformations in the wall, the bending moment starts decreasing. Especially in thick walled pipes the bending moment still increases after initiation of local buckles.

Table 6.9 Comparison of the predicted and the experimentally determined global critical buckling strain of the test piece in the bending test

ε_b test [%]	ε_{cr} Murphy & Langer [%]	ε_{cr} Gresnigt [%]	ε_{cr} DNV [%]
2.63	2.88	2.81	3.89

It should also be realised that the usual underestimation of the critical buckling strain at the test piece low diameter to thickness ratio (15 for TEST-1 and 17 for TEST-2) in the predictions developed by Murphy and Langner [36] and by Gresnigt [23], is compensated by the enhancement of local buckling as a result of the reaction force of the reel on the pipe which is not taken into account in the equations. This has previously been explained in Subsection 5.3.2.3. Moreover, it should be taken into account that the guidance note in the DNV Offshore Standard OS-F101 [11] states that for diameter to thickness ratios smaller than 20 the prediction may only be utilised provided that full scale testing, observation or former experience indicates a sufficient safety margin. The DNV Offshore Standard OS-F101 is also based on pure bending tests not taking the reaction force of the reel on the pipe, enhancing local buckling, into account.

The half wave length (L/m) and the height of the buckle (a) were approximately 150 mm and 1.1 mm, respectively, both measured after bending the pipe on the 5 m reel. The finite element calculation predicted a length of approximately 140 mm [20], [27].

6.4 Conclusions

A full scale bending test was executed on a 12.75 inch outer diameter single walled pipe in preparation of the full scale bending tests of 12.75 inch outer diameter Tight Fit Pipe. The developed theoretical model describing the forces on the 12.75 inch single walled pipe by the full scale bending rig matched the test results well.

The ovality of the 12.75 inch single walled pipe at maximum bending strain as predicted by the DNV Offshore Standard OS-F101 underestimated most values for the ovalisation at maximum bending as measured in the bending test. This can be explained by the fact that this prediction is intended for bending only, while in the tests also a reaction force of the reel on the pipe enhanced ovalisation. Pipe ovalisation measured in the bending test was compared to predictions for ovalisation resulting from the combination of bending and a concentrated transverse load. These predictions are shown to be sensitive to the value of the reaction force of the reel on the pipe used in these equations. It should be taken into account that in these equations the reaction of the reel on the pipe was applied as a concentrated load while in fact it is a distributed load resulting in a conservative approach to the calculation of the ovalisation. It should also be taken into account that these equations are actually designed for different circumstances (lower bending strains, larger pipe outer diameters and stronger material).

Predictions of the critical buckling strain by Murphy and Langer, Gresnigt and the DNV OS F101 code exceeded the global buckling strain determined in the testing from the reel radius and the pipe outer diameter. The local curvature and the local bending strain were in fact larger than the global bending strain because of the extra bending in the weaker pipe in which the buckle developed (the test piece bend tested consisted of a pipe with a higher bending moment capacity (stronger pipe) and a pipe with a lower bending moment capacity (weaker pipe), connected by a weld). Furthermore, the depth of the local deformation was still rather small and it can be questioned whether this should be defined as local buckling.

Some adaptations were made to the full scale bending rig such as:

1. the removal of the lift force because it appeared not needed to avoid excessive ovalisation and local buckling in the beginning of the test, while it does complicate the finite element analysis.
2. the addition of beams behind the reel to reduce rotation of the reel.
3. the addition of measuring equipment (e.g. curvature meters, more ovalisation meters and more strain gauges).

Although some adaptations were made to the full scale bending rig and to the measuring equipment, the fitness for purpose of the rig for performing full scale bending tests on 12.75 inch outer diameter Tight Fit Pipe was proven.

7 Full Scale Reeling Simulation of Tight Fit Pipe

7.1 Introduction

Seven full scale bending tests, in which the pipe was bent on increasingly smaller reels, were executed on 12.75 inch outer diameter Tight Fit Pipe. The objective of these tests was to determine the initiation and the degree of local buckling of the Tight Fit Pipe as well as the degree of ovalisation occurring during the spooling-on phase of the reeling process. Also the influence on liner pipe wrinkling (local buckling of the liner pipe) was determined of (1) the mechanical bonding strength between the liner pipe and the outer pipe in the Tight Fit Pipe, (2) the electric resistance welded longitudinal outer pipe weld and (3) the presence of a Tight Fit Pipe circumferential weld.

The test set-up of the full scale bending tests on the 12.75 inch Tight Fit Pipe is discussed in Subsection 7.2. Experimental results are compared to theoretical predictions in Subsection 7.3. Equations that can be used to predict the liner pipe wrinkle height as a result of spooling-on can be found in Subsection 7.4.

7.2 Test Set-up

7.2.1 Full Scale Bending Rig

Three adaptations were made to the full scale bending rig after it was used in the full scale bending test of the 12.75 inch outer diameter single walled pipe (Chapter 6):

1. Making the bending rig stiffer
2. Removal of the lift force
3. Strengthening of the re-usable pipe

1. Making the bending rig stiffer
Two additional beams were positioned behind the beam adjacent to the reel in order to reduce the rotation of the reel under loading (Figure 7.1 and Figure 7.2).

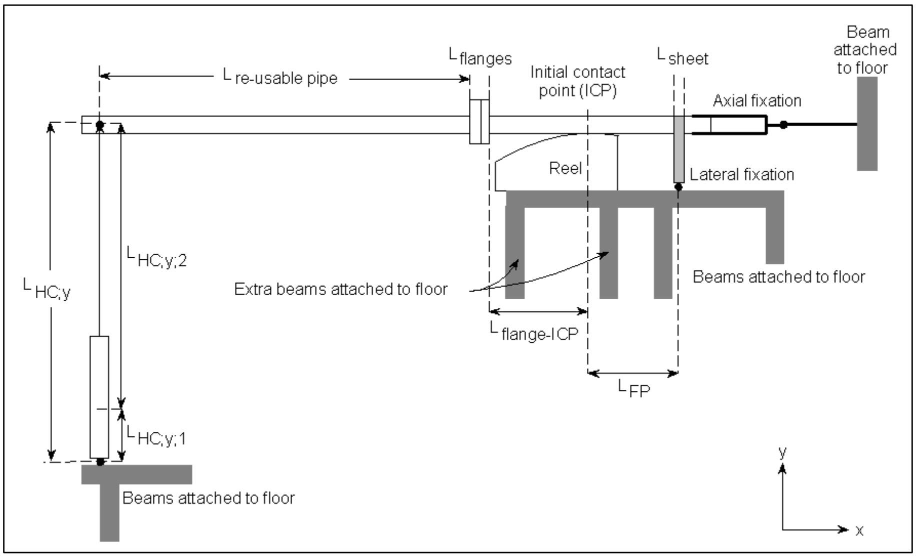

Figure 7.1 Schematic overview of the (optimised) full scale bending rig (not to scale)

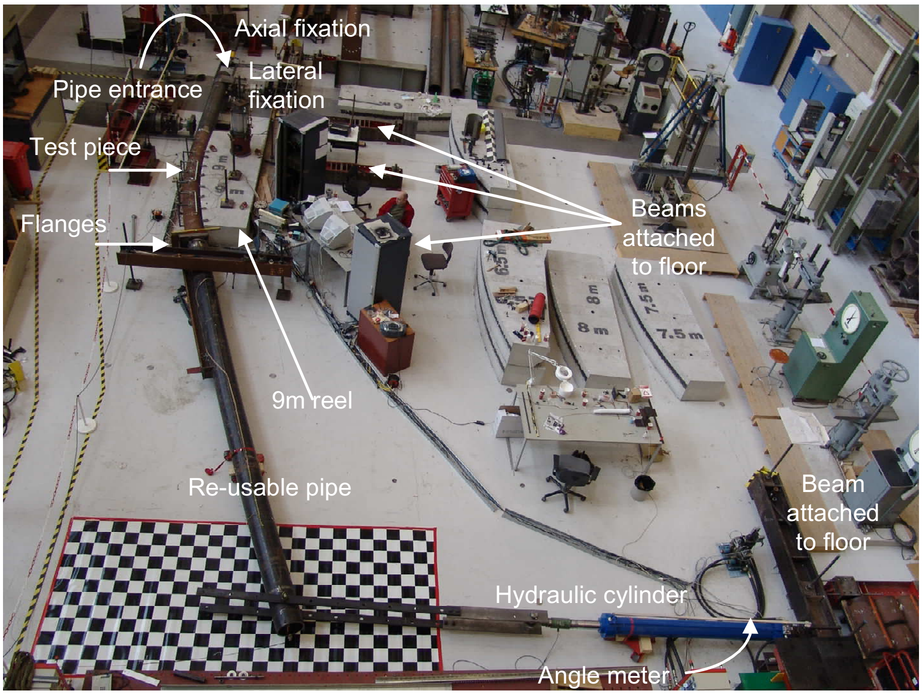

Figure 7.2 (Optimised) full scale bending rig in the laboratory

In each test in the bending rig (Figure 7.1 and Figure 7.2), the length of the re-usable pipe ($L_{re\text{-}usable\ pipe}$) was 6720 mm, the thickness of the flanges of the re-usable pipe and the test piece together ($L_{flanges}$) was 125 mm and the width of the sheet in the lateral fixation point (L_{sheet}) was 300 mm. Other distances in the bending rig (i.e. L_{FP} and $L_{flange\text{-}ICP}$) were not the same in each bending test due to variation in the pipe lengths in the Tight Fit Pipe test pieces. These lengths are provided in Subsection 7.2.3 and Appendix IV.

2. Removal of the lift force

The lift force was removed from the test set-up prior to performing Tight Fit Pipe bending tests (Figure 7.1 and Figure 7.2). It appeared not to be required to avoid excessive ovalisation and local buckling in the beginning of the test, while it does complicate the finite element analysis [20], [27].

3. Strengthening of the re-usable pipe

The re-usable pipe was strengthened near the flange, because the material of the re-usable pipe appeared to be less strong than expected. Because the 12.75 inch single walled pipe (Chapter 6) was also less strong than expected, this was not a problem during this bending test. However, when bending the Tight Fit Pipes with the strong outer pipe (Table 3.2) there was some concern that the re-usable pipe was not strong enough to avoid plastic deformation during testing.

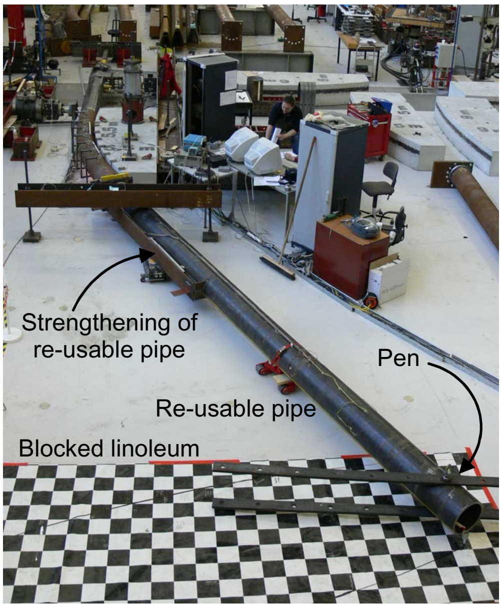

Figure 7.3 Strengthening of the re-usable pipe

7.2.2 Measuring Equipment

Several changes were made to the measuring equipment after it was used in the full scale bending test of the 12.75 inch outer diameter single walled pipe (Chapter 6). Only changes to the measuring equipment as used in the full scale bending test of the 12.75 inch single walled pipe are described below:

1. Curvature meters
2. Type and location of the strain gauges
3. Increase of the number of strain gauges and ovalisation meters
4. Angle meter and displacement meter
5. "Full scale graph"
6. Light sensors instead of copper strips determining angle β
7. Laser trolley scanning the inside of the Tight Fit Pipe for liner pipe wrinkling

1. Curvature meters

Strain and curvature of the pipe were measured by strain gauges and by curvature meters. The curvature meters functioned as back-up to the strain gauges and vice versa, in order to avoid lack of information in case of accidental failure of some measuring equipment. The set-up of the curvature meters can be seen in Figure 7.4.

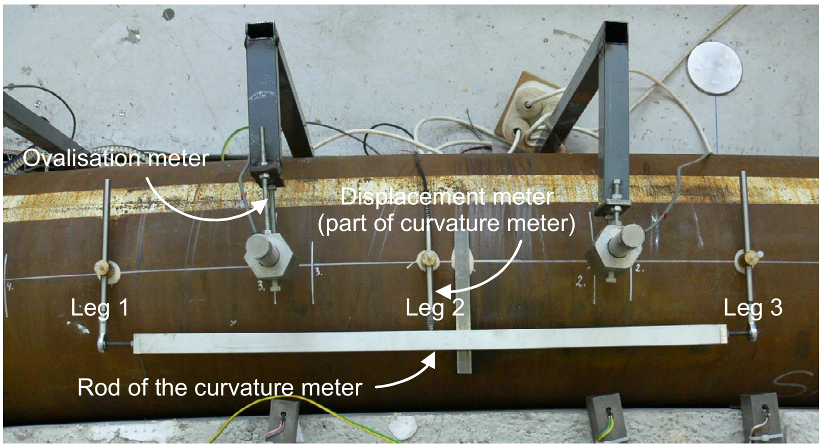

Figure 7.4 Curvature meter attached to the Tight Fit Pipe

Two curvature meters were attached to the Tight Fit Pipe. A displacement meter measured the displacement of the middle of the rod (leg 2) relative to the displacement of both ends of the rod of the curvature meter (leg 1 and leg 3). From this measured distance, ΔL, the average bending radius, the average curvature and the average bending strain of the Tight Fit Pipe over the length of the rod (part of the curvature meter), can be calculated using Equations (7.1), (7.2) and (7.3).

$$R_{TFP} = \frac{(L_{CM})^2}{8 \cdot \Delta L} + \frac{\Delta L}{2} \tag{7.1}$$

$$\kappa = \frac{1}{R_{TFP}} \tag{7.2}$$

$$\varepsilon_b = \kappa \cdot r_{O;o;TFP} \tag{7.3}$$

2. Type and location of the strain gauges

Strain gauges especially suitable for measuring large plastic deformations were used. Strain gauges were applied on the outer fibre of the Tight Fit Pipe in the tension zone. As well, strain gauges were applied in the compression zone of the Tight Fit Pipe, but then 20 mm next to the outer fibre of the Tight Fit Pipe in order to avoid being crushed between the Tight Fit Pipe and the reel when the pipe became in contact with the reel (Figure 7.5).

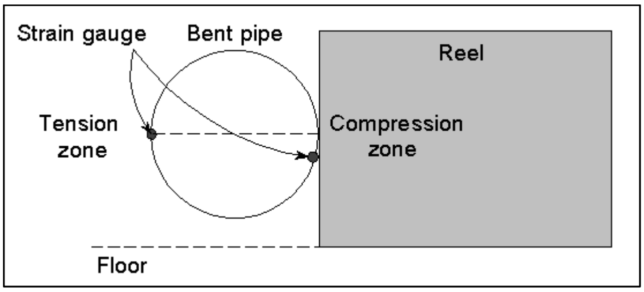

Figure 7.5 Location of the strain gauges attached to the Tight Fit Pipe

It follows from Equation (7.4) that positioning the strain gauges in the compression zone 20 mm next to the outer fibre only gives a negligible difference compared to the strain that would have been measured in the most outer fibre of the compression zone itself.

$$\frac{r_{O;o;TFP} \cdot \cos\left(20/2 \cdot \pi \cdot r_{O;o;TFP}\right)}{r_{O;o;TFP}} \approx 1.00 \tag{7.4}$$

3. Increase of the number of strain gauges and ovalisation meters

The number of strain gauges in the tension zone and in the compression zone as well as the number of ovalisation meters, were increased along the contact length ($L_{contact}$) from four to seven in order to compensate for the fact that strain gauges and ovalisation meters measure strain and ovality locally. Curvature meters measure curvature and thus strain more globally.

Moreover, the ovalisation meter and the strain gauges in the tension zone and in the compression zone most closely to the flange were moved further away from the flange to avoid the influence of the flange on measurements. The strain gauges and the ovalisation meter were located 499 mm from the flange in the test on the 12.75 inch single walled pipe (Chapter 6). In the tests on the 12.75 inch Tight Fit Pipes the strain gauges and the ovalisation meter were located 750 mm from the flange. The influence length of the flange can be calculated using Equation (7.5) [24].

$$l_i = 1.5 \cdot r_{O;o;TFP} \cdot \sqrt{\left(r_{O;o;TFP} / \left(t_O + t_L\right)\right)} \qquad (7.5)$$

The locations of the strain gauges and the ovalisation meters for the five full scale bending tests on the Tight Fit Pipes without a Tight Fit Pipe circumferential weld can be seen in Figure 7.6 and Figure 7.7, respectively. The ovalisation meters and the strain gauges in the tension and compression zones of the test piece were distributed evenly over the distance between the initial contact point and the strain gauges and the ovalisation meter located 750 mm from the flange.

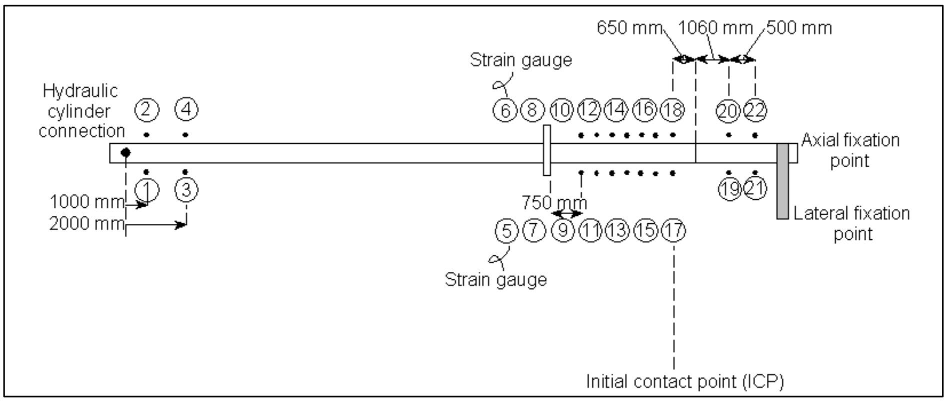

Figure 7.6 Locations of the strain gauges in the five bending tests on the Tight Fit Pipes without a Tight Fit Pipe circumferential weld

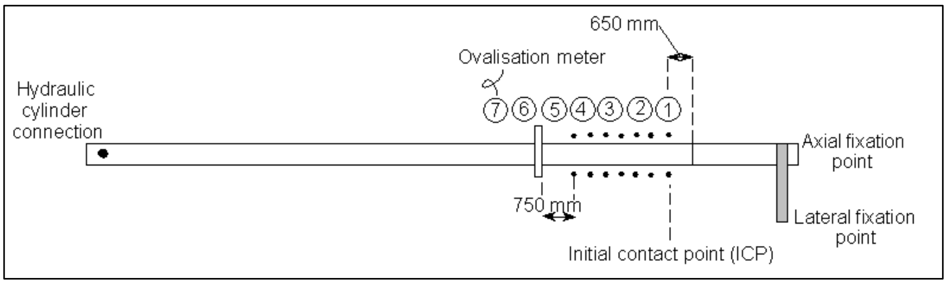

Figure 7.7 Locations of the ovalisation meters in the five bending tests on the Tight Fit Pipes without a Tight Fit Pipe circumferential weld

The locations of the strain gauges and the ovalisation meters for the two full scale bending tests on the Tight Fit Pipes with a Tight Fit Pipe circumferential weld can be seen in Figure 7.8 and Figure 7.9, respectively. In the test piece, a strain gauge was located on top of the weld in the compression zone as well as in the tension zone (strain gauges 15 and 16). The three strain gauges in the compression zone and the three strain gauges in the tension zone were located at 15 mm, 30 mm and 80 mm from the weld (strain gauges 13 and 14, 11 and 12 and 9 and 10, respectively) in the direction of the flange. In the middle between strain gauge 5 and 6 (located 750 mm from the flange) and strain gauge 9 and 10, strain gauge 7 and 8 were located. The strain gauge distribution was identical on both sides of the weld (Figure 7.8).

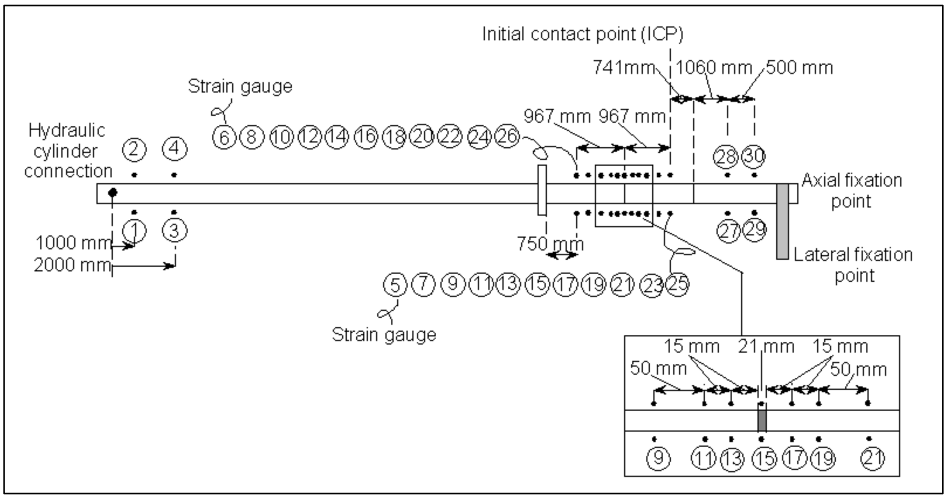

Figure 7.8 Locations of the strain gauges in the two bending tests on the Tight Fit Pipes with a Tight Fit Pipe circumferential weld

In between the weld and the flange, the ovalisation meters were located at the same locations of the strain gauges 5 and 6, 7 and 8 and 9 and 10. One ovalisation meter was located on top of the weld. On the other side of the weld, ovalisation meters were attached to the pipe at the same locations as the strain gauges 21 and 22, 23 and 24 and 25 and 26 (Figure 7.9 and Figure 7.10).

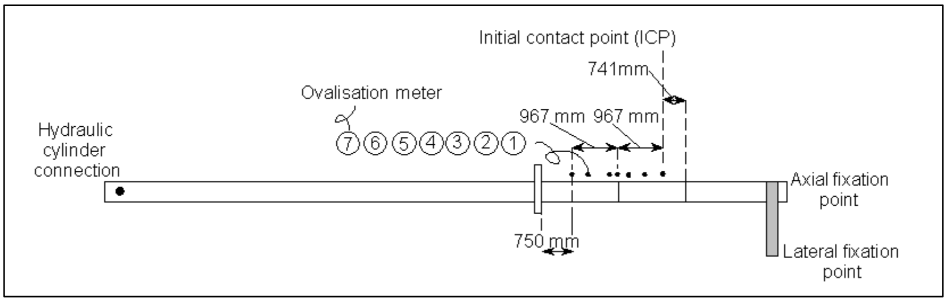

Figure 7.9 Locations of the ovalisation meters in the two bending tests on the Tight Fit Pipes with a Tight Fit Pipe circumferential weld

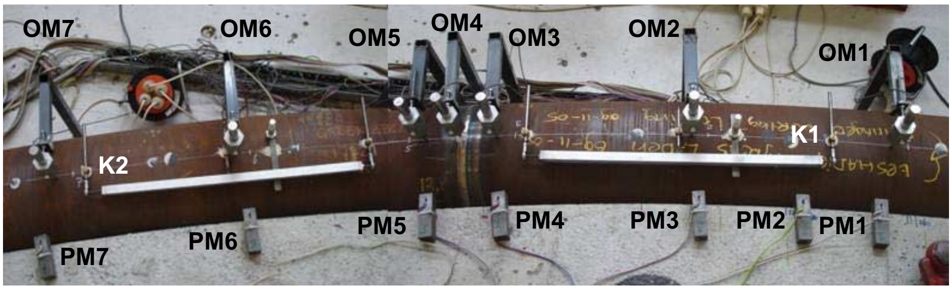

Figure 7.10 Ovalisation meters (OM1-OM7), position meters (PM1-PM7) and curvature meters (K1 and K2) attached to the Tight Fit Pipes in the two bending tests on the Tight Fit Pipes with a Tight Fit Pipe circumferential weld

4. Angle meter and displacement meter

An angle meter was located on top of the hydraulic cylinder to measure the change in orientation (angle ζ; Figure 5.8) during the bending test (Figure 7.2). The angle meter replaced the displacement meter, which measured the movement of the hydraulic cylinder in the x-direction, which was used in the bending test on the single walled pipe.

In the two Tight Fit Pipes with a Tight Fit Pipe circumferential weld (GR-OR-1 and GR-OR-2), the displacement meter returned and was positioned 1000 mm from the hinged connection between the hydraulic cylinder and the beam that was attached to the floor ($L_{HC;y;1}$ in Figure 7.1). The displacement meter measured the movement of the hydraulic cylinder in the x-direction (Figure 7.1). This measurement was used to verify the measurements of the angle meter (Equation (5.1)).

5. "Full scale graph"

The displacement of the connection between the hydraulic cylinder and the re-usable pipe was determined, full scale, by a pen. This pen drew the actual displacement on the blocked linoleum (Figure 7.11). The displacements at maximum bending (Δx_{max} and Δy_{max}; Figure 6.18) and after unloading (Δx_{res} and Δy_{res}; Figure 6.18), drawn on the blocked linoleum by the pen ("full scale graph") were measured and compared with the displacements at maximum bending and after unloading, defined by measurements from the angle meter and from the displacement meter together with Equations (5.1), (6.1) and (6.2). Measurements from the angle meter and from the displacement meter were thus verified by measurements from the "full scale graph". The "full scale graph" also functioned as a back-up system to these measurements.

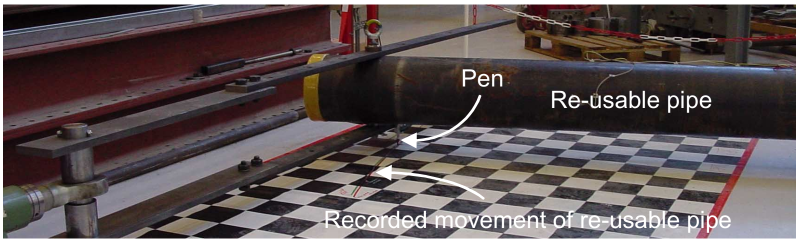

Figure 7.11 Recording the displacement of the end of the re-usable pipe on the linoleum

6. Light sensors instead of copper strips determining angle β

The copper strips used as position meters in the test on the single walled pipe (Chapter 6) were replaced by light sensors (Figure 7.12), because the strips, when compressed between the reel and the pipe, initiated liner pipe wrinkling. This might have been the result of the distributed contact load between the reel and the pipe obtaining a concentrated character due to the copper strip, enhancing liner pipe wrinkling.

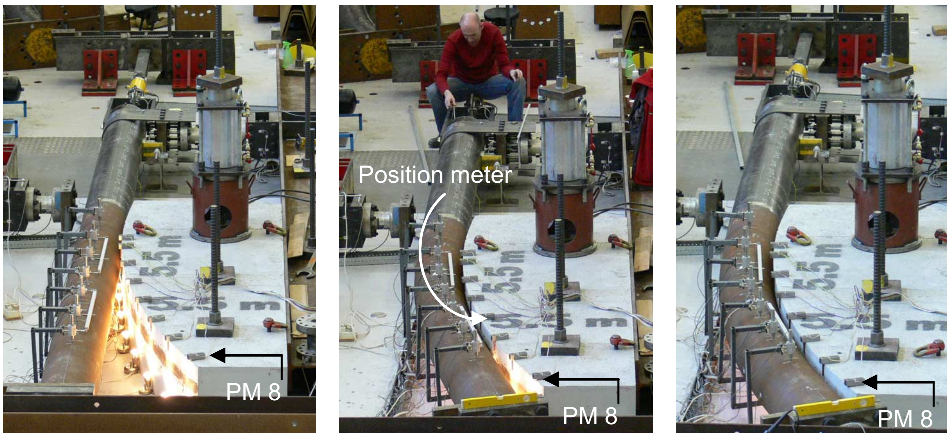

Figure 7.12 Position meters (PM) (light sensors) between the Tight Fit Pipe and the reel

It should be realised that concentrated loads e.g. as a result of possibly stacking different layers of pipeline on top of each other on the reel in a slightly crossing pattern (Figure 7.13), might also initiate liner pipe wrinkling and thus needs to be investigated further.

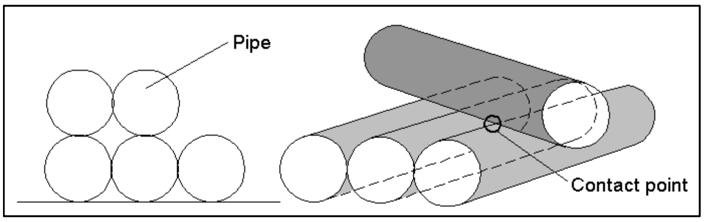

Figure 7.13 Impression of the pipeline stacked on the reel in layers in a slightly crossing pattern, resulting in local contact points

By using the light sensors instead of the copper strips as position meters no imperfections were created between the Tight Fit Pipe and the reel. As soon as the light did not reach the sensor anymore because it was interrupted by the Tight Fit Pipe being in contact with the reel, the computer recorded the force required for the Tight Fit Pipe to come in contact with the reel at this location.

The number of sensors was increased from four to eight, which were placed at regular intervals along the curved part of the former (Figure 7.12). The ovalisation meters and the strain gauges were located on the curved Tight Fit Pipe at exactly these locations. The eighth light sensor, i.e. position meter, was placed where the maximum length of Tight Fit Pipe came in contact with the reel. As soon as the computer indicated that the maximum length of Tight Fit Pipe was in contact with the reel at this position meter, the test was stopped and unloading of the Tight Fit Pipe could begin.

7. Laser trolley scanning the inside of the Tight Fit Pipe for liner pipe wrinkling
A special laser trolley was developed to measure liner pipe wrinkling and ovalisation before, during and after bending the pipe on the reel. The device had a laser measuring distance, an angle meter and two acceleration meters (Figure 7.14).

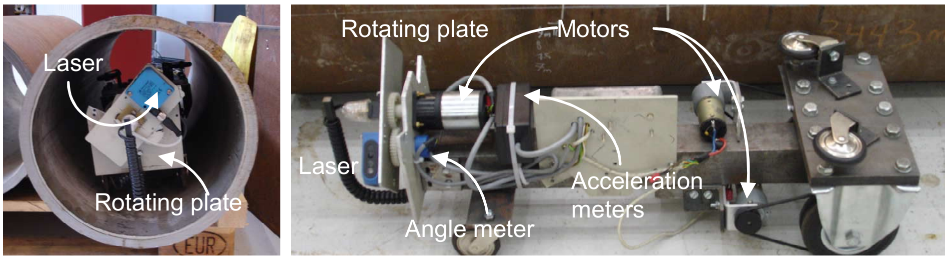

Figure 7.14 Laser trolley measuring liner pipe wrinkling of the Tight Fit Pipe

Two motors were connected to the two rear wheels moving the laser trolley through the pipe. The laser trolley was connected to an external threaded displacement meter, which kept track of the displacement through the pipe. The third motor was located at the front to rotate a plate on which the laser was mounted (Figure 7.14). The laser measured the distance from the inside of the pipe wall to the centre point of the cross section of the pipe at regular intervals (e.g. every 0.5 degrees). The angle meter measured the rotation of the plate. The location of the laser in relation to the centre point of the pipe's cross section was determined by the software from the measurements by the laser and the angle meter. The two acceleration meters were needed to compensate for the rotation of the laser trolley itself.

In order to measure the interior of a pipeline, the laser was located at the beginning of the test region. The laser then made a complete rotation of 360 degrees (making a scan of a cross section of the pipe) and stopped. The laser trolley subsequently moved over the defined interval (e.g. 20 mm) to the next location and stopped there. The measuring process was started again by rotating the laser one complete cycle of 360 degrees (again making a scan of a cross section of the pipe). This process was continued until the end of test region was reached. More information about the laser trolley can be found in Appendix IV.

7.2.3 Test Pipes and the Tests Performed

7.2.3.1 Test Pipes

Seven reeling simulation tests were executed on 12.75 inch outer diameter Tight Fit Pipe with a 3 mm thick 316L liner pipe with a longitudinal weld and an X65, electric resistance welded outer pipe, also with a longitudinal weld (Table 3.2).

The Tight Fit Pipe test pieces which were bent had the identical set-up as the single walled pipe test piece previously bent (Chapter 6): they consisted of pipe connected to a flange (Figure 6.4) and the flange of the test piece was connected to the flange of the re-usable pipe. Five Tight Fit Pipe test pieces (identified as OR-2, GR-1, GR-2, WT-1 and WT-2) consisted of a 3.44 m long, 12.75 inch Tight Fit Pipe connected by a weld on one side to a 2.5 m long, 12.75 inch single walled pipe and on the other side to the flange (Figure 7.15 and Figure 7.16). Two Tight Fit Pipe test pieces (identified as GR-OR-1 and GR-OR-2) with a Tight Fit Pipe circumferential weld in the middle consisted of two pieces of 12.75 inch Tight Fit Pipe, each 1.72 m in length (making up 3.44 m Tight Fit Pipe), connected to a 2.5 m long, 12.75 inch single walled pipe on one side and a flange on the other side (Figure 7.15 and Figure 7.16). The dimensions of the Tight Fit Pipe test pieces with and without a Tight Fit Pipe circumferential weld can be found in Appendix IV.

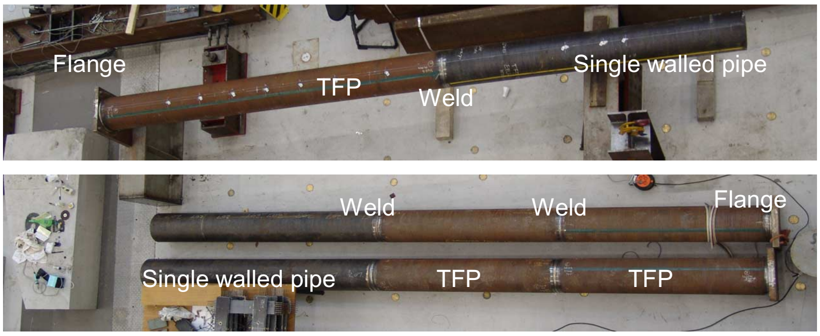

Figure 7.15 Tight Fit Pipe (TFP) test pipes without a Tight Fit Pipe circumferential weld (above) and with a Tight Fit Pipe circumferential weld (below)

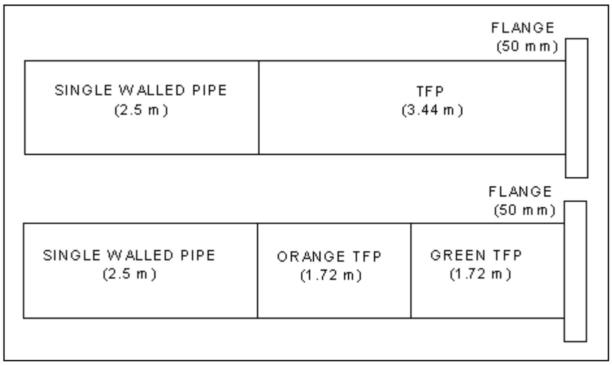

Figure 7.16 Schematic impression of the Tight Fit Pipe (TFP) test pipes (not to scale)

The sequence of welding the two 1.72 m long Tight Fit Pipes (ORANGE and GREEN Tight Fit Pipe) together, comprised the following steps: in step 1 the liner pipe was removed at the ends of the Tight Fit Pipe by machining, after which the liner pipe was welded to the outer pipe by a so called seal weld (step 2). Next, the edges of the Tight Fit Pipe were bevelled (step 3), so the two pipes could be aligned (step 4) and the bevel could be girth welded (step 5).

In order to maintain corrosion resistance in the seal weld, the welding consumable of the seal weld needs to be equally or higher alloyed than the liner pipe material. In order to meet this requirement, the welding consumable of the seal weld was 309 LMo. Welding an alloyed material (girth weld) to another alloyed material (seal weld) can in general only be done using a welding consumable equally or higher alloyed [37]. Therefore duplex was used as a weld consumable for the girth weld. As explained in Subsection 6.2.3, in order to avoid large plastic deformations in the weld during reeling, the girth weld needs to be overmatching [11]. This was another reason to use duplex as a weld consumable for the girth weld. Both the seal weld and the girth weld were TIG welded (GTAW) [10], [17]. The geometry of the Tight Fit Pipe circumferential weld present in the 12.75 inch outer diameter Tight Fit Pipe test pieces GR-OR-1 and GR-OR-2 can be seen in Figure 7.17 [17].

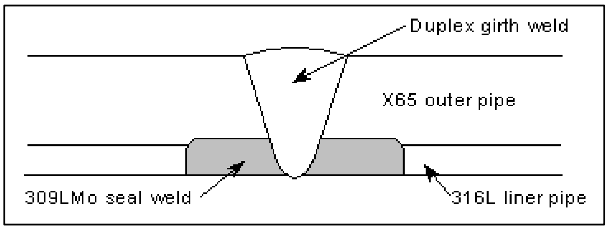

Figure 7.17 Tight Fit Pipe circumferential weld (not to scale)

The seal weld was 25 mm in length (Figure 7.18). This length was chosen such that in case the Tight Fit Pipe girth weld was not meeting the requirements and a new bevel needed to be made, the seal weld would still be intact to prevent impurities (dirt, oil, oxides, etc.) to enter between the liner pipe and the outer pipe. The height of the seal weld was 3.5 mm according to specification [11].

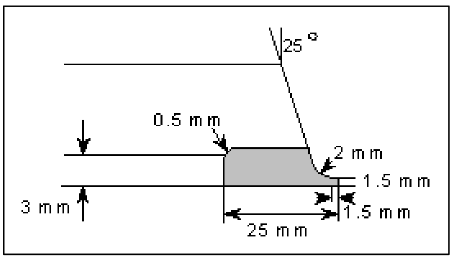

Figure 7.18 Detailed Tight Fit Pipe circumferential weld geometry (not to scale)

7.2.3.2 Tests Performed

Five bending tests were executed on the 12.75 inch Tight Fit Pipe test pieces without a Tight Fit Pipe circumferential weld (Table 7.1). These tests were performed to determine the influence of (1) the mechanical bonding strength, i.e. the residual liner pipe hoop stress (σ_{res}) and (2) the electric resistance welded longitudinal outer pipe weld, on liner pipe wrinkling.

Table 7.1 Overview of the Tight Fit Pipe test pieces without a Tight Fit Pipe circumferential weld

Test piece	σ_{res} [MPa]	ERW Weld	Reel Sizes Tested
GR-1	-199 (high)	compression zone	- 5.5
GR-2	-199 (high)	compression zone	9 - 8 - 7.5 - 7 - 6.5 - 6 - 5.5
OR-2	-178 (high)	compression zone	9 - 8 - 7.5 - 7 - 6.5 - 6 -5.5
WT-1	-53 (low)	neutral zone	9 - 8 - 7.5 - 7 - 6.5 - 6 -5.5
WT-2	-53 (low)	compression zone	9 - 8 - 7.5 - 7 - 6.5 - 6 -5.5

Note:
ERW: Electric resistance welded
The residual liner pipe hoop stresses (σ_{res}) of the Tight Fit Pipes (-199 MPa, -178 MPa and -53 MPa) have been determined in the residual compressive stress test (Subsection 3.4.2) using Equations (3.1) and (3.2).

Two bending tests were executed on the 12.75 inch Tight Fit Pipe test pieces with a Tight Fit Pipe circumferential weld in the middle (Table 7.2) in order to determine the influence of the Tight Fit Pipe circumferential weld on liner pipe wrinkling.

Table 7.2 Overview of the Tight Fit Pipe test pieces with a Tight Fit Pipe circumferential weld

Test piece	σ_{res} [MPa]	ERW weld	Reel sizes tested
GR-OR-1	-199 & -178 (high)	compression zone & tension zone	9 - 8 - 7.5 - 7 - 6.5 - 6 - 5.5
GR-OR-2	-199 & -178 (high)	compression zone & tension zone	9 - 8 - 7.5 - 7 - 6.5 - 6 - 5.5

Note:
ERW: Electric resistance welded
The residual liner pipe hoop stresses (σ_{res}) of the Tight Fit Pipes (-199 MPa and -178 MPa) have been determined in the residual compressive stress test (Subsection 3.4.2) using Equations (3.1) and (3.2).

In order to investigate the influence of the mechanical bonding strength on liner pipe wrinkling, three Tight Fit Pipes with a high mechanical bonding strength (GR-1, GR-2 and OR-2) and two Tight Fit Pipes with a low mechanical bonding strength (WT-1 and WT-2) have been bent. Liner pipe wrinkling due to bending was measured and compared. It should be taken into account that there was some variation present in the mechanical bonding strength along the length of the Tight Fit Pipe section (Subsection 3.4.2).

In order to investigate the influence of the electric resistance welded longitudinal outer pipe weld, this weld was positioned on the neutral axis for test WT-1 while the electric resistance welded longitudinal outer pipe weld was positioned in the compression zone for the test WT-2 (Figure 7.19). Theoretically it is expected that when the weld is positioned in the compression zone, the weld has an influence on liner pipe wrinkling. It is expected that when the electric resistance welded longitudinal outer pipe weld is positioned on the neutral axis it has no influence on liner pipe wrinkling since theoretically there is no bending strain present in the neutral zone (neglecting the axial tension stress for the moment). By bend testing these Tight Fit Pipes and measuring liner pipe wrinkling, the influence of the electric resistance welded outer pipe longitudinal weld on liner pipe wrinkling can be determined.

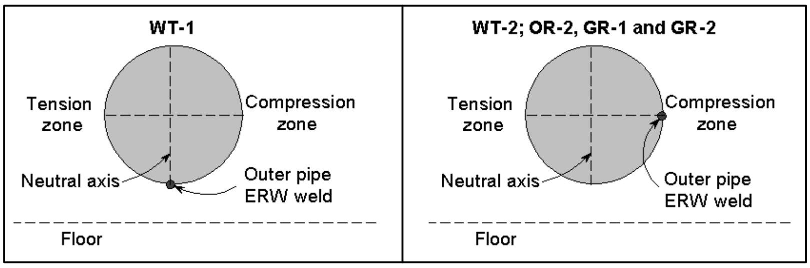

Figure 7.19 Location of the electric resistance welded (ERW) longitudinal outer pipe weld in the Tight Fit Pipe test pieces without a Tight Fit Pipe circumferential weld

In order to determine the influence of the presence of the Tight Fit Pipe circumferential weld on liner pipe wrinkling, the location and the size of the liner pipe wrinkles found in the tests GR-OR-1 and GR-OR-2 were compared to the size and location of the liner pipe wrinkles found in the tests GR-1, GR-2 and OR-2. The electric resistance welded longitudinal outer pipe welds in the GREEN Tight Fit Pipes of test pieces GR-OR-1 and GR-OR-2 were positioned in the compression zone while the electric resistance welded longitudinal outer pipe welds in the adjacent ORANGE Tight Fit Pipes were positioned in the tension zone (Figure 7.20). The electric resistance welded longitudinal outer pipe welds in test pieces GR-1, GR-2 and OR-2 were all located in the compression zone (Figure 7.19).

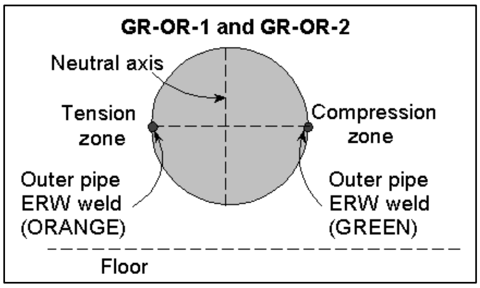

Figure 7.20 Locations of the electric resistance welded (ERW) longitudinal outer pipe weld in the Tight Fit Pipe test pieces with a Tight Fit Pipe circumferential weld

In each bending test the Tight Fit Pipe was stepwise bent to smaller sized reels in order to investigate the initiation of liner pipe wrinkling and when liner pipe wrinkles had appeared, how the liner pipe wrinkle size increased with decreasing reel radii (Table 7.1 and Table 7.2). However, in reality the Tight Fit Pipe is being curved on a single reel in a continuous process. In order to verify the test method and make sure there was no significant difference in liner pipe wrinkling and ovalisation between bending the Tight Fit Pipe stepwise on a certain reel size and bending the Tight Fit Pipe on this reel size in one go, GR-2 was bent stepwise on the 5.5 m radius reel while GR-1 was bent on the 5.5 m radius reel with a continuously increasing load (Table 7.1). Liner pipe wrinkling and ovalisation for both tests have been compared.

7.3 Comparison of the Experimental Data with the Theoretical Predictions

7.3.1 Forces in the Bending Rig

The relevant forces in the bending rig during testing were the hydraulic cylinder force pulling the pipe against the reel (F_{HC}), the axial and lateral components of the hydraulic cylinder force ($F_{HC;A}$ and $F_{HC;P}$), the lateral fixation point force holding the pipe when it was pulled against the reel ($F_{FP;P}$) and the axial fixation point force also holding the pipe when it was pulled against the reel ($F_{FP;A}$). The experimental values of the hydraulic cylinder force (F_{HC}), the components of the hydraulic cylinder force ($F_{HC;A}$ and $F_{HC;P}$) and the lateral fixation point force ($F_{FP;P}$) were compared with the theoretical predictions. The axial fixation point force ($F_{FP;A}$) measured in the test was very small compared to the other forces and not investigated further. The axial fixation point force was measured for future finite element modelling, however.

Prior to comparing the measured hydraulic cylinder force and its components with predictions, the experimentally determined hydraulic cylinder rotation (angle ζ) and the angle β need to be compared with predictions first.

The predicted values for the rotation of the hydraulic cylinder at maximum bending (ζ_{max}) using Equations (5.4), (6.3), (6.4) and (6.6) compare reasonably with the experimental data (Appendix IV). On average there was a 39 %, 23 % and 17 % difference between the theoretically predicted angle ζ_{max} and the experimental data from the angle meter, from the "full scale graph" and from the displacement meter, respectively. The fact that the experimental data exceeded the theoretical prediction for angle ζ_{max} can be explained by the fact that, in order not to make the calculations unnecessarily complex, the theoretical prediction does not take the bending of the pipe between the reel and the hydraulic cylinder into account. Other discrepancies may be the result of the fact that it was difficult to calibrate the angle meter and to take precise measurements needed to determine ζ_{max} (such as Δx_{max} or $L_{HC;y;1}$) in the "full scale graph" and in the bending rig, taking the size of the full scale bending rig into account. It should also be taken into account that these differences in the angle ζ_{max} do not significantly influence the y-component of the hydraulic cylinder force (approximately 1 %) but they do influence the x-component of the hydraulic cylinder force (approximately 40 %). However, the axial component of the hydraulic cylinder force is small compared to the y-component of the hydraulic cylinder force and is of lesser importance for the phenomena like ovalisation and local buckling.

The theoretically predicted and the experimentally determined angle β at maximum bending (β_{max}) correlate well with each other (Appendix IV): the average difference between them is 9 %. Predictions for β_{max} can be made using Equation (5.4). The angle β (Figure 5.8) was determined in the bending test by measuring the angle between the x-axis and the re-usable pipe in the full scale graph. The small discrepancies can be explained by measurement inaccuracies and the fact that in the theoretically determined angle β the bending of the pipe between the reel and the hydraulic cylinder is not taken into account.

The hydraulic cylinder force and the lateral fixation point force at the end of Phases I and II (Figure 5.7) are predicted using Equations (5.8) to (5.10) and Equations (6.3) to (6.7). The predictions are compared with the experimental data. This can only be done for the Tight Fit Pipes without a Tight Fit Pipe circumferential weld, because for the Tight Fit Pipes with a Tight Fit Pipe circumferential weld, measurements of the lateral fixation point force failed in the bending test. Tight Fit Pipe GR-1 does not show up in Figure 7.21 because this pipe was only bent to the 5.5 m radius reel. Figure 7.21 shows that for the Tight Fit Pipes without a Tight Fit Pipe circumferential weld the predicted and measured hydraulic cylinder forces correlate well (average 2 % difference at the end of Phase I and 2 % difference at the end of Phase II). Figure 7.21 also shows that there is an average of 10 % difference between the theoretical predictions of the lateral fixation point force and the experimental data, at the end of Phases I and II.

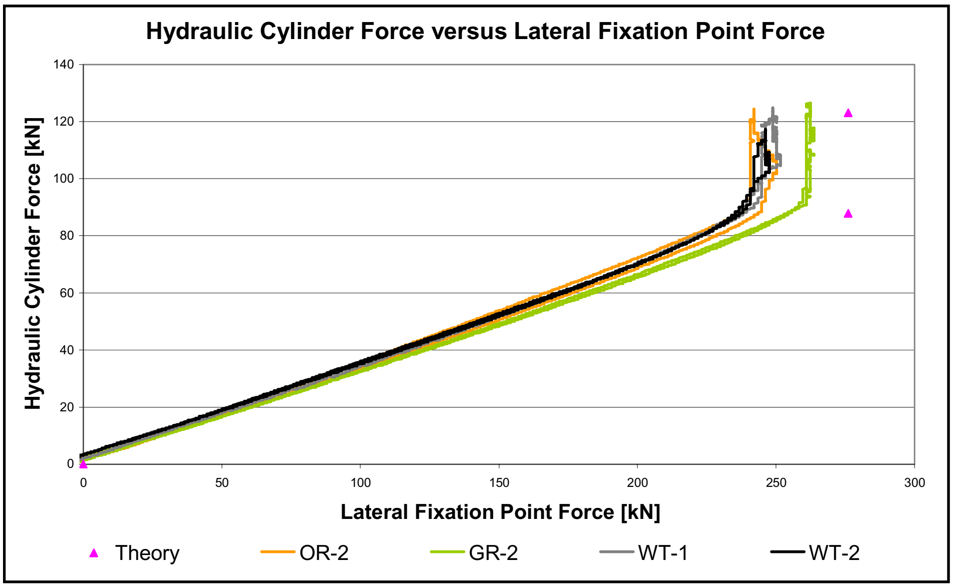

Figure 7.21 Comparison between the theoretically predicted and the measured hydraulic cylinder force and the lateral fixation point force for different Tight Fit Pipes

In the test piece there is a welded transition from the single walled pipe to the Tight Fit Pipe (Figure 7.15). The ratio between the distance between the fixation point and the initial contact point and the distance between the fixation point and the transition is 5:4. The bending moment capacity of the single walled pipe is lower than the bending moment capacity of the Tight Fit Pipe (614 kNm versus 847 kNm). The bending moment in the Tight Fit Pipe at the initial contact point during testing is therefore determined by the bending moment capacity of the single walled pipe at the transition of the single walled pipe to the Tight Fit Pipe (see also Figure 6.20). This bending moment is determined by multiplying the bending moment capacity of the single walled pipe with the ratio 5:4. This bending moment at the initial contact point is used in Equation (5.10) to predict the lateral fixation point force at the end of Phases I and II which shows to overestimate the average measurements by approximately 10 %. This difference may be explained by the fact that the single walled pipe is a seamless pipe with variation in the wall thickness and the yield stress.

The theoretical finding that the lateral fixation point force does not change in value after the end of Phase I (Figure 5.7) was again experimentally proven in these bending tests, after having seen this in the small scale bending tests (Chapter 5). However, this phenomenon was not noticed in the bending test of the single walled 12.75 inch piece (Chapter 6) due to variation in the geometric and the material properties of the test piece.

As will be discussed later, ovalisation and local buckling will be investigated in that part of the Tight Fit Pipe test piece, which was not affected by the boundary conditions (the “test region” in Subsections 7.3.3 and 7.3.4). The experimental values of the hydraulic cylinder force and its axial and perpendicular components influencing ovalisation and local buckling of the pipe in the test region were determined using the measured hydraulic cylinder forces needed to pull the test region on the reel and the measured angles ζ together with the theoretically determined angles β at various locations along this test region. These experimental values for the hydraulic cylinder force and its perpendicular component correlate well with their theoretical predictions along the test region (average 7 % and 7 % difference, respectively). There is a larger difference between the theoretical and the experimental values for the axial components of the hydraulic cylinder force along the test region (average 40 %). However as explained earlier, the axial components of the hydraulic cylinder force are smaller than the perpendicular components of the hydraulic cylinder force and of less influence on phenomena like ovalisation and local buckling.

There appears to be no significant difference between the Tight Fit Pipe test pieces with the high residual liner pipe hoop stress and the low residual liner pipe hoop stress for angle ζ_{max}, angle β_{max}, the hydraulic cylinder force and the lateral fixation point force (Appendix IV). This indicates that the residual liner pipe hoop stress does not really influence the global mechanical behaviour of the system. The same applies for the Tight Fit Pipes bent stepwise or in one go to the 5.5 m radius reel and for the Tight Fit Pipes with the electric resistance welded longitudinal outer pipe weld on the neutral axis and with the electric resistance welded longitudinal outer pipe weld in the compression zone. This also applies for the Tight Fit Pipes with and without a Tight Fit Pipe circumferential weld.

7.3.2 Strain and Curvature

The experimental results from the strain gauges and the curvature meters are compared to the theoretical predictions (Equations (5.16) and (5.17)). The locations of the strain gauges and the curvature meters in the bending rig can be found in Appendix IV as well as in Figure 7.6 (the Tight Fit Pipe test pieces without a Tight Fit Pipe circumferential weld) and in Figure 7.8 (the Tight Fit Pipe test pieces with a Tight Fit Pipe circumferential weld).

Comparison of the theoretically predicted maximum bending strain (ε_b) with the measured maximum bending strains can be found in Table 7.3 for Tight Fit Pipe OR-2 as an example of a Tight Fit Pipe test piece without a Tight Fit Pipe circumferential weld. Strain gauges 11 and 13 (measuring bending strains $\varepsilon_{b;SG11}$ *and* $\varepsilon_{b;SG13}$) were located near curvature meter K1 (measuring bending strain $\varepsilon_{b;K1}$). Strain gauges 5 and 7 (measuring bending strain $\varepsilon_{b;SG5}$ *and* $\varepsilon_{b;SG7}$) were located near curvature meter K2 (measuring bending strain $\varepsilon_{b;K2}$) in the Tight Fit Pipe bending test OR-2. Comparison of the theoretical maximum bending strain (ε_b) with the measured maximum bending strains can be found in Table 7.4 for Tight Fit Pipe GR-OR-1 as an example of a test piece with a Tight Fit Pipe circumferential weld. Strain gauge 23 (measuring bending strain $\varepsilon_{b;SG23}$) was located near curvature meter K1 (measuring bending strain $\varepsilon_{b;K1}$) and strain gauge 7 (measuring bending strain $\varepsilon_{b;SG7}$) was located near curvature meter K2 (measuring bending strain $\varepsilon_{b;K2}$) in the Tight Fit Pipe bending test GR-OR-1. An overview of the bending strain data for the other Tight Fit Pipes (GR-1, GR-2, WT-1, WT-2 and GR-OR-2) can be found in Appendix IV.

Table 7.3 Comparison between the predicted and the measured bending strains (OR-2)

Reel [mm]	$\varepsilon_{b;K1}$ [%]	$\varepsilon_{b;SG11}$ [%]	$\varepsilon_{b;SG13}$ [%]	$\varepsilon_{b;K2}$ [%]	$\varepsilon_{b;SG5}$ [%]	$\varepsilon_{b;SG7}$ [%]	$\varepsilon_{b;SG;average}$ 1) [%]	ε_b theory [%]
9000	-1.94	-1.75	-1.66	-1.41	-1.64	-1.66	-1.72	-1.77
8000	-2.07	-1.77	-1.79	-1.92	-1.76	-1.75	-1.81	-1.99
7500	-2.21	-1.83	-1.89	-2.01	-1.80	-1.81	-1.87	-2.12
7000	-2.29	-1.92	-1.93	-2.25	-1.93	-2.04	-1.98	-2.27
6500	-2.48	-2.03	-2.08	-2.36	-2.03	-2.10	-2.08	-2.44
6000	-2.71	-2.26	-2.25	-2.52	-2.08	-2.10	-2.18	-2.64
5500	-2.95	-2.39	-2.38	-2.72	-2.21	-1.85	-2.23	-2.87

Note:
1) The average bending strain was determined from data from strain gauges 5, 7, 9, 11, 13 and 15

Table 7.4 Comparison between the predicted and the measured bending strains (GR-OR-1)

Reel [mm]	$\varepsilon_{b;K1}$ [%]	$\varepsilon_{b;SG23}$ [%]	$\varepsilon_{b;K2}$ [%]	$\varepsilon_{b;SG7}$ [%]	ε_b theory [%]
9000	-1.66	-1.62	-1.80	-1.77	-1.77
8000	-1.82	-1.71	-1.96	-1.87	-1.99
7500	-1.96	-1.80	-2.01	-1.88	-2.12
7000	-2.07	-1.90	-2.27	-2.00	-2.27
6500	-2.24	-1.96	-2.35	-2.02	-2.44
6000	-2.54	-2.12	-2.65	-2.25	-2.64
5500	-2.82	-2.33	-2.84	-2.34	-2.87

Table 7.3 and Table 7.4 show that for Tight Fit Pipe OR-2 and Tight Fit Pipe GR-OR-1 the experimental bending strain data from the curvature meters and from the strain gauges attached to the Tight Fit Pipe in the region of the curvature meters correlate reasonably, as well as the experimental bending strain and the theoretically predicted bending strain. Differences can be explained by the fact that ovalisation of the Tight Fit Pipe during bending was not taken into account in the theoretical bending strain predictions and in the strains determined from the curvature meter measurements

(Equations (5.16) and (5.17) and Equations (7.2) and (7.3)). Taking ovalisation into account in the theoretical prediction of the bending strain and in the bending strain determined from the curvature meters would have reduced the bending strain (Equation (7.6) and (7.7)).

$$\varepsilon_b = \frac{\left(d_{O;o;TFP} - \Delta d_{O;o;TFP}\right)/2}{\left(D_{reel}/2 + \left(\left(d_{O;o;TFP} - \Delta d_{O;o;TFP}\right)/2\right)\right)} \tag{7.6}$$

$$\varepsilon_b = \kappa \cdot \left(d_{O;o;TFP} - \Delta d_{O;o;TFP}\right) \tag{7.7}$$

Differences between the curvature meters and the strain gauges can also be the result of the fact that strain gauges measure locally while the curvature meters determine the average bending strain over a longer distance.

Table 7.5 shows the bending strains measured in the strain gauges located on top of ($\varepsilon_{b;SG15}$) and around ($\varepsilon_{b;SG9}$, $\varepsilon_{b;SG11}$, $\varepsilon_{b;SG13}$, $\varepsilon_{b;SG17}$, $\varepsilon_{b;SG19}$ and $\varepsilon_{b;SG21}$) the Tight Fit Pipe circumferential weld of Tight Fit Pipe GR-OR-1 and the theoretical predicted bending strain (ε_b). The bending strain data measured on top of and around the Tight Fit Pipe circumferential weld of the Tight Fit Pipe GR-OR-2 can be found in Appendix IV.

Table 7.5 Bending strain measured in the strain gauges around the weld (GR-OR-1)

Distance from weld [mm]		80	30	15	WELD	15	30	80
Reel [mm]	ε_b theory[1)] [%]	$\varepsilon_{b;SG9}$ [%]	$\varepsilon_{b;SG11}$ [%]	$\varepsilon_{b;SG13}$ [%]	$\varepsilon_{b;SG15}$ [%]	$\varepsilon_{b;SG17}$ [%]	$\varepsilon_{b;SG19}$ [%]	$\varepsilon_{b;SG21}$ [%]
9000	-1.77	-1.30	-1.18	-3.86	-2.42	-2.67	-1.81	-2.26
8000	-1.99	-1.97	-1.49	-4.41	-2.60	-2.93	-1.90	-2.40
7500	-2.12	-2.06	-1.55	-4.63	-2.70	-3.07	-1.92	-2.41
7000	-2.27	-2.25	-1.72	-4.65	-2.85	-3.31	-2.03	-2.48
6500	-2.44	-2.45	-1.82	-	-2.98	-3.50	-2.04	-2.48
6000	-2.64	-2.64	-1.99	-	-3.21	-3.82	-2.20	-2.81
5500	-2.87	-2.73	-2.08	-	-3.35	-4.08	-2.29	-2.89

Note:
1) The theoretical bending strain was determined over the length of Tight Fit Pipe in contact with the reel (Table 7.3 and Table 7.4).

Table 7.5 and Appendix IV show that the measured bending strains in the strain gauges varied around the weld. This can be the result of differences in the geometry (the weld and the pipe) and in the material (X65 parent material and a duplex weld consumable). Also the welding heat input, the residual stresses due to the welding heat input and the

Bauschinger effect could have contributed to the variation of the measured strains around the weld.

Instead of comparing the measured bending strain (by the curvature meters and by the strain gauges) with the theoretically predicted bending strain, it is also possible to compare the minimum bending radius measured by the curvature meters ($R_{TFP;K1}$ and $R_{TFP;K2}$) with the theoretically applied bending radius (R_{TFP}). This comparison provides clearer insight into the shape of the Tight Fit Pipe at maximum bending in the bending test. This comparison can be found in Table 7.6 for Tight Fit Pipes OR-2 and GR-OR-1 and in Appendix IV for the other Tight Fit Pipes.

Table 7.6 Comparison between the predicted and the measured bending radius (OR-2 and GR-OR-2)

OR-2		GR-OR-2		
$R_{TFP;K1}$ [mm]	$R_{TFP;K2}$ [mm]	$R_{TFP;K1}$ [mm]	$R_{TFP;K2}$ [mm]	R_{TFP} theory [mm]
8398	9509	9754	9006	9163
7847	8467	8944	8275	8163
7357	8104	8277	8087	7663
7103	7208	7840	7140	7163
6558	6893	7238	6902	6663
5993	6458	6389	6133	6163
5515	5980	5764	5718	5663

The measured and the theoretical bending radii correlated well with each other (Table 7.6 and Appendix IV): the average difference was 5 %. Differences between the measured and the predicted bending radius can be explained by the fact that not all Tight Fit Pipes were in complete contact with the reel at maximum bending. Differences can also be explained by the fact that the curvature meters were sometimes positioned to the side of the pipe length in contact with the reel and may have been influenced by the boundary effect that the pipe curved towards the reel.

Table 7.7 shows that the middle of the Tight Fit Pipe test piece OR-2 at the locations of the position meters PM4 and PM5 ($L_{HC\text{-}PM4}$ and $L_{HC\text{-}PM5}$) was not in contact with the reel at maximum bending. Table 7.7 indicates which position meters (PM) were in contact with the reel at maximum bending in the bending test: a “1” indicates contact while a “0” indicates the position meter was not in contact with the reel. In Appendix IV it can be seen that Tight Fit Pipe GR-2 was also not in contact with the reel in the middle of the Tight Fit Pipe in the bending test at maximum bending. The Tight Fit Pipes GR-1, WT-1 and WT-2 were all completely in contact with the reel during the bending tests at maximum bending. It can be seen in Table 7.8 and Appendix IV that for Tight Fit Pipes GR-OR-1 and GR-OR-2, there was relatively good contact with the reel at maximum bending in the bending tests. Only PM4 next to the weld (Figure 7.10) showed no contact when Tight Fit Pipe GR-OR-1 was bent to the 6.5 and 6 m radius reel and Tight Fit Pipe GR-OR-2 showed no contact in PM4 when it was bent to the 7 m radius reel.

Table 7.7 Position meters (PM) in contact (1) and not in contact (0) with the reel (OR-2)

	PM1	PM2	PM3	PM4	PM5	PM6	PM7	PM8
$L_{HC\text{-}PMn}$ [mm]	9467	9296	8954	8612	8270	7928	7586	7244
9000	1	1	0	0	0	1	1	1
8000	1	1	1	0	0	1	1	1
7500	1	1	1	0	0	1	1	1
7000	1	1	1	0	0	1	1	1
6500	1	1	1	0	1	1	1	1
6000	1	1	1	0	0	1	1	1
5500	1	1	1	0	0	1	1	1

Table 7.8 Position meters (PM) in contact (1) and not in contact (0) with the reel (GR-OR-1)

	PM1	PM2	PM3	PM4	PM5	PM6	PM7	PM8
$L_{HC\text{-}PMn}$ [mm]	9491	9320	9102	8672	8515	8095	7610	7268
9000	1	1	1	1	1	1	1	1
8000	1	1	1	1	1	1	1	1
7500	1	1	1	1	1	1	1	1
7000	1	1	1	1	1	1	1	1
6500	1	1	1	0	1	1	1	1
6000	1	1	1	0	1	1	1	1
5500	1	1	1	1	1	1	1	1

The reason why the Tight Fit Pipes WT-1 and WT-2 (Tight Fit Pipes with a low mechanical bonding strength) were in complete contact with the reel at maximum bending and Tight Fit Pipes OR-2 and GR-2 (Tight Fit Pipes with a high mechanical bonding strength) were not, may be the result of the Tight Fit Pipes WT-1 and WT-2 having a lower bending moment capacity at the same value of bending strain. This lower bending moment capacity may be the result of more liner pipe wrinkles along the Tight Fit Pipe due to bending resulting from a lower mechanical bonding strength between the liner pipe and the outer pipe (this will be explained in Subsection 7.3.4). If more liner pipe wrinkles occur along the Tight Fit Pipe length, the liner pipe and the outer pipe do not function as one integral pipe, resulting in a lower bending moment capacity at the same value of bending strain.

Tight Fit Pipe GR-1 was bent to the 5.5 m reel in one go and was in complete contact with the reel. GR-2 was bent stepwise to the 5.5 m reel and was not in contact with the 5.5 m radius reel in the middle of the Tight Fit Pipe (PM4 and PM5). This might be the result of the following: Tight Fit Pipe GR-2 was not completely curved on the 9 m radius reel due to the fact that the tension in the pipe was not yet high enough in this test. The tension in the pipe increases with decreasing reel radius (Figure 5.8). After unloading, a certain residual curvature was present in the pipe which was influenced by the Tight Fit Pipe not being completely in contact with the 9 m radius reel. This residual curvature influenced the shape of the Tight Fit Pipe GR-2 at decreasing reel sizes and thus the Tight Fit Pipe in contact with the reel at decreasing reel sizes. For the Tight Fit Pipe GR-1 which was bent in one go on the 5.5 m reel, the tension in the pipe was high enough for the Tight Fit Pipe to be in complete contact with the 5.5 m reel. The Tight Fit Pipe GR-1 bent on the 5.5 m reel in one go was not influenced by a bending history. However, the maximum difference between the theoretical bending radius and the bending radius measured for the Tight Fit Pipes GR-1 and GR-2 was only 4 % and 13 %, respectively.

It can be concluded that the mechanical bonding strength between the Tight Fit Pipe liner pipe and the outer pipe as well as the stepwise bending (opposed to bending in one go) show to have no significant influence on the shape of the pipe in bending and thus on the bending radius. The electric resistance welded longitudinal outer pipe weld and the presence of the Tight Fit Pipe circumferential weld also did not seem to have a significant influence on the bending radius.

7.3.3 Ovalisation

In Figure 7.22 ovalisation at maximum bending was compared to the DNV Offshore Standard OS-F101 [11] design formula (Equation (5.15)) using only the outer pipe wall thickness as well as assuming the liner pipe and the outer pipe wall thicknesses "added", representing one single wall thickness.

It should be realised that the experimental values for ovalisation presented in Figure 7.22 are values for ovalisation determined by the vertical change in the diameter measured by the ovalisation meter at maximum bending and the horizontal change in the diameter determined by multiplying the vertical change in the diameter measured by the ovalisation meter at maximum bending with the ratio between the horizontal and the vertical change in the diameter measured by hand after each bending stage ($\Delta d_{O;o;TFP;hor}/\Delta d_{O;o;TFP;ver}$); this procedure has been explained in Subsection 6.2.2.

It should also be noted that the values for the ovalisation presented in Figure 7.22 and in Appendix IV are the average values for ovalisation in the "test region" of each Tight Fit Pipe. The "test region" of a Tight Fit Pipe test piece is the length of the Tight Fit Pipe which was not affected by boundary effects and shows relatively constant values for ovalisation.

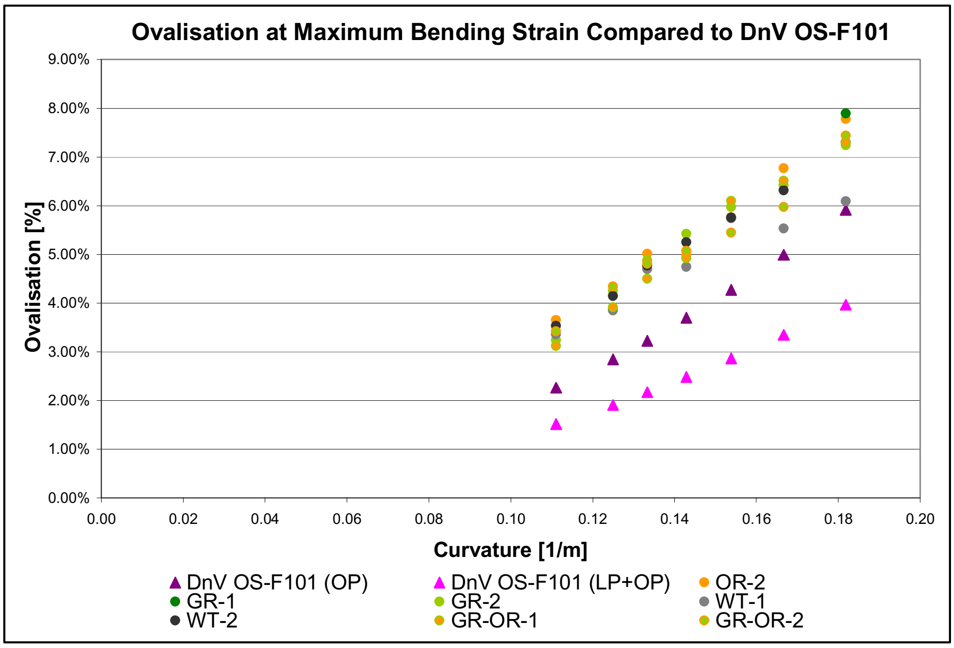

Figure 7.22 Comparison of the experimentally determined ovalisation at maximum bending with the DNV Offshore Standard OS-F101 [11] prediction using only the outer pipe (OP) and the "added" liner pipe and outer pipe (LP+OP) wall thicknesses

It can be seen in Figure 7.22 that the ovalisation at maximum bending is underestimated by the DNV Offshore Standard OS-F101 [11] for all Tight Fit Pipes when assuming the liner pipe and the outer pipe wall thicknesses "added", representing one single wall thickness as well as when only the outer pipe wall thickness is taken into account. Firstly, this underestimation is the result of the DNV Offshore Standard OS-F101 code being based on pure bending tests disregarding the reaction force of the reel on the pipe as has been mentioned in the bending test on the single walled pipe (Chapter 6). Secondly it should be taken into account that the ovalisation at maximum bending by the ovalisation meters is determined using the ratio between the change in the horizontal diameter and the change in the vertical diameter after bending measured by hand (Subsection 6.2.2). This ratio might be slightly different at maximum bending than after unloading. The maximum ovalisation measured after bending in the full scale bending test of the 12.75 inch Tight Fit Pipe exceeded the 3.0 % allowable threshold for ovalisation (after installation) as stated in the DNV OS F101 code [11] when bending it on the 7 m, or smaller radius reel. What ovalisation should be allowed after unreeling and straightening depends on the loads (e.g. water depth) and the required safety margin. Reduction of ovalisation can be obtained by increasing the reel radius (e.g.

Technip Deep Blue has a reel radius of 9.75 m [52] and the Technip Apache has a reel radius of 8.23 m [51]) and/or decreasing the diameter to wall thickness ratio [12].

When comparing Tight Fit Pipes with a high residual bonding strength with the Tight Fit Pipes with a low residual bonding strength, a 20 % average difference was noticed in ovalisation at maximum bending and after unloading using the ovalisation meters; only a 10 % difference was noticed when the ovality hand measurements after unloading were compared (Appendix IV). When comparing Tight Fit Pipes GR-1 (bending in one go) and GR-2 (stepwise bending), there was 8 % average difference in ovalisation. When comparing Tight Fit Pipes WT-1 (electric resistance welded longitudinal outer pipe weld in the neutral axis) with Tight Fit Pipe WT-2 (electric resistance welded longitudinal outer pipe weld in the compression zone), there was 20 % average difference in these measured ovalisation values. When comparing Tight Fit Pipes OR-1, GR-1, GR-2 (Tight Fit Pipes without a Tight Fit Pipe circumferential weld) with Tight Fit Pipes GR-OR-1 and GR-OR-2 (Tight Fit Pipes with a Tight Fit Pipe circumferential weld), there was a 4 % average difference in measured ovalisation in the bending tests.

7.3.4 Local Buckling of the Tight Fit Pipe

7.3.4.1 Defining Local Buckling of the Tight Fit Pipe

With local buckling of the Tight Fit Pipe is meant local buckling of the integral Tight Fit Pipe or liner pipe wrinkling. Local buckling of the integral Tight Fit Pipe means that the outer pipe and thus also the liner pipe is buckled. Liner pipe wrinkling means that local buckling of the liner pipe alone occurs while the outer pipe is still intact. Local buckling of the integral Tight Fit Pipe should be limited because of the following reasons:

1. The Tight Fit Pipe needs to have enough resistance against collapse once it has been installed on the seabed.
2. Local buckling results in loss of moment capacity of the Tight Fit Pipe. If the pipe is loaded e.g. in bending (load controlled) in case of spans in the seabed, concentration of curvature can occur at the location of the local buckle. Excessive local buckling and concentration of curvature of the integral Tight Fit Pipe can obstruct the flow of hydrocarbons and a pig from passing through the pipe.
3. As a result of local buckling, excessive strains can occur at the location of the local buckle. The strain capacity of the pipe material needs to be sufficient, else fractures can occur.
4. During the operation of a buckled Tight Fit Pipe, an increase and a decrease of the operational pressure may increase and decrease the sizes of these local buckles. This increase and decrease in the local buckle size decreases the fatigue life and can possibly cause fractures.

Liner pipe wrinkling should be limited because of the following reasons:

1. During the operation of a Tight Fit Pipe with a wrinkled liner pipe, an increase and a decrease of the operational pressure may increase and decrease the sizes of these liner pipe wrinkles. This increase and decrease in the liner pipe wrinkle size decreases the fatigue life and can possibly cause fractures to develop. Once fractures have been developed in the liner pipe, through-the-liner pipe wall cracks can develop. Once through-the-liner pipe wall cracks have occurred, the corrosion resistance of the liner pipe is not guaranteed anymore.
2. Excessive liner pipe wrinkling obstructs the flow of hydrocarbons and a pig from passing through the pipe.

Whether local buckling of the integral Tight Fit Pipe occurred was detected visually in the bending tests. Detection of the local buckle of the integral Tight Fit Pipe in the test thus depended on the eyesight of the person evaluating the local buckle and was therefore a subjective phenomenon. A special laser trolley has been developed to scan the inside of the Tight Fit Pipe and measure liner pipe wrinkling. Although a very sensitive laser trolley has been built to measure liner pipe wrinkling, detection of liner pipe wrinkling still remains a subjective phenomenon because there is currently no agreement on the definition of a local buckle (liner pipe wrinkling) or of the initiation of local buckling (liner pipe wrinkling).

It is suggested to define the initiation of liner pipe wrinkling as crossing a certain threshold of:

1. the liner pipe wrinkling height.
2. the steepness of the liner pipe wrinkle.
3. the change of steepness, i.e. the curvature, in the liner pipe wrinkle.

The threshold for the liner pipe wrinkle height, the steepness or the curvature could be based on its influence on the fatigue life reduction or the size of a pig and its ability to pass liner pipe wrinkles of a certain height. Research into this subject still has to be performed.

7.3.4.2 Local Buckling of the Integral Tight Fit Pipe

The critical buckling strain of the integral Tight Fit Pipe can be predicted by using the Equations (5.18), (5.19) and (5.20), developed by Murphy and Langner [36] and Gresnigt [23] and stated by DNV [11], respectively. However, these equations predict the critical buckling strain of a single walled pipe while the Tight Fit Pipe is a combination between an inner and an outer pipe. In Table 7.9 the predictions for the critical buckling strain ($\varepsilon_{TFP;cr}$) can be seen, assuming the liner pipe and the outer pipe wall thicknesses "added", representing one single wall thickness. It is noted that it might not be allowed to use the liner pipe and the outer pipe wall thicknesses to function as one in these predictions, because prior to local buckling of the integral Tight Fit Pipe liner pipe wrinkling may occur, resulting in the liner pipe and the outer pipe not to function as one anymore.

Table 7.9 Predictions for the critical buckling strain of the integral Tight Fit Pipe

ε_b test [%]	$\varepsilon_{TFP;cr}$ Murphy & Langer [%]	$\varepsilon_{TFP;cr}$ Gresnigt [%]	$\varepsilon_{TFP;cr}$ DNV [%]
2.87	2.68	2.43	3.56

The equation developed by Gresnigt [23] predicts a critical buckling strain for the integral Tight Fit Pipe of 2.43 % (which will be reached when bending the Tight Fit Pipe on the 6 m radius reel). However, the Tight Fit Pipe did not show any signs of local buckling at this bending strain of 2.43 %. The equation developed by Murphy and Langer [36] predicts the Tight Fit Pipe to buckle at 2.68 % bending strain (which will be reached when bending the Tight Fit Pipe on the 5.5 m radius reel). However, the Tight Fit Pipe did also not show any signs of local buckling in the bending tests at this bending strain of 2.68 %. The DNV OS F101 code [11] predicts that local buckling of the Tight Fit Pipe is not expected to occur during these bending tests, because the maximum bending strain applied in the bending tests was 2.87 % while the critical buckling strain predicted by the DNV OS F101 code is 3.56 %.

As mentioned in Chapter 5 and 6, it should be realised that the predictions developed by Murphy and Langner [36] and by Gresnigt [23] underestimate the critical buckling strain in the lower diameter to thickness ratio region of below 40. The diameter to thickness ratio of the Tight Fit Pipes was 22. Moreover, these predictions developed by Murphy and Langner [36] and Gresnigt [23], as well as the prediction stated by the DNV OS F101 code [11], are design equations. At the same time it should be realised that all three predictions are based on pure bending tests not taking the reaction force of the reel on the pipe into account. This reaction force enhances local buckling.

The Tight Fit Pipe did however clearly show signs of liner pipe wrinkling (local buckling of the liner pipe) prior to local buckling of the integral Tight Fit Pipe. The failure mode of the Tight Fit Pipes in these tests was thus liner pipe wrinkling.

7.3.4.3 Determination of Liner Pipe Wrinkling

Liner pipe wrinkling was detected by the laser trolley (Subsection 7.2.2). Comparing the liner pipe wrinkles of the different Tight Fit Pipes provided insight in the influence on liner pipe wrinkling of (1) the mechanical bonding strength between the liner pipe and the outer pipe, (2) the electric resistance welded longitudinal outer pipe weld, (3) the presence of the Tight Fit Pipe circumferential weld and (4) bending in one go to a final reel radius (5.5 m) versus stepwise bending on this reel radius. Moreover, the influence of the interval measuring length on the measured liner pipe wrinkle height was investigated (5) by scanning the largest wrinkles of Tight Fit Pipe WT-2 with an interval length of 5 mm and an interval length of 20 mm. An overview of the laser trolley measuring specifics is presented in Table 7.10.

Table 7.10 Overview of the details of the liner pipe wrinkling measurements using the laser trolley for all Tight Fit Pipes tested

	AB and MBS	Interval	Laser Scan Steps
OR-2	AB	20 mm	BB-9-8-7.5-7-6.5-6-5.5
GR-1	AB and MBS	20 mm	BB-5.5
GR-2	AB and MBS	20 mm	BB-9-8-7.5-7-6.5-6-5.5
WT-1	AB and MBS	20 mm	BB-9-8-7.5-7-6.5-6-5.5
WT-2	AB and MBS	5 & 20 mm	BB-9-8-7.5-7-6.5-6-5.5
GR-OR-1	AB and MBS	10 mm	BB-9-8-7.5-7-6.5-6-5.5
GR-OR-2	AB and MBS	10 mm	BB-9-8-7.5-7-6.5-6-5.5

Note:

BB: Before bending (the laser trolley scanned the inside of the Tight Fit Pipe before bending the Tight Fit Pipe)

MBS: Maximum bending strain (the laser trolley scanned the inside of the Tight Fit Pipe at maximum bending when the Tight Fit Pipe was in contact with the reel)

AB: After bending testing (the laser trolley scanned the inside of the Tight Fit Pipe after unloading the Tight Fit Pipe)

The scans of the inside of the Tight Fit Pipe made by the laser trolley represent the radial changes of the original inner radius of the Tight Fit Pipe, assumed to be 145 mm. This data needs to be expressed in the liner pipe wrinkle height and the liner pipe wrinkle half wave length, thereby defining the shape of the liner pipe wrinkles in the tested Tight Fit Pipes.

In order to be able to compare the liner pipe wrinkles, a consistent method of analysing liner pipe wrinkling needed to be established for each Tight Fit Pipe:

1. Definition of the test region in the Tight Fit Pipe
2. Determination of the locations of the liner pipe wrinkles in the Tight Fit Pipe
3. Determination of the shape of the liner pipe wrinkles
    a. Determination of the location of the top of a liner pipe wrinkle
    b. Determination of the liner pipe wrinkle height
    c. Determination of the liner pipe wrinkle half wave length
    d. Analysing the residual liner pipe wrinkles in the test region after bending the Tight Fit Pipe on the 5.5 m reel
4. Scanning of the Tight Fit Pipe with a different scanning interval density
5. Increase in liner pipe wrinkling with increase of the curvature
6. Liner pipe wrinkling at maximum bending

1. Definition of the test region in the Tight Fit Pipe

The region of the Tight Fit Pipe test piece which was not affected by boundary effects and was investigated for ovalisation and liner pipe wrinkling was that part of the Tight Fit Pipe test piece which shows relatively constant values for ovalisation. Outside of this test region liner wrinkles did occur, but they were not taken into account during the analysis. The area of the liner pipe surface that was analysed was defined to be between the hand measurement H3 and ovalisation meter measurement OM6 for the Tight Fit Pipes without a Tight Fit Pipe circumferential weld and between H2 and OM6 for the Tight Fit Pipes with a Tight Fit Pipe circumferential weld. In Table 7.11 and Figure 7.23 the distance between the start of the laser and the beginning of the test region ($L_{laser\ hole\text{-}STR}$) can be found and the distance between the start of the laser and the end of the test region ($L_{laser\ hole\text{-}ETR}$).

Table 7.11 Overview of the liner pipe wrinkling data for the Tight Fit Pipes tested

	OR-2	GR-1	GR-2	WT-1	WT-2	GR-OR-1	GR-OR-2
$L_{laser\ hole\text{-}STR}$ [mm]	1172	1201	1196	1189	1175	982	1018
$L_{laser\ hole\text{-}ETR}$ [mm]	2238	2259	2245	2228	2228	2088	2088
Wrinkles in Tight Fit Pipe	W1-W8	W1-W8	W1-W7	W1-W23	W1-W25	W1-W9	W1-W10
Wrinkles in test region	W2-W6 1)	W2-W7 1)	W3-W6	W4-W15	W8-W18	W1-W7	W2-W7 1)
Wrinkles in CZ in test region	W2-W6	W2-W6	W3-W6	W5, W8, W13	W10, W12, W16	W1, W3, W5, W6	W2, W4, W5, W6
Wrinkles next to CZ	-	W7	-	W4, W6, W7, W9-W12, W14, W15	W8, W9, W11, W13-W15, W17, W18	W2, W4, W7	W3, W7
Wrinkle threshold [-]	0.051	0.063	0.084	0.088	0.078	0.120	0.102

Note:

CZ: Compression zone

1) W2 of the Tight Fit Pipes OR-2, GR-1 and GR-OR-2 were located close the beginning of the test region. It was decided to locate these liner pipe wrinkles W2 in the test region.

2. Determination of the locations of the liner pipe wrinkles in the Tight Fit Pipe

The locations of the liner pipe wrinkles in the Tight Fit Pipe were identified using the scans obtained from the laser trolley. Figure 7.23 shows the scan of the Tight Fit Pipe WT-1 made by the laser trolley after bending it on the 5.5 m radius reel.

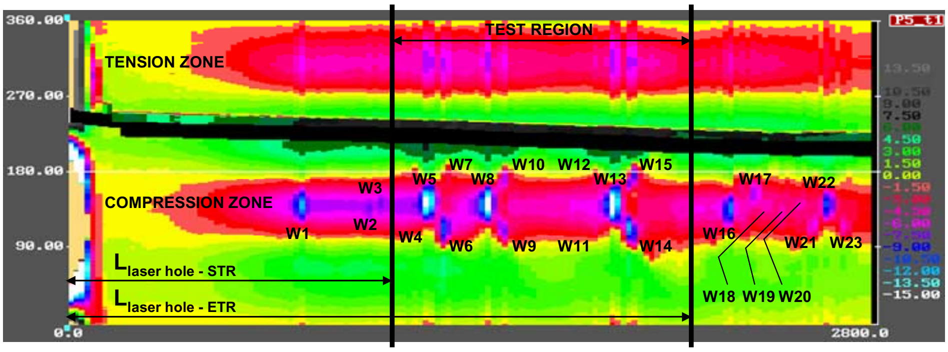

Figure 7.23 Internal scan made by the laser trolley of the Tight Fit Pipe WT-1, identifying the liner pipe wrinkles

The scans of the inside of the Tight Fit Pipe made by the laser trolley represent the radial changes of the average, inner radius of the Tight Fit Pipe prior to testing. The blue and the white colours in the compression zone of the scan identify the largest radial changes, indicating the presence of liner pipe wrinkling. The blue colours in the tension zone identify the locations where the liner pipe came loose from the outer pipe as a result of bending (which is not liner pipe wrinkling).

The laser trolley scan alone was not sufficient to determine the locations of all the liner pipe wrinkles in the Tight Fit Pipe, however. Some liner pipe wrinkles appeared more to the side of the compression zone and were harder to find in the scan. E.g. liner pipe wrinkle W5 of the Tight Fit Pipe WT-1 can be seen in the compression zone of Figure 7.23. However, wrinkle W4 cannot clearly be seen in Figure 7.23. Therefore, various cross-sections of the Tight Fit Pipe WT-1 (e.g. the cross sections made by the laser trolley, 1179 mm and 1217 mm from the start of the laser measurements in Figure 7.24) had to be used as well, in order to find all the liner pipe wrinkles in the Tight Fit Pipe. As mentioned, the laser made a complete rotation of 360 degrees, thereby scanning a cross section of the Tight Fit Pipe, at regular intervals (e.g. 20 mm). The disturbance which can be seen in Figure 7.24 just above the x-axis on the left side is the result of the fact that the laser scans its own cable (this is unavoidable). However, the disturbance is always positioned there where liner pipe wrinkling did not occur.

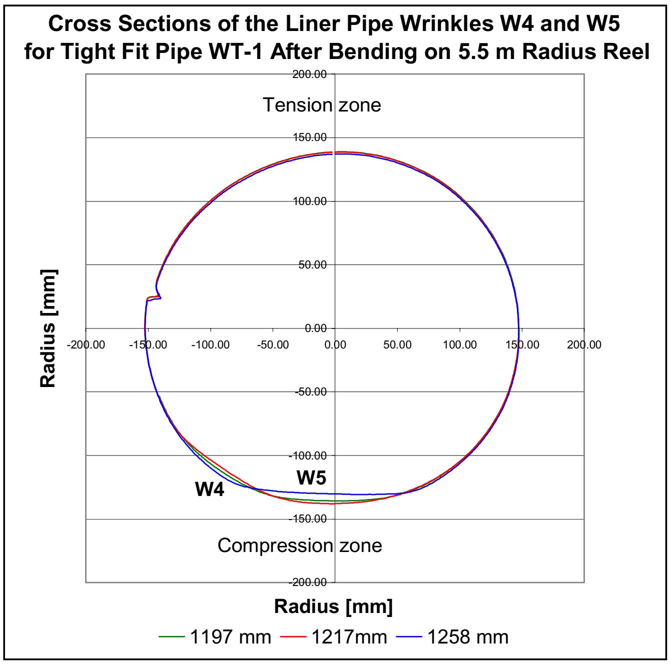

Figure 7.24 Various cross-sections made by the laser trolley used to detect wrinkle W4 in Tight Fit Pipe WT-1

3. Determination of the shape of the liner pipe wrinkles

For all the Tight Fit Pipes, the shape (the liner pipe wrinkle height and the liner pipe wrinkle half wave length) of all the liner pipe wrinkles in the test region were determined after bending the Tight Fit Pipe on the 5.5 m radius reel. The four most significant liner pipe wrinkles were subsequently studied in more detail regarding their development with increasing curvature (see point 5 below).

3a. Determination of the location of the top of a liner pipe wrinkle

The data provided by the laser trolley was put in a matrix, where the columns represented the measurements in axial direction (i.e. one measurement per specified measuring interval of e.g. 5 mm or 20 mm) and the rows in the matrix represented the measurements every half degree in the circumferential direction. As mentioned earlier, the data in this matrix represented the radial changes of the average, inner radius of the Tight Fit Pipe prior to testing, assumed to be 145 mm. The largest negative radial changes of the inner radius in this matrix indicated the locations of the tops of the liner pipe wrinkles.

3b. Determination of the liner pipe wrinkle height

Once the axial and the circumferential locations of the tops of the liner pipe wrinkles were found, the liner pipe wrinkle height needed to be determined. The bottom of the liner pipe wrinkle was defined as the intersection of two lines (Figure 7.25): (1) the line connecting the valley in front of the top of liner pipe wrinkle (prebottom) with the valley behind the top of liner pipe wrinkle (postbottom) and (2) the line dropped perpendicularly down from the top on the pipe axis. The intersection point of these two lines divided the length between both valleys (prebottom and postbottom) into two parts, which differed in size per liner pipe wrinkle as can be seen in Figure 7.25.

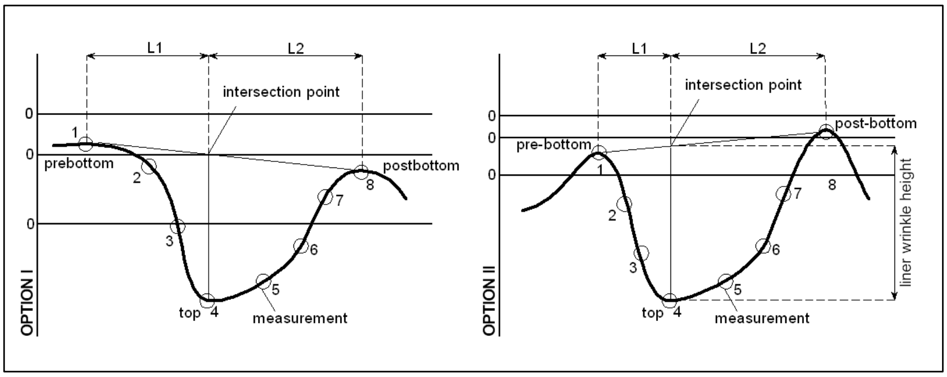

Figure 7.25 Assessment of the liner pipe wrinkle height

When calculating the height of the intersection point, it should be taken into account that the prebottoms and postbottoms could either have a positive or negative value and that the prebottom could either be larger or smaller than the postbottom (Figure 7.25). However, Equation (7.8) defines the height of the intersection point ($\Delta r_{L;i;TFP;bottom}$) for all variations as defined in Figure 7.25.

$$\Delta r_{L;i;TFP;bottom} = \Delta r_{L;i;TFP;pre} + \left(\frac{L_1}{L_1+L_2}\right) \cdot \left(\Delta r_{L;i;TFP;post} - \Delta r_{L;i;TFP;pre}\right) \tag{7.8}$$

The difference in the height between this intersection point and the top of the liner pipe wrinkle was defined as the liner pipe wrinkle height (Equation (7.9)).

$$a = \Delta r_{L;i;TFP;bottom} - \Delta r_{L;i;TFP;top} \tag{7.9}$$

3c. Determination of the liner pipe wrinkle half wave length

The half wave length of a local buckle of a single walled pipe is defined in theory as the length between two adjacent locations where the curvature of the liner pipe wrinkle changes signs [46].

This definition is not applicable to the Tight Fit Pipe liner pipe wrinkling because the measurement density of liner pipe wrinkling is not high enough. One suggestion is to define the liner pipe wrinkle half wave length as the length between the prebottom and the postbottom surrounding the top of the liner pipe wrinkle. However, this would result in too large values for the liner pipe wrinkle half wave length. This was concluded by comparing the liner pipe wrinkle half wave lengths measured by the laser trolley after the Tight Fit Pipe was bent on the 5.5 m radius reel, based on the prebottom and postbottom locations, with measurements by hand. These measurements by hand could only provide an indication of the half wave length, since the start and the end of the liner pipe wrinkle can only be subjectively determined. These subjective measurements by hand could still provide an indication of the liner pipe wrinkle half wave length, however. These hand measurements were performed after testing the Tight Fit Pipe on the 5.5 m radius reel (the Tight Fit Pipes were cut open to be able to do this).

A new approach for determining the liner pipe wrinkle half wave length (L_L/m) is suggested, based on the values for the steepness, the value for dr/dx. The value for dr/dx was determined by dividing the difference in the radial changes ($\Delta r_{L;i;TFP}$) between two laser axial measurements (n), by the interval length between these two axial measurements. The value for dr/dx can be determined for the entire circumference of the Tight Fit Pipe for every interval scanned by the laser trolley. For example, the value dr/dx of 0.31 (Figure 7.26 and Table 7.12) was determined by subtracting the radial displacement $\Delta r_{L;i;TFP}$ of -12.41 mm, measured at the axial location L_{axial} = 1277 mm, from the radial offset $\Delta r_{L;i;TFP}$ of -6.22 mm measured at the axial location L_{axial} = 1297 mm (Table 7.12). This value was subsequently divided by the interval length between these two axial measurements in order to determine dr/dx for this interval.

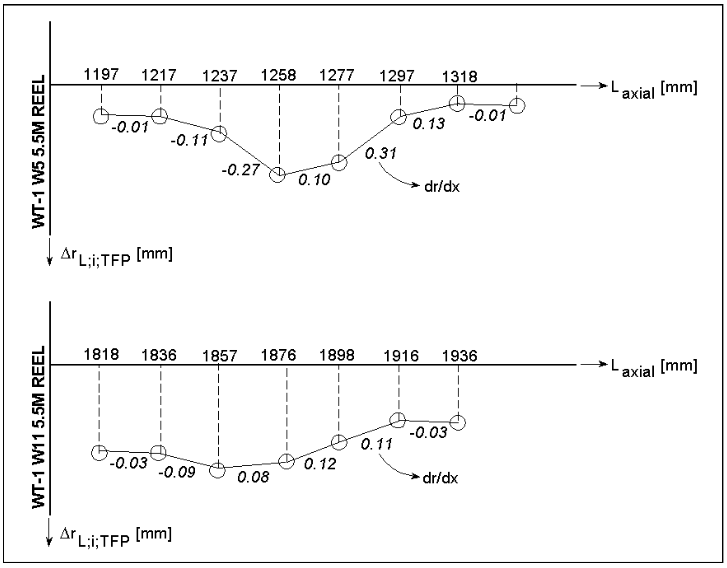

Figure 7.26 Assessment of the liner pipe wrinkle half wave length of liner pipe wrinkles W5 and W11 of Tight Fit Pipe WT-1 after bending and unloading to the 5.5 m radius reel

Table 7.12 Analysis of the liner pipe wrinkle W5 in Tight Fit Pipe WT-1 after bending it on the 5.5m radius reel

L_{axial} [mm]	1117	1137	1157	1177	1197	1217	1237	1258	1277	1297	1318	1337
		pre-bottom						top			post-bottom	
$\Delta r_{L;l;TFP}$ (laser) mm]	-6.34	-6.03	-6.23	-6.41	-6.46	-6.75	-9.01	-14.45	-12.41	-6.22	-3.63	-3.80
n [-]	14	15	16	17	18	19	20	21	22	23	24	25
dr/*dx*		0.02	-0.01	-0.01	0.00	-0.01	-0.11	-0.27	0.10	0.31	0.13	-0.01
L_l/m [mm]						start		top			end	

It can be seen in Table 7.12 that for liner pipe wrinkle W5 in Tight Fit Pipe WT-1 after bending it on the 5.5 m radius reel, *dr*/*dx* has different values along the axis of the Tight Fit Pipe, having larger values (either negative of positive) around a liner pipe wrinkle. There the orientation of the liner pipe made more abrupt changes. The liner pipe wrinkle half wave length was therefore defined as the length over which the values for *dr*/*dx* were larger than a certain threshold value for *dr*/*dx* (Table 7.11).

The threshold value for *dr*/*dx* was determined for a Tight Fit Pipe as follows: all values of *dr*/*dx* in the scan made by the laser trolley before testing were calculated, after which the threshold value for *dr*/*dx* was defined as twice the average of all these values for *dr*/*dx*. The threshold provides an indication of the initial roughness of the liner pipe. This procedure was chosen because results for the liner pipe wrinkle half wave length compared well to hand measurements. As mentioned earlier, these measurements by hand could only provide an indication of the liner pipe wrinkle half wave length, since the start and the end of the liner pipe wrinkle can only be subjectively determined by hand. However, these subjective hand measurements could still provide an indication of the liner pipe wrinkle half wave length.

In this method of Tight Fit Pipe liner pipe wrinkle half wave length analysis, the liner pipe wrinkle half wave length depends on the height of the liner pipe wrinkle. This is not conventional. In the local buckling analysis of a single walled pipe [46] the half wave length of the local buckle remains constant. However, it was noticed in the Tight Fit Pipe bending tests that the liner pipe wrinkle half wave length became slightly larger with increased curvature (Figure 7.27). The increase in the liner pipe wrinkle half wave length with increasing curvature was more pronounced for the highly bonded Tight Fit Pipes than for the less bonded Tight Fit Pipes (Figure 7.27 and Figure 7.28). Furthermore, for someone to asses the liner pipe wrinkles in a Tight Fit Pipe, a higher liner pipe wrinkle height would also make the liner pipe wrinkle more visible and thus seem longer. The method of the half wave length depending on the height of the liner pipe wrinkle (*dr*/*dx*) may be not conventional but is considered practical and therefore useful in the consistent analysis of the liner pipe wrinkles.

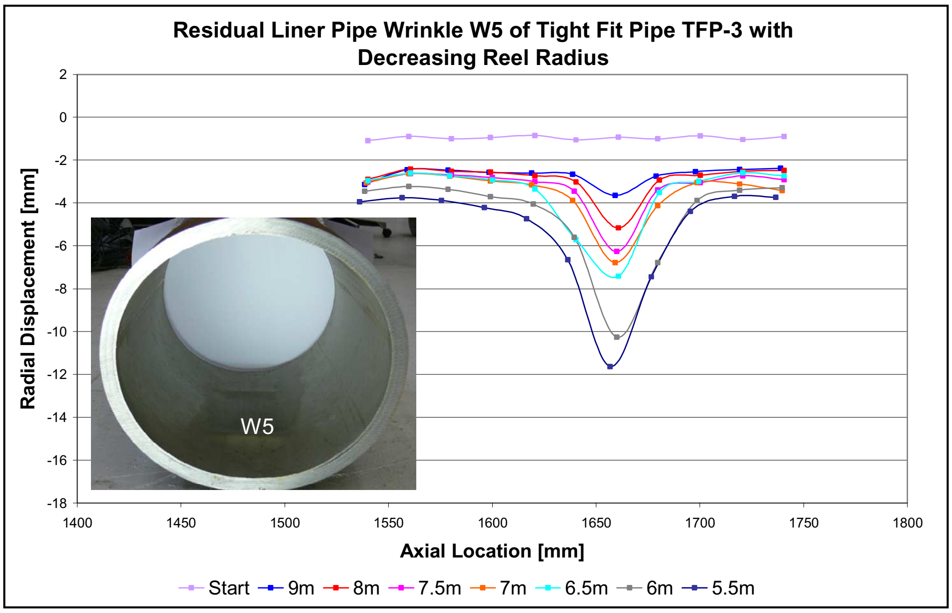

Figure 7.27 Liner pipe wrinkle half wave length growth of W5 in Tight Fit Pipe GR-2

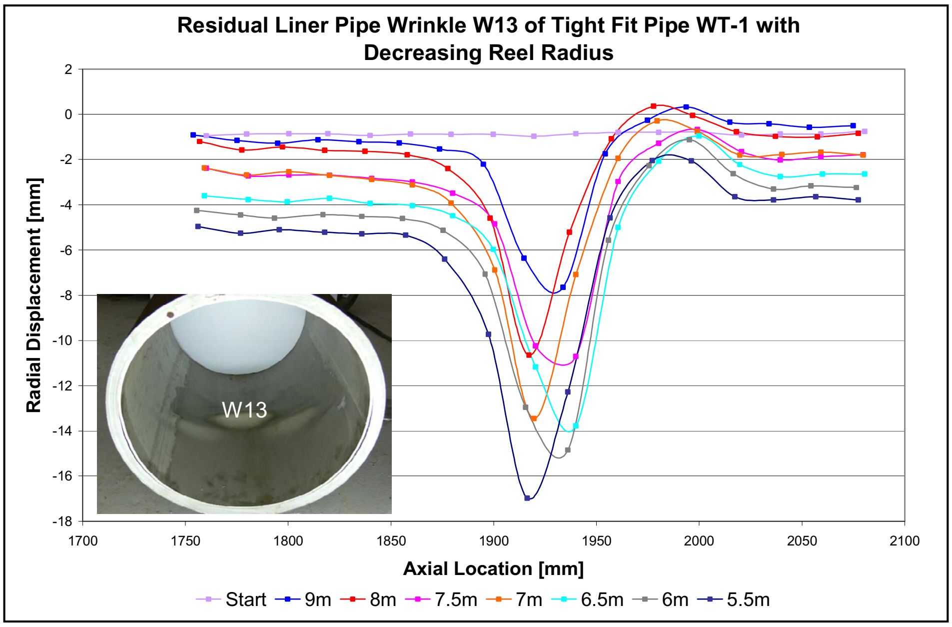

Figure 7.28 Liner pipe wrinkle half wave length growth of W13 in Tight Fit Pipe WT-1

The thresholds for *dr*/*dx* of the Tight Fit Pipes GR-OR-1 and GR-OR-2 were larger than the thresholds of the Tight Fit Pipes OR-2, GR-1, GR-2, WT-1 and WT-2 (Table 7.11). This is the result of the difference in the measuring interval length used by the laser trolley: Tight Fit Pipes GR-OR-1 and GR-OR-2 were scanned with a 10 mm interval instead of a 20 mm interval (Table 7.10). The interval measuring length influences the magnitude of the threshold.

Finally, three aspects should be taken into account when determining the liner pipe wrinkle half wave length:

1. Liner pipe wrinkles always had one or more values for *dr*/*dx* that were negative (indicating an increase in the liner pipe wrinkle height) followed by one or more values for *dr*/*dx* that were positive (indicating a decrease in the liner pipe wrinkle height). If a value for *dr*/*dx* lower than the threshold was located in between a negative and a positive *dr*/*dx* which did exceed the threshold, this *dr*/*dx* was part of the liner pipe wrinkle (Figure 7.26). In this case the top of the liner pipe wrinkle was missed by the laser trolley.
2. If only the negative *dr*/*dx* or the positive *dr*/*dx* of the liner pipe wrinkle exceeded the threshold, it was assumed that the other *dr*/*dx*, not exceeding the threshold, was part of the liner pipe wrinkle half wave length.

3. When determining the *dr/dx* threshold for Tight Fit Pipes GR-OR-1 and GR-OR-2, the area near the weld was not taken into account, due to the residual weld material on the inside of the Tight Fit Pipe.

3d. Analysing the residual liner pipe wrinkles in the test region after bending the Tight Fit Pipe on the 5.5 m reel

The residual liner pipe wrinkle height (a) determined from the laser measurements, the length between the valleys surrounding the top of the liner pipe wrinkle ($L_L/m_{pre\text{-}post}$) measured by the laser, the liner pipe wrinkle half wave length determined from the laser measurements ($L_L/m_{dr/dx}$) and the liner pipe wrinkle half wave length determined by hand (L_L/m) of all the liner pipe wrinkles in the test region of Tight Fit Pipe WT-1 bent on the 5.5 m radius reel are shown in Table 7.13. The residual liner pipe wrinkle half wave length ($L_L/m_{dr/dx}$) and the axial location of the liner pipe wrinkle top ($L_{axial;top}$), both determined from the laser measurements (Table 7.13) were compared with results measured by hand for verification purposes of the laser measurements and the method of analysing this data. The test data for the other Tight Fit Pipes can be found in Appendix IV.

Table 7.13 Details of the liner pipe wrinkles of Tight Fit Pipe WT-1

	a (laser) [mm]	$L_{axial;top}$ (laser) [mm]	$L_{axial;top}$ (hand) [mm]	$L_L/m_{dr/dx}$ (laser) [mm]	$L_L/m_{pre\text{-}post}$ (laser) [mm]	L_L/m (hand) [mm]	Location
W4	3.33	1217	1205	61	61	45	next to CZ
W5	10.02	1258	1253	100	181	80	CZ
W6	4.06	1337	1313	59	120	60	next to CZ
W7	9.77	1318	1308	79	219	70	next to CZ
W8	11.73	1477	1460	79	219	70	CZ
W9	8.12	1536	1516	59	220	60	next to CZ
W10	6.56	1536	1518	80	198	60	next to CZ
W11	4.94	1857	1833	81	160	60	next to CZ
W12	2.51	1857	1826	-	121	45	next to CZ
W13	13.90	1916	1894	101	182	80	CZ
W14	10.98	1996	1963	100	261	70	next to CZ
W15	10.56	1977	1954	81	140	60	next to CZ

For all Tight Fit Pipes, the height (*a*) of the largest residual liner pipe wrinkle in the test region measured by hand was compared with the height of this liner pipe wrinkle, measured by the laser trolley after bending the Tight Fit Pipes to the 5.5 m radius reel. This was done for verification purposes of the laser measurements and the method of analysing this data (Table 7.14). It should be noted that the Tight Fit Pipes GR-OR-1 and GR-OR-2 were scanned with a 10 mm interval measuring length. The liner pipe wrinkle height of the largest liner pipe wrinkle resulting from the 20 mm measuring interval has been calculated by leaving out every other 10 mm measurement. Leaving out every other measurement can be done in two ways: each first or second measurement can be left out. Leaving out the first 10 mm scan resulted in a liner pipe wrinkle height of 6.51 mm for Tight Fit Pipe GR-OR-1 and 7.33 mm for Tight Fit Pipe GR-OR-2 (Table 7.14). Leaving out the second 10 mm scan resulted in a liner pipe wrinkle height of 8.48 mm for Tight Fit Pipe GR-OR-1 and 10.09 mm for Tight Fit Pipe GR-OR-2 (Table 7.14).

Table 7.14 Largest residual liner pipe wrinkle height of Tight Fit Pipes

	OR-2	GR-1	GR-2	WT-1	WT-2	GR-OR-1	GR-OR-2
a (laser 20 mm (1)) [mm]	5.89	6.87	7.92	13.90	10.43	6.51	7.33
a (laser 20 mm (2)) [mm]						8.48	10.09
a (laser 10 mm) [mm]						8.48	9.81
a (hand) [mm]	8.75	8.85	10.1	18.3	13.25	10.40	12.80

The hand measurements were performed by making a plaster print of the liner pipe wrinkle (Figure 7.29, left) and measuring the liner pipe wrinkle depth (Figure 7.29, right). The Tight Fit Pipes were cut open to be able to do this.

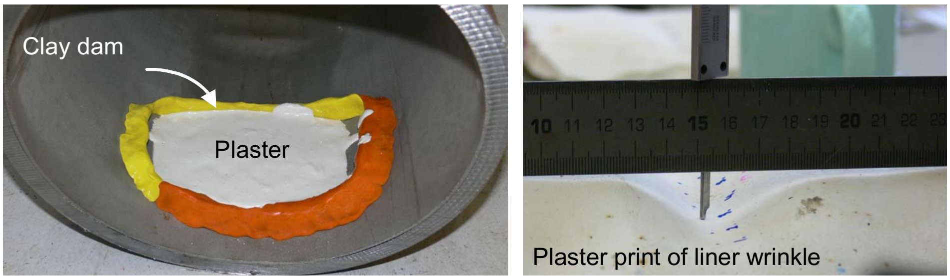

Figure 7.29 Plaster print of the liner pipe wrinkle (left) and measuring the liner pipe wrinkle height (right)

In the hand measurements, the liner pipe wrinkle height was assumed as the difference in the height between the top of the liner pipe wrinkle and the two valleys surrounding the top, printed in the plaster. It occurred most of the times that the valleys were located at the side of the plaster print. The actual valleys surrounding the top of the liner pipe wrinkle were usually not printed in the plaster. It should thus be taken into account that comparing the hand measurements with the data from the laser scan will result in differences. However, comparison of the liner pipe wrinkle height measured by hand with the laser trolley results provides a verification of the laser trolley data.

Hand measurements of the liner pipe wrinkle height correlated sufficiently with the laser trolley results (Table 7.14). It should be taken into consideration that a larger interval length of the laser trolley (20 mm instead of 10 mm) provided less accurate results for the liner pipe wrinkle height. The influence of the scanning density on the liner pipe wrinkle height and half wave length is discussed hereafter.

4. Scanning of the Tight Fit Pipe with a different scanning interval density

In order to investigate the influence of measuring the liner pipe wrinkles with different scanning interval lengths, a few buckles of the Tight Fit Pipe WT-2 were scanned into more detail at maximum bending strain and after bending, using a laser trolley measuring interval of 5 mm instead of 20 mm. Although a smaller scanning interval results in an increase in the threshold for *dr/dx*, the same threshold had to be used in the analysis because the Tight Fit Pipe was not scanned prior to bending using a 5 mm laser trolley interval (Table 7.11).

A scan with a smaller interval measuring length can result in either an increase or a decrease of the measured liner pipe wrinkle height. As an example, Figure 7.30 and Figure 7.31 are presented comparing the rough scanning measurements (20 mm measuring interval) with the detailed scanning measurements (5 mm measuring interval) for the liner pipe wrinkles W16 and W18 of Tight Fit Pipe WT-2, respectively. It occurred in the analysis of these wrinkles that the location of the prebottom and postbottom was found closer to the top indicating a less deep valley (Figure 7.31). This resulted in the intersection point to be closer to the top resulting in a lower value of the measured liner pipe wrinkle height (W18 of Tight Fit Pipe WT-2). However, it also occurred in the analysis that the more detailed scan found a higher top and deeper valleys (prebottom and postbottom) surrounding the top, resulting in finding a larger liner pipe wrinkle height (W16 of Tight Fit Pipe WT-2 in Figure 7.30). It should also be taken into account, that it was impossible for the laser to exactly duplicate the measurements. The fact that the laser scanned the inside of the Tight Fit Pipe at slightly different locations resulted in a different laser output and thus in a different liner pipe wrinkle height determination.

Calculations for several liner pipe wrinkles in Tight Fit Pipe WT-2 (at maximum bending and after bending) in Appendix IV show that when the measuring interval of the laser decreased from 20 mm to 5 mm for Tight Fit Pipe WT-2, the liner pipe wrinkle height can vary from -15% to +25 % with an average of +9 %.

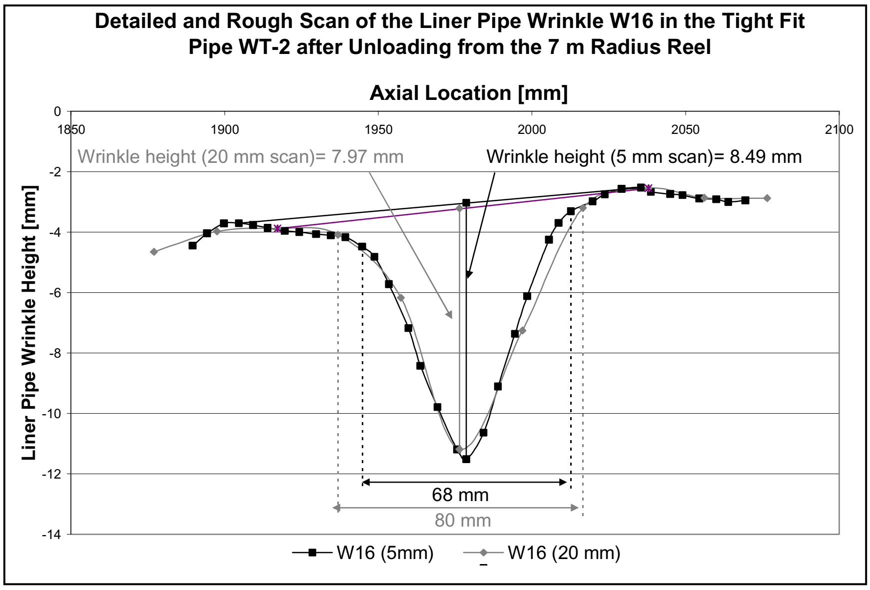

Figure 7.30 Comparison of a detailed (5 mm) and a rough (20 mm) scan of the residual liner pipe wrinkle W16 after unloading the Tight Fit Pipe WT-2 from a 7 m radius reel

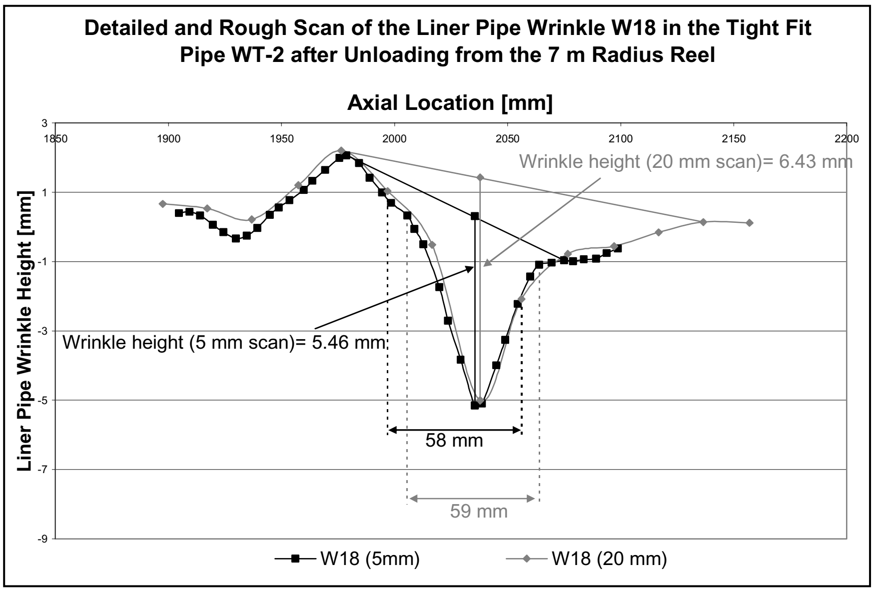

Figure 7.31 Comparison of a detailed (5 mm) and a rough (20 mm) scan of the residual liner pipe wrinkle W18 after unloading the Tight Fit Pipe WT-2 from a 7 m radius reel

Calculations for several liner pipe wrinkles in Tight Fit Pipe WT-2 (at maximum bending and after bending) in Appendix IV show that a scan with a smaller interval measuring length can result in either an increase or a decrease of the measured liner pipe wrinkle half wave length. This was the result of the (consequent) method of analysing the liner pipe wrinkles and the result of the fact that it was impossible for the laser to exactly duplicate its measurements. Calculations for several liner pipe wrinkles in Tight Fit Pipe WT-2 (at maximum bending and after bending), show that the half wave length of the liner pipe wrinkle varies from -26 % to +34 % with an average of -3 %, based on the same threshold for *dr*/*dx*.

5. Increase in liner pipe wrinkling with increase of the curvature

In order to determine at which curvature (i.e. reel radius) the liner pipe of the Tight Fit Pipe started wrinkling, it would be possible, as mentioned earlier, to use a certain value of the liner pipe wrinkle height as a threshold for liner pipe wrinkling initiation. The development of the liner pipe wrinkle height with increasing curvature needed to be monitored in order to be able to do this. In Figure 7.32 the residual liner pipe wrinkle height can be seen as a function of the Tight Fit Pipe curvature for Tight Fit Pipe WT-1. It can be seen how the initial liner pipe imperfections (measured by the laser prior to bending) develop into liner pipe wrinkles with a certain liner pipe wrinkle height. This procedure has been performed for the four largest liner pipe wrinkles in the test region of the Tight Fit Pipe.

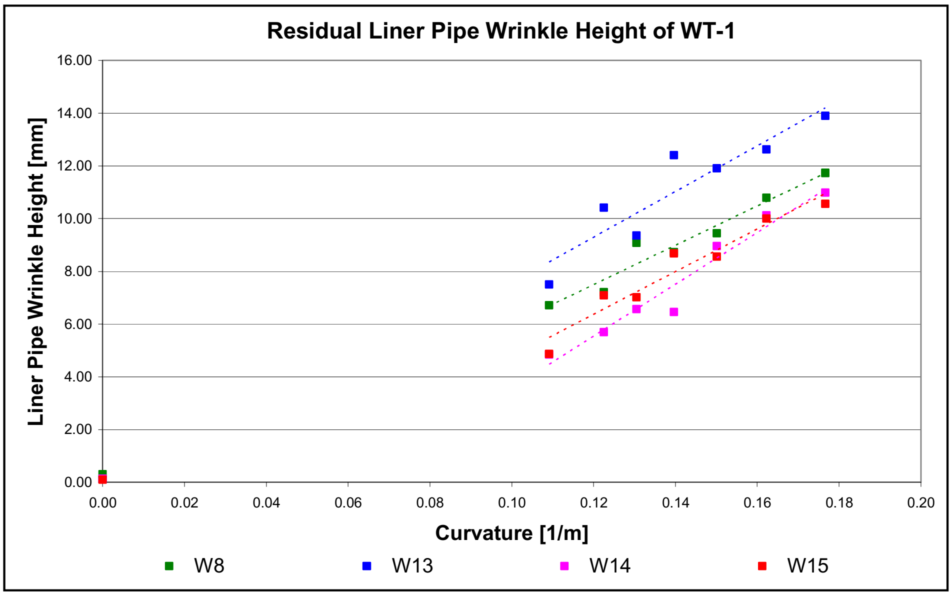

Figure 7.32 Residual liner pipe wrinkle height as a function of the applied curvature for Tight Fit Pipe WT-1

The height of the initial imperfection was determined in exactly the same manner as the liner pipe wrinkle height (*a*) was determined in the analysis of liner pipe wrinkling. The average height of the initial imperfections at the locations where the four largest liner pipe wrinkles occurred can be found in Table 7.15 for all Tight Fit Pipes. The average lengths between the adjacent valleys (prebottom and postbottom) of the initial imperfections ($L_L/m_{pre\text{-}post}$) at these locations are also provided in Table 7.15.

Table 7.15 Initial imperfections of the Tight Fit Pipes measured by the laser trolley

	OR-2	GR-1	GR-2	WT-1	WT-2	GR-OR-1	GR-OR-2
a [mm]	0.15	0.25	0.25	0.20	0.21	0.14	0.28
$L_L/m_{pre\text{-}post}$ [mm]	66	60	72	80	84	38	53

Note:
Tight Fit Pipes GR-OR-1 and GR-OR-2 were scanned with a 10 mm interval measuring length. The other Tight Fit Pipes were scanned with a 20 mm interval measuring length.

6. Liner pipe wrinkling at maximum bending

The liner pipe wrinkles had on average a higher liner pipe wrinkle height and a larger liner pipe wrinkle half wave length at maximum bending (i.e. when the Tight Fit Pipe was in contact wit the reel) than after unloading. These measurements also supported the observation in the liner pipe wrinkling analysis that liner pipe wrinkles with a larger wrinkle height usually also had a larger liner pipe wrinkle half wave length (Figure 7.27), taking into account that these liner pipe wrinkle half wave lengths were based on the *dr*/*dx* threshold.

7.3.4.4 Discussion of the Test Results

As pointed out earlier, there is an option to use the liner pipe wrinkle height as a measure for the liner pipe wrinkle initiation. Based on the liner pipe wrinkle height, several observations can be made in regard to the influence on liner pipe wrinkling of:

1. the mechanical bonding strength
2. the electric resistance welded longitudinal outer pipe weld
3. the presence of the Tight Fit Pipe circumferential weld
4. stepwise bending versus continuous bending

1. Mechanical bonding strength

As can be seen in Figure 7.33, Tight Fit Pipes without a Tight Fit Pipe circumferential weld and a higher mechanical bonding strength show a decrease in the residual liner pipe wrinkle height of the largest wrinkle. It should be observed that the height of the residual liner pipe wrinkles in a Tight Fit Pipe with a high mechanical bonding strength and no Tight Fit Pipe circumferential weld (OR-2, GR-1 and GR-2) are more exponentially dependent on the tested curvatures while the residual liner pipe wrinkles in a Tight Fit Pipe with a low mechanical bonding strength and no Tight Fit Pipe circumferential weld (WT-1 and WT-2) are more linearly dependent on the tested curvatures.

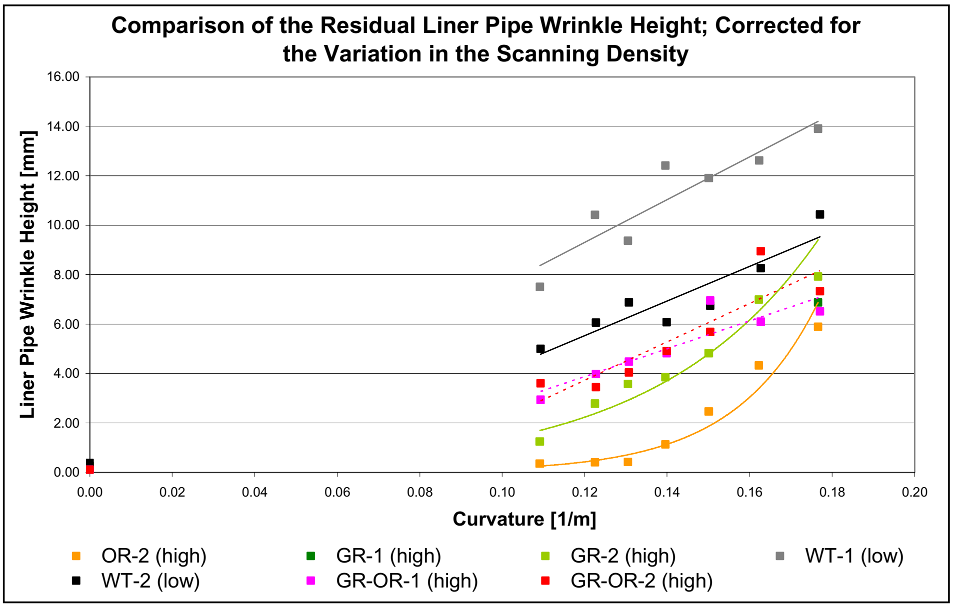

Figure 7.33 Comparison of the residual liner pipe wrinkle height in the various Tight Fit Pipes at different curvatures; wrinkle height corrected for scanning density

An increase in the mechanical bonding strength also results in a smaller number of liner pipe wrinkles with a different distribution over the Tight Fit Pipe inner surface (Tight Fit Pipes without a Tight Fit Pipe circumferential weld; Figure 7.34).

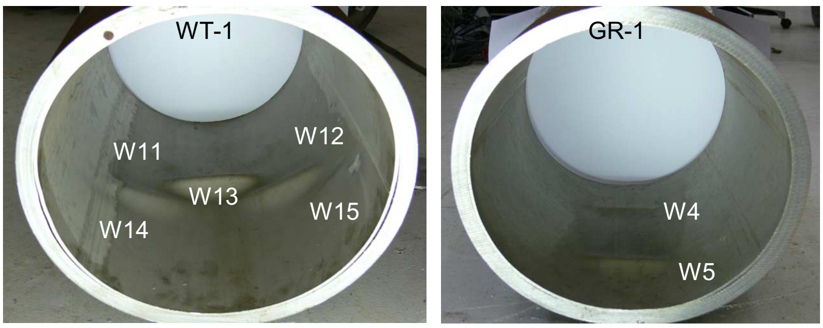

Figure 7.34 Liner pipe wrinkles in the Tight Fit Pipes with a low (left) and a high (right) mechanical bonding strength (no Tight Fit Pipe circumferential weld)

When the mechanical bonding strength was low, residual liner pipe wrinkles were located in groups: liner pipe wrinkles (W11, W12, W14 and W15 in Figure 7.34) were located around one very large liner pipe wrinkle (W13 in Figure 7.34) in the compression zone. Liner pipe wrinkles W11, W12, W14 and W15 were located more towards the neutral axis next to the compression zone. If the mechanical bonding strength was high, liner pipe wrinkling occurred only in the compression zone (W4 and W5 in Figure 7.34). However, for the highly bonded Tight Fit Pipes, the initiation of the liner pipe wrinkles to the side of the compression zone was already slightly visible during the bending tests.

This decrease in liner pipe wrinkling with a higher mechanical bonding strength (i.e. a higher radial contact stress between the liner pipe and the outer pipe) can be explained by the fact that the higher radial contact stress between the liner pipe and the outer pipe indicates a higher axial friction between the liner pipe and the outer pipe. This higher axial friction avoids liner pipe material "feeding in" to the liner pipe wrinkle. At a certain curvature, this results in less liner pipe wrinkling for Tight Fit Pipes with a high mechanical bonding strength than for Tight Fit Pipes with a lower mechanical bonding strength.

2. The electric resistance welded longitudinal outer pipe weld

It can be seen in Figure 7.33 that the electric resistance welded longitudinal outer pipe weld did not cause higher liner pipe wrinkles at the curvatures tested. This may be explained by the fact that this weld is continuous along the length of the Tight Fit Pipe and did not function as a local imperfection.

3. The presence of the Tight Fit Pipe circumferential weld

When comparing the Tight Fit Pipes with a Tight Fit Pipe circumferential weld (GR-OR-1 and GR-OR-2) with the Tight Fit Pipes without a Tight Fit Pipe circumferential weld (OR-2, GR-1 and GR-2) it has to be taken into account that the scans for GR-OR-1 and GR-OR-2 were performed with a smaller scanning interval (10 mm interval length) than the scans for Tight Fit Pipes OR-2, GR-1 and GR-2 (20 mm interval length). The scanning density of the laser trolley may influence the measurements of the liner pipe wrinkle height (*a*). As explained earlier, an increase in the scanning measuring length from 10 mm to 20 mm can result in a decrease or an increase of the liner pipe wrinkle height, depending on which 10 mm scan is left out of the analysis (Table 7.16).

Table 7.16 Influence of the laser scanning density on the liner pipe wrinkle height

	Interval length [mm]	$L_{axial;top}$ [mm]	*a* [mm]
W6 (GR-OR-1)	10 mm	1820	8.48
W6 (GR-OR-1)-1	20 mm	1830	6.51
W6 (GR-OR-1)-2	20 mm	1820	8.48
W6 (GR-OR-2)	10 mm	1910	9.81
W6 (GR-OR-1)-1	20 mm	1900	7.33
W6 (GR-OR-2)-2	20 mm	1910	10.09

Figure 7.33 shows that the presence of a Tight Fit Pipe circumferential weld in the highly bonded Tight Fit Pipes resulted in higher liner pipe wrinkles at the lower curvatures tested than when no Tight Fit Pipe circumferential weld was present: the residual liner pipe wrinkle height of W5 in GR-2 after testing on the 9 m radius reel was 1.25 mm and of W6 in GR-OR-1 was 2.93 mm or 3.09 mm (values compensated for the interval measuring length). The residual liner pipe wrinkle height of W5 in GR-2 after testing on the 5.5 m radius reel was 7.92 mm and of W6 in GR-OR-1 was 6.51 mm or 8.48 mm.

The liner pipe wrinkling behaviour of the highly bonded Tight Fit Pipes with a Tight Fit Pipe circumferential weld depends more linearly on the curvature than when no Tight Fit Pipe circumferential weld is present in the highly bonded Tight Fit Pipes: these Tight Fit Pipes show an exponential dependence on the increasing curvature. Moreover, the liner pipe wrinkles of the highly bonded Tight Fit Pipes with a Tight Fit Pipe circumferential weld were located in as well as next to the compression zone. Poorly bonded Tight Fit Pipes without a Tight Fit Pipe circumferential weld show a same distribution. In other words, the behaviour of the highly bonded Tight Fit Pipes with a Tight Fit Pipe circumferential weld resembled more the behaviour of the less bonded Tight Fit Pipes without a Tight Fit Pipe circumferential weld at the same curvatures tested.

The occurrence of higher liner pipe wrinkles at lower curvature for highly bonded Tight Fit Pipes with a Tight Fit Pipe circumferential weld may be explained by the fact that the presence of the weld resulted in a less even distribution of the contact stress between the reel and the Tight Fit Pipe during bending. This was the result of the fact that the Tight Fit Pipe was in contact with the reel at the location of weld cap and some distance further along the reel. The locally higher contact forces there where the Tight Fit Pipe came in contact with the reel again further along the reel from the weld cap resulted in small indentations in the pipe wall that triggered the initiation of the wrinkles (tests GR-OR-1 and GR-OR-2).

4. Stepwise bending versus continuous bending

Comparing wrinkle height of the largest liner pipe wrinkle for GR-1, bending in one go, and GR-2, step by step bending, (the largest: 7.92 mm versus 6.87 mm, respectively) indicates that stepwise bending does not result in unacceptable higher liner pipe wrinkles (Figure 7.33). Since there was also no unacceptable difference in ovalisation between Tight Fit Pipes GR-1 and GR-2 (8 %), the test method of step by step bending to find the initiation of liner pipe wrinkling can be concluded to be an acceptable testing procedure.

7.4 Equations to Predict the Liner Pipe Wrinkle Height as a Result of Spooling-on

This research indicates that the residual liner pipe wrinkle height (a) as a result of spooling-on depends on the applied curvature, the mechanical bonding strength and the diameter to thickness ratios of the liner pipe and the outer pipe (Equation (7.10)). In order to reduce liner pipe wrinkling during spooling on, the mechanical bonding strength should be as high as possible. Further measures to reduce liner pipe wrinkling are decreasing the applied curvature (increase the reel radius) and decreasing the diameter to thickness ratio of the liner pipe. Decreasing the diameter to thickness ratio of the outer pipe will result in a lower ovalisation and thereby also have a beneficial effect on liner pipe wrinkling. Further research may indicate dependence of the liner pipe wrinkle height on more parameters than those mentioned in Equation (7.10).

$$a = f(\kappa), f(\sigma_{res}), f\left(d_{L;o;TFP}/t_L\right), f\left(d_{O;o;TFP}/t_O\right) \tag{7.10}$$

In order to predict the residual liner pipe wrinkling height as a result of spooling-on to reel sizes between 5.5 m and 9 m, of a 12.75 inch Tight Fit Pipe (3 mm 316L liner pipe and a 14.3 mm X65 outer pipe) without a Tight Fit Pipe circumferential weld, with a residual liner pipe hoop stress varying between 53 MPa (low) and 189 MPa (high), Equation (7.11) can be used. In Equation (7.11) only $f(\kappa)$ and $f(\sigma_{res})$ are addressed. $f(d_{L;o;TFP}/t_L)$ and $f(d_{O;o;TFP}/t_O)$ could not be addressed because only one value for $d_{L;o;TFP}/t_L$ and $d_{O;o;TFP}/t_O$ was tested. Equation (7.11) is based on the best fit of the test results (Figure 7.35).

$$a=\left(\left[74.898\cdot\kappa-1.7459\right]-\left[0.0127\cdot e^{34.402\cdot\kappa}\right]\right)\cdot\left(\frac{189-\sigma_{res}}{189-53}\right)+\left[0.0127\cdot e^{34.402\cdot\kappa}\right] \tag{7.11}$$

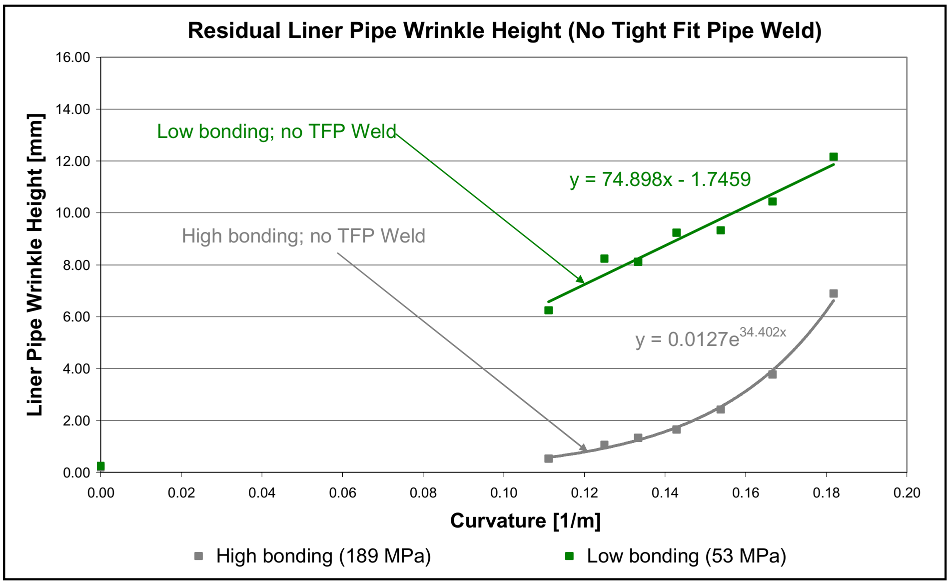

Figure 7.35 Liner pipe wrinkle height with increasing curvature; without a Tight Fit Pipe (TFP) circumferential weld; with a low and a high mechanical bonding strength

In order to predict the residual liner pipe wrinkling height as a result of spooling-on to reel sizes between 5.5 m and 9 m, of a 12.75 inch Tight Fit Pipe (3 mm 316L liner pipe and a 14.3 mm X65 outer pipe) with a Tight Fit Pipe circumferential weld, with a residual liner pipe hoop stress of 189 MPa (high), Equation (7.12) can be used. In Equation (7.12) only $f(\kappa)$ is addressed. $f(\sigma_{res})$, $f(d_{L;o}/t_L)$ and $f(d_{O;o}/t_O)$ could not be addressed because only one value for σ_{res}, $d_{L;o;TFP}/t_L$ and $d_{O;o;TFP}/t_O$ was tested. Equation (7.12) is based on the best fit of the test results (Figure 7.36).

$$a = 72.755 \cdot \kappa + 4.9471 \tag{7.12}$$

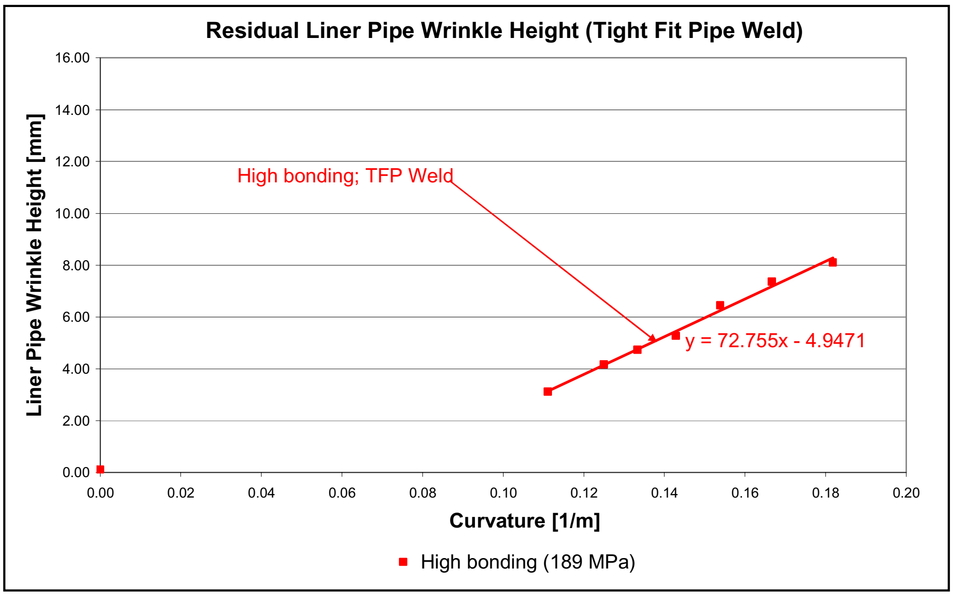

Figure 7.36 Liner pipe wrinkle height with increasing curvature; with a Tight Fit Pipe (TFP) circumferential weld; with a high mechanical bonding strength

7.5 Mechanical Bonding Strength in a Tight Fit Pipe after Spooling-on

In order to investigate the influence of spooling-on of Tight Fit Pipe on the mechanical bonding strength between the liner pipe and the outer pipe, the residual compressive stress test (described in Chapter 3.4.2) was performed on rings, cut from the Tight Fit Pipes WT-1 and GR-2, after these test pipes were bend tested and unloaded in the bending rig. Three rings of approximately 100 mm were cut from each Tight Fit Pipe, two rings at a location where no liner pipe wrinkling had occurred although the Tight Fit Pipe was plastically deformed (WT-A, WT-B, GR-A and GR-B) and one where a liner pipe wrinkle had occurred (WT-C and GR-C). In Figure 7.37 the locations of the test specimens are shown.

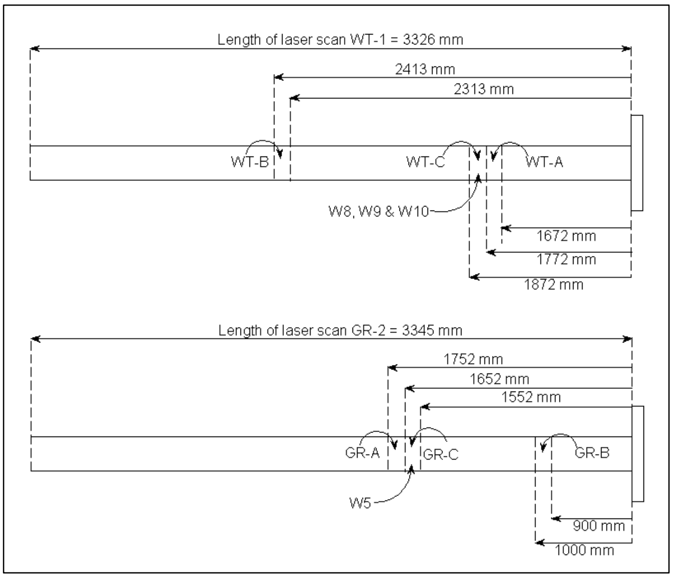

Figure 7.37 Locations of the Tight Fit Pipe test specimens used in the residual compressive stress tests performed after unloading

Figure 7.38 indicates the locations of the strain gauges that were attached to the inside of the specimens (WT-A, WT-B, WT-C, GR-A, GR-B and GR-C) [1].

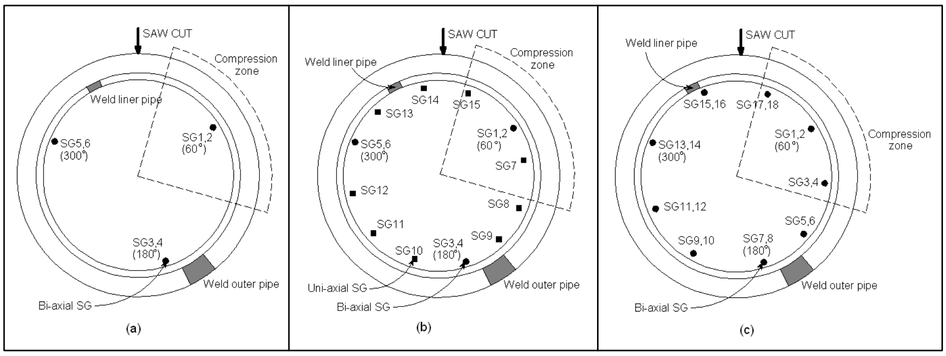

Figure 7.38 Locations of the strain gauges (a) for WT-A, WT-B and GR-A, (b) for GR-B and (c) for WT-C and GR-C (SG = strain gauge)

The locations of the strain gauges in the compression zone can be seen for the wrinkled Tight Fit Pipe specimens WT-C and GR-C in Figure 7.39. The bi-axial strain gauge SG17,18 was located just next to liner pipe wrinkle W10 in the test, SG1,2 was located in between W8, W9 and W10 while SG3,4 was located on top of the liner pipe wrinkle. For the Tight Fit Pipe specimen GR-C the bi-axial strain gauge SG1,2 was located on top of the liner pipe wrinkle W5.

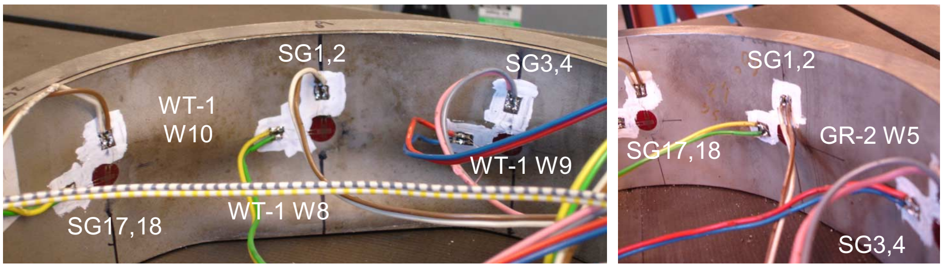

Figure 7.39 Locations of the strain gauges (SG) for WT-C (left) and GR-C (right)

The test results (Figure 7.40 and Figure 7.41) indicated that the measured residual hoop and axial strains in the liner pipe were small and differed in the circumference for the Tight Fit Pipes.

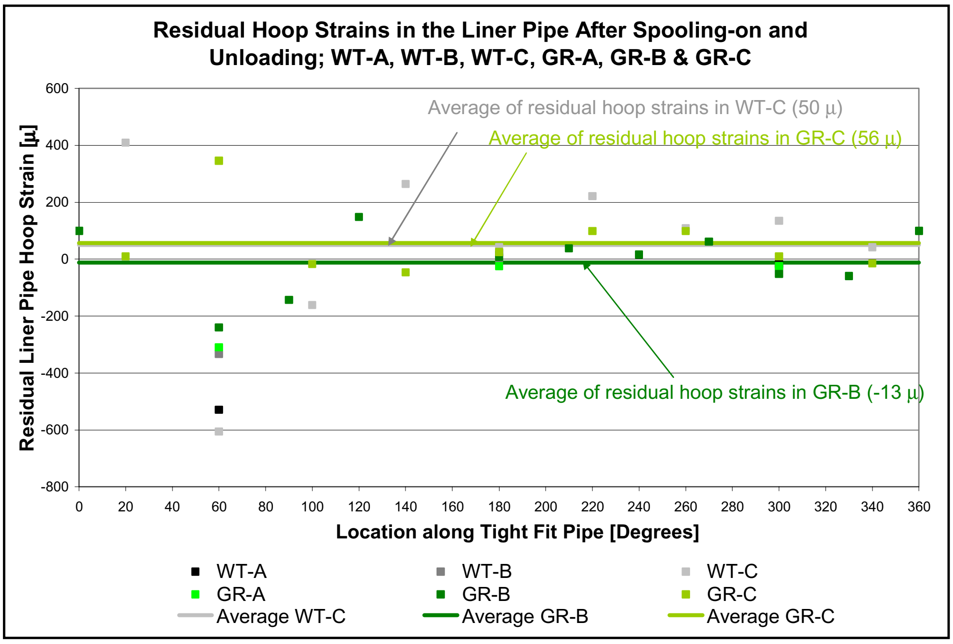

Figure 7.40 Hoop strains in the liner pipe, measured in the residual compressive stress test, performed after unloading the Tight Fit Pipe in the bending tests

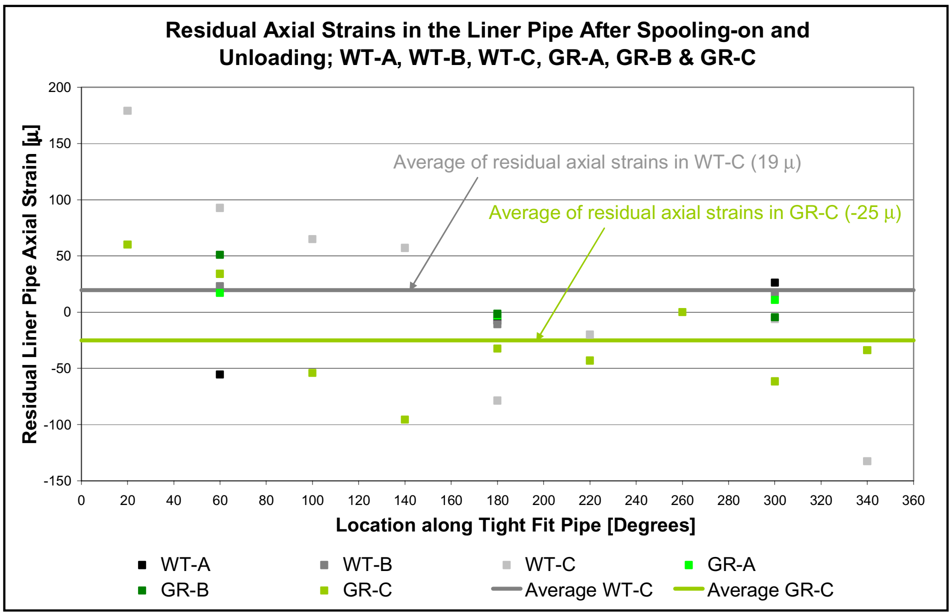

Figure 7.41 Axial strains in the liner pipe, measured in the residual compressive stress test, performed after unloading the Tight Fit Pipe in the bending tests

The variation in the measured strains could be attributed to changes in the ovalisation between the situation where the strain gauges were attached to the liner pipe still inside the outer pipe and after saw cutting the outer pipe. Test results indicated as well that in the Tight Fit Pipes, initially either with a high or a low mechanical bonding strength, negligible average residual hoop and axial strains in the liner pipe remained after spooling-on and unloading. This means that in the Tight Fit Pipes tested in this research, initially with either a high or a low mechanical bonding strength, a negligible average residual mechanical bonding strength remained after spooling-on and unloading.

The decrease of the mechanical bonding strength can be explained with the normality principle used in plastic theory [23]. After manufacturing Tight Fit Pipe, a radial contact stress σ_C (i.e. the mechanical bonding strength) is present (point A in Figure 7.42). Then, the Tight Fit Pipe is bent during spooling-on and the bending moment (M) is increased until the yield surface is reached (point B). Further increases of the deformations have to obey the normality principle (the deformation vector at the yield surface). At point B this means a decrease of the diameter $\Delta d_{L;a;TFP}$ and an increase of the curvature κ. This means that the deformation vector at point B is not correct. The yield point gradually moves from point B via point C to point D in order to obey the normality principle. In point D the contact pressure σ_C is decreased to zero. In other words, the structure offers maximum resistance in the direction of deformation. In other directions where no deformation is applied, it does not need to maintain stresses. Note: Figure 7.42 only provides an impression of the yield surface and the normality principle; the yield surface shown in Figure 7.42 is not supported by specific equations yet.

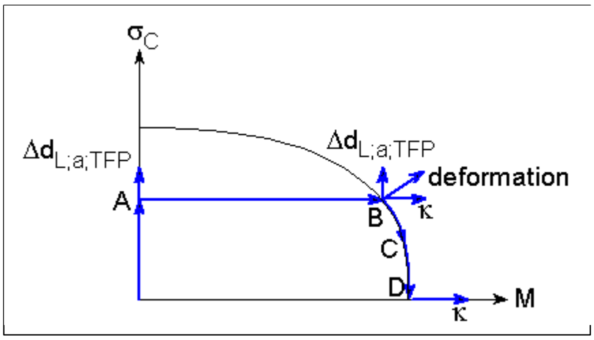

Figure 7.42 Impression of the yield surface for the load case of a bending moment and a contact pressure

These initial findings justify further research into the phenomena as it may be vital for its anticipated application during operation.

7.6 Conclusions

Seven full scale bending tests, in which the pipe was bent on increasingly smaller reels, were executed on 12.75 inch outer diameter Tight Fit Pipe. Results of these tests indicated that:

1. the developed theoretical model describing the forces on the 12.75 inch Tight Fit Pipe by the full scale bending rig matched the test results well.
2. the DNV OS F101 prediction for ovalisation, assuming the liner pipe and the outer pipe wall thicknesses “added”, representing one single wall thickness in this prediction, resulted in an underestimate of the measured ovalisation. This underestimate is attributed to the fact that this prediction is intended for bending only, while in the tests also a reaction force of the reel on the Tight Fit Pipe enhanced ovalisation.
3. no local buckling of the 12.75 inch integral Tight Fit Pipe was encountered during testing, although it was predicted to occur by equations by Murphy and Langer and Gresnigt, assuming the liner pipe and the outer pipe wall thicknesses “added”, representing one single wall thickness in these predictions. The underestimate of the critical buckling strain may be the result of the equations’ underestimation of the critical buckling strain at this Tight Fit Pipe’s low diameter to thickness ratio of 22 and the fact that these equations are design formulae. It is noted that it might not be allowed to use the liner pipe and the outer pipe wall

thicknesses to function as one in these predictions, because prior to local buckling of the integral Tight Fit Pipe liner pipe wrinkling may occur, resulting in the liner pipe and the outer pipe not functioning as one anymore.

4. liner pipe wrinkling was observed during the testing.
5. the extent of the liner pipe wrinkling decreased if Tight Fit Pipe with a high mechanical bonding strength between the liner pipe and the outer pipe in the Tight Fit Pipe was used. This can be explained by the fact the higher radial contact stress between the liner pipe and the outer pipe results in a higher axial friction between the liner pipe and the outer pipe. This higher axial friction avoids liner pipe material “feeding in” to the liner pipe wrinkle.
6. the presence of a Tight Fit Pipe circumferential weld in the highly bonded Tight Fit Pipes caused higher liner pipe wrinkles at the lower curvatures tested. This may be the consequence of the weld resulting in a less even distribution of the contact stress between the reel and the Tight Fit Pipe during bending. Locally higher contact forces resulted in small indentations in the pipe wall that triggered the initiation of the liner pipe wrinkles.
7. the electric resistance welded longitudinal outer pipe weld did not cause higher liner pipe wrinkles at the curvatures tested. This may be explained by the fact that this weld is continuous along the length of the Tight Fit Pipe and did not function as a local imperfection.
8. there was no unacceptable difference in liner pipe wrinkling and ovalisation between a Tight Fit Pipe bent stepwise on a 5.5 m radius reel and a Tight Fit Pipe which was bent in one go on the 5.5 m radius reel. This proved that the test method of step by step increasing the curvature of the pipe while bending it on a curved former (simulating the reel) in order to find the initiation of liner pipe wrinkling, was confirmed.

API residual compressive stress tests showed that the initial mechanical bonding strength in the 12.75 inch Tight Fit Pipe bend tested in this research was significantly reduced, irrespective of whether a high or a low initial mechanical bonding strength had been used prior to spooling-on. This decrease of the mechanical bonding strength can be explained with the normality principle used in plastic theory. These findings justify further research into this phenomenon as the eventual mechanical bonding strength after reeling installation may be vital for its anticipated application during operation.

8 Conclusions and Recommendations

8.1 Conclusions

Axial compression tests on 10.75 and 12.75 inch outer diameter Tight Fit Pipe

1. Results of the axial compression tests indicated that the liner pipe buckling capacity was significantly increased by the support of the outer pipe (compared to buckling of the liner pipe only).
2. Results of the axial compression tests indicated that an increase in the mechanical bonding strength between the liner pipe and the outer pipe in the Tight Fit Pipe increased the buckling strength of the liner pipe.

Small scale reeling simulation of 22 mm outer diameter single walled pipe

3. The developed theoretical model describing the forces on the pipe by the small scale bending rig proved to be acceptable and could be used in the design of the full scale bending rig.
4. The eventual full scale bending rig had the same test set-up as the small scale bending rig at the end of the small scale reeling simulation testing: the pipe was axially and laterally fixed on one side while a hydraulic cylinder pulled the pipe against different reel sizes in order to study the initiation and the degree of local buckling as well as the degree of ovalisation of the pipe with increasing curvature.
5. Small scale bending test experience was useful in the preparation and the execution of the full scale bending tests.
6. Although ovalisation was difficult to measure due to the small size of the pipe, the ovality of the pipes measured after the bending tests approached the DNV Offshore Standard OS-F101 prediction for ovalisation at maximum bending strain.
7. The buckling strain of the pipe in the bending tests compared well with the predictions from Murphy and Langer and Gresnigt. However, it should be realised that these predictions underestimate the buckling strain for pipes with a low diameter to thickness ratio (lower than 40). The diameter to thickness ratio of the pipe tested in the small scale bending rig was 17. On the other hand the predictions are intended for bending only, while in the tests also a reaction force of the reel on the pipe contributed to the occurrence of local buckling. Both phenomena compensated each other resulting in the predictions to compare well with the buckling strains in the bending tests.

Full scale reeling simulation of 12.75 inch outer diameter single walled pipe

8. The developed theoretical model describing the forces on the 12.75 inch single walled pipe by the full scale bending rig matched the test results well.
9. The ovality of the 12.75 inch single walled pipe at maximum bending strain as predicted by the DNV Offshore Standard OS-F101 underestimated most values

for the ovalisation at maximum bending as measured in the bending test. This can be explained by the fact that this prediction is intended for bending only, while in the tests also a reaction force of the reel on the pipe enhanced ovalisation.

10. Pipe ovalisation measured in the bending test was compared to predictions for ovalisation resulting from the combination of bending and a concentrated transverse load. These predictions were shown to be sensitive to the value of the reaction force of the reel on the pipe used in these equations. It should be taken into account that in these equations the reaction of the reel on the pipe was applied as a concentrated load while in fact it is a distributed load resulting in a conservative approach to calculate the ovalisation.
11. Predictions of the critical buckling strain by Murphy and Langer, Gresnigt and the DNV OS F101 code exceeded the global buckling strain determined in the testing from the reel radius and the pipe outer diameter. The local curvature and the local bending strain were in fact larger than the global bending strain because of the extra bending in the weaker pipe in which the buckle developed (the test piece bend tested consisted of a pipe with a higher bending moment capacity (stronger pipe) and a pipe with a lower bending moment capacity (weaker pipe), connected by a weld). Furthermore, the depth of the local deformation was still rather small and it can be questioned whether this should be defined as local buckling.
12. Although some adaptations were made to the full scale bending rig and to the measuring equipment, the fitness for purpose of the rig for performing full scale bending tests on 12.75 inch outer diameter Tight Fit Pipe was proven.

Full scale reeling simulation of 12.75 inch Tight Fit Pipe

13. The developed theoretical model describing the forces on the 12.75 inch Tight Fit Pipe by the full scale bending rig matched the test results well.
14. The DNV OS F101 prediction for ovalisation, assuming the liner pipe and the outer pipe wall thicknesses “added”, representing one single wall thickness in this prediction, resulted in an underestimate of the measured ovalisation. This underestimate is attributed to the fact that this prediction is intended for bending only, while in the tests also a reaction force of the reel on the Tight Fit Pipe enhanced ovalisation.
15. No local buckling of the 12.75 inch integral Tight Fit Pipe was encountered during testing, although it was predicted to occur by equations by Murphy and Langer and Gresnigt, assuming the liner pipe and the outer pipe wall thicknesses “added”, representing one single wall thickness in these predictions. The underestimate of the critical buckling strain may be the result of the equations’ underestimation of the critical buckling strain at this Tight Fit Pipe’s low diameter to thickness ratio of 22 and the fact that these equations are design formulae. It is noted that it might not be allowed to use the liner pipe and the outer pipe wall thicknesses to function as one in these predictions, because prior to local buckling of the integral Tight Fit Pipe liner pipe wrinkling may occur, resulting in the liner pipe and the outer pipe not to function as one anymore.
16. Liner pipe wrinkling was observed during the testing.

17. In the testing, the extent of the liner pipe wrinkling decreased if Tight Fit Pipe with a high mechanical bonding strength between the liner pipe and the outer pipe in the Tight Fit Pipe was used. This can be explained by the fact the higher radial contact stress between the liner pipe and the outer pipe results in a higher axial friction between the liner pipe and the outer pipe. This higher axial friction avoids liner pipe material “feeding in” to the liner pipe wrinkle.
18. In the testing, the presence of a Tight Fit Pipe circumferential weld in the highly bonded Tight Fit Pipes caused higher liner pipe wrinkles at the lower curvatures tested. This may be the consequence of the weld resulting in a less even distribution of the contact stress between the reel and the Tight Fit Pipe during bending. Locally higher contact forces resulted in small indentations in the pipe wall that triggered the initiation of the liner pipe wrinkles.
19. In the testing, the electric resistance welded longitudinal outer pipe weld did not cause higher liner pipe wrinkles at the curvatures tested. This may be explained by the fact that this weld is continuous along the length of the Tight Fit Pipe and did not function as a local imperfection.
20. The fact that there was no unacceptable difference in liner pipe wrinkling and ovalisation between a Tight Fit Pipe bent stepwise on a 5.5 m radius reel and a Tight Fit Pipe which was bent in one go on the 5.5 m radius reel, proved that the test method of step by step increasing the curvature of the pipe while bending it to a reel in order to find the initiation of liner pipe wrinkling, was confirmed.
21. In order to make it technically possible to install Tight Fit Pipe by means of reeling it is necessary, besides adhering to other requirements (e.g. the integrity of the Tight Fit Pipe circumferential weld), to minimise liner pipe wrinkling and ovalisation during the reeling process. Reducing the bending curvature or decreasing of the diameter to thickness ratio of the Tight Fit Pipe by either increasing the liner pipe or the outer pipe wall thickness, will result in a decrease of ovalisation of the Tight Fit Pipe. It is expected that liner pipe wrinkling will be reduced if the ovalisation of the Tight Fit Pipe is reduced, since ovalisation contributes to the extent of liner pipe wrinkling. The full scale bending tests also revealed that an increase in the mechanical bonding strength reduces liner pipe wrinkling and therefore increases the suitability of Tight Fit Pipe for reeling installation.

Manufacturing process of Tight Fit Pipe

22. A sensitivity analysis of the manufacturing process was performed using a two dimensional analytical model and a three dimensional, one layer thick, finite element model of the manufacturing process of Tight Fit Pipe.
23. This sensitivity analysis showed that the most efficient way to increase the mechanical bonding strength of a Tight Fit Pipe thereby minimising liner pipe wrinkling occurring during reeling, is to increase the liner pipe material strength and to minimise the contact time between the liner pipe and the outer pipe during the manufacturing process.

Mechanical bonding strength in the 12.75 inch Tight Fit Pipe after spooling-on

24. API residual compressive stress tests showed that the initial mechanical bonding strength in the 12.75 inch Tight Fit Pipe bend tested in this research was significantly reduced, irrespective of whether a high or a low initial mechanical bonding strength had been used prior to spooling-on.
25. This decrease of the mechanical bonding strength can be explained with the normality principle used in plastic theory.

8.2 Recommendations

Finite element modelling simulating the spooling-on process of Tight Fit Pipe

1. Now that the influence of the parameters such as the bending strain and the mechanical bonding strength between the liner pipe and the outer pipe in a Tight Fit Pipe on liner pipe wrinkling during the spooling-on phase of the reeling process has been investigated experimentally, it is recommended to develop a finite element model to simulate the observed behaviour. Then, after validation of the finite element model, parameter studies can be performed to quantify the influence of the various parameters on liner pipe wrinkling.
2. More experiments need to be performed to verify the finite element model of the spooling-on process regarding other parameters not tested in this research (e.g. the diameter to thickness ratio of the liner pipe).

Loss of the mechanical bonding strength between the liner pipe and the outer pipe in the Tight Fit Pipe

3. The significant reduction of the mechanical bonding strength as a consequence of spooling-on needs to be verified in a finite element model of the spooling-on process described above.
4. The influence of the significant reduction of the mechanical bonding strength as a consequence of reeling needs to be investigated for its anticipated use during operation.

Acceptable liner pipe wrinkling height

5. There is currently no agreement on the definition of liner pipe wrinkling and liner pipe wrinkling initiation due to the fact that it is currently unknown how liner pipe wrinkling is related to the possible reduction of the fatigue life or to the obstruction of a pig passing through the pipe. This needs to be investigated in order to define acceptance criteria for liner pipe wrinkling as a result of reeling installation.

Finite element modelling simulating the entire reeling process of Tight Fit Pipe

6. It is advised to simulate the entire reeling process of Tight Fit Pipe in a finite element model using a pipe that will show minimal liner pipe wrinkling and acceptable ovalisation.

7. By simulating the entire reeling process using the 12.75 inch Tight Fit Pipe from this research, the influence of pulling the pipeline straight between the reel and the aligner, the influence of aligning and the influence of straightening on the size of the liner pipe wrinkles (e.g. the wrinkle height) created during the spooling-on phase, can be investigated; it is expected that also experiments are needed to validate these finite element calculations.

Manufacturing process of Tight Fit Pipe

8. To verify theoretical assumptions in the two dimensional analytical model and in the three dimensional, one layer thick, finite element model of the manufacturing process of Tight Fit Pipe, it is recommended to experimentally investigate the influence of the contact time of the cooled liner pipe with the hot outer pipe during the manufacturing process using two identical Tight Fit Pipes, in one test case using a long contact time and in another test case using a short duration of the contact time. The temperature of the liner pipe should be monitored throughout the manufacturing process.
9. By developing a Tight Fit Pipe (with a diameter to thickness ratio of approximately 15) with e.g. a duplex liner pipe and a 316L liner pipe, the theoretical prediction that a liner pipe with a higher strength will result in a higher mechanical bonding strength and thus in less liner pipe wrinkling, can be verified.

Influence of a concentrated load on liner pipe wrinkling

10. Since results of the Tight Fit Pipe bending tests have shown that during reeling concentrated loads may result in liner pipe wrinkling, further investigation into this phenomenon is necessary. Parameters of influence on this phenomenon (e.g. the wall thickness of the Tight Fit Pipe or the mechanical bonding strength), need to be quantified.

Analytical models

11. In conjunction with the finite element calculations described above and the experimental research performed, analytical models should be developed to enhance the understanding of the behaviour of the Tight Fit Pipe and to form a basis for the development of design recommendations.

References

[1] **API** (1998) *Specification for CRA Clad or Lined Steel Pipe API Specification 5LD* American Petroleum Institute, 2nd Edition

[2] **API** (1999) *RP 1111 Design, Construction, Operation and Maintenance of Offshore Hydrocarbon Pipelines - Limit State Design* American Petroleum Institute, 3rd Edition

[3] **API** (2004) *Specification Line Pipe API Specification 5L* American Petroleum Institute, 43rd Edition

[4] **Batterman, S.C.** (1972) *Plastic Buckling of the Axially Compressed Cylindrical Shells* AIAA Journal 1965 Vol. 3 (2): 316-325 and Vol. 3 (9)

[5] **Brown, G., Thomson, P. and Fryer, M.** (2004) *World's First 18 inch Reeled Pipe Installation* Pipeline Technology Conference

[6] **Chaudhury, G.** (2004) *Reeling of Pipes with Thick Insulation, A Simple New Calculation Procedure* Proceedings of the Offshore Technology Conference, OTC 16111

[7] **Clarkson Research Services** (2006) *Construction Vessels of the World* ISBN 1-902157-70-2, Eighth Edition

[8] **Craig, B.D.** (1992), *The Economics of the Application of CRA Clad Steel versus Carbon Steel with Inhibitors: Factors Involved and Examples* Metallurgical Consultants Inc., First International Conference on Clad Engineering, Aberdeen, Scotland

[9] **Craig, B.D. and Thompson, R.S.** (1995) *The Influence of Risk Analysis on the Economics of Carbon Steel and CRA Clad Flowlines* Metallurgical Consultants Inc. and the Petroleum Engineering Department of the Colorado School of Mines, Proceedings of the Offshore Technology Conference 1995, p.829-835, OTC 7788, Houston, USA

[10] **De Koning, A.C., Nakasugi, H. and Li Ping** (2004) *TFP and TFT Back in Town (Tight Fit CRA Lined Pipe and Tubing)* Stainless Steel World, January/ February 2004, p.53-61

[11] **DNV** (2000) *Offshore Standard OS-F101 Submarine Pipeline Systems* Det Norske Veritas

[12] **DNV** (2005) *Reel Installation of Clad Steel Pipe* DNV Pipeline Committee 18.02.2005, Det Norske Veritas

[13] **DNV** (2006) *Technical Report, JIP Participants, State-of-the-Art Report Lined and Clad Pipeline Materials* Report No.2006-3119, Det Norske Veritas

[14] **Focke, E.S., Gresnigt, A.M. and Bijlaard, F.S.K.** (2003) *A Theoretical Model of Straightening without an Aligner during the Reeling Installation Process* Proceedings of the 13th ISOPE Conference, pp. 52-61

[15] **Focke, E.S., Gresnigt, A.M., Meek, J. and Nakasugi, H.** (2004) *The 2-Dimensional Modelling of the Manufacturing Process of Tight Fit Pipe (TFP)* Proceedings of the 14th ISOPE Conference, pp.82-91

[16] **Focke, E.S., Gresnigt, A.M., Meek, J. and Nakasugi, H.** (2005) *Experimental Behaviour on Local Buckling Behaviour of Tight Fit Pipe* Proceedings of the 15th International Symposium of Offshore and Polar Engineering, pp.76-84

[17] **Focke, E.S., van Oosten, J., Gresnigt, A.M., Meek, J. and Nakasugi, H.** (2005) *The Influence of the Reeling Installation Method on the Integrity of Circumferential Welds in Tight Fit Pi*pe Proceedings of the 15th International Symposium of Offshore and Polar Engineering, pp.31-38

[18] **Focke, E.S., Gresnigt, A.M., Meek, J. and Nakasugi, H.** (2006) *The Influence of Heating of the Liner Pipe during the Manufacturing Process of Tight Fit Pipe* Proceedings of the 16th ISOPE Conference, pp. 228-236

[19] **Focke, E.S., Gresnigt, A.M. and Meek, J.** (2006) *Small Scale Reeling Tests* Proceedings of the 16th ISOPE Conference, pp.118-126

[20] **Focke, E.S., Karjadi, E., Gresnigt, A.M. and Meek, J.** (2007) *Reeling of Tight Fit Pipe (TFP)* Proceedings of the 26th International Conference on Offshore Mechanics and Arctic Engineering, (to be published)

[21] **Gerard, G.** (1956) *Compressive and Torsional Buckling of Thin Walled Cylinders in the Yield Region* NACA TN 3726

[22] **Graf, M.K., von Hagen, I. and Niederhoff, K.A.** (1992) *Production of Large Diameter Line Pipe for the Transportation of Highly Corrosive Crude Oil and Natural Gas* Europipe and Mannesmannröhren-Werke AG Germany, Offshore South East Asia, 9th Conference and Exhibition, Singapore

[23] **Gresnigt, A.M.** (1986) *Plastic Design of Buried Pipelines in Settlement Areas* HERON, Volume 31, No.4

[24] **Gresnigt, A.M. and van Foeken, R.** (1990) *Local Loads on Buried Pipelines* TNO-IBBC Report B-90-434 for NV Nederlandse Gasunie (in Dutch)

[25] **Gresnigt, A.M. and van Foeken, R.** (2001) *Local Buckling of UOE and Seamless Steel Pipes* Proceedings of the Eleventh International Offshore and Polar Engineering Conference, Stavanger, Norway

[26] **Kane, R.D., Wilhelm, S.M. and McIntyre, D.R.** (1990) *Evaluation of Bimetallic Pipe for Oilfield Flowline Service Involving* H_2S *and* CO_2 NACE Corrosion

[27] **Karjadi, E.** (2006) *Full Scale Bending Tests for Reeling Simulation of Single Walled Pipe: Experiment vs ABAQUS Calculation* ABAQUS Benelux User's Meeting 2006, Leuven, Belgium, November 16-17, 2006

[28] **Kaye, D.** (2002) *CSO Deep Blue: Field Experience with a New UDW Pipelay Vessel* Technip-Coflexip, Conference Documentation of the Offshore Pipeline Technology Conference 2002

[29] **Kyriakides, S. and Shaw, P.K.** (1987) *Inelastic Buckling of Tubes Under Cyclic Bending* Journal of Pressure Vessel Technology, Vol. 109

[30] **Lee, L.H.N.** (1962) *Inelastic Buckling of Initially Imperfect Cylindrical Shells Subject to Axial Compression* Journal of the Aerospace Sciences, January, pp.87-95

[31] **MARC** (2001) *Introductory Course 2001* MSC. Software Corporation

[32] **Matsui, S.** (1989) *Implosion Strength of Liner Tube on Double Wall Pipe* Journal of High Pressure Institute of Japan, Vol. 27, No. 3, p.152

[33] **Matsui, S., Kakei, K. Iwase, T., Chino, H., Suzuki, M. and Murakami, Y.** (1990) *Manufacturing of Mechanically Bonded Bi-metallic Pipe* Proceedings of the Offshore Pipeline Technology Conference, Paris, France

[34] **Mills, A.F.** (1999) *Basic Heat and Mass Transfer* Prentice Hall, ISBN 0130962473

[35] **Mizumura, M., Hiroyuki, M., Naoi, H. and Higashiyama, H.** (1992) *Behaviour of Mechanically Bonding Double Wall Pipe under Various Loading Conditions* Proceedings of the Second International Offshore and Polar Engineering Conference 1992, pp.142-150

[36] **Murphey, C.E. and Langner, C.G.** (1985) *Ultimate Pipe Strength under* Bending, Collapse and Fatigue Proceedings of the Offshore Mechanics and Arctic Engineering Conference

[37] **Neessen, F.** (2004) *Stainless Steel Welding Seminar* Welding Course by Lincoln Smit Weld BV

[38] **NEN** (2003) Staal Katern 6 Bijlagen E en F NEN 3650-2

[39] **Rommerskirchen, I. et al** (2003) *New Liner Materials Used in Bubi-Pipes* Stainless Steel World 2003, 2003 KCI Publishing BV

[40] **Sasaki, T., Ume, K., Tohma, H., Kobayashi, Y., Tsuji, M and Itoh, M.** (1990) *Corrosion Resistant Clad Pipes Manufactured by UOE Process* NKK Corporation, Proceedings of the Pipeline Technology Conference 1990, p. 3.9-3.16, Oostende, Belgium

[41] **Smith, L.M.** (1992) *Clad Steel: An Engineering Option* Proceedings of the Offshore Technology Conference 1992, OTC 6911, p. 343-355, Houston, USA

[42] **Smith, L.M. and Celant, M.** (2000) *CASTI Handbook of Cladding Technology* ISBN 1894038304, 2nd Edition, CASTI Publishing Inc., Canada

[43] **STOS** (2004) *Pohokura Subsea Pipeline Material Specification For Lined Pipe* Document No. 292100-TCN-M0058 Shell Todd Oil Services Report No. 2389

[44] **Suer, H.S., Harris, L.A., Skene, W.T. and Benjamin, R.J.** (1958) *The Bending Stability of Thin-Walled Unstiffenend Circular Cylinders Including the Effects of Internal Pressure* Journal of the Aeronautical Sciences, Vol.25, No.5, pp.281-287

[45] **Suschitz, L.** (2000) *Reeling Study for Ultra-deepwater Pipelay Vessel Development* Coflexip Stena Offshore, Deep Offshore Technology

[46] **Timoshenko, S.P. and Gere, J.M.** (1961) *Theory of Elastic Stability* McGraw-Hill, second edition

[47] **Torselletti, E., Levold, E., Vitali, L. and Mørk, K.** (2005) *Submarine Pipeline Installation JIP: Strength and Deformation Capacity of Pipes Passing over the S-lay Stinger* Proceedings of the 25th International Offshore Mechanics and Arctic Engineering, OMAE2006-92378, pp.1-9

[48] **Yoshida, T., Matsui, S., Atsuta, T. and Itoga, K.** (1980) *Corrosion Problems of Pipeline and a Solution* Proceedings of the Offshore Technology Conference 1980, OTC 3891, p.361-364, Houston, USA

[49] **Yoshida, T., Matsuda, S., Matsui, S., Atsuta, T., Toma, S. and Igota, K.** (1981) *The Development of Corrosion-Resistant Tubing* Proceedings of the Offshore Technology Conference 1981, OTC 4153, p.365-368

[50] **Yoshida, T., Matsui, S., Atsuta, T., Hasegewa, H., Kakehi, K., Iwase, T. and Kuboyama, K**. (1986) *Mechanical-Bonded Double-Wall Pipe for Severe Corrosion Environment* Evaluation Materials Conference KOBE

[51] http://www.technip.com/pdf/Apache.pdf
[52] http://www.technip.com/pdf/Deep_Blue.pdf
[53] http://www.edvermeuelen.com/statoilclad180205.pdf
[54] http://www.leidschdagblad.nl/article875603.ece
[55] http://www.offshore-technology.com/contractors/pipes/proclad/
[56] http://archive.metalformingmagazine.com
[57] http://www.weldingengineer.com/Stainless%20Steel.htm
[58] http://en.wikipedia.org/wiki/Stainless_steel
[59] http://www.genesisoilandgasconsultants.com/pdf/Deep_Blue.pdf
[60] http://www2.steel.sandvik.com/sandvik/0140/internet/se01598.nsf/cdatas/C3F37C589CDFC86241256618006F1E50
[61] http://www.mace.manchester.ac.uk/project/research/structures/strucfire/materialInFire/Steel/HotRolledCarbonSteel/mechanicalProperties.htm
[62] http://www.jfe-steel.co.jp/en/products/stainless/07jisstandardchemical composition.html
[63] http://www.astm.org/cgi-bin/SoftCart.exe/index.shtml?E+mystore
[64] http://www.thefabricator.com/ResistanceWelding/ ResistanceWelding _Article.cfm?ID=89
[65] http://www.tenaris.com/shared/documents/files/CB152.pdf
[66] http://www.thermotech.co.uk/pictures/dss-ssc-big.html
[67] http://www.azom.com/details.asp?ArticleID=863
[68] http://www.engineeringtoolbox.com

Appendix I
Possibilities to Resist Corrosion in Steel Pipelines

I.1 Introduction

Hydrocarbons can contain H_2S, CO_2 and other corrosive products that can result in different types of corrosion problems in flowlines as is described below in Appendix I.2. Several methods exist to cope with corrosion problems in these flowlines as is described in Appendix I.3. However, a very aggressive environment (such as corrosive products in combination with high pressure and high temperature) may require a different approach such as the use of Tight Fit Pipe, a promising cost efficient concept for offshore transportation of corrosive hydrocarbons. A comparison between Tight Fit Pipe and other measures against corrosion problems in pipelines is made in Appendix I.4.

I.2 Different Types of Corrosion

Several types of corrosion exist, caused by different phenomena [48], [49].

1. General corrosion

General corrosion implies an overall weight loss of the pipe. Oil containing brine causes general corrosion because of the chloride ions present. Secondary recovery further enhances this type of corrosion.

2. Stress corrosion cracking

Stress corrosion cracking can be sulphide stress corrosion cracking or chloride stress corrosion cracking. H_2S causes sulphide stress corrosion cracking. The harder a material and the higher the tensile stress in the pipe, the lower the sulphide stress corrosion cracking resistance. Since well tubing is subjected to high tensile stresses, sulphide stress corrosion cracking turns out to be a larger problem for well tubing than for flowlines. Oil containing brine causes chloride stress corrosion cracking because of the chloride ions present in the brine. Tests with liner pipes manufactured from austenitic stainless steel (for example AISI 316L) show susceptibility to chloride stress corrosion cracking in a sour environment. If the temperature in the pipeline increases, the cracking time decreases.

3. Pitting corrosion

Pitting corrosion occurs in sour and sweet conditions. Due to wet CO_2 gas (resolved in oil and gas) sweet corrosion occurs in the flowline ($Fe^{++} + CO_2 + H_2O \rightarrow FeCO_3 + 2H^+$); due to wet H_2S gas (resolved in oil and gas) sour corrosion arises in the pipe ($Fe^{++} + H_2S \rightarrow FeS + 2H^+$). Moreover, pitting corrosion can occur when stainless steel is subjected to high concentration of chloride ions and moderately high temperatures [58].

4. Crevice corrosion

When the flow velocity is low, a discontinuity in the shape of the inner surface of the pipeline causes crevice erosion under deposits in concaves.

5. Blistering

Blistering takes place when the diffusive hydrogen is accumulated at a non-metallic inclusion located near the internal surface.

6. Erosion corrosion

When the flow velocity is high, a discontinuity in the shape of the inner surface of the pipeline causes erosion corrosion due to turbulence. This abrasion is especially a problem when sand particles are included in the rapid flow.

I.3 Solutions to Corrosion Problems

Several solutions to corrosion problems are described below:

1. Corrosion inhibitors

Inhibitors form a film on the inner surface of the pipe, thus protecting against corrosion. A disadvantage of this technique is that it adds considerably to operating costs and requires special equipment to operate. Moreover, formation of deposits due to inhibitors may cause the shutdown of the treating unit [49], [50]. Batch inhibition is effective up to approximately 150 °C but the technology can be extended to higher temperatures by continuous injection [26].

2. Plastic coating

The plastic coating protects the pipe against corrosion. Perfect bonding however, is hardly obtained and separation occurs when high pressure goes underneath the coating through holidays [49]. Besides, implosion of the liner pipe is a well known problem from onshore pipelines with a liner pipe made of plastic materials. In case a pressure builds up in between the liner pipe and the outer pipe, a sudden de-pressurisation of the pipeline may cause a high enough over-pressure between the liner pipe and the outer pipe to collapse or implode the liner pipe [13]. Further, their reliability at elevated temperatures is a problem and sealing at mechanical joints tends to be troublesome. In addition, abrasion occurs due to rapid flow containing sand [49].

3. Corrosion allowance

Where the duration of a project is relatively short, the amount of corrosion arising on carbon steel may be tolerated by allowing extra wall thickness, which is consumed during its lifetime [42].

4. Solid corrosion resistant alloys

Solid corrosion resistant alloys are (highly) alloyed materials, which provide improved corrosion resistance and thus extended service life compared to carbon steels. Such alternative materials may include various grades of stainless steels, nickel alloys or titanium alloys, its use depending on the environment [22], [48], [49]. Most widely used are stainless steels and nickel alloys. Three types of stainless steels that can be used as corrosion resistant alloy material are martensitic stainless steels, austenitic stainless steels and duplex stainless steels.

Martensitic stainless steels, represented by 13 % Cr, are advantageous in strength and general corrosion resistance. These materials are susceptible to sulphide and chloride stress corrosion cracking, so they should not be used in sour conditions. Austenitic stainless steels [57], [58], are effective in sour conditions but are generally susceptible to chloride stress corrosion cracking. Duplex steels with an austenitic-ferretic structure exhibit superior resistance to both general corrosion and stress corrosion cracking. The corrosion resistance of austenitic-ferritic duplex steels greatly depends on the ratio of austenite to ferrite content. By applying a heat treatment between 1020 °C and 1100 °C the austenite-to-ferrite content is between 40:60 and 60:40 and the microstructure is sufficiently free of precipitates (a solid or solid phase separated from the microstructure). Yield strengths for duplex stainless steels are high (965 MPa) and consequently are suited for use as high strength solid pipes [22], [26], [40], [48], [49].

Super nickel alloys are suitable for services at high temperatures. These materials exhibit excellent performance both in strength and corrosion resistance [22], [48], [49]. Under circumstances such as high production rates, high temperatures, high pressures, remote operations and demand of long term reliability, corrosion resistant alloy materials may provide an attractive alternative to conventional steels used in combination with chemical inhibitors. Corrosion resistant alloy materials however, are slow to weld and may require special line-up procedures resulting in additional costs [26].

5. Double walled pipe

Carbon steel or solid corrosion resistant alloy alone are not able to combine strength, corrosion resistance and cost-effectiveness: strong and economical carbon steel is lacking corrosion resistance and corrosion resistant alloys are expensive and not sufficient in strength. In order to fill this gap, the manufacturing of double walled pipeline (and tubing) started (at the end of the 1970-s), where the outer pipe is made of carbon steel and the liner pipe (inner pipe) of corrosion resistant alloy material. Difference is made between clad pipe and lined pipe; clad pipe is a bimetallic pipe composed of an internal corrosion resistant alloy layer metallurgical bonded to the carbon steel base metal while lined pipe is a bimetallic pipe composed of an internal corrosion resistant alloy liner pipe mechanically bonded to the carbon steel base metal [42].

The liner pipe of the double walled pipe is selected for its resistance to corrosion and the backing material is chosen to meet the necessary mechanical requirements. In many cases the backing steel strength exceeds the corrosion resistant alloy strength, so that in designs where the strength requirement controls the design wall thickness, the use of clad steel can result in a thinner overall wall thickness when compared to the use of solid corrosion resistant alloy [42].

Although the capital cost of double walled pipe is quite high, the subsequent operating costs over the life of the project are relatively low. The opposite is true for carbon steel where relatively low initial costs may be coupled with significant operating and repair costs [9]. Reduced risk of pipeline failure (which is not always taken into account into economic analysis) is however most often sufficient to justify the additional initial costs of a more corrosion resistant solution [8]. The cost benefit of using a double walled solution rather than a solid corrosion resistant alloy for flowlines may be very attractive for deep water developments where high pressure and high temperature conditions of the hydrocarbons may be very aggressive, requiring highly alloyed materials to prevent corrosion [42].

5a. Clad pipe (metallurgical bonded double walled pipe)

As mentioned before, clad pipe is a bimetallic pipe composed of an internal corrosion resistant alloy layer metallurgical bonded to the carbon steel base metal. There may be limitations to the possible combinations of alloys and backing steels when using clad pipe due to the fact that heat treatment optimises the corrosion properties of the cladding material but at the same time the backing steel has to fulfil its mechanical properties. These two requirements may be in conflict. The clad pipe often needs to be demagnetised after production because of residual magnetism, which can be strong enough to cause arc blow during welding [56]. Since pipes could also re-magnetise during transport and storage, the pipe sometimes need to be demagnetised after fit up [42].

Clad pipe exists in the form of longitudinal welded pipe and seamless pipe [41]. For longitudinally welded pipe a clad plate is transformed into clad pipe in a UOE press (the press transforms the flat plate first into a U-shape, then into an O-shape after which the pipe is expanded to enhance its roundness) or rolling mill. The clad plate can be manufactured in three ways: hot roll bonding, explosive bonding and weld overlaying. For hot roll bonding the cleaned surfaces of the cladding and backing steel are brought together. It is normal to prepare a sandwich of two clad slabs with the clad surfaces together with a layer of separating compound to prevent the surfaces sticking together. The two slabs are welded at the edges to prevent separation during rolling. The advantages are that the cladding layer does not contact the steel rolls during the rolling so that it is not contaminated. Rolling two slabs together allows thinner plates to be produced. Explosive bonding can best be achieved in materials with high impact toughness and high ductility. For weld overlaying, a high deposition rate process may appear to be fast (therefore reducing labour costs) but if the heat input is too high, excessive dilution with the underlying base metal may mean that a second layer is required [42].

The other type of clad pipe is the seamless clad pipe. Seamless clad pipe can be fabricated by overlay welding [55], explosion, extrusion, by the centricast method or by means of hot isostatic pressing. Extruded pipe products use a composite billet of CRA pipe nested inside a steel pipe. For clad pipes produced by the centricast pipe the molten steel is poured into a rotating metal mould with a flux and after solidification, the molten CRA is introduced into the opposite end of the mould with a new flux. When using the hot isostatic pressing method, the alloy may be in the form of a powder or as a solid lining. By controlling the temperature and holding time the diffusion zone depth can be controlled and limited, so there is no zone of dilution [42].

5b. Lined Pipe (Mechanically Bonded Double Walled Pipe)

Lined pipe is a combination of a corrosion resistant alloy liner pipe tightly fixed inside a carbon steel pipe (mechanically bonded). The tight fit of the liner pipe to the carbon steel outer pipe can be achieved in three ways, as described hereafter [42].

The first method is the thermal shrink fit method. A liner pipe is inserted into the outer pipe, while the outer pipe has been expanded by heating. As the outer pipe is cooled, the liner pipe and the outer pipe become tightly fitted together, owing to the thermal shrinkage of the outer pipe and the resistance to this shrinkage of the liner pipe. Precise machining is needed in such a manner that the outer diameter of the liner pipe is slightly larger than the inner diameter of the outer pipe (before heating), by the amount predetermined from the required fit-in stress magnitude. In addition, a high degree of straightness and roundness must be achieved for the smooth insertion of the liner pipe. Unfortunately, these two requirements are practically impossible which makes this process economically not attractive [49].

The second method, the hydraulic expansion method, does not require precise dimensions nor a high degree of straightness of pipes since the liner pipe is loosely inserted into the outer pipe before both are expanded. There is however a limitation on the selection of backing steel and liner pipe materials. Since the fitting is achieved by the larger elastic spring-back of the outer pipe than that of the liner pipe, the strength of the outer pipe must be higher than liner pipe strength. If the strength of the outer pipe does not exceed the strength of the liner pipe, a gap occurs between the two pipes after manufacturing [39].

Although there are combinations of backing steel and liner pipe materials where the fit is achieved, it should be noted that a very high expanding pressure is required [49]. The third method is the thermal hydraulic expansion method which is the manufacturing method for the Tight Fit Pipe (Chapter 2 and Appendix II).

I.4 Comparison of Solutions to Corrosion Problems

For severe environments (such as high pressure, high temperature production environments) where the corrosion resistance has to be guaranteed for a long period of time, corrosion inhibitors, plastic coating and corrosion allowance using carbons steel are not feasible options. Attention has to be focused on either solid corrosion resistant alloy materials or double walled pipe (metallurgical or mechanically bonded double walled pipe). For the mechanically bonded double walled pipe there is the choice between pipe manufactured through either the hydraulic expansion method or the thermo-hydraulic gripping method.

When double walled pipe (mechanically or metallurgical bonded) is compared to solid corrosion resistant alloy pipe, double walled pipe behaves in a more complicated manner. At the same time however, double walled pipe has the advantage of obtaining optimum properties of mechanical strength (outer pipe) and corrosion resistance (liner pipe) and is often more economical and easier to handle during transport and installation (special tools are necessary during transport and installation to handle solid corrosion resistant alloy material).

When mechanically bonded double walled pipe (lined pipe) is compared to metallurgical bonded double walled pipe (clad pipe), lined pipe may have a few disadvantages but also has distinct advantages. Although lined pipe behaves in a more complex manner than clad pipe (because inner and outer pipes are bonded only mechanically), the compressive residual stress in the liner pipe prevents stress corrosion cracking phenomenon such as sulphide stress corrosion cracking and chloride stress corrosion cracking [50]. Moreover, the mechanical properties of the backing steel can be optimised during normal pipe production and the liner pipe can then be inserted into the finished pipe. This opens up the possibility for use of a wider range of alloys [42]. Most importantly, lined pipe is less costly than clad pipe.

When thermo-hydraulically fitted pipe (Tight Fit Pipe) is compared to the hydraulically expanded pipe (e.g. a BuBi-pipe manufactured by Butting in Germany), the Tight Fit Pipe may be more expensive, but a higher confinement of the liner pipe in the outer pipe is guaranteed. In addition, the manufacturing method of Tight Fit Pipe makes more combinations of liner pipe and the outer pipe possible. A duplex or super duplex liner pipe for example cannot be manufactured with the hydraulic expansion method, for the high yield strength of the liner pipe material versus the lower yield strength of the carbon steel.

Appendix II
Analytical Model of the Manufacturing Process of Tight Fit Pipe

II.1 Liner Pipe Temperature during Manufacturing

For six manufactured Tight Fit Pipes the average temperature of the liner pipe due to contact with the outer pipe ($T_{L;a;PH}$) was determined using Equation (II. 1) to (II. 6) [34]. Liner pipe and outer pipe characteristics of the six manufactured Tight Fit Pipes (Table I. 1) were used to determine these (average) liner pipe temperatures.

Table I. 1 Input parameters used to determine the liner pipe average temperature resulting from contact with the hot outer pipe for six Tight Fit Pipes manufactured by Kuroki T&P

	1	2	3	4	5	6
$r_{L;i;TFP}$ [mm]	44.25	44.59	86.80	86.45	125.36	125.52
$r_{L;o;TFP}$ [mm]	46.15	46.15	88.69	88.47	127.75	127.89
$r_{O;i;TFP}$ [mm]	46.15	46.15	88.69	88.47	127.75	127.89
$r_{O;o;TFP}$ [mm]	57.45	57.45	97.25	97.25	137.10	137.18
L_{TFP} [mm]	1	1	1	1	1	1
$T_{O;max}$ [K]	638	655	650	655	580	680
T_{CW} [K]	283	293	298	293	300	298
k_O [W/(mK)]	50	50	50	50	50	50
k_L [W/(mK)]	15	15	15	15	15	15

$$\Omega_L = \ln\left(r_{L;o;TFP} / r_{L;i;TFP}\right) / \left(2 \cdot \pi \cdot k_L \cdot L_{TFP}\right) \tag{II. 1}$$

$$\Omega_O = \ln\left(r_{O;o;TFP} / r_{O;i;TFP}\right) / \left(2 \cdot \pi \cdot k_O \cdot L_{TFP}\right) \tag{II. 2}$$

$$UA = 1 / \left(\Omega_L + \Omega_O\right) \tag{II. 3}$$

$$Q = UA \cdot \left(T_{O;\max} - T_{CW}\right) \tag{II. 4}$$

$$T_{L-O} = Q \cdot \Omega_L + T_{CW} \tag{II. 5}$$

$$T_{L;a;PH} = \left(T_{CW} + T_{L-O}\right) / 2 \tag{II. 6}$$

II.2 Step 1: Identification of the Parameters

In step 1 the dimensions of the outer pipe and the liner pipe are stated in Equations (II. 7) to (II. 10).

$$d_{O;o;1}=d_{O;o}\ ;\ d_{O;a;1}=d_{O;o;1}-t_O\ ;\ d_{O;i;1}=d_{O;o;1}-2\cdot t_O \tag{II. 7}$$

$$d_{L;o;1}=d_{O;i;1}-2\cdot g\ ;\ d_{L;a;1}=d_{L;o;1}-t_L\ ;\ d_{L;i;1}=d_{L;o;1}-2\cdot t_L \tag{II. 8}$$

$$r_{O;o;1}=d_{O;o;1}/2\ ;\ r_{O;a;1}=d_{O;a;1}/2\ ;\ r_{O;i;1}=d_{O;i;1}/2 \tag{II. 9}$$

$$r_{L;o;1}=d_{L;o;1}/2\ ;\ r_{L;a;1}=d_{L;a;1}/2\ ;\ r_{L;i;1}=d_{L;i;1}/2 \tag{II. 10}$$

The hoop stresses in the liner pipe ($\sigma_{O;h;1}$) and in the outer pipe ($\sigma_{L;h;1}$) are zero.

II.3 Step 2: Cooling of the Liner Pipe

The liner pipe is assumed to be $T_{environment}$ at the beginning of the manufacturing process. As soon as the hydraulic expansion machine (which is also a cooling machine as mentioned in assumption 3 in Subsection 2.3.1) is inserted into the liner pipe, the liner pipe cools down from $T_{environment}$ to T_{CW}.

$$T_{L;1} = T_{environment}\ ;\ T_{L;2}=T_{CW} \tag{II. 11}$$

$$\Delta T_{L;1-2}=T_{L;2}-T_{L;1} \tag{II. 12}$$

$$d_{O;o;2}=d_{O;o;1}\ ;\ d_{O;a;2}=d_{O;a;1}\ ;\ d_{O;i;2}=d_{O;i;1} \tag{II. 13}$$

$$d_{L;o;2}=d_{L;o;1}+d_{L;a;1}\cdot\alpha_L\cdot\Delta T_{L;1-2}\ ;\ d_{L;a;2}=d_{L;a;1}+d_{L;a;1}\cdot\alpha_L\cdot\Delta T_{L;1-2}\ ;\ d_{L;i;2}=d_{L;i;1}+d_{L;a;1}\cdot\alpha_L\cdot\Delta T_{L;1-2} \tag{II. 14}$$

$$r_{O;o;2}=d_{O;o;2}/2\ ;\ r_{O;a;2}=d_{O;a;2}/2\ ;\ r_{O;i;2}=d_{O;i;2}/2 \tag{II. 15}$$

$$r_{L;o;2}=d_{L;o;2}/2\ ;\ r_{L;a;2}=d_{L;a;2}/2\ ;\ r_{L;i;2}=d_{L;i;2}/2 \tag{II. 16}$$

$$\Delta r_{O;a;1-2}=r_{O;a;2}-r_{O;a;1}\ ;\ \Delta r_{L;a;1-2}=r_{L;a;2}-r_{L;a;1} \tag{II. 17}$$

The hoop stresses in the liner pipe ($\sigma_{O;h;2}$) and in the outer pipe ($\sigma_{L;h;2}$) are zero.

II.4 Step 3: Heating of the Outer Pipe

The outer pipe is heated from $T_{environment}$ to the maximum temperature of the outer pipe, which is identical to the oven temperature ($T_{O;max}$).

$$T_{O;2} = T_{environment} \; ; \; T_{O;3} = T_{O;max} \tag{II. 18}$$

$$\Delta T_{O;2-3} = T_{O;3} - T_{O;2} \tag{II. 19}$$

$$d_{O;o;3} = d_{O;o;2} + d_{O;a;2} \cdot \alpha_O \cdot \Delta T_{O;2-3} \; ; \; d_{O;a;3} = d_{O;a;2} + d_{O;a;2} \cdot \alpha_O \cdot \Delta T_{O;2-3} \; ; \; d_{O;i;3} = d_{O;i;2} + d_{O;a;2} \cdot \alpha_O \cdot \Delta T_{O;2-3} \tag{II. 20}$$

$$d_{L;o;3} = d_{L;o;2} \; ; \; d_{L;a;3} = d_{L;a;2} \; ; \; d_{L;i;3} = d_{L;i;2} \tag{II. 21}$$

$$r_{O;o;3} = d_{O;o;3}/2 \; ; \; r_{O;a;3} = d_{O;a;3}/2 \; ; \; r_{O;i;3} = d_{O;i;3}/2 \tag{II. 22}$$

$$r_{L;o;3} = d_{L;o;3}/2 \; ; \; r_{L;a;3} = d_{L;a;3}/2 \; ; \; r_{L;i;3} = d_{L;i;3}/2 \tag{II. 23}$$

$$\Delta r_{O;a;2-3} = r_{O;a;3} - r_{O;a;2} \; ; \; \Delta r_{L;a;2-3} = r_{L;a;3} - r_{L;a;2} \tag{II. 24}$$

The hoop stresses in the liner pipe ($\sigma_{O;h;3}$) and in the outer pipe ($\sigma_{L;h;3}$) are zero.

II.5 Step 4: Expansion of the Liner Pipe to Yield

In step 4 the liner pipe is expanded to yield.

$$P_{i;4} = \left(\sigma_{L;y} \cdot 2 \cdot t_L\right) / d_{L;i;3} \tag{II. 25}$$

$$\mathrm{d}_{O;o;4} = \mathrm{d}_{O;o;3} \; ; \; d_{O;a;4} = d_{O;a;3} \; ; \; d_{O;i;4} = d_{O;i;3} \tag{II. 26}$$

$$\begin{aligned} d_{L;o;4} &= d_{L;o;3} + d_{L;a;3} \cdot \left(\sigma_{L;y}/E_L\right); \\ d_{L;a;4} &= d_{L;a;3} + d_{L;a;3} \cdot \left(\sigma_{L;y}/E_L\right); \\ d_{L;i;4} &= d_{L;i;3} + d_{L;a;3} \cdot \left(\sigma_{L;y}/E_L\right) \end{aligned} \tag{II. 27}$$

$$r_{O;o;4} = d_{O;o;4}/2 \; ; \; r_{O;a;4} = d_{O;a;4}/2 \; ; \; r_{O;i;4} = d_{O;i;4}/2 \tag{II. 28}$$

$$r_{L;o;4} = d_{L;o;4}/2 \; ; \; r_{L;a;4} = d_{L;a;4}/2 \; ; \; r_{L;i;4} = d_{L;i;4}/2 \tag{II. 29}$$

$$\Delta r_{O;a;3-4} = r_{O;a;4} - r_{O;a;3} \; ; \; \Delta r_{L;a;3-4} = r_{L;a;4} - r_{L;a;3} \tag{II. 30}$$

The hoop stress in the outer pipe ($\sigma_{O;h;4}$) is zero. The hoop stress in the liner pipe equals the yield stress.

$$\sigma_{L;h;4} = \sigma_{L;y} \tag{II. 31}$$

II.6 Step 5: Expansion of the Liner Pipe until it is in Contact with the Outer Pipe

In step 5 the liner pipe is expanded plastically until it is in contact with the outer pipe.

$$P_{i;5} = P_{i;4} \tag{II. 32}$$

$$\Delta d_{L;a;4-5} = d_{O;i;4} - d_{L;o;4} \tag{II. 33}$$

$$d_{O;o;5} = d_{O;o;4}\ ;\ d_{O;a;5} = d_{O;a;4}\ ;\ d_{O;i;5} = d_{O;i;4} \tag{II. 34}$$

$$d_{L;o;5} = d_{L;o;4} + \Delta d_{L;a;4-5}\ ;\ d_{L;a;5} = d_{L;a;4} + \Delta d_{L;a;4-5}\ ;\ d_{L;i;5} = d_{L;i;4} + \Delta d_{L;a;4-5} \tag{II. 35}$$

$$r_{O;o;5} = d_{O;o;5}/2\ ;\ r_{O;a;5} = d_{O;a;5}/2\ ;\ r_{O;i;5} = d_{O;i;5}/2 \tag{II. 36}$$

$$r_{L;o;5} = d_{L;o;5}/2\ ;\ r_{L;a;5} = d_{L;a;5}/2\ ;\ r_{L;i;5} = d_{L;i;5}/2 \tag{II. 37}$$

$$\Delta r_{O;a;4-5} = r_{O;a;5} - r_{O;a;4}\ ;\ \Delta r_{L;a;4-5} = r_{L;a;5} - r_{L;a;4} \tag{II. 38}$$

The hoop stress in the outer pipe ($\sigma_{L;h;5}$) is zero. The hoop stress in the liner pipe equals the yield stress.

$$\sigma_{L;5} = \sigma_{L;y} \tag{II. 39}$$

II.7 Step 6: Increase of the Internal Pressure to Maximum

In step 6 the internal pressure reaches its maximum value.

$$\Delta P_{i;5-6} = P_{i;\max} - P_{i;5} \tag{II. 40}$$

$$\Delta\sigma_{O;h;5-6} = \left(\Delta P_{i;5-6} \cdot d_{L;i;5} - \sigma_{L;h;5} \cdot 2 \cdot t_L\right) / (2 \cdot t_O) \tag{II. 41}$$

There is no change in hoop stress in the liner pipe from step 5 to step 6.

$$d_{O;o;6} = d_{O;o;5} + d_{O;a;5} \cdot \left(\Delta\sigma_{O;h;5-6}/E_O\right);\ d_{O;a;6} = d_{O;a;5} + d_{O;a;5} \cdot \left(\Delta\sigma_{O;h;5-6}/E_O\right);\ d_{O;i;6} = d_{O;i;5} + d_{O;i;5} \cdot \left(\Delta\sigma_{O;h;5-6}/E_O\right) \tag{II. 42}$$

$$d_{L;o;6} = d_{O;i;6}\ ;\ d_{L;a;6} = d_{L;o;6} - t_L\ ;\ d_{L;a;6} = d_{L;o;6} - 2 \cdot t_L \tag{II. 43}$$

$$r_{O;o;6} = d_{O;o;6}/2\ ;\ r_{O;a;6} = d_{O;a;6}/2\ ;\ r_{O;i;6} = d_{O;i;6}/2 \tag{II. 44}$$

$$r_{L;o;6}=d_{L;o;6}/2\ ;\ r_{L;a;6}=d_{L;a;6}/2\ ;\ r_{L;i;6}=d_{L;i;6}/2 \tag{II. 45}$$

$$\Delta r_{O;a;5-6}=r_{O;a;6}-r_{O;a;5}\ ;\ \Delta r_{L;a;5-6}=r_{L;a;6}-r_{L;a;5} \tag{II. 46}$$

$$\sigma_{O;h;6}=\Delta\sigma_{O;h;5-6} \tag{II. 47}$$

$$\sigma_{L;h;6}=\sigma_{L;y} \tag{II. 48}$$

There should be equilibrium which can be checked using Equation (II. 49).

$$\Delta\sigma_{O;h;5-6}\cdot 2\cdot t_O+\sigma_{L;y}\cdot 2\cdot t_L-\Delta P_{i;5-6}\cdot d_{L;i;5}=0 \tag{II. 49}$$

It needs to be checked whether the outer pipe hoop stress in step 6 ($\sigma_{O;h;6}$) remains below the outer pipe yield stress ($\sigma_{O;y}$).

II.8 Step 7: Heating of the Liner Pipe

It is assumed that due to contact of the cooled liner pipe with the heated outer pipe, the liner pipe heats up to either $T_{L;a;PH}$ or to $T_{L;a;CH}$ depending on partial or complete heating assumption of the liner pipe. From step 6 to step 7a it is assumed the liner pipe heats up without the confinement of the outer pipe.

$$T_{L;7a}=T_{L;a;PH/CH} \tag{II. 50}$$

$$\Delta T_{L;6-7a}=T_{L;7a}-T_{L;6} \tag{II. 51}$$

$$\Delta d_{L;a;6-7a}=d_{L;a;6}\cdot\Delta T_{L;6-7a}\cdot\alpha_L \tag{II. 52}$$

$$d_{L;o;7a}=d_{L;o;6}+\Delta d_{L;a;6-7a}\ ;\ d_{L;a;7a}=d_{L;a;6}+\Delta d_{L;a;6-7a}\ ;\ d_{L;i;7a}=d_{L;i;6}+\Delta d_{L;a;6-7a} \tag{II. 53}$$

$$d_{O;o;7a}=d_{O;o;6}\ ;\ d_{O;a;7a}=d_{O;a;6}\ ;\ d_{O;i;7a}=d_{O;i;6} \tag{II. 54}$$

From step 7a to step 7b it is assumed the liner pipe is confined back inside the outer pipe.

$$d_{7b}=d_{O;i;7a}+\Delta d_{O;i;7a-7b} \tag{II. 55}$$

$$d_{7b}=d_{L;o;7a}-\Delta d_{L;o;7a-7b} \tag{II. 56}$$

$$\Delta d_{O;i;7a-7b}=\Delta\varepsilon_{O;h;7a-7b}\cdot(d_{7b}+t_O)=(\Delta\sigma_{O;h;7a-7b}/E_O)\cdot(d_{7b}+t_O) \tag{II. 57}$$

$$\Delta d_{O;i;7a-7b}=\left((\Delta\sigma_{C;7a-7b}\cdot d_7)/(2\cdot t_O\cdot E_O)\right)\cdot(d_{7b}+t_O) \tag{II. 58}$$

$$\Delta d_{L;o;7a-7b}=\Delta\varepsilon_{L;h;7a-7b}\cdot(d_{7b}-t_L)=(\Delta\sigma_{L;h;7a-7b}/E_L)\cdot(d_{7b}-t_L) \tag{II. 59}$$

$$\Delta d_{L;o;7a-7b} = \left(\left(\Delta\sigma_{C;7a-7b} \cdot d_7\right) / \left(2 \cdot t_L \cdot E_L\right)\right) \cdot \left(d_{7b} - t_L\right) \tag{II. 60}$$

Implementing Equations (II. 59) and (II. 60) in Equations (II. 55) and (II. 56) results in Equations (II. 61) and (II. 62).

$$d_{7b} = d_{O;i;7a} + \left(\left(\Delta\sigma_{C;7a-7b} \cdot d_{7b}\right) / \left(2 \cdot t_O \cdot E_O\right)\right) \cdot \left(d_{7b} + t_O\right) \tag{II. 61}$$

$$d_{7b} = d_{L;o;7a} - \left(\left(\Delta\sigma_{C;7a-7b} \cdot d_{7b}\right) / \left(2 \cdot t_L \cdot E_L\right)\right) \cdot \left(d_{7b} - t_L\right) \tag{II. 62}$$

Two equations with two unknowns can be developed and the two unknown variables, the equilibrium diameter (d_{7b}) and the change in contact pressure between the liner pipe and the outer pipe ($\Delta\sigma_{C;7a-7b}$), can be solved for (Equations (II. 63) and (II. 64).

$$d_{7b} = d_{O;i;7a} + \left(\left(\Delta\sigma_{C;7a-7b} \cdot d_{7b}\right) / \left(2 \cdot t_O \cdot E_O\right)\right) \cdot \left(d_{7b} + t_O\right) \tag{II. 63}$$

$$\Delta\sigma_{C;7a-7b} = \left(-d_{7b} + d_{L;o;7a}\right) \cdot \left(\left(2 \cdot t_L \cdot E_L\right) / \left(\left(d_{7b}\right)^2 - t_L \cdot d_{7b}\right)\right) \tag{II. 64}$$

The inner diameter of the outer pipe in step 7b and the outer diameter of the liner pipe in step 7b are set equal to the equilibrium diameter in step 7b (d_{7b}). The average and outer diameter of the outer pipe and the average and inner diameter of the liner pipe are calculated from the equilibrium diameter.

$$d_{O;o;7b} = d_{7b} + 2 \cdot t_O \,;\; d_{O;a;7b} = d_{7b} + t_O \,;\; d_{O;i;7b} = d_{7b} \tag{II. 65}$$

$$d_{L;o;7b} = d_{7b} \,;\; d_{L;a;7b} = d_{7b} - t_L \,;\; d_{L;a;7b} = d_{7b} - 2 \cdot t_L \tag{II. 66}$$

$$r_{O;o;7b} = d_{O;o;7b}/2 \,;\; r_{O;a;7b} = d_{O;a;7b}/2 \,;\; r_{O;i;7b} = d_{O;i;7b}/2 \tag{II. 67}$$

$$r_{L;o;7b} = d_{L;o;7b}/2 \,;\; r_{L;a;7b} = d_{L;a;7b}/2 \,;\; r_{L;i;7b} = d_{L;i;7b}/2 \tag{II. 68}$$

$$\Delta r_{O;a;6-7b} = r_{O;a;7b} - r_{O;a;6} \,;\; \Delta r_{L;a;7a-6} = r_{L;a;7b} - r_{L;a;6} \tag{II. 69}$$

$$\begin{gathered} \Delta\sigma_{O;h;6-7b} = \left(\left(\Delta\sigma_{C;7a-7b} \cdot d_{7b}\right) / 2 \cdot t_O\right); \\ \Delta\sigma_{L;h;6-7b} = -\left(\left(\Delta\sigma_{C;7a-7b} \cdot d_{7b}\right) / 2 \cdot t_L\right) \end{gathered} \tag{II. 70}$$

$$\sigma_{O;h;7b} = \sigma_{O;h;6} + \Delta\sigma_{O;h;6-7b} \,;\; \sigma_{L;h;7b} = \sigma_{L;h;6} + \Delta\sigma_{L;h;6-7b} \tag{II. 71}$$

$$IF \sigma_{L;h;7b} \rangle - \sigma_{L;y} THEN \sigma_{L;h;7b} ; ELSE - \sigma_{L;y} \tag{II. 72}$$

$$\sigma_{O;h;7b} = \left(\Delta P_{i;5-6} \cdot d_{L;i;5} - \sigma_{L;h;7b} \cdot 2 \cdot t_L\right) / \left(2 \cdot t_O\right) \tag{II. 73}$$

It needs to be checked whether the outer pipe hoop stress in step 7 ($\sigma_{O;h;7b}$) remains below the outer pipe yield stress ($\sigma_{O;y}$).

II.9 Step 8: Reduction of the Internal Pressure

In step 8, the internal pressure is reduced to atmospheric level while the liner pipe is heated due to contact with the outer pipe. Firstly from step 6 to step 8a, dimensions and stresses of the liner pipe and the outer pipe are calculated for the situation where the internal pressure is assumed to be reduced to atmospheric level but the liner pipe is assumed not to be heated due to contact with the outer pipe.

$$d_{O;o;8a}=d_{O;o;3}\ ;\ d_{O;a;8a}=d_{O;a;3}\ ;\ d_{O;i;8a}=d_{O;i;3} \tag{II. 74}$$

$$d_{L;o;8a}=d_{L;o;6}+d_{L;a;6}\cdot\left(\sigma_{L;h;6}/E_L\right);\ d_{L;a;8a}=d_{L;a;6}+d_{L;a;6}\cdot\left(\sigma_{L;h;y}/E_L\right);\ d_{L;i;8a}=d_{L;i;6}+d_{L;a;6}\cdot\left(\sigma_{L;h;y}/E_L\right) \tag{II. 75}$$

$$r_{O;o;8a}=d_{O;o;8a}/2\ ;\ r_{O;a;8a}=d_{O;a;8a}/2\ ;\ r_{O;i;8a}=d_{O;i;8a}/2 \tag{II. 76}$$

$$r_{L;o;8a}=d_{L;o;8a}/2\ ;\ r_{L;a;8a}=d_{L;a;8a}/2\ ;\ r_{L;i;8a}=d_{L;i;8a}/2 \tag{II. 77}$$

$$\Delta r_{O;a;6-8a}=r_{O;a;8a}-r_{O;a;6}\ ;\ \Delta r_{L;a;6-8a}=r_{L;a;8a}-r_{L;a;6} \tag{II. 78}$$

The hoop stress present in the liner pipe ($\sigma_{L;h;8a}$) and the outer pipe ($\sigma_{O;h;8a}$) are zero. Secondly from step 8a to step 8b, the expansion of the liner pipe as a result of contact with the hot outer pipe is calculated, assuming the expansion of the liner pipe is not restricted by the confinement of the outer pipe (the internal pressure is at atmospheric level).

$$\Delta d_{L;a;8a-8b}=d_{L;a;8a}\cdot\Delta T_{L;8a-8b}\cdot\alpha_L \tag{II. 79}$$

$$d_{O;o;8b}=d_{O;o;8a}\ ;\ d_{O;a;8b}=d_{O;a;8a}\ ;\ d_{O;i;8b}=d_{O;i;8a} \tag{II. 80}$$

$$d_{L;o;8b}=d_{L;o;8a}+\Delta d_{L;a;8a-8b}\ ;\ d_{L;a;8b}=d_{L;a;8a}+\Delta d_{L;a;8a-8b}\ ;\ d_{L;i;8b}=d_{L;i;8a}+\Delta d_{L;a;8a-8b} \tag{II. 81}$$

Thirdly from step 8b to step 8c, the unrestrictedly expanded, heated up liner pipe is assumed to be confined back into the outer pipe while the internal pressure is still at atmospheric level. Calculations in step 8b and 8c are identical to calculations in step 7a and step 7b. It needs to be checked whether the outer pipe hoop stress in step 8c ($\sigma_{O;h;8c}$) remains below the outer pipe yield stress ($\sigma_{O;y}$).

$$d_{8c}=d_{O;i;8b}+\left(\left(\Delta\sigma_{C;8b-8c}\cdot d_{8c}\right)/\left(2\cdot t_O\cdot E_O\right)\right)\cdot\left(d_{8c}+t_O\right) \tag{II. 82}$$

$$\Delta\sigma_{C;8b-8c}=\left(-d_{8c}+d_{L;o;8b}\right)\cdot\left(\left(2\cdot t_L\cdot E_L\right)\Big/\left(\left(d_{8c}\right)^2-t_L\cdot d_{8c}\right)\right) \tag{II. 83}$$

$$d_{O;o;8c}=d_{8c}+2\cdot t_O\ ;\ d_{O;a;8c}=d_{8c}+t_O\ ;\ d_{O;i;8c}=d_{8c} \tag{II. 84}$$

$$d_{L;o;8c} = d_{8c}\ ;\ d_{L;a;8c} = d_{8c} - t_L\ ;\ d_{L;a;8c} = d_{8c} - 2 \cdot t_L \qquad \text{(II. 85)}$$

$$r_{O;o;8c} = d_{O;o;8c}/2\ ;\ r_{O;a;8c} = d_{O;a;8c}/2\ ;\ r_{O;i;8c} = d_{O;i;8c}/2 \qquad \text{(II. 86)}$$

$$r_{L;o;8c} = d_{L;o;8c}/2\ ;\ r_{L;a;8c} = d_{L;a;8c}/2\ ;\ r_{L;i;8c} = d_{L;i;8c}/2 \qquad \text{(II. 87)}$$

$$\Delta r_{O;a;6-8c} = r_{O;a;8c} - r_{O;a;6}\ ;\ \Delta r_{L;a;6-8c} = r_{L;a;8c} - r_{L;a;6} \qquad \text{(II. 88)}$$

$$\sigma_{O;h;8c} = \left(\left(\Delta\sigma_{C;8b-8c} \cdot d_{8c}\right)/2 \cdot t_O\right);\ \sigma_{L;h;8c} = -\left(\left(\Delta\sigma_{C;8b-8c} \cdot d_{8c}\right)/2 \cdot t_L\right) \qquad \text{(II. 89)}$$

$$IF \sigma_{L;h;8c} \rangle - \sigma_{L;y} THEN \sigma_{L;h;8c}; ELSE - \sigma_{L;y} \qquad \text{(II. 90)}$$

$$\sigma_{O;h;8c} = \left(\sigma_{L;h;8c} \cdot t_L\right)/\left(t_O\right) \qquad \text{(II. 91)}$$

II.10 Step 9: Cooling down of the Liner Pipe and the Outer Pipe to T_{end}

In step 9 the outer pipe cools down in the atmosphere to temperature T_{end} (343 K (70°C)), the temperature at which active cooling of the liner pipe is stopped. Because active cooling of the liner pipe is stopped at temperature T_{end}, the liner pipe then obtains the same temperature T_{end} as the outer pipe. It is therefore assumed that the liner pipe and outer pipe both cool down in step 9 to T_{end}.

Firstly in step 9a, the liner pipe and the outer pipe are assumed to cool down separately from each other and due to their difference in temperature and material characteristics, they decrease to different dimensions.

$$T_{L;8c} = T_{7a} = T_{L;a;PH/CH}\ ;\ T_{O;8c} = T_{O;3} = T_{O;\max} \qquad \text{(II. 92)}$$

$$T_{L;9a} = T_{end}\ ;\ T_{O;9a} = T_{end} \qquad \text{(II. 93)}$$

$$\Delta T_{L;8c-9a} = T_{L;9a} - T_{L;8c}\ ;\ \Delta T_{O;8c-9a} = T_{O;9a} - T_{O;8c} \qquad \text{(II. 94)}$$

$$\Delta d_{L;a;8c-9a} = d_{L;a;8c} \cdot \Delta T_{L;8c-9a} \cdot \alpha_L\ ;$$
$$\Delta d_{O;a;8c-9a} = d_{O;a;8c} \cdot \Delta T_{O;8c-9a} \cdot \alpha_O \qquad \text{(II. 95)}$$

$$d_{L;o;9a} = d_{L;o;8c} + \Delta d_{L;a;8c-9a}\ ;\ d_{L;a;9a} = d_{L;a;8c} + \Delta d_{L;a;8c-9a}\ ;$$
$$d_{L;i;9a} = d_{L;i;8c} + \Delta d_{L;a;8c-9a} \qquad \text{(II. 96)}$$

$$d_{O;o;9a} = d_{O;o;8c} + \Delta d_{O;a;8c-9a}\ ;\ d_{O;a;9a} = d_{O;a;8c} + \Delta d_{O;a;8c-9a}\ ;$$
$$d_{O;i;9a} = d_{O;i;8c} + \Delta d_{O;a;8c-9a} \qquad \text{(II. 97)}$$

Secondly in step 9b, the liner pipe is assumed to be confined back into the outer pipe, thereby calculating an equilibrium diameter and the related stresses as has been described in step 7. It needs to be checked whether the outer pipe hoop stress in step 9b ($\sigma_{O;h;9b}$) remains below the outer pipe yield stress ($\sigma_{O;y}$).

$$d_{9b}=d_{O;i;9a}+\left(\left(\Delta\sigma_{C;9a-9b}\cdot d_{9b}\right)/\left(2\cdot t_O\cdot E_O\right)\right)\cdot\left(d_{9b}+t_O\right) \quad \text{(II. 98)}$$

$$\Delta\sigma_{C;9a-9b}=\left(-d_{9b}+d_{L;o;9a}\right)\cdot\left(\left(2\cdot t_L\cdot E_L\right)/\left(\left(d_{9b}\right)^2-t_L\cdot d_{9b}\right)\right) \quad \text{(II. 99)}$$

$$d_{O;o;9b}=d_{9b}+2\cdot t_O\ ;\ d_{O;a;9b}=d_{9b}+t_O\ ;\ d_{O;i;9b}=d_{9b} \quad \text{(II. 100)}$$

$$d_{L;o;9b}=d_{9b}\ ;\ d_{L;a;9b}=d_{9b}-t_L\ ;\ d_{L;a;9b}=d_{9b}-2\cdot t_L \quad \text{(II. 101)}$$

$$r_{O;o;9b}=d_{O;o;9b}/2\ ;\ r_{O;a;9b}=d_{O;a;9b}/2\ ;\ r_{O;i;9b}=d_{O;i;9b}/2 \quad \text{(II. 102)}$$

$$r_{L;o;9b}=d_{L;o;9b}/2\ ;\ r_{L;a;9b}=d_{L;a;9b}/2\ ;\ r_{L;i;9b}=d_{L;i;9b}/2 \quad \text{(II. 103)}$$

$$\Delta r_{O;a;8c-9b}=r_{O;a;9b}-r_{O;a;8c}\ ;\ \Delta r_{L;a;8c-9b}=r_{L;a;9b}-r_{L;a;8c} \quad \text{(II. 104)}$$

$$\Delta\sigma_{O;h;8c-9b}=\left(\left(\Delta\sigma_{C;9a-9b}\cdot d_{9b}\right)/2\cdot t_O\right)\ ;$$
$$\Delta\sigma_{L;h;8c-9b}=-\left(\left(\Delta\sigma_{C;9a-9b}\cdot d_{9b}\right)/2\cdot t_L\right) \quad \text{(II. 105)}$$

$$\sigma_{O;h;9b}=\sigma_{O;h;8c}+\Delta\sigma_{O;h;8c-9b}\ ;\ \sigma_{L;h;9b}=\sigma_{L;h;8c}+\Delta\sigma_{L;h;8c-9b} \quad \text{(II. 106)}$$

$$IF\sigma_{L;h;9b}\rangle-\sigma_{L;y}THEN\sigma_{L;h;9b};ELSE-\sigma_{L;y} \quad \text{(II. 107)}$$

$$\sigma_{O;h;9b}=\left(\sigma_{L;h;9b}\cdot t_L\right)/\left(t_O\right) \quad \text{(II. 108)}$$

II.11 Step 10: Final Cooling down of the Liner Pipe and the Outer Pipe

In step 10 the liner pipe and the outer pipe cool down to environmental temperature. Firstly in step 10a the liner pipe and the outer pipe are assumed to cool down to the environmental temperature separately from each other.

$$T_{L;9b}=T_{end}\ ;\ T_{O;9b}=T_{end} \quad \text{(II. 109)}$$

$$T_{L;10a}=T_{environment}\ ;\ T_{O;10a}=T_{environment} \quad \text{(II. 110)}$$

$$\Delta T_{L;9b-10a}=T_{L;10a}-T_{L;9b}\ ;\ \Delta T_{O;9b-10a}=T_{O;10a}-T_{O;9b} \quad \text{(II. 111)}$$

$$\Delta d_{L;a;9b-10a}=d_{L;a;9b}\cdot\Delta T_{L;9b-10a}\cdot\alpha_L\ ;$$
$$\Delta d_{O;a;9b-10a}=d_{O;a;9b}\cdot\Delta T_{O;9b-10a}\cdot\alpha_O \quad \text{(II. 112)}$$

$$d_{L;o;10a}=d_{L;o;9b}+\Delta d_{L;a;9b-10a}\ ;\ d_{L;a;10a}=d_{L;a;9b}+\Delta d_{L;a;9b-10a}\ ;$$
$$d_{L;i;10a}=d_{L;i;9b}+\Delta d_{L;a;9b-10a} \quad \text{(II. 113)}$$

$$d_{O;o;10a} = d_{O;o;9b} + \Delta d_{O;a;9b-10a}\ ;\ d_{O;a;10a} = d_{O;a;9b} + \Delta d_{O;a;9b-10a}\ ;\ d_{O;i;10a} = d_{O;i;9b} + \Delta d_{O;a;9b-10a} \quad \text{(II. 114)}$$

Secondly in step 10b, the liner pipe is assumed to be confined back into the outer pipe. Calculations are identical as in step 7.

$$d_{10b} = d_{O;i;10a} + \left(\left(\Delta\sigma_{C;10a-10b} \cdot d_{10b}\right) / (2 \cdot t_O \cdot E_O)\right) \cdot (d_{10b} + t_O) \quad \text{(II. 115)}$$

$$\Delta\sigma_{C;10a-10b} = \left(-d_{10b} + d_{L;o;10a}\right) \cdot \left((2 \cdot t_L \cdot E_L) \Big/ \left((d_{10b})^2 - t_L \cdot d_{10b}\right)\right) \quad \text{(II. 116)}$$

$$d_{O;o;10b} = d_{10b} + 2 \cdot t_O\ ;\ d_{O;a;10b} = d_{10b} + t_O\ ;\ d_{O;i;10b} = d_{10b} \quad \text{(II. 117)}$$

$$d_{L;o;10b} = d_{10b}\ ;\ d_{L;a;10b} = d_{10b} - t_L\ ;\ d_{L;a;10b} = d_{10b} - 2 \cdot t_L \quad \text{(II. 118)}$$

$$r_{O;o;10b} = d_{O;o;10b}/2\ ;\ r_{O;a;10b} = d_{O;a;10b}/2\ ;\ r_{O;i;10b} = d_{O;i;10b}/2 \quad \text{(II. 119)}$$

$$r_{L;o;10b} = d_{L;o;10b}/2\ ;\ r_{L;a;10b} = d_{L;a;10b}/2\ ;\ r_{L;i;10b} = d_{L;i;10b}/2 \quad \text{(II. 120)}$$

$$\Delta r_{O;a;9b-10b} = r_{O;a;10b} - r_{O;a;9b}\ ;\ \Delta r_{L;a;9b-10b} = r_{L;a;10b} - r_{L;a;9b} \quad \text{(II. 121)}$$

$$\Delta\sigma_{O;h;9b-10b} = \left(\left(\Delta\sigma_{C;10a-10b} \cdot d_{10b}\right) / 2 \cdot t_O\right)\ ;\ \Delta\sigma_{L;h;9b-10b} = -\left(\left(\Delta\sigma_{C;10a-10b} \cdot d_{10b}\right) / 2 \cdot t_L\right) \quad \text{(II. 122)}$$

$$\sigma_{O;h;10b} = \sigma_{O;h;9b} + \Delta\sigma_{O;h;9b-10b}\ ;\ \sigma_{L;h;10b} = \sigma_{L;h;9b} + \Delta\sigma_{L;h;9b-10b} \quad \text{(II. 123)}$$

$$\sigma_{O;h;10b} = \left(\sigma_{L;h;10b} \cdot t_L\right) / (t_O) \quad \text{(II. 124)}$$

Using this model the residual liner pipe hoop stress in the outer pipe ($\sigma_{O;h;10b}$) and the residual liner pipe hoop stress in the liner pipe ($\sigma_{L;h;10b}$) can be determined.

II.12 Material Properties of the Liner Pipes

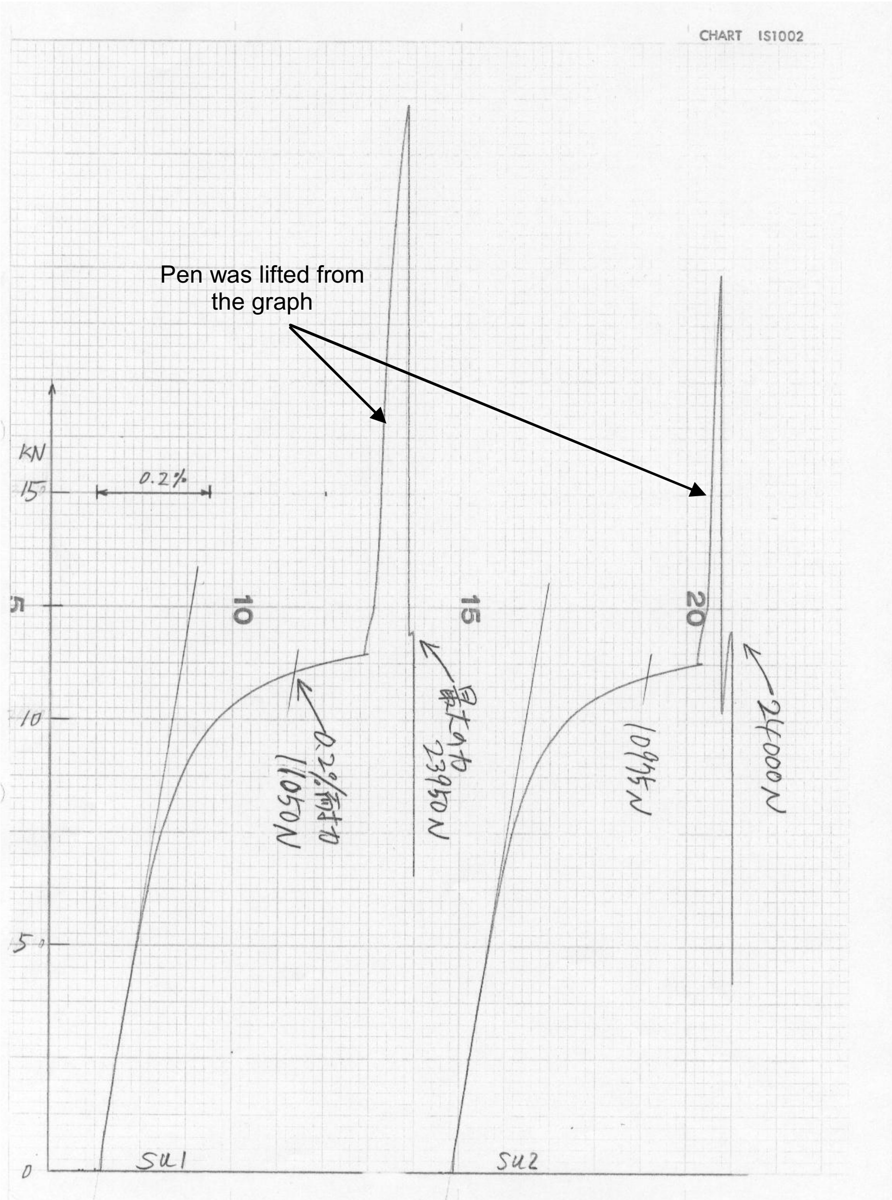

Figure II. 1 Tensile test results for 1.97 x 19.08 mm SUS304 specimen (test case 1)

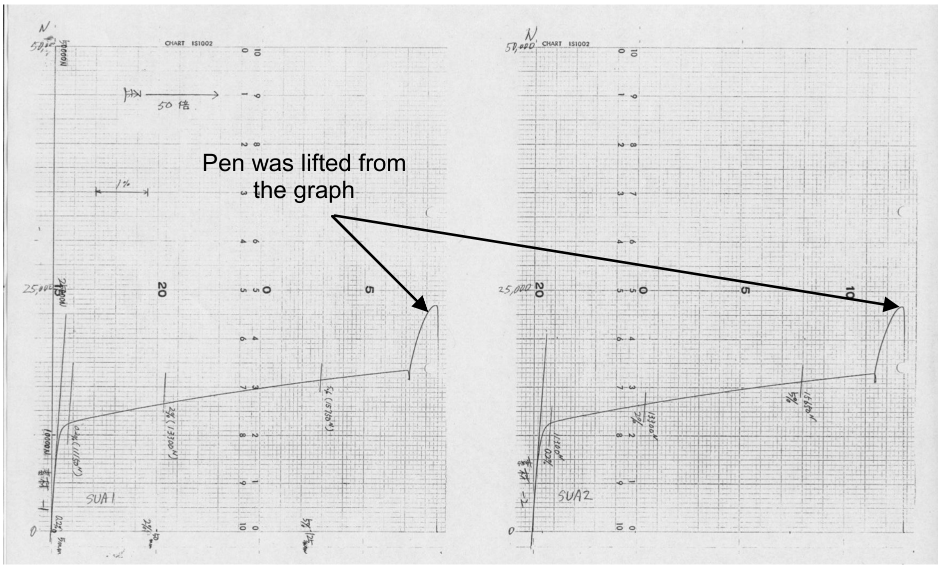

Figure II. 2 Tensile test results for 1.60 x 20.01 mm UNS N08825 specimen (test case 3)

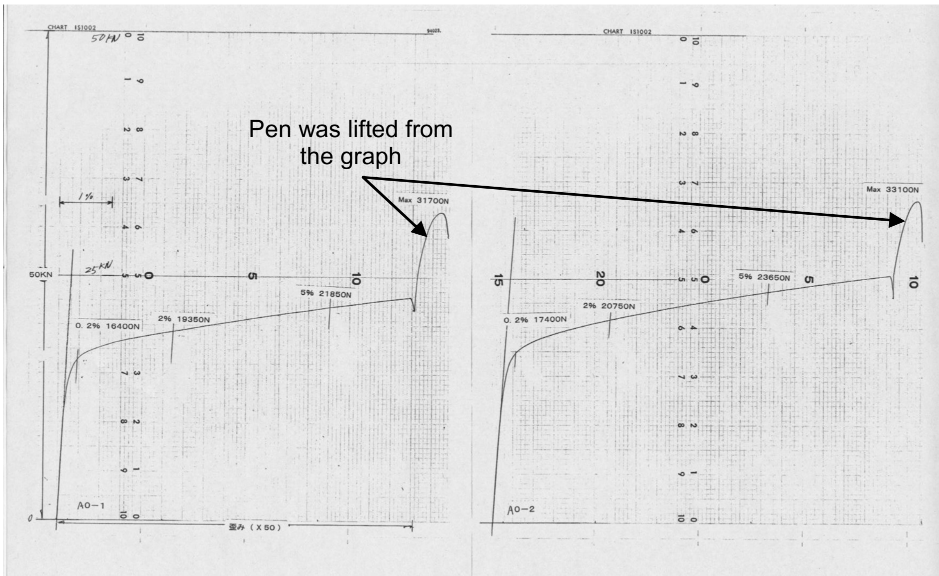

Figure II. 3 Tensile test results for 2.09 x 19.12 mm UNS N08031 specimen (test case 4)

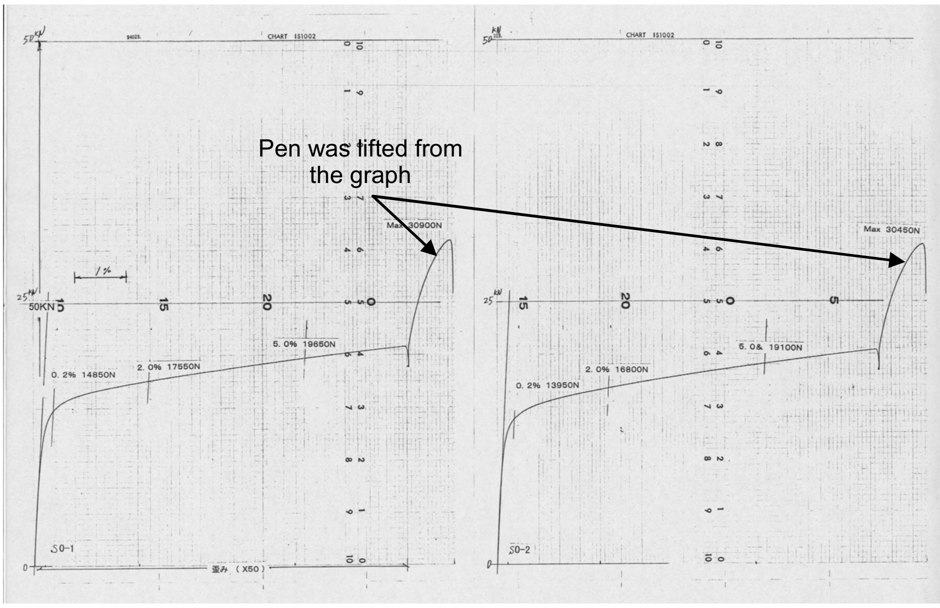

Figure II. 4 Tensile test results for 2.52 x 19.13 mm UNS N08031 specimen (test case 5 and 6)

Appendix III
Properties of the Available Pipes

Figure III. 1 and Figure III. 2 show the stress strain diagrams in axial and hoop direction of the liner pipes and the outer pipes of the ORANGE and GREEN Tight Fit Pipes.

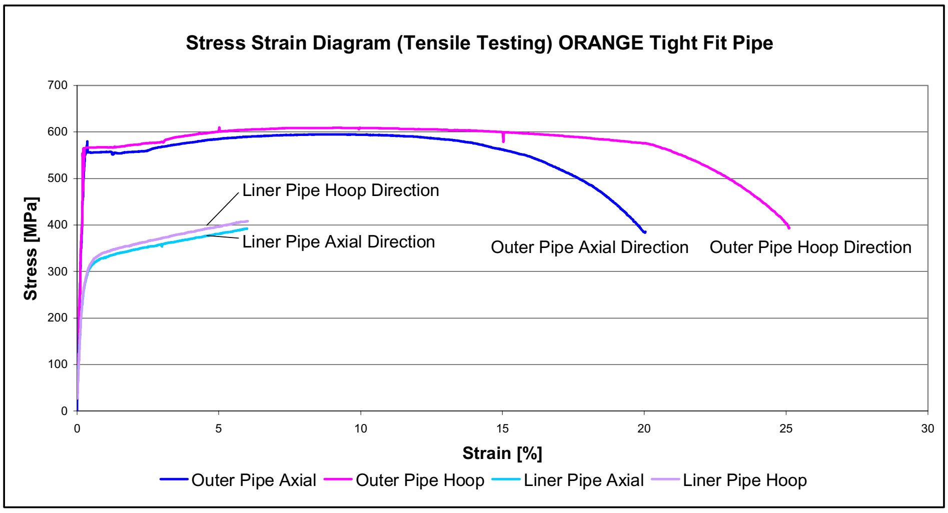

Figure III. 1 Stress strain diagrams of the 316L liner pipe and the X65 outer pipe of the ORANGE Tight Fit Pipe

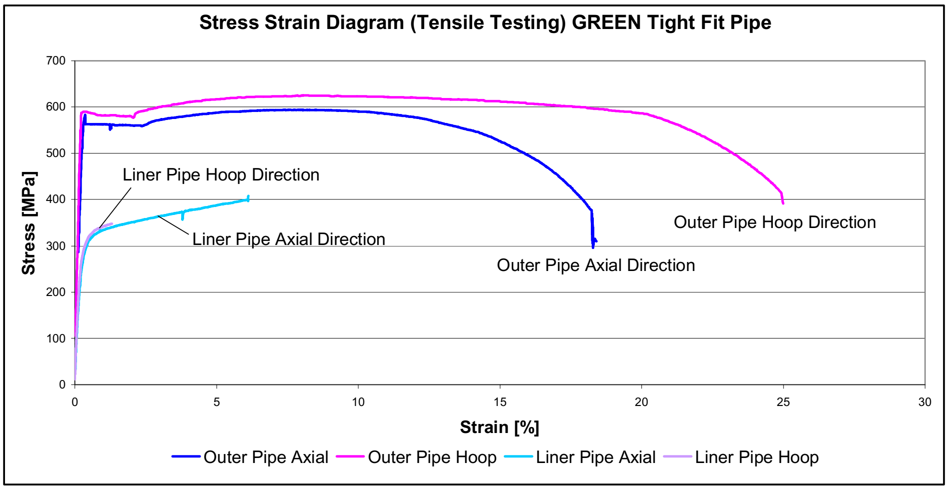

Figure III. 2 Stress strain diagram of the 316L liner pipe and the X65 outer pipe of the GREEN Tight Fit Pipe

In Figure III. 3 below the stress strain diagrams of the liner pipe and the outer pipe of the WHITE Tight Fit Pipe can be found in axial direction.

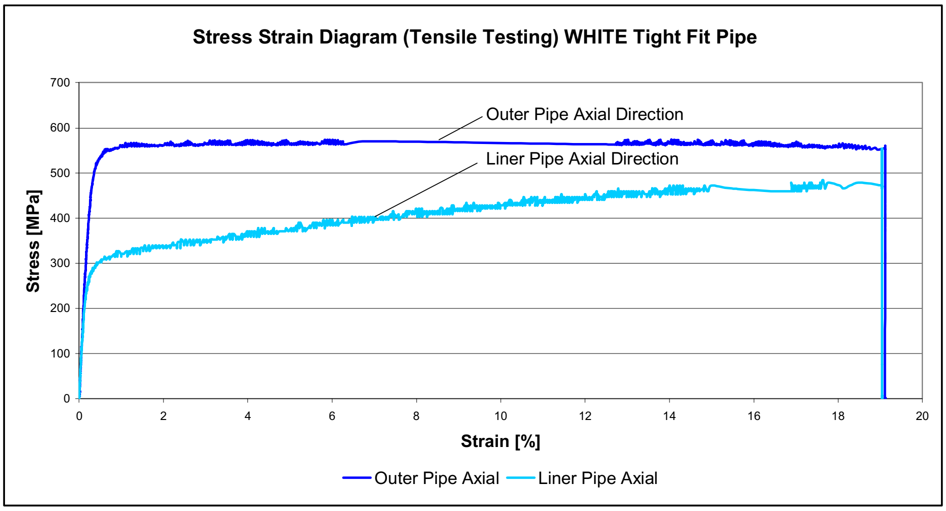

Figure III. 3 Stress strain diagram of the 316L liner pipe and the X65 outer pipe of the WHITE Tight Fit Pipe

In Figure III. 4 below the stress strain diagrams for the single walled pipes TEST-1 and TEST-2 can be found in axial and hoop direction.

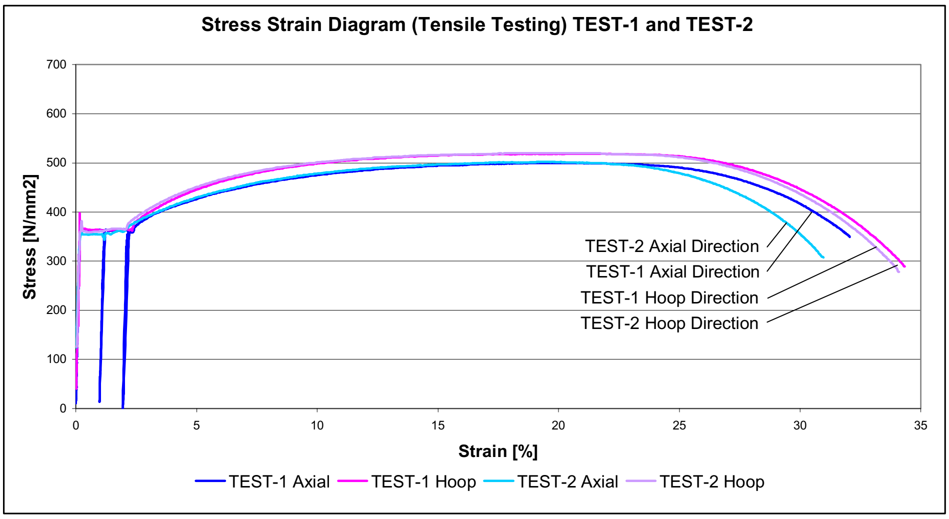

Figure III. 4 Stress strain diagrams in axial and hoop direction of TEST-1 and TEST-2

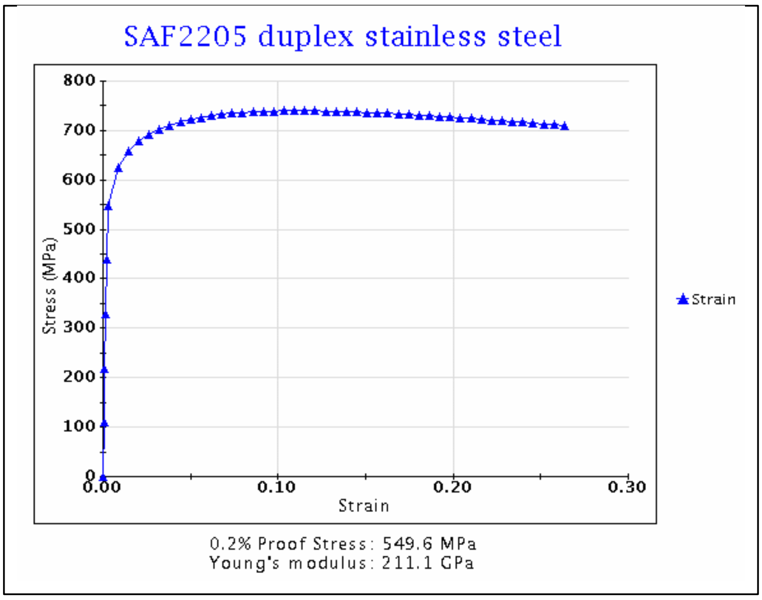

Figure III. 5 An example of a stress strain diagram of duplex [66]

Appendix IV
Detailed Information of Tests on 12.75 Inch Tight Fit Pipe

IV.1 Specification of the Laser Trolley

A laser trolley was developed to measure the internal diameter and ovalisation of the pipe in straight form and in bent form, during and after bending the pipe to the reel. The device consisted of three motors, a laser that measured distance, an angle meter and two acceleration meters (Figure IV. 1). Furthermore the laser trolley was connected to an external treaded displacement meter.

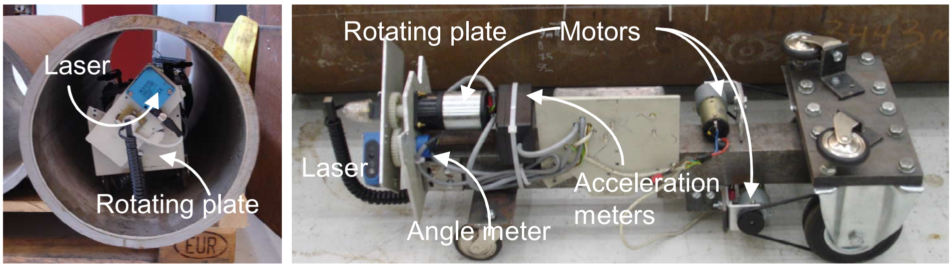

Figure IV. 1 Laser trolley measuring Tight Fit Pipe liner pipe wrinkling and ovalisation

Two motors were connected to the two rear wheels moving the device through the pipe. The third motor was located at the front to rotate a plate on which the laser was mounted. The rotation was such that, when the laser rotated, it exactly scanned a cross-section of the inside of the pipe. It was thus possible to determine the distance from the inside of the pipe wall to the centre of the pipe.

Coupled to the rotating plate was the angle meter that measured the angle of the laser in relation to the laser trolley itself. In order to determine the radial location of the spot where the laser touched the inside of the pipe wall, it was also necessary to determine the exact location of the laser trolley itself in relation to the pipe, or in other words, in relation to the surrounding world. The laser trolley did not only move in axial direction along the pipe, but it was also possible that the trolley rotated inside the pipe. Axial and radial displacement of the laser trolley had to be taken into account.

The location in the axial direction of the laser trolley (i.e. the movement of the laser trolley into the pipe) was determined by the external threaded displacement meter. The thread of the sensor was attached to the laser trolley, while the sensor itself was attached to a fixed object located in front of the pipe.

The rotation of the laser trolley was determined using two acceleration meters. The first acceleration meter was located such that when the laser trolley was positioned horizontally, it measured the acceleration of the earth (9.81 m/s^2). The other acceleration meter was positioned under an angle of 90 degrees and measured 0 m/s^2 acceleration under these circumstances. When the laser trolley rotated the first acceleration meter measured less than 9.81 m/s^2 while the second acceleration meter measured more than 0 m/s^2 acceleration. From the ratio of the output of these two acceleration meters, the exact rotation of the laser trolley was determined.

All measured signals (distance of the laser to the inside of the pipe wall, laser angle, both the acceleration meters and the axial displacement of the laser trolley) were sent to the computer by cable. The software calculated the rotation of the laser trolley from the data coming from the acceleration meters and used this as a correction on the laser angle. The centre of the rotating plate would in most cases not be identical to the centre of the pipe that was measured. This caused the signal of the laser, measuring a perfect round pipe, not to have a constant value, but more of a sinusoidal from. To correct this, the software determined the position of the laser in relation to the centre of the pipe (i.e. the offset in relation to the centre of the pipe) from all measured data during a complete rotation of the laser. Using this offset, the measured data from the laser (distance of the laser to the inside of the pipe wall and the laser angle) was corrected.

The two motors which moved the laser trolley into the pipe in axial direction were also operated by the software using a PI operational device. The set point for this device came from the software which followed a grid. The feedback came from the threaded displacement meter which measured the exact position of the laser trolley in axial direction. It was possible to position the trolley at any location within the measuring range. The motor causing the rotation of the laser was also operated by the software based on a speed of several degrees per second. The feedback came from the angle meter of the laser. The software defined 720 measurements per complete rotation of 360 degrees, i.e. one measurement per half degree. When the rotational speed of the laser was low, more measurements were taken within the half degree. In this case an average was calculated from these measurements. This provided an improvement of the surrounding noise. When the rotational speed of the laser was high, it was possible that there were locations without a measurement. In that case the software interpolated between the surrounding measurements. A good compromise between speed and quality was chosen.

In order to measure the interior of a pipeline, the laser was located at the beginning of the test region. After entering the name of the file and the length of the test region, the measuring process could begin. The software then took over the complete operation of the laser trolley and allowed the laser to make a complete rotation of 360 degrees and then stopped. The measured data was saved. The laser trolley subsequently moved over the defined interval (e.g. 20 mm) to the next location and stopped there. The measuring process was started again by rotating the laser one complete cycle of 360 degrees. This process was continued until the end of test region was reached.

IV.2 Dimensions of the Full Scale Bending Rig and the Tight Fit Pipe Test Pipe Lengths

Dimensions of the full scale bending rig and lengths of the 12.75 inch outer diameter Tight Fit Pipe in the bending rig can be found in the tables below. The 12.75 inch Tight Fit Pipe has a 3 mm thick, 316L liner pipe and a 14.3 mm thick, X65 outer pipe.

Table IV. 1 Overview of the dimensions in the bending rig for the Tight Fit Pipe test pieces without a Tight Fit Pipe circumferential weld

	OR-2	GR-1	GR-2	WT-1	WT-2
L_{TFP} [mm]	3420	3432	3433	3420	3420
$L_{weld\ TFP\text{-}EP}$ [mm]	19	24	23	22	23
L_{EP} [mm]	2537	2505	2588	2503	2558
$L_{flange\ -\ ICP}$ [mm]	2793	2785	2783	2776	2808
$L_{HC;x}$ [mm]	9638	9630	9628	9621	9653
L_{FP} [mm]	2847	2856	2859	2701	2707
$L_{DM\ axial}$ [mm]	723	693	810	694	722
$L_{LFP\text{-}end}$ [mm]	186	170	229	168	213
$L_{laser\ hole\text{-}weld}$ [mm]	90	84	88	94	97
$L_{HC;y}$ [mm]	8835	8855	8945	8945	8860

Table IV. 2 Overview of the dimensions in the bending rig for the Tight Fit Pipe test pieces with a Tight Fit Pipe circumferential weld

	GR-OR-1	GR-OR-2
L_{TFP} (GREEN TFP) [mm]	1708	1705
$L_{weld\ TFP}$ [mm]	19	21
L_{TFP} (ORANGE TFP) [mm]	1696	1697
$L_{weld\ TFP\text{-}EP}$ [mm]	26	21
L_{EP} [mm]	2573	2536
$L_{flange\ -\ ICP}$ [mm]	2817	2869
$L_{HC;x}$ [mm]	9662	9714
L_{FP} [mm]	2831	2775
$L_{DM\ axial}$ [mm]	725	665
$L_{LFP\text{-}end}$ [mm]	224	186
$L_{laser\ hole\text{-}weld}$ [mm]	141	136
$L_{HC;y}$ [mm]	8830	8825
$L_{HC;y;1}$ [mm]	1000	1000

Table IV. 3 Distances between the connection between the hydraulic cylinder and the re-usable pipe and the strain gauge locations in the compression and tension zone

	OR-2	GR-1	GR-2	WT-1	WT-2	GR-OR-1	GR-OR-2
$L_{HC\text{-}SG1;2}$ [mm]	1000	1000	1000	1000	1000	1000	1000
$L_{HC\text{-}SG3;4}$ [mm]	2000	2000	2000	2000	2000	2000	2000
$L_{HC\text{-}SG5;6}$ [mm]	7597	7595	7590	7595	7601	7590	7593
$L_{HC\text{-}SG7;8}$ [mm]	7937	7934	7945	7943	7940	8039	8037
$L_{HC\text{-}SG9;10}$ [mm]	8285	8273	8293	8267	8281	8487	8480
$L_{HC\text{-}SG11;12}$ [mm]	8617	8611	8615	8607	8621	8530	8530
$L_{HC\text{-}SG13;14}$ [mm]	8960	8952	8952	8953	8969	8545	8545
$L_{HC\text{-}SG15;16}$ [mm]	9302	9291	9297	9286	9299	8564	8560
$L_{HC\text{-}SG17;18}$ [mm]	9638	9780	9780	9771	9776	8574	8574
$L_{HC\text{-}SG19;20}$ [mm]	11367	11361	11361	11347	11348	8590	8590
$L_{HC\text{-}SG21;22}$ [mm]	11867	11861	11861	11847	11848	8631	8640
$L_{HC\text{-}SG23;24}$ [mm]						9100	9085
$L_{HC\text{-}SG25;26}$ [mm]						9531	9527
$L_{HC\text{-}SG27;28}$ [mm]						11354	11349
$L_{HC\text{-}SG29;30}$ [mm]						11854	11849

Table IV. 4 Distances between the connection between the hydraulic cylinder and the re-usable pipe and the legs of curvature meters

	OR-2	GR-1	GR-2	WT-1	WT-2	GR-OR-1	GR-OR-2
$L_{HC\text{-}K1;leg1}$ [mm]	8448	8777	8443	8763	8783	8723	8707
$L_{HC\text{-}K1;leg2}$ [mm]	8788	9120	8785	9106	9125	9066	9049
$L_{HC\text{-}K1;leg3}$ [mm]	9127	9463	9127	9448	9467	9409	9391
	SG11; SG13	SG13; SG15	SG11; SG13	SG13; SG15	SG13; SG15	SG23	SG23
$L_{HC\text{-}K2;leg1}$ [mm]	7422	7764	7417	7754	7765	7655	7682
$L_{HC\text{-}K2;leg2}$ [mm]	7764	8107	7759	8097	8107	7997	8024
$L_{HC\text{-}K2;leg3}$ [mm]	8106	8450	8101	8439	8449	8339	8366
	SG5; SG7	SG7; SG9	SG5; SG7	SG7; SG9	SG7; SG9	SG7	SG7

Table IV. 5 Distances between the hydraulic cylinder connection to the re-usable pipe and the locations of the ovalisation meters

	OR-2	GR-1	GR-2	WT-1	WT-2	GR-OR-1	GR-OR-2
$L_{HC\text{-}H1}$ [mm]	9688	9820	9820	9810	9808	9495	9566
$L_{HC\text{-}H2}$ [mm]	9343	9331	9338	9321	9331	9145	9114
$L_{HC\text{-}H3}$ [mm]	9003	8992	8994	8982	8993	8675	8681
$L_{HC\text{-}H4}$ [mm]	8659	8651	8655	8647	8653	WELD	WELD
$L_{HC\text{-}H5}$ [mm]	8318	8313	8333	8309	8313	8450	8439
$L_{HC\text{-}H6}$ [mm]	7977	7974	7986	7973	7976	8079	8080
$L_{HC\text{-}H7}$ [mm]	7637	7635	7631	7634	7636	7705	7647

Table IV. 6 Distances between the hydraulic cylinder connection to the re-usable pipe and the locations of the ovalisation hand measurements after bending

	OR-2	GR-1	GR-2	WT-1	WT-2	GR-OR-1	GR-OR-2
$L_{HC\text{-}OM1}$ [mm]	9638	9780	9780	9771	9776	2686	2683
$L_{HC\text{-}OM2}$ [mm]	9302	9291	9297	9286	9299	2255	2234
$L_{HC\text{-}OM3}$ [mm]	8960	8952	8952	8953	8969	1786	1796
$L_{HC\text{-}OM4}$ [mm]	8617	8611	8615	8607	8621	1719	1712
$L_{HC\text{-}OM5}$ [mm]	8285	8273	8293	8267	8281	1642	1632
$L_{HC\text{-}OM6}$ [mm]	7937	7934	7945	7943	7940	1194	1199
$L_{HC\text{-}OM7}$ [mm]	7597	7595	7590	7595	7601	745	760

IV.3 Angle ζ_{max}

In the tables below the comparison can be found between the theoretically predicted angle ζ_{max} and measurements for ζ_{max} from the angle meter, the full scale graph and the displacement meter (only for GR-OR-1 and GR-OR-2).

The fact that the experimental data exceeded the theoretical prediction for angle ζ_{max} can be explained by the fact that, in order not to make the calculations unnecessarily complex, the theoretical prediction does not take the bending of the pipe between the reel and the hydraulic cylinder into account. Other discrepancies may be the result of the fact that it was difficult to calibrate the angle meter and to take precise measurements needed to determine ζ_{max} (such as Δx_{max} or $L_{HC;y;1}$) in the “full scale graph” and in the bending rig, taking the size of the full scale bending rig into account.

It should also be taken into account that these differences in angle ζ_{max} do not significantly influence the y-component of the hydraulic cylinder force (approximately 1 %) but they do influence the x-component of the hydraulic cylinder force (approximately 40 %). However, the axial component of the hydraulic cylinder force is small compared to the y-component of the hydraulic cylinder force and is less of importance for the phenomena like ovalisation and local buckling.

Table IV. 7 Comparison of experimental and predicted angle ζ_{max} (OR-2)

Reel [mm]	ζ_{max} AM [rad]	ζ_{max} FSG [rad]	ζ_{max} theory [rad]
9000	0.06	0.06	0.04
8000	0.08	0.08	0.06
7500	0.09	0.09	0.07
7000	0.11	0.10	0.08
6500	0.13	0.12	0.09
6000	0.16	0.15	0.11
5500	0.19	0.17	0.14

Note:
AM: Angle meter
FSG: Full scale graph

Table IV. 8 Comparison of experimental and predicted angle ζ_{max} (GR-1)

Reel [mm]	ζ_{max} AM [rad]	ζ_{max} FSG [rad]	ζ_{max} theory [rad]
5500	0.17	0.15	0.14

Note:
AM: Angle meter
FSG: Full scale graph

Table IV. 9 Comparison of experimental and predicted angle ζ_{max} (GR-2)

Reel [mm]	ζ_{max} AM [rad]	ζ_{max} FSG [rad]	ζ_{max} theory [rad]
9000	0.06	0.05	0.04
8000	0.08	0.06	0.06
7500	0.09	0.07	0.06
7000	0.10	0.09	0.08
6500	0.12	0.10	0.09
6000	0.15	0.12	0.11
5500	0.18	0.15	0.14

Note:
AM: Angle meter
FSG: Full scale graph

Table IV. 10 Comparison of experimental and predicted angle ζ_{max} (WT-1)

Reel [mm]	ζ_{max} AM [rad]	ζ_{max} FSG [rad]	ζ_{max} theory [rad]
9000	0.07	0.06	0.04
8000	0.09	0.08	0.06
7500	0.11	0.09	0.06
7000	0.12	0.10	0.08
6500	0.16	0.12	0.09
6000	0.16	0.14	0.11
5500	0.20	0.17	0.14

Note:
AM: Angle meter
FSG: Full scale graph

Table IV. 11 Comparison of experimental and predicted angle ζ_{max} (WT-2)

Reel [mm]	ζ_{max} AM [rad]	ζ_{max} FSG [rad]	ζ_{max} theory [rad]
9000	0.05	0.05	0.04
8000	0.08	0.07	0.06
7500	0.08	0.08	0.07
7000	0.10	0.10	0.08
6500	0.12	0.12	0.09
6000	0.14	0.14	0.11
5500	0.17	0.16	0.14

Note:
AM: Angle meter
FSG: Full scale graph

Table IV. 12 Comparison of experimental and predicted angle ζ_{max} (GR-OR-1)

Reel [mm]	ζ_{max} AM [rad]	ζ_{max} FSG [rad]	ζ_{max} DM [rad]	ζ_{max} theory [rad]
9000	0.07	0.06	0.06	0.04
8000	0.09	0.07	0.08	0.06
7500	0.09	0.08	0.08	0.07
7000	0.11	0.10	0.09	0.08
6500	0.11	0.11	0.10	0.09
6000	0.14	0.14	-	0.11
5500	0.16	0.17	-	0.14

Note:
AM: Angle meter
FSG: Full scale graph
DM: Displacement meter

Table IV. 13 Comparison of experimental and predicted angle ζ_{max} (GR-OR-2)

Reel [mm]	ζ_{max} AM [rad]	ζ_{max} FSG [rad]	ζ_{max} DM [rad]	ζ_{max} theory [rad]
9000	0.05	0.05	0.05	0.04
8000	0.06	0.07	0.07	0.06
7500	0.07	0.08	0.07	0.07
7000	0.09	0.09	0.08	0.08
6500	0.10	0.11	0.09	0.09
6000	0.12	0.13	0.10	0.11
5500	0.21	0.16	0.15	0.14

Note:
AM: Angle meter
FSG: Full scale graph
DM: Displacement meter

IV.4 Angle β_{max}

In the tables below the comparison can be found between the theoretically predicted angle β_{max} (Figure 5.8) and measurements for β_{max} from full scale graph.

Table IV. 14 Comparison of experimental and predicted angle β_{max} (OR-2)

Reel [mm]	β_{max} FSG [rad]	β_{max} theory [rad]
9000	-	0.27
8000	-	0.30
7500	0.31	0.32
7000	-	0.34
6500	0.40	0.37
6000	0.40	0.40
5500	0.41	0.44

Note:
FSG: Full scale graph

Table IV. 15 Comparison of experimental and predicted angle β_{max} (GR-1 and GR-2)

	GR-1		GR-2	
Reel [mm]	β_{max} FSG [rad]	β_{max} theory [rad]	β_{max} FSG [rad]	β_{max} theory [rad]
9000			0.27	0.27
8000			0.35	0.30
7500			0.34	0.32
7000			0.35	0.34
6500			0.37	0.37
6000			0.41	0.40
5500	0.44	0.44	0.39	0.44

Note:
FSG: Full scale graph

Table IV. 16 Comparison of experimental and predicted angle β_{max} (WT-1 and WT-2)

	WT-1		WT-2	
Reel [mm]	β_{max} FSG [rad]	β_{max} theory [rad]	β_{max} FSG [rad]	β_{max} theory [rad]
9000	0.27	0.27	0.32	0.27
8000	-	0.30	0.34	0.30
7500	0.34	0.32	0.24	0.32
7000	0.40	0.34	0.39	0.34
6500	0.39	0.37	0.41	0.37
6000	0.39	0.40	0.43	0.40
5500	0.47	0.44	-	0.44

Note:
FSG: Full scale graph

Table IV. 17 Comparison of experimental and predicted angle β_{max}
(GR-OR-1 and GR-OR-2)

	GR-OR-1		GR-OR-2	
Reel [mm]	β_{max} FSG [rad]	β_{max} theory [rad]	β_{max} FSG [rad]	β_{max} theory [rad]
9000	0.22	0.27	0.21	0.27
8000	0.22	0.30	0.30	0.30
7500	0.37	0.32	0.30	0.32
7000	0.37	0.34	-	0.34
6500	0.43	0.37	0.38	0.37
6000	0.45	0.40	0.36	0.40
5500	0.47	0.44	0.43	0.44

Note:
FSG: Full scale graph

IV.5 Maximum Bending Strain in Outer Fibre of TFP

In the tables below the comparison can be found between the theoretically predicted global bending strain using Equations (5.16) and (5.17) and measurements from the strain gauges and the curvature meters.

Table IV. 18 Comparison between theory, the bending strain determined by the strain gauges and the bending strain determined by curvature meters (GR-1)

Reel [mm]	$\varepsilon_{b;K1}$ [%]	$\varepsilon_{b;SG13}$ [%]	$\varepsilon_{b;SG15}$ [%]	$\varepsilon_{b;K2}$ [%]	$\varepsilon_{b;SG7}$ [%]	$\varepsilon_{b;SG9}$ [%]	$\varepsilon_{b;SG;average}$ [1] [%]	ε_b theory [%]
5500	-2.85	-2.92	-2.43	-2.77	-2.33	-2.39	-2.61	-2.87%

Note:
1) The average bending strain is determined averaging strain gauges 5, 7, 9, 11, 13 and 15

Table IV. 19 Comparison between theory, the bending strain determined by the strain gauges and the bending strain determined by curvature meters (GR-2)

Reel [mm]	$\varepsilon_{b;K1}$ [%]	$\varepsilon_{b;SG11}$ [%]	$\varepsilon_{b;SG13}$ [%]	$\varepsilon_{b;K2}$ [%]	$\varepsilon_{b;SG5}$ [%]	$\varepsilon_{b;SG7}$ [%]	$\varepsilon_{b;SG;average}$ [1] [%]	ε_b theory [%]
9000	-1.90	-1.50	-1.68	-1.57	-1.49	-1.53	-1.67	-1.77
8000	-2.08	-1.69	-1.84	-1.79	-1.65	-1.74	-1.82	-1.99
7500	-2.26	-1.81	-1.97	-1.92	-1.74	-1.86	-1.92	-2.12
7000	-2.36	-1.91	-2.04	-2.10	-1.82	-2.04	-2.02	-2.27
6500	-2.56	-2.02	-2.24	-2.16	-1.92	-2.10	-2.13	-2.44
6000	-3.01	-2.24	-2.45	-2.50	-1.96	-2.20	-2.28	-2.64
5500	-3.24	-2.40	-2.72	-2.73	-2.18	-2.39	-2.47	-2.87

Note:
1) The average bending strain is determined averaging strain gauges 5, 7, 9, 11 and 13

Table IV. 20 Comparison between theory, the bending strain determined by the strain gauges and the bending strain determined by curvature meters (WT-1)

Reel [mm]	$\varepsilon_{b;K1}$ [%]	$\varepsilon_{b;SG13}$ [%]	$\varepsilon_{b;SG15}$ [%]	$\varepsilon_{b;K2}$ [%]	$\varepsilon_{b;SG7}$ [%]	$\varepsilon_{b;SG9}$ [%]	$\varepsilon_{b;SG;average}$ [1] [%]	ε_b theory [%]
9000	-1.51	-1.61	-1.51	-1.81	-1.56	-2.06	-1.69	-1.77
8000	-1.69	-1.89	-1.70	-2.03	-1.78	-2.26	-1.88	-1.99
7500	-1.86	-2.05	-1.74	-2.11	-1.64	-2.35	-1.95	-2.12
7000	-1.99	-2.16	-1.84	-2.33	-2.05	-2.50	-2.15	-2.27
6500	-2.21	-2.33	-2.06	-2.50	-2.14	-2.75	-2.31	-2.44
6000	-2.22	-2.33	-2.08	-2.51	-2.14	-2.76	-2.32	-2.63
5500	-2.51	-2.56	-2.37	-2.73	-2.34	-2.91	-2.52	-2.87

Note:
1) The average bending strain is determined averaging strain gauges 5, 7, 9, 11, 13 and 15

Table IV. 21 Comparison between theory, the bending strain determined by the strain gauges and the bending strain determined by curvature meters (WT-2)

Reel [mm]	$\varepsilon_{b;K1}$ [%]	$\varepsilon_{b;SG13}$ [%]	$\varepsilon_{b;SG15}$ [%]	$\varepsilon_{b;K2}$ [%]	$\varepsilon_{b;SG7}$ [%]	$\varepsilon_{b;SG9}$ [%]	$\varepsilon_{b;SG;average}$ 1) [%]	ε_b theory [%]
9000	-1.60	-1.64	-1.32	-1.78	-1.55	-1.68	-1.77	-1.77
8000	-1.73	-1.86	-1.66	-2.02	-2.73	-2.76	-1.99	-1.99
7500	-1.88	-2.00	-1.67	-2.08	-2.89	-2.81	-2.12	-2.12
7000	-2.02	-2.08	-1.71	-2.32	-3.11	-2.90	-2.27	-2.27
6500	-2.22	-2.17	-1.95	-2.44	-	-3.04	-2.44	-2.44
6000	-2.39	-2.41	-2.00	-2.66	-	-3.20	-2.63	-2.64
5500	-2.71	-2.64	-2.49	-2.90	-	-3.36	-2.87	-2.87

Note:
1) The average bending strain is determined averaging strain gauges 5, 7, 9, 11, 13 and 15

Table IV. 22 Comparison between theory, the bending strain determined by the strain gauges and the bending strain determined by curvature meters (GR-OR-2)

Reel [mm]	ε_b theory [%]	$\varepsilon_{b;K1}$ [%]	$\varepsilon_{b;SG23}$ [%]	$\varepsilon_{b;K2}$ [%]	$\varepsilon_{b;SG7}$ [%]
9000	-1.77	-1.77	-1.78	-1.71	-1.57
8000	-1.99	-1.89	-1.83	-1.87	-1.67
7500	-2.12	-2.00	-1.94	-1.95	-1.72
7000	-2.27	-2.10	-2.00	-2.15	-1.81
6500	-2.44	-2.27	-2.09	-2.27	-1.90
6000	-2.64	-2.43	-2.24	-2.46	-2.07
5500	-2.87	-2.73	-2.53	-2.84	-2.23

Table IV. 23 Bending strain measured by the strain gauges around the weld (GR-OR-2)

Distance from weld [mm]		80	30	15	WELD	15	30	80
Reel [mm]	ε_b theory [%]	$\varepsilon_{b;SG9}$ [%]	$\varepsilon_{b;SG11}$ [%]	$\varepsilon_{b;SG13}$ [%]	$\varepsilon_{b;SG15}$ [%]	$\varepsilon_{b;SG17}$ [%]	$\varepsilon_{b;SG19}$ [%]	$\varepsilon_{b;SG21}$ [%]
9000	-1.77	-0.89	-1.47	-3.92	-3.05	-2.98	-2.02	-2.29
8000	-1.99	-1.34	-1.59	-4.23	-3.15	-3.10	-2.08	-2.34
7500	-2.12	-1.48	-1.63	-4.35	-3.22	-3.18	-2.11	-2.36
7000	-2.27	-1.70	-1.78	-4.60	-3.37	-3.33	-2.17	-2.41
6500	-2.44	-1.91	-1.88	-5.00	-3.50	-3.50	-2.23	-2.44
6000	-2.64	-2.04	-1.93	-5.26	-3.61	-3.66	-2.31	-2.54
5500	-2.87	-2.18	-1.97	-5.48	-3.71	-3.84	-2.53	-2.67

IV.6 Bending Radius

In the tables below the comparison can be found between the theoretically predicted applied bending radius of the Tight Fit Pipe during testing ($D_{reel}/2 + r_{O;o;TFP}$) and measurements from the curvature meters. Differences between the measured and the predicted bending radius can be explained by the fact that not all Tight Fit Pipes were in complete contact with the reel at maximum bending. Differences can also be explained by the fact that the curvature meters were sometimes positioned to the side of the pipe length in contact with the reel and may have been influenced by the boundary effect that the pipe curved towards the reel.

Table IV. 24 Comparison between the applied bending radius and the bending radius measured by curvature meters K1 and K2 for GR-1 and GR-2

9120	8107	$L_{HC\text{-}Km;leg2}$ [mm]	8785	7759	$L_{HC\text{-}Km;leg2}$ [mm]
$R_{TFP;K1}$ [mm]	$R_{TFP;K2}$ [mm]	R_{TFP} theory [mm]	$R_{TFP;K1}$ [mm]	$R_{TFP;K2}$ [mm]	R_{TFP} theory [mm]
			8542	10320	9162
			7792	9051	8162
			7191	8462	7662
			6880	7746	7162
			6346	7537	6662
			5391	6486	6162
5706	5872	5662	5014	5951	5662

Table IV. 25 Comparison between the applied bending radius and the bending radius measured by curvature meters K1 and K2 for WT-1 and WT-2

9106	8097	$L_{HC\text{-}Km;leg2}$ [mm]	9125	8107	$L_{HC\text{-}Km;leg2}$ [mm]
$R_{TFP;K1}$ [mm]	$R_{TFP;K2}$ [mm]	R_{TFP} theory [mm]	$R_{TFP;K1}$ [mm]	$R_{TFP;K2}$ [mm]	R_{TFP} theory [mm]
10716	8972	9162	10170	9131	9162
9590	7991	8162	9400	8042	8162
8710	7686	7662	8651	7799	7662
8142	6980	7162	8049	7007	7162
7354	6488	6662	7295	6649	6662
7317	6468	6162	6790	6097	6162
6463	5981	5662	5993	5592	5662

Table IV. 26 Comparison between applied bending radius and bending radius measured by curvature meters K1 and K2 for GR-OR-2

9049	8024	$L_{HC\text{-}Km;leg2}$ [mm]
$R_{TFP;K1}$ [mm]	$R_{TFP;K2}$ [mm]	R_{TFP} theory [mm]
9154	9477	9162
8590	8681	8162
8112	8322	7662
7742	7560	7162
7151	7145	6662
6677	6594	6162
5950	5720	5662

IV.7 Position Meters

The tables below indicate which position meters (PM) were in contact with the reel at maximum bending in the bending test: a “1” indicates contact while a “0” indicates the PM was not in contact with the reel

Table IV. 27 Position meters in contact with the reel for GR-1

	PM1	PM2	PM3	PM4	PM5	PM6	PM7	PM8
$L_{HC\text{-}PMn}$ [mm]	9459	9288	8946	8604	8262	7920	7578	7236
5500	1	1	1	1	1	1	1	1

Note:
PM: Position meter

Table IV. 28 Position meters in contact with the reel for GR-2

	PM1	PM2	PM3	PM4	PM5	PM6	PM7	PM8
$L_{HC\text{-}PMn}$ [mm]	9457	9286	8944	8602	8260	7918	7576	7234
9000	1	1	1	0	0	1	1	1
8000	1	1	1	0	0	1	1	1
7500	1	1	1	0	0	0	1	1
7000	1	1	1	0	0	0	1	1
6500	1	1	1	1	1	1	1	1
6000	1	1	0	0	0	1	1	1
5500	1	1	1	0	0	1	1	1

Note:
PM: Position meter

Table IV. 29 Position meters in contact with the reel for WT-1

	PM1	PM2	PM3	PM4	PM5	PM6	PM7	PM8
$L_{HC\text{-}PMn}$ [mm]	9450	9279	8937	8595	8253	7911	7569	7227
9000	1	1	1	1	1	1	1	1
8000	1	1	1	1	1	1	1	1
7500	1	1	1	1	1	1	1	1
7000	1	1	1	1	1	1	1	1
6500	1	1	1	1	1	1	1	1
6000	1	1	1	1	1	1	1	1
5500	1	1	1	1	1	1	1	1

Note:
PM: Position meter

Table IV. 30 Position meters in contact with the reel for WT-2

	PM1	PM2	PM3	PM4	PM5	PM6	PM7	PM8
$L_{HC\text{-}PMn}$ [mm]	9482	9311	8969	8627	8285	7943	7601	7259
9000	1	1	1	1	1	1	1	1
8000	1	1	1	1	1	1	1	1
7500	1	1	1	1	1	1	1	1
7000	1	1	1	1	1	1	1	1
6500	1	1	1	1	1	1	1	1
6000	1	1	1	1	1	1	1	1
5500	1	1	1	1	1	1	1	1

Note:
PM: Position meter

Table IV. 31 Position meters in contact with the reel for GR-OR-2

	PM1	PM2	PM3	PM4	PM5	PM6	PM7	PM8
$L_{HC\text{-}PMn}$ [mm]	9524	9353	9135	8705	8548	8128	7643	7301
9000	1	1	1	1	1	1	1	1
8000	1	1	1	1	1	1	1	1
7500	1	1	1	1	1	1	1	1
7000	1	1	1	0	1	1	1	1
6500	1	1	1	1	1	1	1	1
6000	1	1	1	1	1	1	1	1
5500	1	1	1	1	1	1	1	1

Note:
PM: Position meter

IV.8 Ovalisation

VI.8.1 Ovalisation after Bending

It should be noted that the average values for ovalisation after bending for Tight Fit Pipes OR-2, GR-1, GR-2, WT-1 and WT-2 (Tight Fit Pipes with no Tight Fit Pipe circumferential weld) are determined only using values at locations 3, 4, 5 and 6 (Figure 7.7). Ovalisation values at these locations are more or less the same. Average values for ovalisation after bending for GR-OR-1 and GR-OR-2 (Tight Fit Pipes with a Tight Fit Pipe circumferential weld) are determined using measurements from locations 2, 3, 5 and 6 (Figure 7.9). Values for ovalisation at these locations are also more or less the same. Values at the other locations (locations 1, 2 and 7 for the Tight Fit Pipes with no Tight Fit Pipe circumferential weld and locations 1, 4 and 7 for the Tight Fit Pipes with a Tight Fit Pipe circumferential weld) are affected by boundary conditions and are not taken into account. It should also be take into account that the ovalisation meter can only measure the increase in diameter in the vertical plane. As has been explained in Subsection 6.2.2 a procedure has been developed to calculate the ovalisation from the ovalisation meter measurements.

Table IV. 32 Ovalisation after bending measured by hand (OR-2)

Reel [mm]	BB	9000	8000	7500	7000	6500	6000	5500
f_{H1} [%]	-0.09	-0.18	0.00	0.18	0.83	0.65	0.37	1.58
f_{H2} [%]	-0.14	1.08	2.09	2.31	2.95	3.35	3.55	4.69
f_{H3} [%]	-0.15	1.94	2.54	2.71	3.23	3.69	4.05	5.17
f_{H4} [%]	-0.09	1.63	2.17	2.40	2.92	3.51	4.35	4.98
f_{H5} [%]	-0.09	1.94	2.28	2.40	3.02	3.51	4.20	4.92
f_{H6} [%]	-0.05	1.45	2.35	2.62	3.05	3.38	4.05	4.71
f_{H7} [%]	-0.12	1.51	2.08	2.03	2.83	3.08	3.48	4.12
$f_{H;average}$ [%]	-0.10	1.74	2.33	2.53	3.05	3.52	4.16	4.95

Table IV. 33 Ratio of the change in diameter in the horizontal plane to the change in diameter in the vertical plane measured by hand after bending (OR-2)

Reel [mm]	9000	8000	7500	7000	6500	6000	5500
$\Delta d_{O;o;TFP;hor}/\Delta d_{O;o;TFP;ver}$ (H1)	0.95	-1.00	-85.00	0.35	4.35	-12.20	1.03
$\Delta d_{O;o;TFP;hor}/\Delta d_{O;o;TFP;ver}$ (H2)	0.85	2.17	2.01	1.67	2.12	2.01	1.88
$\Delta d_{O;o;TFP;hor}/\Delta d_{O;o;TFP;ver}$ (H3)	2.51	1.71	2.27	1.77	1.80	1.89	1.76
$\Delta d_{O;o;TFP;hor}/\Delta d_{O;o;TFP;ver}$ (H4)	2.81	1.67	1.79	1.57	1.60	1.58	1.59
$\Delta d_{O;o;TFP;hor}/\Delta d_{O;o;TFP;ver}$ (H5)	1.63	1.75	2.26	1.58	1.54	1.63	1.54
$\Delta d_{O;o;TFP;hor}/\Delta d_{O;o;TFP;ver}$ (H6)	1.78	1.60	1.84	1.83	1.75	1.61	1.66
$\Delta d_{O;o;TFP;hor}/\Delta d_{O;o;TFP;ver}$ (H7)	2.28	1.88	2.31	1.43	1.57	1.90	1.61
$\Delta d_{O;o;TFP;hor}/\Delta d_{O;o;TFP;ver}$ (average)	2.18	1.68	2.04	1.69	1.67	1.68	1.64

Table IV. 34 Ovalisation after bending measured by ovalisation meter (OR-2)

Reel [mm]	9000	8000	7500	7000	6500	6000	5500
$f_{OM1;AB}$ [%]	0.05	0.00	-10.89	0.34	2.07	-5.27	-
$f_{OM2;AB}$ [%]	1.39	2.91	3.05	3.18	4.61	4.79	-
$f_{OM3;AB}$ [%]	2.33	2.22	3.34	3.23	4.04	4.98	-
$f_{OM4;AB}$ [%]	1.83	1.56	1.87	2.06	2.61	3.53	4.29
$f_{OM5;AB}$ [%]	1.85	2.48	3.25	3.11	3.47	4.46	-
$f_{OM6;AB}$ [%]	1.44	2.07	2.61	3.50	3.77	4.26	-
$f_{OM7;AB}$ [%]	1.79	2.12	2.62	2.50	2.94	3.90	-
$f_{OM;average;AB}$ [%]	1.86	2.08	2.77	2.97	3.47	4.31	4.29

Table IV. 35 Ovalisation after bending measured by hand and by ovalisation meter and the ratio of the change in diameter in the horizontal plane to the change in diameter in the vertical plane measured by hand after bending (GR-1)

Reel [mm]	BB	5500	Reel [mm]	5500	Reel [mm]	5500
f_{H1} [%]	-0.20	0.42	$f_{OM1;AB}$ [%]	0.51	$\Delta d_{O;o;TFP;hor}/\Delta d_{O;o;TFP;ver}$ (H1)	0.79
f_{H2} [%]	0.02	4.19	$f_{OM2;AB}$ [%]	4.79	$\Delta d_{O;o;TFP;hor}/\Delta d_{O;o;TFP;ver}$ (H2)	1.52
f_{H3} [%]	-0.15	5.14	$f_{OM3;AB}$ [%]	5.99	$\Delta d_{O;o;TFP;hor}/\Delta d_{O;o;TFP;ver}$ (H3)	1.67
f_{H4} [%]	-0.08	5.20	$f_{OM4;AB}$ [%]	4.36	$\Delta d_{O;o;TFP;hor}/\Delta d_{O;o;TFP;ver}$ (H4)	1.58
f_{H5} [%]	-0.15	4.89	$f_{OM5;AB}$ [%]	5.28	$\Delta d_{O;o;TFP;hor}/\Delta d_{O;o;TFP;ver}$ (H5)	1.58
f_{H6} [%]	-0.18	4.74	$f_{OM6;AB}$ [%]	5.39	$\Delta d_{O;o;TFP;hor}/\Delta d_{O;o;TFP;ver}$ (H6)	1.68
f_{H7} [%]	-0.15	3.72	$f_{OM7;AB}$ [%]	4.07	$\Delta d_{O;o;TFP;hor}/\Delta d_{O;o;TFP;ver}$ (H7)	1.78
$f_{H;average}$ [%]	-0.14	4.99	$f_{OM;average;AB}$ [%]	5.26	$\Delta d_{O;o;TFP;hor}/\Delta d_{O;o;TFP;ver}$ (average)	1.63

Table IV. 36 Ovalisation after bending measured by hand (GR-2)

Reel [mm]	BB	9000	8000	7500	7000	6500	6000	5500
f_{H1} [%]	-0.17	-0.05	0.00	0.09	0.22	0.40	0.40	0.38
f_{H2} [%]	-0.14	2.02	2.20	2.76	3.11	3.76	4.16	4.96
f_{H3} [%]	-0.03	2.19	2.62	3.14	3.37	4.09	4.56	5.59
f_{H4} [%]	-0.09	2.26	2.54	2.86	3.26	3.97	4.63	5.43
f_{H5} [%]	-0.02	2.32	2.46	3.42	3.49	3.82	5.17	5.57
f_{H6} [%]	-0.15	2.34	2.51	3.06	3.52	3.71	4.23	5.43
f_{H7} [%]	-0.15	1.72	2.29	2.49	2.89	3.20	3.39	4.40
$f_{H;average}$ [%]	-0.07	2.28	2.53	3.12	3.41	3.90	4.65	5.51

Table IV. 37 Ratio of the change in diameter in the horizontal plane to the change in diameter in the vertical plane measured by hand after bending (GR-2)

Reel [mm]	9000	8000	7500	7000	6500	6000	5500
$\Delta d_{O;o;TFP;hor}/\Delta d_{O;o;TFP;ver}$ (H1)	-0.26	-1.00	0.22	1.84	1.01	1.91	2.15
$\Delta d_{O;o;TFP;hor}/\Delta d_{O;o;TFP;ver}$ (H2)	1.57	2.11	1.72	1.59	1.68	1.62	1.58
$\Delta d_{O;o;TFP;hor}/\Delta d_{O;o;TFP;ver}$ (H3)	1.59	1.62	1.65	1.64	1.49	1.58	1.42
$\Delta d_{O;o;TFP;hor}/\Delta d_{O;o;TFP;ver}$ (H4)	1.34	1.23	1.70	1.62	1.33	1.32	1.29
$\Delta d_{O;o;TFP;hor}/\Delta d_{O;o;TFP;ver}$ (H5)	1.22	1.32	1.39	1.58	1.67	1.20	1.37
$\Delta d_{O;o;TFP;hor}/\Delta d_{O;o;TFP;ver}$ (H6)	1.21	1.77	1.49	1.49	1.57	1.33	1.25
$\Delta d_{O;o;TFP;hor}/\Delta d_{O;o;TFP;ver}$ (H7)	1.49	1.57	1.57	1.65	1.51	1.59	1.25
$\Delta d_{O;o;TFP;hor}/\Delta d_{O;o;TFP;ver}$ (average)	1.34	1.48	1.56	1.58	1.51	1.36	1.33

Table IV. 38 Ovalisation after bending measured by OM (GR-2)

Reel [mm]	9000	8000	7500	7000	6500	6000	5500
$f_{OM1;AB}$ [%]	0.04	0.00	0.21	0.63	0.57	1.00	1.21
$f_{OM2\,;AB}$ [%]	2.40	3.40	3.26	3.49	4.37	4.60	5.58
$f_{OM3;AB}$ [%]	2.22	2.73	3.28	3.56	4.09	4.89	5.64
$f_{OM4;AB}$ [%]	1.52	1.88	2.64	2.78	2.84	3.57	4.02
$f_{OM5;AB}$ [%]	1.97	2.58	3.07	3.79	4.31	4.40	5.38
$f_{OM6;AB}$ [%]	1.78	2.92	2.95	3.53	3.92	4.09	4.70
$f_{OM7;AB}$ [%]	1.67	2.24	2.55	3.10	3.10	3.67	3.79
$f_{OM;average;AB}$ [%]	1.87	2.53	2.98	3.41	3.79	4.24	4.93

Table IV. 39 Ovalisation after bending measured by hand (WT-1)

Reel [mm]	BB	9000	8000	7500	7000	6500	6000	5500
f_{H1} [%]	0.14	0.00	0.15	0.37	0.25	0.48	0.65	1.00
f_{H2} [%]	0.12	2.13	2.62	3.00	3.20	4.02	4.36	5.21
f_{H3} [%]	0.14	2.31	3.08	3.39	3.81	4.28	4.98	5.85
f_{H4} [%]	0.09	2.05	2.76	2.93	3.54	4.13	4.47	6.27
f_{H5} [%]	0.17	2.03	2.56	2.60	3.03	3.76	4.44	5.48
f_{H6} [%]	0.18	1.46	2.30	2.40	3.11	3.36	4.31	5.16
f_{H7} [%]	0.28	1.59	1.88	2.22	3.02	3.33	3.53	4.67
$f_{H;average}$ [%]	0.15	1.96	2.67	2.83	3.37	3.88	4.55	5.69

Table IV. 40 Ratio of the change in diameter in the horizontal plane to the change in diameter in the vertical plane measured by hand after bending (WT-1)

Reel [mm]	9000	8000	7500	7000	6500	6000	5500
$\Delta d_{O;o;TFP;hor}/\Delta d_{O;o;TFP;ver}$ (H1)	-1.00	0.12	0.86	-0.24	1.84	1.01	0.67
$\Delta d_{O;o;TFP;hor}/\Delta d_{O;o;TFP;ver}$ (H2)	1.47	1.40	1.44	1.51	1.46	1.55	1.43
$\Delta d_{O;o;TFP;hor}/\Delta d_{O;o;TFP;ver}$ (H3)	1.38	1.25	1.53	1.47	1.55	1.41	1.39
$\Delta d_{O;o;TFP;hor}/\Delta d_{O;o;TFP;ver}$ (H4)	1.51	1.24	1.41	1.21	1.46	1.48	0.93
$\Delta d_{O;o;TFP;hor}/\Delta d_{O;o;TFP;ver}$ (H5)	1.28	1.22	1.45	1.38	1.37	1.32	1.12
$\Delta d_{O;o;TFP;hor}/\Delta d_{O;o;TFP;ver}$ (H6)	1.32	1.49	1.65	1.27	1.51	1.21	1.12
$\Delta d_{O;o;TFP;hor}/\Delta d_{O;o;TFP;ver}$ (H7)	1.34	0.94	1.40	1.45	1.43	1.44	1.01
$\Delta d_{O;o;TFP;hor}/\Delta d_{O;o;TFP;ver}$ (average)	1.37	1.30	1.51	1.33	1.47	1.36	1.14

Table IV. 41 Ovalisation after bending measured by OM (WT-1)

Reel [mm]	9000	8000	7500	7000	6500	6000	5500
$f_{OM1;AB}$ [%]	0.00	0.07	0.18	0.14	0.75	0.55	0.63
$f_{OM2\ ;AB}$ [%]	2.22	2.58	2.91	3.44	4.02	4.24	5.10
$f_{OM3;AB}$ [%]	2.40	2.63	3.45	3.70	4.42	4.22	5.36
$f_{OM4;AB}$ [%]	1.41	1.64	1.94	2.04	2.73	2.77	2.71
$f_{OM5;AB}$ [%]	1.76	2.16	2.66	2.93	3.65	3.63	3.96
$f_{OM6;AB}$ [%]	1.36	1.97	2.38	2.57	3.28	2.92	3.47
$f_{OM7;AB}$ [%]	1.48	1.70	2.22	3.00	3.26	3.30	3.07
$f_{OM;average;AB}$ [%]	1.73	2.10	2.61	2.81	3.52	3.39	3.88

Table IV. 42 Ovalisation after bending measured by hand (WT-2)

Reel [mm]	BB	9000	8000	7500	7000	6500	6000	5500
f_{H1} [%]	-0.15	-0.34	-0.09	-0.02	0.00	0.20	0.31	0.51
f_{H2} [%]	-0.14	1.57	2.26	2.48	3.07	3.65	3.91	4.87
f_{H3} [%]	-0.25	2.26	2.60	3.08	3.22	3.48	5.15	5.15
f_{H4} [%]	-0.12	1.65	2.10	2.45	2.77	3.33	4.08	4.45
f_{H5} [%]	-0.12	1.46	1.94	2.26	2.71	2.91	3.42	4.42
f_{H6} [%]	-0.15	1.46	1.91	2.00	2.54	2.77	3.45	4.56
f_{H7} [%]	-0.26	1.14	1.71	1.77	2.31	2.68	3.20	3.54
$f_{H;average}$ [%]	-0.16	1.71	2.14	2.45	2.81	3.12	4.02	4.64

Table IV. 43 Ratio of the change in diameter in the horizontal plane to the change in diameter in the vertical plane measured by hand after bending (WT-2)

Reel [mm]	9000	8000	7500	7000	6500	6000	5500
$\Delta d_{O;o;TFP;hor}/\Delta d_{O;o;TFP;ver}$ (H1)	1.48	6.00	-0.46	-1.00	5.07	5.36	0.72
$\Delta d_{O;o;TFP;hor}/\Delta d_{O;o;TFP;ver}$ (H2)	1.08	1.44	1.59	1.55	1.32	1.61	1.65
$\Delta d_{O;o;TFP;hor}/\Delta d_{O;o;TFP;ver}$ (H3)	1.62	1.48	1.53	1.61	1.48	1.07	1.35
$\Delta d_{O;o;TFP;hor}/\Delta d_{O;o;TFP;ver}$ (H4)	1.81	1.47	1.52	1.60	1.37	1.47	1.37
$\Delta d_{O;o;TFP;hor}/\Delta d_{O;o;TFP;ver}$ (H5)	1.78	1.37	1.22	1.25	1.42	1.44	1.47
$\Delta d_{O;o;TFP;hor}/\Delta d_{O;o;TFP;ver}$ (H6)	1.31	1.33	1.65	1.79	1.60	1.60	1.26
$\Delta d_{O;o;TFP;hor}/\Delta d_{O;o;TFP;ver}$ (H7)	0.57	1.26	1.34	2.05	1.41	1.63	1.32
$\Delta d_{O;o;TFP;hor}/\Delta d_{O;o;TFP;ver}$ (average)	1.63	1.41	1.48	1.56	1.47	1.40	1.36

Table IV. 44 Ovalisation after bending measured by OM (WT-2)

Reel [mm]	9000	8000	7500	7000	6500	6000	5500
$f_{OM1;AB}$ [%]	-0.07	0.37	0.04	0.00	1.36	1.84	0.65
$f_{OM2\ ;AB}$ [%]	1.90	2.73	3.14	3.43	3.70	4.55	5.75
$f_{OM3;AB}$ [%]	2.51	2.89	3.43	3.77	4.07	4.03	5.63
$f_{OM4;AB}$ [%]	1.42	2.16	2.43	2.79	2.92	3.74	4.26
$f_{OM5;AB}$ [%]	1.63	2.38	2.46	2.83	3.73	4.51	5.34
$f_{OM6;AB}$ [%]	1.24	1.82	2.34	3.19	3.32	3.97	4.16
$f_{OM7;AB}$ [%]	0.59	1.86	1.98	3.66	3.02	3.97	3.91
$f_{OM;average;AB}$ [%]	1.70	2.31	2.66	3.14	3.51	4.06	4.85

Table IV. 45 Ovalisation after bending measured by hand (GR-OR-1)

Reel [mm]	BB	9000	8000	7500	7000	6500	6000	5500
f_{H1} [%]	0.00	1.37	1.55	1.87	2.12	2.91	3.96	4.11
f_{H2} [%]	0.03	3.05	2.72	2.69	3.37	3.83	4.80	5.82
f_{H3} [%]	0.06	2.06	2.42	2.75	3.09	3.42	4.26	5.33
f_{H4} [%]	-	-	-	-	-	-	-	-
f_{H5} [%]	0.23	2.23	3.16	2.70	3.04	3.62	4.73	5.99
f_{H6} [%]	0.24	2.11	2.58	2.89	3.27	3.47	4.49	5.37
f_{H7} [%]	-0.08	1.88	2.24	2.27	3.02	3.32	4.79	4.91
$f_{H;average}$ [%]	0.14	2.36	2.72	2.76	3.19	3.59	4.57	5.63

Table IV. 46 Ratio of the change in diameter in the horizontal plane to the change in diameter in the vertical plane measured by hand after bending (GR-OR-1)

Reel [mm]	9000	8000	7500	7000	6500	6000	5500
$\Delta d_{O;o;TFP;hor}/\Delta d_{O;o;TFP;ver}$ (H1)	0.93	0.95	1.25	0.79	1.39	1.01	1.25
$\Delta d_{O;o;TFP;hor}/\Delta d_{O;o;TFP;ver}$ (H2)	1.04	1.68	1.32	1.62	1.49	1.10	1.29
$\Delta d_{O;o;TFP;hor}/\Delta d_{O;o;TFP;ver}$ (H3)	1.50	1.50	1.60	1.52	1.55	1.60	1.36
$\Delta d_{O;o;TFP;hor}/\Delta d_{O;o;TFP;ver}$ (H4)	-	-	-	-	-	-	-
$\Delta d_{O;o;TFP;hor}/\Delta d_{O;o;TFP;ver}$ (H5)	1.03	1.02	1.42	1.51	1.74	1.29	1.06
$\Delta d_{O;o;TFP;hor}/\Delta d_{O;o;TFP;ver}$ (H6)	1.76	1.33	1.31	1.19	1.63	1.45	1.37
$\Delta d_{O;o;TFP;hor}/\Delta d_{O;o;TFP;ver}$ (H7)	1.65	1.82	1.37	1.52	1.58	0.99	1.22
$\Delta d_{O;o;TFP;hor}/\Delta d_{O;o;TFP;ver}$ (average)	1.33	1.38	1.41	1.46	1.60	1.36	1.27

Table IV. 47 Ovalisation after bending measured by OM (GR-OR-1)

Reel [mm]	9000	8000	7500	7000	6500	6000	5500
$f_{OM1;AB}$ [%]	0.99	1.26	1.56	1.53	2.28	2.52	3.17
$f_{OM2;AB}$ [%]	1.95	2.86	2.81	3.49	3.86	4.08	5.48
$f_{OM3;AB}$ [%]	1.69	2.15	2.55	2.78	3.28	4.54	4.98
$f_{OM4;AB}$ [%]	-	-	-	-	-	-	-
$f_{OM5;AB}$ [%]	1.19	1.67	2.28	2.74	3.68	3.96	4.23
$f_{OM6;AB}$ [%]	1.96	2.21	2.41	2.86	3.91	4.67	5.23
$f_{OM7;AB}$ [%]	1.74	2.34	2.01	2.84	2.95	2.91	3.79
$f_{OM;average;AB}$ [%]	1.70	2.22	2.51	2.97	3.68	4.31	4.98

Table IV. 48 Ovalisation after bending measured by hand (GR-OR-2)

Reel [mm]	BB	9000	8000	7500	7000	6500	6000	5500
f_{H1} [%]	-0.28	1.05	1.40	1.51	1.93	2.40	3.06	3.37
f_{H2} [%]	-0.12	2.28	2.58	2.86	3.13	3.59	5.42	5.65
f_{H3} [%]	0.08	2.39	2.52	2.78	2.96	3.77	4.50	5.38
f_{H4} [%]	-	-	-	-	-	-	-	-
f_{H5} [%]	0.25	1.99	2.10	2.47	2.74	3.64	4.27	4.92
f_{H6} [%]	0.18	2.22	2.61	2.77	3.21	3.81	4.54	5.23
f_{H7} [%]	-0.03	2.13	2.36	2.40	2.91	3.39	3.90	4.44
$f_{H;average}$ [%]	0.10	2.22	2.45	2.72	3.01	3.70	4.68	5.29

Table IV. 49 Ratio of the change in diameter in the horizontal plane to the change in diameter in the vertical plane measured by hand after bending (GR-OR-2)

Reel [mm]	9000	8000	7500	7000	6500	6000	5500
$\Delta d_{O;o;TFP;hor}/\Delta d_{O;o;TFP;ver}$ (H1)	1.59	1.53	1.07	1.53	1.58	1.53	1.49
$\Delta d_{O;o;TFP;hor}/\Delta d_{O;o;TFP;ver}$ (H2)	1.89	1.58	1.52	1.55	1.49	1.00	1.53
$\Delta d_{O;o;TFP;hor}/\Delta d_{O;o;TFP;ver}$ (H3)	1.45	1.73	1.49	1.42	1.45	1.38	1.34
$\Delta d_{O;o;TFP;hor}/\Delta d_{O;o;TFP;ver}$ (H4)	-	-	-	-	-	-	-
$\Delta d_{O;o;TFP;hor}/\Delta d_{O;o;TFP;ver}$ (H5)	1.33	1.96	1.77	1.67	1.29	1.48	1.48
$\Delta d_{O;o;TFP;hor}/\Delta d_{O;o;TFP;ver}$ (H6)	1.56	1.47	1.63	1.52	1.24	1.28	1.37
$\Delta d_{O;o;TFP;hor}/\Delta d_{O;o;TFP;ver}$ (H7)	1.29	1.25	1.78	1.56	1.36	1.27	1.26
$\Delta d_{O;o;TFP;hor}/\Delta d_{O;o;TFP;ver}$ (average)	1.56	1.69	1.60	1.54	1.37	1.29	1.43

Table IV. 50 Ovalisation after bending measured by OM (GR-OR-2)

Reel [mm]	9000	8000	7500	7000	6500	6000	5500
$f_{OM1;AB}$ [%]	1.41	1.72	1.54	2.21	2.75	3.04	3.40
$f_{OM2\,;AB}$ [%]	2.49	2.50	2.88	3.20	3.67	3.47	5.54
$f_{OM3;AB}$ [%]	1.87	2.54	2.56	2.84	3.38	3.98	4.72
$f_{OM4;AB}$ [%]	-	-	-	-	-	-	-
$f_{OM5;AB}$ [%]	1.10	2.15	2.32	2.68	2.94	3.79	4.55
$f_{OM6;AB}$ [%]	2.08	2.57	3.05	3.35	3.46	4.12	5.04
$f_{OM7;AB}$ [%]	1.56	1.99	2.53	3.12	3.09	3.46%	4.06
$f_{OM;average;AB}$ [%]	1.88	2.44	2.70	3.02	3.36	3.84	4.96

VI.8.2 Ovalisation at Maximum Bending

It should be noted that the average values for ovalisation at maximum bending for Tight Fit Pipes OR-2, GR-1, GR-2, WT-1 and WT-2 (Tight Fit Pipes with no Tight Fit Pipe circumferential weld) are determined only using values at locations 3, 4, 5 and 6 (Figure 7.7). Ovalisation values at these locations are more or less the same. Average values for ovalisation at maximum bending for GR-OR-1 and GR-OR-2 (Tight Fit Pipes with a Tight Fit Pipe circumferential weld) are determined using measurements from locations 2, 3, 5 and 6 (Figure 7.9). Values for ovalisation at these locations are also more or less the same. Values at the other locations (locations 1, 2 and 7 for the Tight Fit Pipes with no Tight Fit Pipe circumferential weld and locations 1, 4 and 7 for the Tight Fit Pipes with a Tight Fit Pipe circumferential weld) are affected by boundary conditions and are not taken into account. It should also be take into account that the ovalisation meter can only measure the increase in diameter in the vertical plane. As has been explained in Subsection 6.2.2 a procedure has been developed to calculate the ovalisation from the ovalisation meter measurements.

Table IV. 51 Ovalisation at maximum bending measured by OM (OR-2)

Reel [mm]	9000	8000	7500	7000	6500	6000	5500
$f_{OM1;MBS}$ [%]	0.80	0.00	-52.18	1.05	5.17	-12.68	2.58
$f_{OM2;MBS}$ [%]	2.55	5.23	5.46	5.30	7.36	7.58	8.65
$f_{OM3;MBS}$ [%]	4.52	4.25	6.12	5.51	6.67	7.81	8.96
$f_{OM4;MBS}$ [%]	3.72	3.09	3.55	3.70	4.52	5.64	6.45
$f_{OM5;MBS}$ [%]	3.37	4.35	5.66	5.10	5.67	6.93	7.69
$f_{OM6;MBS}$ [%]	3.00	3.80	4.73	5.64	6.15	6.69	8.01
$f_{OM7;MBS}$ [%]	3.46	3.84	4.65	4.12	4.83	6.18	6.36
$f_{OM;average;MBS}$ [%]	3.65	3.88	5.02	4.99	5.76	6.77	7.78

Table IV. 52 Ovalisation at maximum bending measured by OM (GR-1)

Reel [mm]	5500
$f_{OM1;MBS}$ [%]	1.56
$f_{OM2;MBS}$ [%]	7.40
$f_{OM3;MBS}$ [%]	8.87
$f_{OM4;MBS}$ [%]	6.59
$f_{OM5;MBS}$ [%]	8.04
$f_{OM6;MBS}$ [%]	8.08
$f_{OM7;MBS}$ [%]	6.21
$f_{OM;average;MBS}$ [%]	7.89

Table IV. 53 Ovalisation at maximum bending measured by OM (GR-2)

Reel [mm]	9000	8000	7500	7000	6500	6000	5500
$f_{OM1;MBS}$ [%]	0.29	0.00	0.73	2.05	1.63	2.68	3.09
$f_{OM2;MBS}$ [%]	4.19	5.89	5.54	5.76	6.97	7.16	8.31
$f_{OM3;MBS}$ [%]	3.93	4.77	5.50	5.87	6.52	7.48	8.27
$f_{OM4;MBS}$ [%]	2.68	3.20	4.37	4.46	4.51	5.46	5.99
$f_{OM5;MBS}$ [%]	3.27	4.17	4.79	5.81	6.63	6.44	7.75
$f_{OM6;MBS}$ [%]	3.06	4.86	4.81	5.54	6.22	6.31	6.96
$f_{OM7;MBS}$ [%]	3.02	3.86	4.25	5.00	4.87	5.71	5.70
$f_{OM;average;MBS}$ [%]	3.24	4.25	4.87	5.42	5.97	6.42	7.25

Table IV. 54 Ovalisation at maximum bending measured by OM (WT-1)

Reel [mm]	9000	8000	7500	7000	6500	6000	5500
$f_{OM1;MBS}$ [%]	0.00	0.51	1.00	0.51	2.30	1.77	1.61
$f_{OM2;MBS}$ [%]	4.13	4.56	5.08	5.66	6.40	6.84	7.56
$f_{OM3;MBS}$ [%]	4.26	4.53	5.78	5.92	6.89	6.64	7.93
$f_{OM4;MBS}$ [%]	2.86	3.07	3.60	3.53	4.59	4.67	4.43
$f_{OM5;MBS}$ [%]	3.32	3.86	4.81	4.91	5.83	5.81	6.25
$f_{OM6;MBS}$ [%]	2.98	3.95	4.60	4.60	5.66	5.01	5.77
$f_{OM7;MBS}$ [%]	2.97	3.06	3.77	4.92	5.22	5.18	4.83
$f_{OM;average;MBS}$ [%]	3.35	3.85	4.70	4.74	5.74	5.53	6.10

Table IV. 55 Ovalisation at maximum bending measured by OM (WT-2)

Reel [mm]	9000	8000	7500	7000	6500	6000	5500
$f_{OM1;MBS}$ [%]	0.86	3.41	0.29	0.00	4.72	5.66	1.75
$f_{OM2;MBS}$ [%]	3.51	4.79	5.42	5.74	5.93	7.15	8.53
$f_{OM3;MBS}$ [%]	4.53	4.98	5.76	6.09	6.45	6.09	8.18
$f_{OM4;MBS}$ [%]	3.05	3.74	4.28	4.60	4.72	5.74	6.41
$f_{OM5;MBS}$ [%]	3.61	4.19	4.44	4.71	6.06	6.86	7.99
$f_{OM6;MBS}$ [%]	2.92	3.65	4.56	5.60	5.79	6.56	6.62
$f_{OM7;MBS}$ [%]	1.44	3.43	3.45	5.99	4.89	6.21	6.03
$f_{OM;average;MBS}$ [%]	3.53	4.14	4.76	5.25	5.75	6.31	7.30

Table IV. 56 Ovalisation at maximum bending measured by OM (GR-OR-1)

Reel [mm]	9000	8000	7500	7000	6500	6000	5500
$f_{OM1;MBS}$ [%]	2.01	2.38	2.90	2.69	3.96	4.04	5.02
$f_{OM2;MBS}$ [%]	3.25	4.72	4.62	5.54	6.01	5.92	7.69
$f_{OM3;MBS}$ [%]	3.18	3.92	4.74	4.74	5.64	6.91	7.37
$f_{OM4;MBS}$ [%]	-	-	-	-	-	-	-
$f_{OM5;MBS}$ [%]	2.42	3.10	4.37	4.71	6.33	6.10	6.37
$f_{OM6;MBS}$ [%]	3.64	3.92	4.27	4.69	6.44	7.10	7.75
$f_{OM7;MBS}$ [%]	3.11	4.02	3.16	4.56	4.53	4.43	5.64
$f_{OM;average;MBS}$ [%]	3.12	3.92	4.50	4.92	6.10	6.51	7.30

Table IV. 57 Ovalisation at maximum bending measured by OM (GR-OR-2)

Reel [mm]	9000	8000	7500	7000	6500	6000	5500
$f_{OM1;MBS}$ [%]	2.78	3.20	2.88	4.03	4.74	5.08	5.56
$f_{OM2;MBS}$ [%]	4.28	4.30	4.83	5.23	5.79	5.25	8.04
$f_{OM3;MBS}$ [%]	3.29	4.39	4.52	4.71	5.43	6.12	7.06
$f_{OM4;MBS}$ [%]	-	-	-	-	-	-	-
$f_{OM5;MBS}$ [%]	2.47	4.21	4.61	4.79	4.94	6.09	7.08
$f_{OM6;MBS}$ [%]	3.64	4.46	5.28	5.57	5.63	6.43	7.59
$f_{OM7;MBS}$ [%]	2.80	3.33	4.03	4.85	4.75	5.22	5.99
$f_{OM;average;MBS}$ [%]	3.42	4.34	4.81	5.07	5.45	5.97	7.44

VI.8.3 Overview of Ovalisation

In the tables below an overview is presented of the average ovalisation in the Tight Fit Pipe test region (1) measured by hand after bending, (2) measured by ovalisation meter after bending and (3) measured by ovalisation meter at maximum bending.

Table IV. 58 Overview of ovalisation (OR-2)

Reel [mm]	9000	8000	7500	7000	6500	6000	5500
$f_{H;average}$ [%]	1.74	2.33	2.53	3.05	3.52	4.16	4.95
$f_{OM;average;AB}$ [%]	1.86	2.08	2.77	2.97	3.47	4.31	4.29
$f_{OM;average;MBS}$ [%]	3.65	3.88	5.02	4.99	5.76	6.77	7.78

Table IV. 59 Overview of ovalisation (GR-1)

Reel [mm]	5500
$f_{H;average}$ [%]	4.99
$f_{OM;average;AB}$ [%]	5.26
$f_{OM;average;MBS}$ [%]	7.89

Table IV. 60 Overview of ovalisation (GR-2)

Reel [mm]	9000	8000	7500	7000	6500	6000	5500
$f_{H;average}$ [%]	2.28	2.53	3.12	3.41	3.90	4.65	5.51
$f_{OM;average;AB}$ [%]	1.87	2.53	2.98	3.41	3.79	4.24	4.93
$f_{OM;average;MBS}$ [%]	3.24	4.25	4.87	5.42	5.97	6.42	7.25

Table IV. 61 Overview of ovalisation (WT-1)

Reel [mm]	9000	8000	7500	7000	6500	6000	5500
$f_{H;average}$ [%]	1.96	2.67	2.83	3.37	3.88	4.55	5.69
$f_{OM;average;AB}$ [%]	1.73	2.10	2.61	2.81	3.52	3.39	3.88
$f_{OM;average;MBS}$ [%]	3.35	3.85	4.70	4.74	5.74	5.53	6.10

Table IV. 62 Overview of ovalisation (WT-2)

Reel [mm]	9000	8000	7500	7000	6500	6000	5500
$f_{H;average}$ [%]	1.71	2.14	2.45	2.81	3.12	4.02	4.64
$f_{OM;average;AB}$ [%]	1.70	2.31	2.66	3.14	3.51	4.06	4.85
$f_{OM;average;MBS}$ [%]	3.53	4.14	4.76	5.25	5.75	6.31	7.30

Table IV. 63 Overview of ovalisation (GR-OR-1)

Reel [mm]	9000	8000	7500	7000	6500	6000	5500
$f_{H;average}$ [%]	2.36	2.72	2.76	3.19	3.59	4.57	5.63
$f_{OM;average;AB}$ [%]	1.70	2.22	2.51	2.97	3.68	4.31	4.98
$f_{OM;average;MBS}$ [%]	3.12	3.92	4.50	4.92	6.10	6.51	7.30

Table IV. 64 Overview of ovalisation (GR-OR-2)

Reel [mm]	9000	8000	7500	7000	6500	6000	5500
$f_{H;average}$ [%]	2.22	2.45	2.72	3.01	3.70	4.68	5.29
$f_{OM;average;AB}$ [%]	1.88	2.44	2.70	3.02	3.36	3.84	4.96
$f_{OM;average;MBS}$ [%]	3.42	4.34	4.81	5.07	5.45	5.97	7.44

IV.9 Liner pipe wrinkling

VI.9.1 Comparison of Rough and Detailed Scans for TFP WT-2

In the tables below the effect of the measuring density of the laser trolley scan (20 mm versus 5 mm) on various measured data. This effect has been studied for Tight Fit Pipe WT-2 at several radii reels.

Table IV. 65 Comparison of detailed and rough scan measurements of residual liner pipe wrinkles and wrinkles at maximum bending strain (TFP WT-2)

	20 mm	5 mm	20 mm	5 mm	Δ [%]	20 mm	5 mm	Δ [%]
	$L_{axial;top}$ [mm]	$L_{axial;top}$ [mm]	$\Delta r_{L;i;TFP;top}$ [mm]	$\Delta r_{L;i;TFP;top}$ [mm]		$L_L/m_{dr/dx}$ [mm]	$L_L/m_{dr/dx}$ [mm]	
7mAB								
W16	1976	1979	-11.19	-11.52	3	80	68	-15
W18	2038	2036	-5.01	-5.15	3	59	58	-2
6.5mAB								
W10	1379	1388	-10.62	-12.10	14	58	78	34
W12	1636	1634	-11.89	-11.89	0	80	73	-10
W16	1978	1980	-12.76	-12.43	-3	81	70	-14
6.5mMBS								
W10	1392	1391	-14.52	-14.45	0	80	79	-1
W12	1631	1634	-13.37	-13.96	4	81	73	-11
W16	1972	1980	-13.69	-15.30	12	81	79	-2
6mAB								
W10	1379	1389	-12.38	-13.56	10	79	73	-7
W12	1638	1633	-12.38	-12.93	4	81	69	-15
W16	1978	1975	-14.16	-14.24	1	80	78	-2
6mMBS								
W10	1387	1390	-15.53	-16.16	4	79	89	13
W12	1644	1634	-13.79	-15.27	11	100	74	-26
W16	1985	1980	-15.71	-16.63	6	81	88	9
5.5mAB								
W10	1385	1385	-14.94	-14.87	0	80	79	-1
W12	1624	1628	-12.65	-14.15	12	80	74	-8
W16	1983	1974	-14.28	-15.54	9	81	70	-14
5.5mMBS								
W10	1393	1389	-17.54	-17.53	0	79	95	20
W12	1631	1633	-16.45	-16.67	1	81	80	-2
W16	1972	1974	-17.46	-18.05	3	101	96	-5

Table IV. 66 Comparison of detailed and rough scan measurements of residual liner pipe wrinkle height and wrinkle height at maximum bending strain (TFP WT-2)

	20 mm	5 mm	Δ [%]
	a [mm]	a [mm]	
W16 (7mAB)	7.97	8.49	7
W18 (7mAB)	6.43	5.46	-15
W10 (6.5mAB)	6.75	8.41	25
W12 (6.5mAB)	8.35	8.57	3
W12 (6.5mMBS)	8.61	9.25	7
W16 (6.5mMBS)	8.91	10.43	17
W12 (6mAB)	8.34	9.00	8
W12 (6mMBS)	8.42	9.98	19
W16 (6mMBS)	10.43	11.64	12
W12 (5.5mAB)	8.08	9.67	20
W12 (5.5mMBS)	10.43	10.68	2

Table IV. 67 Comparison of detailed and rough scan measurements of residual liner pipe wrinkles W16 and W18 (WT-2)

	W16 (WT-2)			W18 (WT-2)		
	20 mm	5 mm	Δ [%]	20 mm	5 mm	Δ [%]
$\Delta r_{L;i;TFP;top}$ [mm]	-11.19	-11.52	3	-5.01	-5.15	3
$\Delta r_{L;i;TFP;pre}$ [mm]	-3.88	-3.71		2.20	2.06	
$\Delta r_{L;i;TFP;post}$ [mm]	-2.55	-2.53		0.14	-0.96	
$L_{axial;top}$ [mm]	1976	1979		2038	2036	
$L_{axial;pre}$ [mm]	1917	1905		1976	1979	
$L_{axial;post}$ [mm]	2038	2036		2137	2075	
$L_{axial;start;dr/dx}$ [mm]	1937	1945		1997	2006	
$L_{axial;end;dr/dx}$ [mm]	2017	2013		2056	2064	
$L/m_{pre\text{-}post}$ [mm]	121	131	9	160	96	-40
$L/m_{dr/dx}$ [mm]	80	68	-15	59	58	-2
$\Delta r_{L;i;TFP;bottom}$ [mm]	-3.22	-3.03		1.42	0.31	
a [mm]	7.97	8.49	7	6.43	5.46	-15

VI.9.2 Results from Scans for Tight Fit Pipes

In the figures below the laser trolley scans of the insides of the Tight Fit Pipes can be found after bending the pipes to the 5.5 m radius reel. Also figures are shown in which the residual liner pipe wrinkle heights for various Tight Fit Pipes as a function of increasing curvature are presented. The tables below provide information on the largest liner wrinkles present in the test regions of the various Tight Fit Pipes.

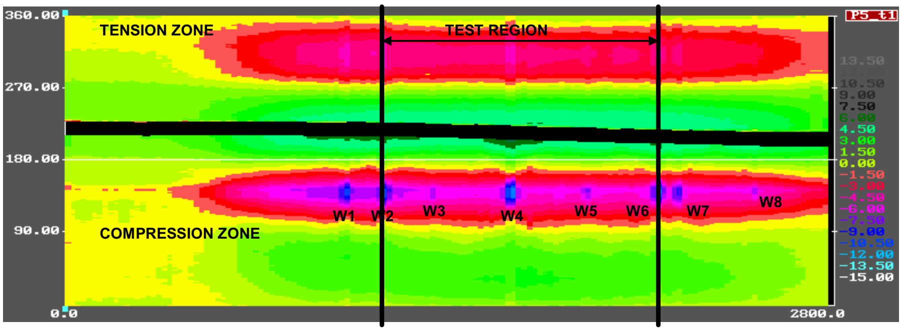

Figure IV. 2 Overview of the liner pipe wrinkles after bending Tight Fit Pipe OR-2 to the 5.5 m radius reel

Table IV. 68 Liner pipe wrinkles of TFP OR-2

	a (laser) [mm]	$L_{axial;top}$ (laser) [mm]	$L_{axial;top}$ (hand) [mm]	$L_L/m_{dr/dx}$ (laser) [mm]	$L_L/m_{pre-post}$ (laser) [mm]	L_L/m (hand) [mm]	Location
W2	4.00	1161	1174	61	81	65	CZ
W3	0.93	1341	1358	-	159	45	CZ
W4	5.89	1640	1626	81	178	85	CZ
W5	1.74	1920	1923	-	100	45	CZ
W6	4.32	2180	2178	60	139	65	CZ

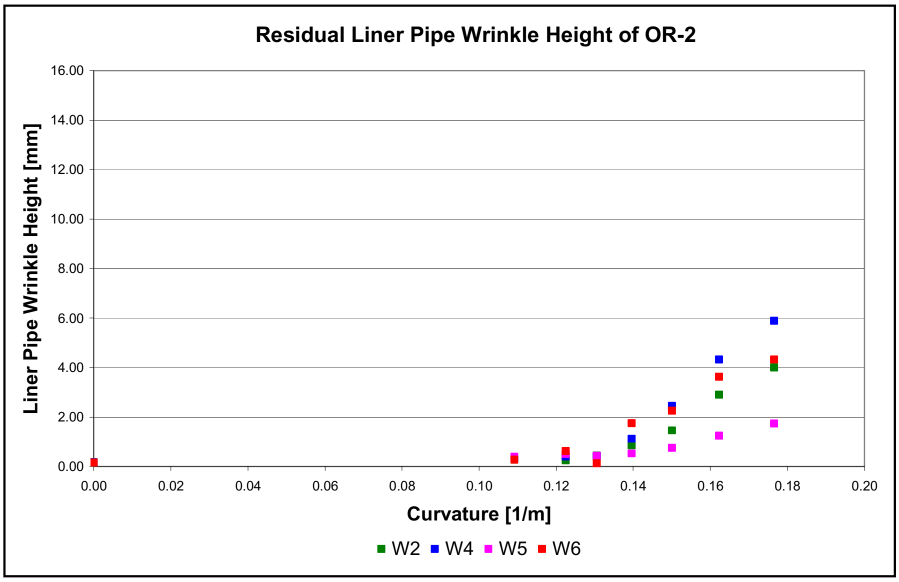

Figure IV. 3 Residual wrinkle height as a function of the increasing curvature (OR-2)

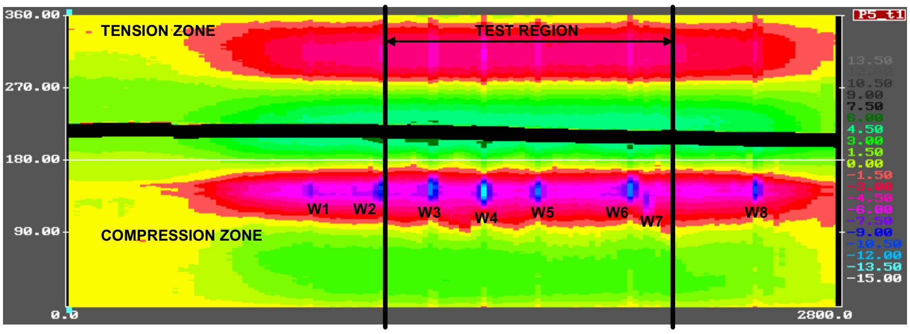

Figure IV. 4 Overview of the liner pipe wrinkles after bending Tight Fit Pipe GR-1 to the 5.5 m radius reel

Table IV. 69 Liner pipe wrinkles of TFP GR-1

	a (laser) [mm]	$L_{axial;top}$ (laser) [mm]	$L_{axial;top}$ (hand) [mm]	$L_L/m_{dr/dx}$ (laser) [mm]	$L_L/m_{pre\text{-}post}$ (laser) [mm]	L_L/m (hand) [mm]	Location
W2	3.70	1162	1148	60	80	65	CZ
W3	5.21	1341	1332	60	219	70	CZ
W4	6.87	1541	1523	79	140	85	CZ
W5	5.44	1741	1713	81	120	75	CZ
W6	5.88	2077	2058	78	240	75	CZ
W7	3.14	2137	2118	61	140	55	next to CZ

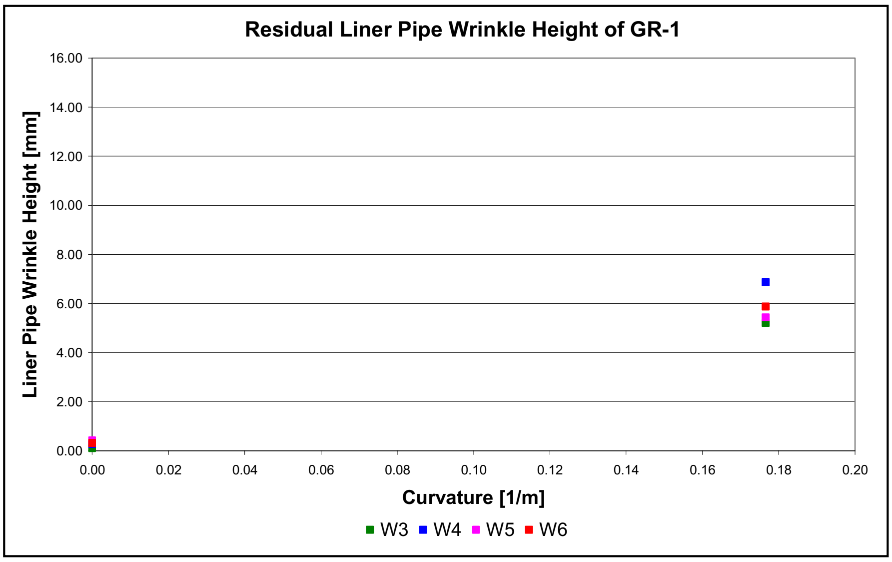

Figure IV. 5 Residual wrinkle height as a function of increasing curvature (GR-1)

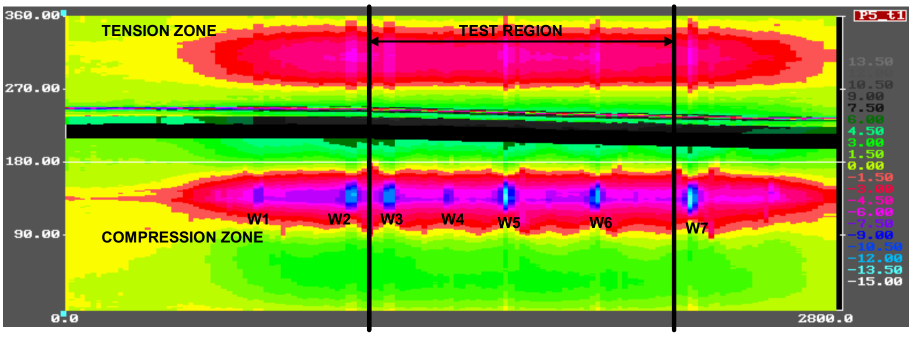

Figure IV. 6 Overview of the liner pipe wrinkles after bending Tight Fit Pipe GR-2 to the 5.5 m radius reel

Table IV. 70 Liner pipe wrinkles of TFP GR-2

	a (laser) [mm]	$L_{axial;top}$ (laser) [mm]	$L_{axial;top}$ (hand) [mm]	$L_L/m_{dr/dx}$ (laser) [mm]	$L_L/m_{pre\text{-}post}$ (laser) [mm]	L_L/m (hand) [mm]	Location
W3	6.21	1216	1217	61	181	65	CZ
W4	3.00	1438	1400	41	140	45	CZ
W5	7.92	1657	1610	79	160	65	CZ
W6	6.59	1995	1968	59	160	65	CZ

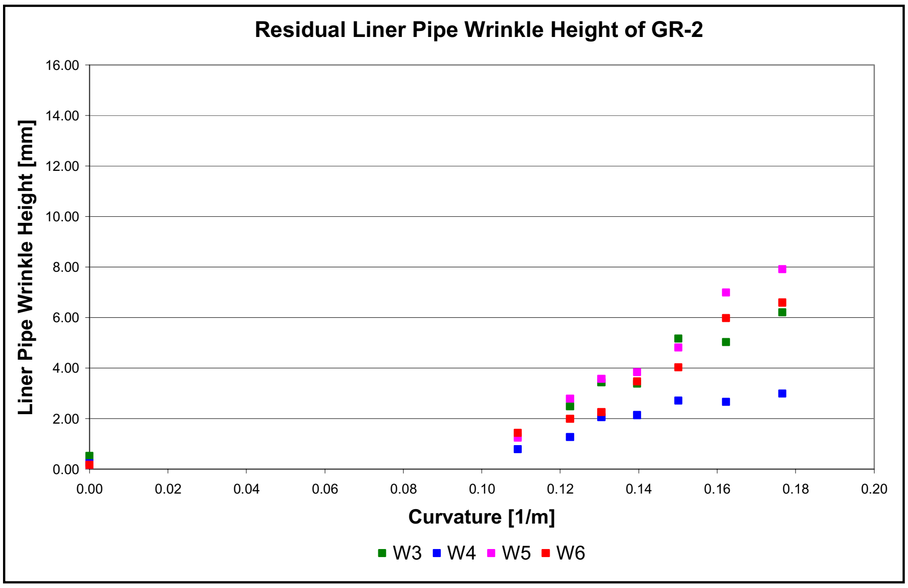

Figure IV. 7 Residual wrinkle height as a function of increasing curvature (GR-2)

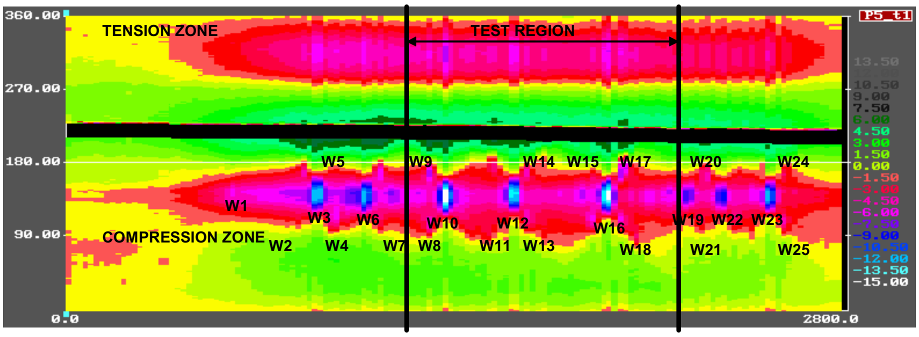

Figure IV. 8 Overview of the liner pipe wrinkles after bending Tight Fit Pipe WT-2 to the 5.5 m radius reel

Table IV. 71 Liner pipe wrinkles of TFP WT-2

	a (laser) [mm]	$L_{axial;top}$ (laser) [mm]	$L_{axial;top}$ (hand) [mm]	$L_L/m_{dr/dx}$ (laser) [mm]	$L_L/m_{pre\text{-}post}$ (laser) [mm]	L_L/m (hand) [mm]	Location
W8	6.55	1325	1324	59	181	65	next to CZ
W9	4.85	1325	1326	39	200	50	next to CZ
W10	10.43	1385	1389	80	218	85	CZ
W11	4.37	1563	1545	60	120	50	next to CZ
W12	8.08	1624	1623	80	140	80	CZ
W13	4.66	1682	1671	61	141	60	next to CZ
W14	2.92	1682	1682	40	141	60	next to CZ
W15	3.96	1924	1909	60	120	60	next to CZ
W16	9.73	1983	1969	81	140	80	CZ
W17	4.94	2024	2019	62	160	60	next to CZ
W18	7.98	2044	2023	80	222	60	next to CZ

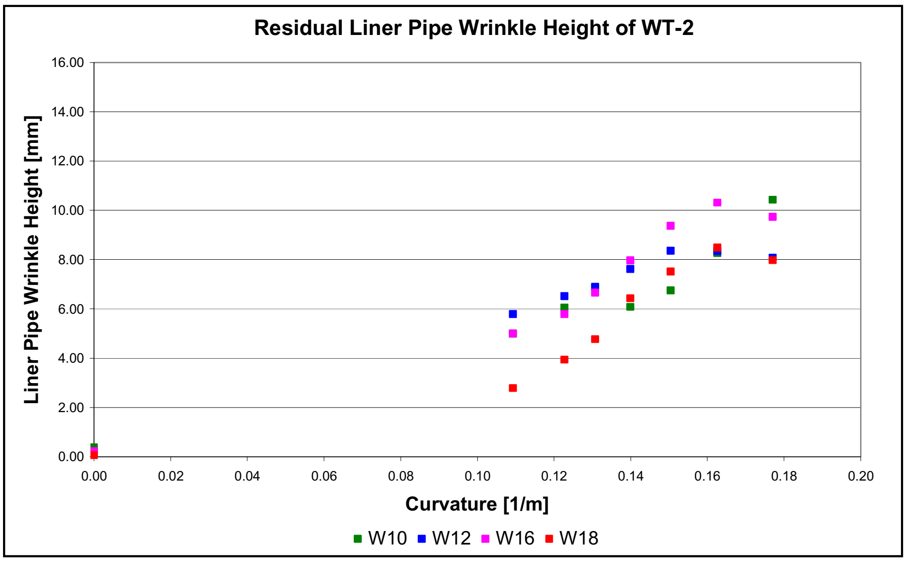

Figure IV. 9 Residual wrinkle height as a function of increasing curvature (WT-2)

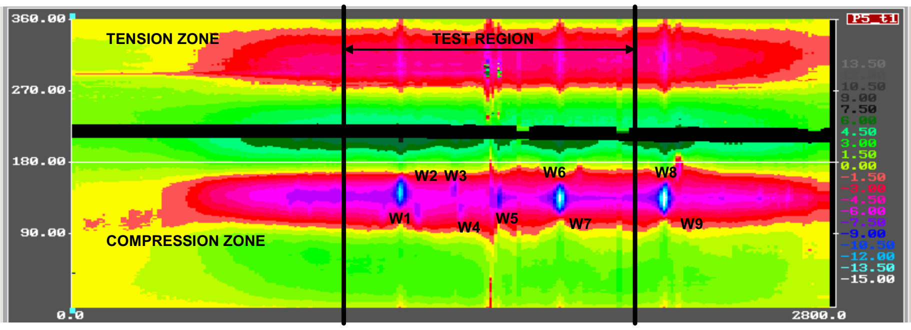

Figure IV. 10 Overview of the liner pipe wrinkles after bending Tight Fit Pipe GR-OR-1 to the 5.5 m radius reel

Table IV. 72 Liner pipe wrinkles of TFP GR-OR-1

	a (laser) [mm]	$L_{axial;top}$ (laser) [mm]	$L_{axial;top}$ (hand) [mm]	$L_L/m_{dr/dx}$ (laser) [mm]	$L_L/m_{pre\text{-}post}$ (laser) [mm]	L_L/m (hand) [mm]	Location
W1	6.77	1220	1216	50	190	70	CZ
W2	2.67	1290	1285	20	100	50	Next to CZ
W3	2.16	1430	1415	-	70	45	CZ
W4	1.82	1450	1449	-	60	45	Next to CZ
W5	2.59	1590	1576	30	70	50	CZ
W6	8.48	1820	1794	60	200	80	CZ
W7	3.09	1890	1884	-	150	45	Next to CZ

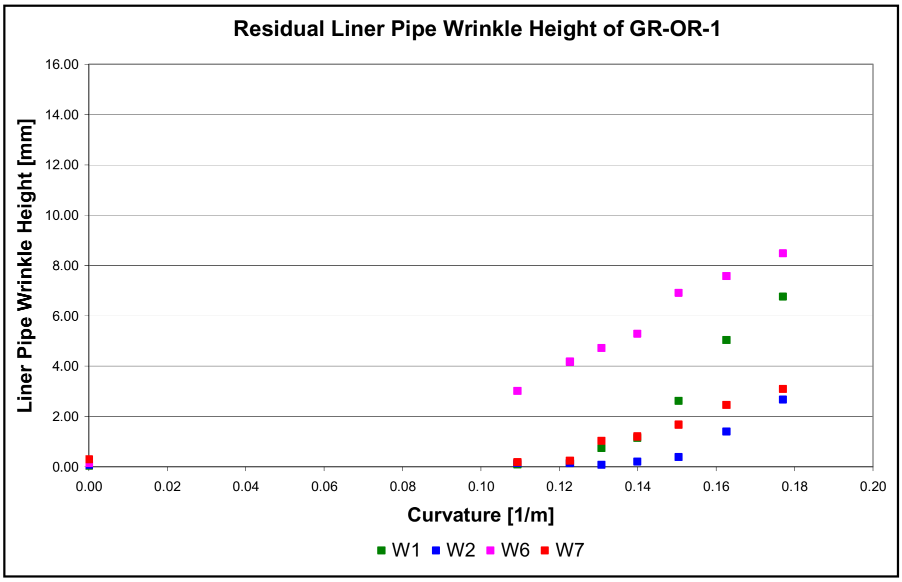

Figure IV. 11 Residual wrinkle height as function of increasing curvature (GR-OR-1)

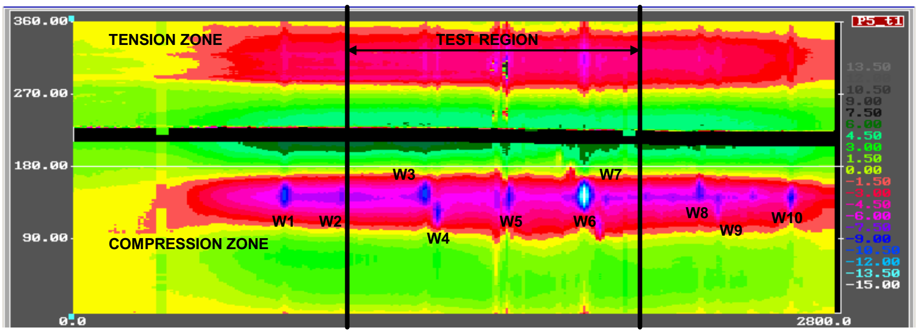

Figure IV. 12 Overview of the liner pipe wrinkles after bending Tight Fit Pipe GR-OR-2 to the 5.5 m radius reel

Table IV. 73 Liner pipe wrinkles of TFP GR-OR-2

	a (laser) [mm]	$L_{axial;top}$ (laser) [mm]	$L_{axial;top}$ (hand) [mm]	$L_L/m_{dr/dx}$ (laser) [mm]	$L_L/m_{pre\text{-}post}$ (laser) [mm]	L_L/m (hand) [mm]	Location
W2	1.10	1000	998	0	45	90	CZ
W3	5.24	1320	1292	60	60	110	Next to CZ
W4	5.09	1360	1337	40	50	120	CZ
W5	4.11	1630	1593	40	50	90	CZ
W6	9.81	1910	1868	80	80	110	CZ
W7	4.46	1970	1928	50	50	90	Next to CZ

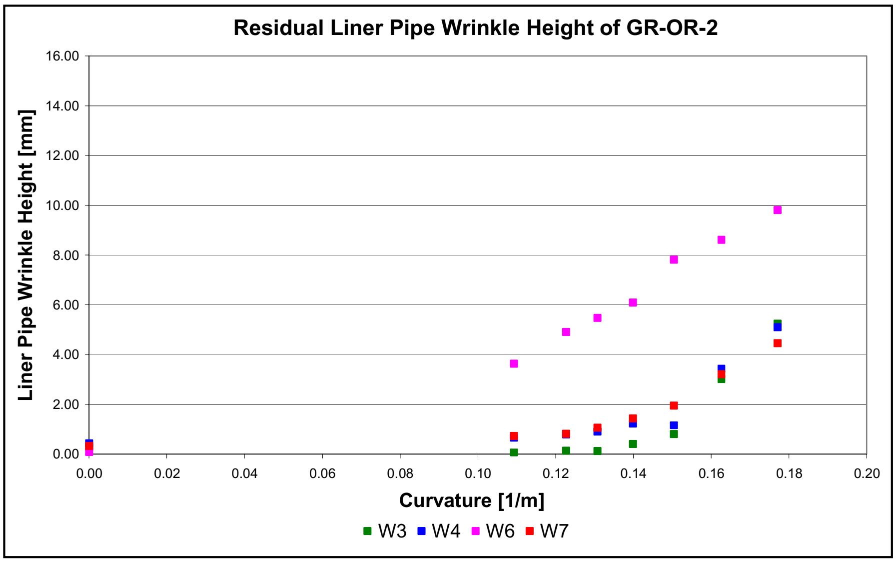

Figure IV. 13 Residual wrinkle height as function of increasing curvature (GR-OR-2)

Samenvatting

Als het mogelijk zou zijn om Tight Fit Pipe te installeren met behulp van de reeling methode zou dit een aantrekkelijke optie zijn voor de exploitatie van offshore velden die corrosief olie en gas bevatten. Tight Fit Pipe is een dubbelwandige pijp waarbij een dunne, corrosie bestendige, binnenpijp in een dikkere stalen buitenpijp is geklemd via een thermo-hydraulisch fabricage proces. Reeling is een offshore pijpleiding installatie methode waarbij een pijpleiding op een spoel wordt gewikkeld die op een schip staat. Het schip vaart vervolgens naar de offshore locatie waar de pijpleiding wordt afgewikkeld, rechtgebogen en neergelegd op de zeebodem. Reeling van Tight Fit Pipe is echter nog geen bewezen technologie. Reeling veroorzaakt namelijk hoge plastische rekken (ten gevolge van het buigen) in de Tight Fit Pipe, die mogelijk onacceptabel plooien van de binnenpijp en onacceptabele ovalisatie kunnen veroorzaken. Dit promotie project beoogt een bijdrage te leveren aan de ontwikkeling van Tight Fit Pipe installatie met behulp van reeling. Het onderzoek richtte zich op de initiatie en de ontwikkeling van het plooien van de binnenpijp en de mate van pijp ovalisatie gedurende het opspoel proces van het reelen. Dit gebeurde zowel theoretisch als experimenteel, het laatste door middel van reeling simulatie testen van 12.75 inch Tight Fit Pipes, schaal 1:1. Deze testen richtten zich op het opspoelen omdat plooi initiatie van de binnenpijp verwacht wordt in deze fase van het reelen: dan treden namelijk de grootste buigrekken op.

Axiale druk testen op 10.75 en 12.75 inch Tight Fit Pipe en buigtesten van kleine enkelwandige 22 mm pijpen in een mini buiginstallatie zijn uitgevoerd ter voorbereiding van het ontwerp en de bouw van een grote buiginstallatie. Deze buiginstallatie is gebruikt voor het uitvoeren van schaal 1:1 reeling simulatie testen van Tight Fit Pipe. Een buigtest is uitgevoerd op een 12.75 inch enkelwandige pijp om de bruikbaarheid van de installatie te verifiëren voor het uitvoeren van de 12.75 inch Tight Fit Pipe buigtesten. Zeven 12.75 inch Tight Fit Pipe test stukken zijn vervolgens stapsgewijs gebogen tegen steeds kleinere reel radii. De reel radii in de buiginstallatie waren 9 m, 8 m, 7.5 m, 7 m, 6.5 m, 6 m, en 5.5 m. Een van de doelen van de Tight Fit Pipe buigtesten was om plooi initiatie van de binnenpijp te bepalen. Er bestaat alleen nog geen algemene overeenstemming over de definitie van plooi initiatie van een pijp. Daarom is voorgesteld om het overschrijden van een zekere plooihoogte aan te nemen als criterium voor plooi initiatie. De waarde voor dit criterium kan bijvoorbeeld worden gebaseerd op de invloed van de plooihoogte op de vermoeiingslevensduur of op de maat van een “pig” en de mogelijkheid om plooien van een zekere hoogte te passeren.

Test resultaten van de reeling simulatie testen van de 12.75 inch Tight Fit Pipe geven aan dat:

1. de voorspellingen voor de krachten op de 12.75 inch Tight Fit Pipe geleverd door de buiginstallatie goed overeenkomen met de gemeten waarden.

2. de DNV OS F101 voorspelling voor ovalisatie, waarbij de binnen- en de buitenpijp als één pijp worden aangenomen, de gemeten waarden voor ovalisatie onderschat. Dit kan worden verklaard door het feit dat in deze formule de reactie kracht van de reel op de buis niet wordt meegenomen.
3. een verhoging van de mechanische verbindingssterkte in de Tight Fit Pipe de mate van plooien van de binnenpijp vermindert. Dit kan worden verklaard door het feit dat een hogere mechanische verbindingssterkte meer axiale frictie veroorzaakt tussen de binnen- en de buitenpijp wat de toevoer van materiaal naar de plooi belemmert.
4. de aanwezigheid van een rondlas in de Tight Fit Pipe hogere plooien veroorzaakt bij de lagere gemeten krommingen. Dit zou het gevolg kunnen zijn van het feit dat de pijp minder gelijkmatig aanligt op de reel ten gevolge van de rondlas. Hierdoor kan de contactdruk tussen de reel en de Tight Fit Pipe lokaal worden verhoogd wat plooi initiatie zou kunnen “triggeren”.
5. de “electric resistance welded” langsnaad in de buitenpijp geen hogere plooien veroorzaakt bij de gemeten krommingen. Dit zou kunnen worden verklaard door het feit dat deze langsnaad langs de gehele lengte van de Tight Fit Pipe aanwezig is, waardoor deze niet functioneert als een locale imperfectie.

Om gedurende het opspoel proces van de Tight Fit Pipe plooien van de binnenpijp te minimaliseren, is het aan te raden de diameter tot wanddikte verhouding van de binnen- en de buitenpijp zo laag mogelijk te kiezen en de radius van de reel en de mechanische verbindingssterkte zo hoog mogelijk te nemen. Een gevoeligheidsanalyse van het fabricage proces van Tight Fit Pipe heeft aangetoond dat de mechanische verbindingssterkte gunstig beïnvloed wordt door het materiaal van de binnenpijp zo sterk mogelijk te kiezen en de contact tijd tussen de binnen- en de buitenpijp gedurende het fabricage proces te minimaliseren. Formules zijn ontwikkeld die gebruikt kunnen worden om de hoogte van de plooien in de binnenpijp te voorspellen als je de 12.75 inch Tight Fit Pipe die gebruikt is in dit onderzoek buigt tegen reel radii tussen 5.5 m en 9 m. De mechanische verbindingssterkte van deze 12.75 inch Tight Fit Pipe moet zich tussen de 53 MPa en de 189 MPa bevinden.

API “residual compressive stress testen” hebben aangetoond dat de initiële mechanische verbindingssterkte sterk gereduceerd wordt ten gevolge van het opspoel proces, ongeacht of initieel een hoge of een lage mechanische verbindingssterkte in de Tight Fit Pipe aanwezig was. Deze afname van de mechanische verbindingssterkte kan worden verklaard met het normaliteitprincipe gebruikt in plastische theorieën. Deze initiële bevindingen moeten verder worden onderzocht omdat de afname van de mechanische verbindingssterkte ten gevolge van het reeling proces van belang zou kunnen zijn bij het uiteindelijke gebruik van Tight Fit Pipe.

Curriculum Vitae

Eelke Focke was born in Willemstad, Curacao on October 14th 1976. She completed the Gymnasium in Leiden in 1995 after which she started her studies in Civil Engineering at the Delft University of Technology. During her studies she spent one year being a treasurer in the board of her students' union, this year being supported by the university. Working experience was gained abroad doing an internship in Norway at Boskalis Offshore A.S. She also studied in the United States twice, once attending a summer course at Texas A&M University in 2000 and once at the University of Texas at Austin as an exchange student during the spring semester of 2001. She graduated cum laude for her MSc. degree in May 2002 in the field of Offshore Engineering on her thesis titled: "*Straightening without an Aligner during the Reeling Installation Process".*

After defending her master thesis, she worked at the Centro de Investigación Industrial in Buenos Aires, Argentina, for three months after which, at the end of 2002, she could start her PhD research. The PhD project, titled "*Reeling of Tight Fit Pipe*", was a cooperation between the Delft University of Technology, Heerema Marine Contractors, Dosto Engineering and Kuroki T&P in Japan. A grant was received from SenterNovem (the department of Economical Affairs of the Dutch government) to execute the project.

Employed by Heerema Marine Contractors, she combined her PhD project with industry related work. During the PhD she also coached many students in BSc. and MSc. projects, published several papers and gave various presentations on the subject of "*Reeling of Tight Fit Pipe*". She also was awarded the Offshore Mechanics Scholarship Award at the ISOPE conference in June 2006.

Her hobbies are travelling, cooking Indonesian rice tables, sports (squash, running, skiing and diving) and reading.

STELLINGEN BEHOREND BIJ HET PROEFSCHRIFT

‘REELING OF TIGHT FIT PIPE’

E.S. FOCKE

1. Om de mechanische verbindingssterkte in een Tight Fit Pipe te bepalen verdient het de voorkeur om de “residual compressive stress test” te gebruiken in plaats van de “liner push out test”.

2. Als reeling gesimuleerd wordt door een vier-punts-buigproef wordt ovalisatie van de pijp onderschat omdat de reactie kracht van de reel op de pijp niet wordt meegenomen.

3. In geval van buiging vermindert een verhoging van de mechanische verbindingssterkte in een Tight Fit Pipe de plooihoogte van de binnenpijp.

4. Hoewel het waarschijnlijk mogelijk is om Tight Fit Pipe te installeren met behulp van reeling zonder onacceptabel plooigedrag van de binnenpijp te veroorzaken, zal eerst moeten worden onderzocht of de uiteindelijke afname van de mechanische verbindingssterkte ten gevolge van het reeling proces van belang zou kunnen zijn bij het uiteindelijke gebruik van Tight Fit Pipe.

5. Experimenteel onderzoek is net als wokken; de voorbereiding kost de meeste tijd.

6. Polygamie biedt ruimte voor de ontwikkeling van een vrouw.

7. Het Amerikaanse systeem op universiteiten waarbij je voortdurend bezig bent met huiswerkopgaven, resulteert in betere beheersing van een vak dan het Delfts blokken systeem waarin je 7 weken “niets” doet aan je studie, je 2 weken heel hard studeert en je “het meeste” de dag na je tentamen weer vergeten bent.

8. Het personeel op de Nederlandse terrassen zou moeten werken op basis van individuele fooien.

9. Gratis kinderopvang zal niet resulteren in een hogere arbeidsparticipatiegraad in Nederland.

10. Het is onzin om ons door de Chinese regering te laten voorschrijven hoe wij buitenlandse eigennamen moeten schrijven (Pinyin transcriptie): je hoeft niet naar Peking om Beijing eend te eten.

Deze stellingen worden opponeerbaar en verdedigbaar geacht en zijn als zodanig goedgekeurd door de promotoren, prof. ir. J. Meek en prof. ir. F.S.K. Bijlaard.

PROPOSITIONS PERTINENT TO THE DISSERTATION

'REELING OF TIGHT FIT PIPE'

E.S. FOCKE

1. To determine the mechanical bonding strength in a Tight Fit Pipe, it is recommended to use the "residual compressive stress test" rather than the "liner push out test".

2. If reeling is simulated by a four-point-bending test, ovalisation will be underestimated due to the fact that the reaction force of the reel on the pipe is not taken into account.

3. An increase in the mechanical bonding strength in a Tight Fit Pipe will reduce the liner pipe wrinkle height during bending.

4. Although it is most likely possible to install Tight Fit Pipe using the reeling installation method without causing unacceptable liner wrinkling, it should first be investigated whether the eventual reduction in the mechanical bonding strength due to the reeling process may be crucial for its anticipated application during operation.

5. Experimental research is like Chinese wok-cooking: the preparations take the most time.

6. Polygamy allows for the development of women.

7. The American university system where one is continuously engaged in homework assignments, results in better knowledge of a subject than the block system at the Delft University of Technology where one does "not" study for seven weeks, learns extremely hard for two weeks and forgets "almost everything" the day after the examination.

8. Employees at Dutch terraces should be paid on the basis of individual tips.

9. Free child care will not add to the level of labour participation in the Netherlands.

10. It is strange to let the Chinese government prescribe us how to write proper names (Pinyin transcription): you don't have to go to Peking to eat Beijing duck.

These propositions are considered opposable and defendable and as such have been approved by the supervisors, prof. ir. J. Meek and prof. ir. F.S.K. Bijlaard.

If it would be possible to install Tight Fit Pipe by means of reeling, it would be an attractive new option for the exploitation of offshore oil and gas fields containing corrosive hydrocarbons. Tight Fit Pipe is a mechanically bonded double walled pipe where a corrosion resistant alloy liner pipe is mechanically fitted inside a carbon steel outer pipe through a thermo-hydraulic manufacturing process. Reeling is a fast method of offshore pipeline installation where a pipe is spooled on a reel, which is positioned on a vessel. The vessel subsequently sails to the offshore location where the pipe is unwound, straightened and deployed to the seabed. Reeling of Tight Fit Pipe is not yet proven technology, however. The reeling process imposes high plastic strains (due to bending) in the pipe, which may cause unacceptable liner pipe wrinkling and Tight Fit Pipe ovalisation. This PhD project aimed to make a contribution to the possible development of the installation of Tight Fit Pipe by means of the reeling method. The focus of this research was on the initiation and the degree of liner pipe wrinkling as well as the degree of ovalisation occurring during the reeling process, both theoretically and experimentally; the latter by performing full scale bending tests on 12.75 inch outer diameter Tight Fit Pipe.

Eelke S. Focke